

University of Kentucky

UKnowledge

---

Theses and Dissertations--Microbiology,  
Immunology, and Molecular Genetics

Microbiology, Immunology, and Molecular  
Genetics

---

2021

# APPLICATION OF GENETIC TECHNIQUES TO INVESTIGATE CHLAMYDIA TRACHOMATIS TYPE III SECRETION EFFECTOR BIOLOGY

Gabrielle Keb

University of Kentucky, gabbykeb@gmail.com

Author ORCID Identifier:

 <https://orcid.org/0000-0001-8563-7593>

Digital Object Identifier: <https://doi.org/10.13023/etd.2021.223>

[Right click to open a feedback form in a new tab to let us know how this document benefits you.](#)

## Recommended Citation

Keb, Gabrielle, "APPLICATION OF GENETIC TECHNIQUES TO INVESTIGATE CHLAMYDIA TRACHOMATIS TYPE III SECRETION EFFECTOR BIOLOGY" (2021). *Theses and Dissertations--Microbiology, Immunology, and Molecular Genetics*. 25.

[https://uknowledge.uky.edu/microbio\\_etds/25](https://uknowledge.uky.edu/microbio_etds/25)

This Doctoral Dissertation is brought to you for free and open access by the Microbiology, Immunology, and Molecular Genetics at UKnowledge. It has been accepted for inclusion in Theses and Dissertations--Microbiology, Immunology, and Molecular Genetics by an authorized administrator of UKnowledge. For more information, please contact [UKnowledge@lsv.uky.edu](mailto:UKnowledge@lsv.uky.edu).

## **STUDENT AGREEMENT:**

I represent that my thesis or dissertation and abstract are my original work. Proper attribution has been given to all outside sources. I understand that I am solely responsible for obtaining any needed copyright permissions. I have obtained needed written permission statement(s) from the owner(s) of each third-party copyrighted matter to be included in my work, allowing electronic distribution (if such use is not permitted by the fair use doctrine) which will be submitted to UKnowledge as Additional File.

I hereby grant to The University of Kentucky and its agents the irrevocable, non-exclusive, and royalty-free license to archive and make accessible my work in whole or in part in all forms of media, now or hereafter known. I agree that the document mentioned above may be made available immediately for worldwide access unless an embargo applies.

I retain all other ownership rights to the copyright of my work. I also retain the right to use in future works (such as articles or books) all or part of my work. I understand that I am free to register the copyright to my work.

## **REVIEW, APPROVAL AND ACCEPTANCE**

The document mentioned above has been reviewed and accepted by the student's advisor, on behalf of the advisory committee, and by the Director of Graduate Studies (DGS), on behalf of the program; we verify that this is the final, approved version of the student's thesis including all changes required by the advisory committee. The undersigned agree to abide by the statements above.

Gabrielle Keb, Student

Dr. Kenneth A. Fields, Major Professor

Dr. Carol Pickett, Director of Graduate Studies

**APPLICATION OF GENETIC TECHNIQUES TO INVESTIGATE CHLAMYDIA  
TRACHOMATIS TYPE III SECRETION EFFECTOR BIOLOGY**

---

DISSERTATION

---

A dissertation submitted in partial fulfillment of the  
requirements for the degree of Doctor of Philosophy in the  
College of Medicine at the University of Kentucky

By

Gabrielle Keb

Lexington, Kentucky

Director: Dr. Kenneth A. Fields, Chair and Professor of  
Microbiology, Immunology, and Molecular Genetics

Lexington, Kentucky

2021

Copyright © Gabrielle Keb 2021  
<https://orcid.org/0000-0001-8563-7593>

## ABSTRACT OF DISSERTATION

### APPLICATION OF GENETIC TECHNIQUES TO INVESTIGATE CHLAMYDIA TRACHOMATIS TYPE III SECRETION EFFECTOR BIOLOGY

*Chlamydia trachomatis* is the causative agent of the most reported bacterial sexually transmitted disease in the United States. The establishment of an intracellular niche within mucosal epithelium is sufficient to drive immunopathology and disease sequela. As obligate intracellular bacteria, *Chlamydia* spp. have evolved numerous mechanisms for establishing an intracellular growth environment. The type III secretion system (T3SS) delivers effector proteins to the host cytosol and is essential for *C. trachomatis* invasion and development. The effectors TmeA, TmeB, and TarP, are all secreted during *C. trachomatis* invasion. TarP and TmeA have been associated with manipulation of actin networks and are essential for normal invasion levels. The functions of TarP are well established, whereas TmeA is less well characterized, and the role of TmeB is entirely unknown.

Recent progress in elucidating and characterizing these effectors has been bolstered by the development of techniques enabling basic genetic tractability of *C. trachomatis* L2. Florescence-reported allelic exchange mutagenesis (FRAEM) couples chromosomal gene deletion with the insertion of a selection cassette encoding antibiotic resistance and green fluorescent protein (GFP); however, FRAEM-mediated deletion of *Chlamydia trachomatis* *tmeA* produces a polar effect on the downstream gene, *tmeB*, and negatively impacts its expression. Our laboratory has adapted FRAEM technology by employing a *gfp-bla* cassette flanked by *loxP* sites. Conditional expression of Cre recombinase in *C. trachomatis* *tmeA* null strain containing a floxed cassette resulted in the deletion of the marker cassette and restoration of *tmeB* expression.

The work presented here utilizes the novel marker-less *C. trachomatis* deletion mutant to determine the importance of TmeA and TmeB during development and identify their eukaryotic host targets. We leverage chlamydial genetics and proximity labeling to

provide evidence that TmeA directly targets host N-WASP to promote Arp2/3-dependent actin polymerization. Our work also shows that TmeA and TarP influence separate yet synergistic pathways to accomplish chlamydial entry, while TmeB functions antagonistically to TmeA and inhibits Arp2/3-mediated actin polymerization.

KEYWORDS: FLAEM, FRAEM, TmeA, TmeB, *C. trachomatis*

---

Gabrielle E Keb  
*(Name of Student)*

---

06/08/2021

---

Date

APPLICATION OF GENETIC TECHNIQUES TO INVESTIGATE CHLAMYDIA  
TRACHOMATIS TYPE III SECRETION EFFECTOR BIOLOGY

By  
Gabrielle Keb

Kenneth A. Fields

---

Director of Thesis

Carol Pickett

---

Director of Graduate Studies

06/08/2021

---

Date

## DEDICATION

To my grandparents, Dr. Alan H. Jacobs, Marilyn C. Jacobs, and Dolores S. Heidanus

## ACKNOWLEDGMENTS

First and foremost, I would like to thank my advisor, Dr. Ken Fields. Ken, thank you for your unwavering support over the last five years and for shaping me into the scientist I am today. You have challenged me to work hard and to “build character.” Though I had a steep learning curve at the beginning of grad school, I appreciate your patience, flexibility, and understanding when I broke glassware or completely messed up an experiment. I am proud to say I have come a long way. You have also been a great mentor outside of the lab and have made me feel like a part of your family. Thank you for including me in so many adventures and celebrations like axe throwing, fishing, shooting at the range, boating, camping, rock climbing, birthdays, Super Bowl parties, and cookouts.

I would also like to thank my advisory committee, Dr. Brian Stevenson, Dr. Sarah D’Orazio, Dr. Carrie Shaffer, Dr. Haining Zhu, and Dr. Hunter Moseley. All of my committee members have been excellent. I appreciate their flexibility to meet and answer questions, their insightful suggestions, and encouragement.

I also owe a huge thank you to my lab mates Robert Hayman, Maria Boderó, and Dr. Kate Wolf. I genuinely believe we are more like family than colleagues at this point. Robert and Maria, you are two of my closest friends, and I thank you from the bottom of my heart for all the support, laughs, tears, and adventures. I would have lost my mind a long time ago if I didn’t have you to dance and sing with during long days. Kate, thank you for always sharing your wisdom about experiments and life. I have learned a lot from you.

I must also give a special thanks to Melissa Hollifield. Melissa, you consistently go above and beyond when chaos arises, whether it be solving technical problems, being a

friend before a seminar, or maintaining a steady supply of coffee. You are simply the best, and we would all be lost without you. Thank you so much for your help, your friendship, your advice, and my super fantastic color-changing lab scissors.

Beth Oates and Holden Williams, thank you, thank you, thank you. Beth, thank you for putting up with me for all these years and always being there when I need you. Thank you for staying late in the office with me and sharing Chinese food, thank you for magically appearing when I need a second pair of hands in lab, thank you for letting me “V8” you when I’m bored (except we’re never bored because grad students don’t get bored), and thank you for being my partner in crime. Holden, thank you for encouraging me, supporting me, and for working through tricky cell pathways with me. The two of you have been with me through the best and worst of grad school, and I am so grateful for your love and support.

Finally, I would like to thank my family. You have been my biggest cheerleaders, and I am so lucky to have you. I would not be where I am today without you believing in me. I love you.

# TABLE OF CONTENTS

<b>ACKNOWLEDGMENTS .....</b>	<b>iii</b>
<b>TABLE OF CONTENTS .....</b>	<b>v</b>
<b>LIST OF TABLES .....</b>	<b>viii</b>
<b>LIST OF FIGURES .....</b>	<b>ix</b>
<b>CHAPTER 1. INTRODUCTION .....</b>	<b>1</b>
1.1. <i>Chlamydia trachomatis</i> Infection and Disease .....	1
1.2. Immune Responses to <i>C. trachomatis</i> Infection.....	3
1.3. The <i>C. trachomatis</i> Developmental Cycle .....	10
1.4. <i>C. trachomatis</i> Type III Secretion System .....	12
1.5. Slc1 Chaperoned T3SS Effectors and Their Role During Development .....	14
1.5.1. TarP .....	14
1.5.2. TepP .....	16
1.5.3. TmeA and TmeB.....	16
1.6. Actin Dynamics and Cytoskeletal Response to <i>C. trachomatis</i> Invasion .....	17
1.7. <i>Chlamydia</i> Genetics.....	19
1.8. Overall Hypothesis .....	21
<b>CHAPTER 2: METHODS .....</b>	<b>22</b>
2.1. Organisms.....	22
2.2. DNA Methods .....	25
2.2.1. Cloning.....	25
2.2.2. PCR Screening.....	31
2.2.3. Quantitative PCR Screening and RNA detection .....	31
2.3. Genetic manipulation of chlamydiae.....	32
2.4. <i>Chlamydia</i> Fitness Models .....	33
2.4.1. Direct IFU Counts.....	33
2.4.2. Progeny IFU Enumeration .....	34
2.4.3. Genome Quantity over Multiple Passages and Penicillin Sensitivity Assay..	34
2.4.4. Quantifying Inclusion Area.....	35
2.5. Immunoblotting .....	35
2.6. Plaque Assay .....	38

2.7. Rifampin Resistance Co-infections .....	38
2.8. Microscopy .....	39
2.8.1. <i>E. coli</i> Colonies .....	39
2.8.2. N-WASP Localization .....	39
2.9. Percent Invasion Assay.....	40
2.10. Inhibitor Assays.....	40
2.10.1. Percent Invasion.....	40
2.10.2. Percent IFU Recovery.....	41
2.11. BirA Biotinylation .....	41
2.12. Apex Biotinylation .....	42
2.13. Mass Spectrometry Based Protein Identification .....	42
2.14. FLAG-Tag Immunoprecipitations.....	43
2.15. Pyrene Assay .....	44
2.16. 2D Gels.....	44
2.17. Mouse Infections .....	45
2.18. Statistical Analysis .....	46
2.19. Image Creation .....	46
<b>CHAPTER 3: Floxed-Cassette Allelic Exchange Mutagenesis Enables Markerless Gene Deletion in <i>Chlamydia trachomatis</i> and Can Reverse Cassette-Induced Polar Effects.....</b>	<b>47</b>
3.1. Summary.....	47
3.2. Introduction .....	48
3.3. Results .....	50
3.4. Discussion.....	61
<b>CHAPTER 4: Non-physiological Levels of TmeB Impacts Intracellular <i>C. trachomatis</i> Development.....</b>	<b>65</b>
4.1. Summary.....	65
4.2. Introduction: .....	66
4.3. Results: .....	67
4.4. Discussion.....	82
<b>CHAPTER 5: <i>Chlamydia trachomatis</i> TmeA Directly Activates N-WASP to Promote Actin Polymerization and Functions Synergistically with TarP during Invasion ....</b>	<b>88</b>

5.1. Summary.....	88
5.2. Introduction .....	89
5.3. Results .....	92
5.4. Discussion.....	110
<b>CHAPTER 6: <i>Chlamydia trachomatis</i> TmeB Functions Antagonistically to TmeA and Inhibits Arp2/3-Mediated Actin Polymerization.....</b>	<b>118</b>
6.1. Summary.....	118
6.2. Introduction .....	119
6.3. Results .....	120
6.4. Discussion.....	131
<b>CHAPTER 7: Summary and Future Directions.....</b>	<b>135</b>
<b>APPENDICES.....</b>	<b>154</b>
APPENDIX 1. List of Abbreviations .....	154
APPENDIX 2. Complete List of Materials .....	156
APPENDIX 3. Detailed Protocols.....	161
3.1. Direct IFU Counts.....	161
3.2. Progeny IFU Enumeration.....	163
3.3. Quantifying Genomes over Multiple Passages and Penicillin Sensitivity Assay .....	164
3.4. 2D Gels .....	166
3.5. Percent Invasion Assay .....	170
3.6. N-WASP Localization .....	172
3.7. Nucleofection.....	174
3.8. Apex Biotinylation.....	175
3.9. FLAG-Tag Immunoprecipitations .....	178
3.9. Plaque Assay .....	180
APPENDIX 4. Loss of TmeA and Tarp Does Not Indirectly Impact Invasion via Effects on TepP or TmeB .....	182
APPENDIX 5. Cis Complementation of TmeA.....	183
APPENDIX 6. Complementation of Mutants Restores Invasion Efficiency and WT Sensitivity to the Respective Inhibitors.....	184
<b>REFERENCES.....</b>	<b>185</b>
<b>VITA.....</b>	<b>229</b>

## LIST OF TABLES

<b>Table 1:</b> <i>C. trachomatis</i> Strains .....	24
<b>Table 2:</b> Oligonucleotide Primer Sets .....	26
<b>Table 3:</b> List of Antibodies Used .....	36
<b>Table 4:</b> MS Identification of Host Proteins Uniquely Proximal to TmeA-BirA .....	98
<b>Table 5:</b> Selected Enriched Gene Ontology (GO) Molecular Functions Identified Among Host Proteins Targeted by TmeA-BirA .....	101

## LIST OF FIGURES

<b>Figure 1:</b> Vector maps and mutagenesis strategy. ....	51
<b>Figure 2.</b> Cre recombinase excises a fluorescence cassette in <i>E. coli</i> . ....	52
<b>Figure 3.</b> Cre is expressed in <i>Chlamydia</i> spp. and does not impact development. ....	54
<b>Figure 4.</b> Construction of a markerless <i>C. trachomatis tmeA</i> mutant. ....	56
<b>Figure 5.</b> Direct evidence of <i>gfp-bla</i> excision. ....	58
<b>Figure 6.</b> Removal of the reporter cassette relieves polar effects on <i>tmeB</i> . ....	60
<b>Figure 7.</b> Rif resistance does not negatively affect <i>C. trachomatis</i> L2 development. ....	68
<b>Figure 8.</b> <i>C. trachomatis</i> L2 $\Delta tmeA-lx$ manifests a developmental defect in tissue culture. ....	70
<b>Figure 9.</b> <i>C. trachomatis</i> L2 $\Delta tmeA-lx$ manifests a greater developmental defect in tissue culture as compared to $\Delta tmeA$ . ....	72
<b>Figure 10.</b> Overexpression of <i>tmeB</i> negatively impacts <i>C. trachomatis</i> L2 development. ....	73
<b>Figure 11.</b> Increased TmeB levels negatively impact <i>C. trachomatis</i> L2 invasion. ....	75
<b>Figure 12.</b> <i>C. trachomatis</i> L2 $\Delta tmeB$ form larger plaques compared to WT. ....	77
<b>Figure 13.</b> <i>C. trachomatis</i> L2 WT <sup>Rif</sup> outcompetes WT+pTmeB compared to WT. ....	78
<b>Figure 14.</b> <i>C. trachomatis</i> L2 lacking both <i>tmeA</i> and <i>tmeB</i> are not deficient in producing infectious progeny. ....	80
<b>Figure 15.</b> <i>C. trachomatis</i> L2 strains lacking both TmeA and TmeB or over-expressing TmeA and TmeB produce fewer progeny genomes over multiple passages than WT. ....	81
<b>Figure 16.</b> Conformation of <i>tarp tmeA</i> double deletion mutant. ....	94
<b>Figure 17.</b> <i>C. trachomatis</i> lacking <i>tmeA</i> and <i>tarp</i> are attenuated during development. ....	95
<b>Figure 18.</b> Detection of biotinylated host proteins via immunoblot. ....	100
<b>Figure 19.</b> A TmeA-APEX fusion is functional when expressed in <i>C. trachomatis</i> and biotinylates proximal proteins. ....	102
<b>Figure 20.</b> TmeA interacts with N-WASP, and TmeA is required for N-WASP recruitment to sites of invading EBs. ....	105
<b>Figure 21.</b> <i>C. trachomatis</i> $\Delta tmeA-lx$ is less susceptible to Cdc42 and N-WASP inhibition, whereas $\Delta tarp$ is less susceptible to Rac1 inhibition compared to WT. ....	107
<b>Figure 22.</b> TmeA activates N-WASP-Arp2/3-dependent actin polymerization, and rates are further enhanced in the presence of TarP. ....	109
<b>Figure 23.</b> Proposed model of <i>C. trachomatis</i> TmeA and TarP of Arp2/3-mediated actin polymerization. ....	111
<b>Figure 24.</b> Levels of phosphorylated cofilin are decreased in the absence of TmeB. ...	122
<b>Figure 25.</b> <i>C. trachomatis</i> WT+pTmeB is more susceptible than WT to actin, Rac1, and N-WASP inhibition, but not Arp2/3 inhibition. ....	124
<b>Figure 26.</b> FLAG-tagged TmeB precipitates with the Arp2/3 complex. ....	126
<b>Figure 27.</b> TmeB decreases the rate of N-WASP-Arp2/3-dependent actin polymerization. ....	128
<b>Figure 28.</b> <i>C. trachomatis</i> WT+pTmeB form smaller inclusions than WT. ....	130

<b>Figure 29.</b> <i>C. trachomatis</i> L2 <i>tmeB</i> mutant strains in a murine model. ....	131
<b>Figure 30.</b> A schematic representation of the possible relationships between TmeA and TarP.....	143
<b>Figure 31.</b> Proposed model of <i>C. trachomatis</i> effectors TmeA, TmeB, TarP, and TepP interacting with host actin signaling pathways. ....	152
<b>Figure 32.</b> Proposed model of potential roles of <i>C. trachomatis</i> TmeA and TmeB during early, mid, and late chlamydial development. ....	153

## CHAPTER 1. INTRODUCTION

### 1.1. *Chlamydia trachomatis* Infection and Disease

*Chlamydia trachomatis* is an obligate intracellular bacterial pathogen that represents a significant burden to human health. *C. trachomatis* belongs to the family *Chlamydiaceae*, which are diverse in their ability to infect eukaryotic hosts ranging from amoebas to humans (1, 2). Three species in the *Chlamydia* genus are known to cause human disease: *C. trachomatis*, *C. pneumoniae*, and *C. psittaci*. The species *C. trachomatis* contains strains that cause ocular infections and strains that cause genital tract infections (3-5). *Chlamydia pneumoniae* causes infection of the upper respiratory tract and is responsible for 10-20% of adult community-acquired pneumonia (6). *Chlamydia psittaci* is a zoonotic infection spread by birds and causes acute respiratory pneumonia which can be fatal with animal handlers being the most commonly infected (7). *C. trachomatis* is most significant to human health as it continues to be the most common bacterial sexually transmitted infection (STI) in the US, with over 1.7 million cases in 2018 (8), and it is costly to treat (9).

*C. trachomatis* preferentially infects columnar epithelial cells and includes 15 different serovars. The serovars are defined by antibody reactivity to four variable domains of the major outer-membrane protein (MOMP) and correlate with tissue specificity during infection (10, 11). Serovars A-C are associated with ocular infections and blinding trachoma, a leading cause of infectious blindness in third-world countries (12). Serovars D-K infect the genitals and are a primary cause of sexually transmitted disease (STD),

along with serovars L1-L3 which are more invasive and traffic to local lymph nodes and cause lymphogranuloma venereum (LGV).

The prevalence and disease severity of sexually transmitted *C. trachomatis* highlights this organism as an important human pathogen. The actual number of yearly infections likely exceeds 3 million because nearly 80% of sexually transmitted infections are asymptomatic (13). Ages 15-24 are the most likely to become infected, and disease outcomes are more severe for women than men, especially women of color (8, 14). Cervical ectopy, where columnar epithelium from the inner cervical canal extends onto the cervix's external surface, is common in young women and is susceptible to damage during intercourse. Damage to this tissue increases vulnerability to *C. trachomatis* infection. From the lower genital tract, the infection can ascend into the upper genital tract (UGT), including the uterus and fallopian tubes. Additionally, *C. trachomatis* genital infection is associated with increased susceptibility and transmission of other STIs, such as HIV (15, 16).

Host, environmental, and bacterial virulence factors all determine the severity of disease sequelae. Only 44.7% of asymptomatic and untreated women clear the infection within one year (17). Failure to clear the infection and repeated exposure can result in pelvic inflammatory disease (PID), fallopian tube scarring, infertility, and ectopic pregnancy. Even women who have no infection symptoms, such as painful urination, vaginal discharge, and pelvic pain, can develop tubal factor infertility without any history of PID (18). Disease pathologies spur from tissue injury during the host immune response to the infection (19).

Physicians treat diagnosed infections with antibiotics such as doxycycline and azithromycin; however, an efficacious vaccine is not yet on the market. Vaccine development has been challenged by inadequate protective immunity and increased pathology (reviewed in (20, 21)). In 2019, the first phase 1 clinical trial was completed for a *C. trachomatis* vaccine candidate. Researchers found that the vaccine was safe and immunogenic, yet more testing is required (22). The high incidence of asymptomatic infections makes the timely administration of antibiotics challenging to prevent disease pathologies; thus, an effective vaccine is essential. Although the disease consequences of infection are well characterized, the *Chlamydia*-induced mechanisms by which they occur are not fully understood and represent an important research area.

## **1.2. Immune Responses to *C. trachomatis* Infection.**

*Chlamydia* spp. maintain a finely tuned relationship with their host to avoid immune recognition and clearance. Careful regulation of the immune response by the host is essential for disease outcomes since excessive inflammation can increase tissue damage and scarring in the fallopian tubes (23). The physical consequence of scarring in the fallopian tubes may lead to tubal occlusion and infertility. *C. trachomatis* infection also induces the loss of microvilli and cilia from the ciliated epithelial cells within the fallopian tubes, which play a part in fertility (24). Disease outcomes depend on many factors, including chlamydial antigens, cytokine profile, HLA subtypes, host genetic factors, and infectious load.

Innate and adaptive immune responses are both elicited during *C. trachomatis* infection where innate immunity contributes to limiting ascension and adaptive immunity contributes to clearance of the infection. Infected epithelial cells initiate inflammation by producing multiple cytokines such as tumor necrosis factor- $\alpha$  (TNF- $\alpha$ ), granulocyte macrophage-colony stimulating factor (GM-CSF), interleukin (IL)-1, IL-6, and IL-8 (25). IL-8 attracts leukocytes such as neutrophils, macrophages, dendritic cells (DCs), T-cells, and natural killer (NK) cells to the site of infection (26). The ability of polymorphonuclear cells (PMNs) to eliminate *Chlamydia* is species-specific because *C. pneumoniae*, for example, can replicate inside PMNs instead of being killed (27). Macrophages contribute to controlling infections by phagocytosing extracellular *Chlamydia* and produce IFN- $\gamma$  (49, 50). Macrophages, along with DCs, also recruit NK cells, B cells, and T cells to the infected area (49). Due to ethical limitations in collecting human tissue samples, mouse models are commonly used to study the inflammatory response during infection. In mice, the infiltration of neutrophils and, to a lesser extent, monocytes occurs within 1-2 days, however innate immunity is not sufficient for chlamydial clearance (28-30).

Interferon- $\gamma$  (IFN- $\gamma$ ) producing CD4<sup>+</sup> Th1 cells are the prominent cell type involved in the clearance of *Chlamydia* infection and aid in preventing accession into the UGT. IFN- $\gamma$  can activate infected cells to produce the tryptophan-catabolizing enzyme, indoleamine 2,3-dioxygenase (IDO). *Chlamydia* require tryptophan for survival; thus, IFN- $\gamma$ -activated IDO production limits intracellular growth (31). Interestingly, *C. trachomatis* strains isolated from human urogenital tracts have been shown to synthesize tryptophan from indole. The microbiota of the genital tract produce indole, which may provide *C. trachomatis* a way to circumvent the inhibitory effects of IFN- $\gamma$  (32, 33); however, HIV-

positive women, with decreased CD4<sup>+</sup> T cell counts, have an increased risk for developing *Chlamydia*-related PID (34).

TNF- $\alpha$  is also a key factor in controlling infection. Recombinant TNF- $\alpha$  alone inhibits *C. trachomatis* growth in cell culture (35). The potency of TNF- $\alpha$  growth inhibition is synergistic with IFN- $\gamma$  and increases 100-fold (35). This effect may be due to an enhanced mechanism for tryptophan depletion (36). One study examining mononuclear cells from *Chlamydia*-infected women found that the predominant Th-1 associated cytokine response was T cell derived TNF- $\alpha$  and not IFN- $\gamma$  (37).

CD8<sup>+</sup> T cells have also been observed at the infection site in non-human primate models, although their specific role has not been well defined (38). Gene knockout studies have shown that CD4<sup>+</sup> T cells play a more prominent role in controlling infection and that CD8<sup>+</sup> T cell-deficient mice do not have altered disease outcomes in response to infection (39, 40). Antibody-producing B-cells can inactivate extracellular *Chlamydia*; although, the presence of *Chlamydia*-specific antibodies during reinfection does not correlate with increased infection resolution and instead correlates with increased morbidity (41, 42).

Toll-like receptors (TLRs) recognize a variety of pathogen-associated molecular patterns (PAMPs). TLR4 is a primary signal transducer in response to LPS, and TLR2 detects a variety of ligands, including bacterial lipoproteins, lipopeptides, and peptidoglycan. TLR2 is the most significant TRL during *Chlamydia* infection while TLR4 may play a lesser role. Chlamydial LPS is structurally different from many enteric gram-negative bacteria since it lacks an extended oligosaccharide chain, has five instead of six fatty acid chains, and has 100-fold lower endotoxic activity compared to *Escherichia coli* or *Neisseria gonorrhoeae* (43-45); however, it does appear to bind TLR4 for signaling

activity and TNF stimulation (46). Compared to TLR4, TLR2 appears to have a more predominant role during infection. Along with MyD88, a TLR adapter protein for nuclear factor kappa-light-chain enhanced of activated B cells (NF- $\kappa$ B) activation, TLR2 localizes to the inclusion membrane, where it likely engages in active signaling during chlamydial development (47). TLR2 also stimulates proinflammatory cytokines during infection like TNF- $\alpha$ , IL-1beta, IL-6, and IL-8 (47, 48). In mouse models, TLR2-deficient mice did not develop oviduct pathology after chlamydial infection. TLR4-deficient mice did not manifest changes in susceptibility to *C. muridarum* infection in terms of duration of infection and pathology. Thus, TLR2, but not TLR4, is involved in disease progression (48).

A chlamydial lipoprotein macrophage infectivity potentiator (MIP) has also been shown to stimulate TLR2/TLR6 and CD14 induction of proinflammatory cytokines (49). These studies used a recombinant MIP due to the lack of a chlamydial mutant; thus, further exploration is still required. TLR3 has more recently been shown to contribute to IFN- $\beta$  response in *Chlamydia*-infected oviduct epithelial cells; however, these studies did not investigate disease in TLR3 knockout mice (50). TLR3 is known to recognize viral double-stranded RNA to induce an IFN- $\beta$  response and is located within intracellular compartments of dendritic cells or on the surface of fibroblasts (51). The chlamydial ligand for TLR3 has not been determined.

Nucleotide oligomerization domain (NOD) proteins also recognize intracellular pathogens by sensing peptidoglycan to initiate inflammatory responses. Muramic acid, the major component of peptidoglycan, has not been found in *Chlamydia* spp.; however, *Chlamydia* contain the genes encoding peptidoglycan precursors (52). NOD-deficient

fibroblasts had significantly reduced NF- $\kappa$ B activation after chlamydial infection suggesting a role in inflammation; however, NOD1-deficient mice showed no difference in cytokine production as compared to WT mice. Therefore, NOD1-mediated recognition of *Chlamydia* likely plays a minor role (53).

Two models describe the progression of immunopathology: the “immunological and cellular” paradigms (23). The “immunological paradigm” explains the importance of antigen-specific adaptive immune responses. The chlamydial heat shock protein 60 (HSP60) and other antigens may have a high degree of homology to human proteins. *C. trachomatis* continually stimulates anti-chlamydial immune responses by repeated exposure and may cause delayed-type hypersensitivity or autoimmunity through molecular mimicry (reviewed in (54)). The “cellular paradigm” of chlamydial pathogenesis describes the host response to *Chlamydia* as initiated and sustained by infected epithelial cells (19). Intracellular infection leads to prolonged cytokine responses and low-level immune stimulation. The “cellular paradigm” underscores the importance of understanding the factors governing *C. trachomatis* intracellular survival.

Chronic immune stimulation in response to *C. trachomatis* promotes tissue injury and fibrosis through host proteins such as Caspase-1 and matrix metalloproteinase (MMP-9). When activated, Caspase-1 is an enzyme that cleaves pro-IL-1 $\beta$  to form mature IL-1 $\beta$ , a potent proinflammatory cytokine that activates neutrophils, monocytes, and macrophages while inducing Th1 and Th17 responses (reviewed in (55)). In the absence of infiltrating leukocytes, IL-1 $\beta$  and IL-1 receptor synthesis was upregulated in epithelial cells after *C. trachomatis* infection and resulted in the destruction of fallopian tubes in an *ex vivo* model (56). These data support the “cellular paradigm” model where epithelial cells are the

primary drivers of pathology; however, a complete mechanism by which fallopian tube damage occurs remains unresolved. MMPs produced by neutrophils (57) also significantly contribute to *Chlamydia*-induced tubal factor infertility. MMPs are endopeptidases and are involved in various processes like skeletal growth and remodeling, wound healing, and cancer. MMPs can degrade the basement membranes of tissues and extracellular matrix components like collagen I and collagen IV, and they play a role in several inflammatory and fibrotic diseases (58). MMPs have been identified in *Chlamydia*-infected fallopian tube organ cultures (59) and are linked to oviduct fibrosis and scarring (MMP-2) (60).

Not all women develop scarring in the reproductive tract after *C. trachomatis* genital infection, so there are likely multiple genetic host factors that influence disease outcomes. For example, variation in the expression of IL-10 and IFN- $\gamma$  genes are associated with the intensity of lymphocyte proliferation during the immune response (23) and influence *Chlamydia*-infected women's chances of fallopian tube damage (38, 61).

Chronic *C. trachomatis* infections are common and result from repeated exposure or persistence after failure to resolve the infection without treatment (62-64). With a dependence on intracellular development and a long evolution with eukaryotic hosts, it is not surprising that *C. trachomatis* have established multiple strategies to avoid immune clearance. For example, *C. trachomatis* are largely resistant to the membrane attack complex/Perforin (MACPF)-domain proteins (reviewed in (65)). The MACPF-containing host proteins Perforin-2 and Complement C9 represent innate immune effectors and act by killing microbes via the polymerization of MACPF proteins to form a membrane-spanning pore (66, 67). Complement is a central defense mechanism of the innate immune response and culminates in a C9-mediated pore. During chlamydial infection, complement is

activated via the antibody-independent alternative pathway; however, *Chlamydia* are resistant to C9 attack. Multiple studies have shown that infectious *Chlamydia* particles incubated with normal human serum fail to establish an intracellular niche, yet late complement factors C5-C9 are dispensable (68-72). Current hypotheses suggest the anaphylatoxin activities of C5a and C3a are responsible for the complement-dependent effects on infectivity *in vivo*. *Chlamydia* are also resistant to NK cell- and cytotoxic CD8<sup>+</sup> T cell-derived perforin (73, 74). Perforin knockout mice are not compromised in their ability to clear infection (75, 76); however, NK cells promote infection clearance. Their role is likely to through IFN-  $\gamma$  production (77).

Unlike perforin-1 and C9 MACPF-domain proteins, *Chlamydia* are conditionally susceptible to perforin-2, which is trafficked to bacteria-containing vacuoles within the cell (66, 78). Perforin-2 is ubiquitously expressed in professional phagocytes, like macrophages, where *Chlamydia* are susceptible to perforin-2-mediated killing. However, *Chlamydia* induce perforin-2 downregulation in infected epithelial cells and subvert perforin-2-mediated attack (79).

Overall, once the infection is cleared and the inflammatory responses subside, the result can be chronic scarring, contributing to infertility. IFN-  $\gamma$  producing CD4<sup>+</sup> T cells are the central mechanism of infection control by hosts, and *Chlamydia* have many strategies to counter immune recognition. Furthermore, the inflammatory response and harmful disease sequela are initiated by infection of epithelial cells. Because immunoreactivity associated with reinfection and vaccines often makes pathology worse, it is essential to understand how *Chlamydia* invade and survive within epithelial cells and the mechanisms used to trigger or suppress host cell immune responses.

### 1.3. The *C. trachomatis* Developmental Cycle

All *Chlamydia* spp. have a biphasic developmental cycle consisting of two bacterial forms, and establish an intracellular membrane-bound vacuole, termed an inclusion, for survival. Elementary bodies (EBs) are the infectious developmental form and are referred to as spore-like for their small size (approximately  $0.03 \mu\text{m}^3$ ) and rigid cell wall (80). EBs are highly resistant to mechanical and osmotic pressures due to the network of disulfide-linked proteins in their membrane (81). EBs are minimally metabolically active (82), and the 1 MB chlamydial genome is tightly compacted (viewed by electron microscopy (80)).

Invasion of non-phagocytic epithelial cells occurs rapidly following EB attachment. Low-affinity interactions are established between host heparan sulfate proteoglycans and chlamydial outer membrane proteins like MOMP, OmcA, and OmcB (83). Next, high-affinity interactions occur with host receptors, such as  $\beta 1$  integrin (84), epidermal growth factor receptor (EGFR) (85), ephrin receptor A2 (EPHA2) (86), and a protein complex that includes protein disulfide isomerase (PDI) (87). Actin is rapidly recruited to the site of EB attachment, and the host cytoskeleton is remodeled to engulf the adherent EB. The EB-containing inclusion pinches off into the cytoplasm through a process resembling macropinocytosis (88). The newly formed inclusion quickly dissociates from the canonical endosomal pathway to avoid lysosomal fusion. The established inclusion membrane lacks all major endolysosomal markers and the lumen of the inclusion does not acidify (89). The inclusion provides a protective niche for the bacteria and is impermeable to molecules larger than 520 Da by simple diffusion (90). Once the inclusion is established, EBs differentiate into metabolically active, non-infectious, reticulate bodies (RBs).

RBs have reduced disulfide linkages in their cell wall and are nearly 33 times the size of EBs ( $RB \approx 1 \mu\text{m}^3$ ) (80). RBs begin to divide 9-12 hours post-infection (hpi). A single RB will replicate to produce approximately 1000 progeny bacteria (80). In a process that requires chlamydial transcription and translation, the inclusion migrates to a peri-Golgi region within 6 hours of infection (91-93). The inclusion migrates in the minus direction along microtubules by interacting with the microtubule motor protein, dynein (94). During development, *Chlamydia* intercept and fuse with vesicles trafficking from the Golgi apparatus containing nutrients and structural molecules like sphingomyelin and cholesterol (95). Along with inclusion migration, fusion with trafficking vesicles requires chlamydial protein synthesis, indicating *Chlamydia* actively orchestrates these events (89).

About 20 hpi, RBs asynchronously differentiate back to the infectious EB form for subsequent rounds of infection. The signal for differentiation is not well understood, yet multiple hypotheses exist. There is evidence to support that the conversion signal is size-dependent (80) and that it depends on the interaction between the RB and the inclusion membrane (96-98); however, it is unclear if RB detachment from the inclusion membrane is the signal for RB-EB differentiation or a result.

Once redifferentiation occurs, progeny EBs exit the host cell using the lysis or extrusion pathway (99). For *C. trachomatis* L2, host cell exit occurs between 44 - 48 hpi. The lysis pathway is described by rupturing the inclusion membrane, other intracellular compartments, and then the host plasma membrane, which is dependent upon intracellular calcium levels (99). Membrane permeabilizations are strongly associated with cysteine proteases secreted by *Chlamydia* (99). Once the inclusion and host cell membranes lyse, infectious EBs are released into the extracellular space and diffuse to nearby cells. The

extrusion pathway differs from the lysis pathway in that neither the inclusion nor host cell lyse. Extrusion is a packaged release mechanism that resembles exocytosis. The whole or partial inclusion buds off from the host cell leaving the inclusion intact. The extrusion pathway requires actin polymerization, neural Wiskott-Aldrich syndrome protein (N-WASP), Myosin II, and Rho GTPases (99).

#### **1.4. *C. trachomatis* Type III Secretion System**

*Chlamydia* spp. orchestrate changes in host cell biology to create and maintain a productive growth environment. Major affected pathways include the host cytoskeleton, vesicle trafficking, cell survival, and immune signaling (reviewed in (100)). Like other Gram-negative pathogens (101), *Chlamydia* spp. express a type III secretion system (T3SS) that translocates effector proteins (T3SE) directly into the host cell cytosol (reviewed in (100)). EBs are decorated with fully assembled T3SSs; however, the T3SS is highly crosslinked and inactive until contact with the host cell surface (reviewed in (102)). Contact-dependent T3SS activity occurs as early as EB attachment and continues throughout development (103, 104).

All sequenced *Chlamydiaceae* genomes contain highly conserved genes encoding the secretion system (105-108). There are four major components of the secretion system: the membrane-associated basal apparatus; the needle and tip complex, which span the space between the bacterial and host membranes; the secreted translocon proteins that form a membrane-spanning pore in the host membrane; and ancillary components, which include chaperones and regulatory factors (reviewed in (102)).

The needle-like apparatus is anchored in the bacterial cell wall. The basal apparatus of the T3SS is structurally related to flagella but is functionally distinct (109). The injectosome, basal apparatus, and translocon are made of 20-25 different proteins. Chaperone proteins are required to facilitate the targeting of effectors to the T3SS, prevent premature folding, and regulate secretion timing (110, 111). Surrogate T3SSs and protein localization studies have previously been leveraged to identify an additional pool of chlamydial effectors that are translocated beyond the inclusion membrane and target host proteins within the cytoplasm or organelles (reviewed in (100)). The total number of T3S substrates likely exceeds 60 effectors, yet most of these proteins' functional role remains an open question (102).

Effectors that intercalate into the inclusion membrane, integral membrane proteins (Incs), represent the most thoroughly characterized group of chlamydial T3SEs. Incs aid in intercepting trafficking vesicles from the exocytic pathway (112), multivesicular bodies (113), and lipid droplets (114) for nutrient acquisition. For example, Inca is a SNARE-like protein that facilitates homotypic vesicle fusion (115).

*C. trachomatis* also encodes type II and type V secretion systems. Type II secretion in *Chlamydia* is a two-step process where proteins are transported across the inner membrane, using the Sec system, and into the periplasmic space, then are secreted through the outer membrane. The *Chlamydia* protease-like activity factor (CPAF) may be secreted via type II secretion (100). Type V secretion proteins are autotransporters. The POMP family proteins are suspected to be secreted via this pathway (116). All three secretion methods contribute to *C. trachomatis* survival.

## 1.5. Slc1 Chaperoned T3SS Effectors and Their Role During Development

Slc1 is a T3S chaperone that facilitates the secretion of effectors from *Chlamydia*. Slc1 (SycE-like chaperone) is named for its structural similarity to SycE in *Yersinia enterocolitica* (117). In *C. trachomatis*, Slc1 chaperones a family of effectors, including the translocated actin recruiting phosphoprotein (TarP), the translocated early phosphoprotein (TepP), and the translocated membrane-associated effectors A and B (111, 117). All four effectors are expressed late-cycle by RBs and are packaged into infectious EBs for secretion during invasion (118).

### 1.5.1. TarP

TarP was the first effector discovered to be deployed during invasion (119). Now, TarP is well-established as an effector that spatially and temporally recruits actin to the site of invading EBs (reviewed in (120)). TarP is a multi-domain protein containing: a tyrosine-rich N-terminal repeat domain, a proline-rich domain, one G-actin binding domain, two C-terminal F-actin binding domains (121), and domains impacting the dynamics of focal adhesions (122). Once secreted, TarP is immediately phosphorylated at tyrosine residues by src family tyrosine kinases and others, such as Abl and Syk kinases (123-125). Although all pathogenic *Chlamydia* spp contain a TarP ortholog, only *C. trachomatis* TarP contains a tyrosine-rich repeat domain which is phosphorylated after secretion (126). It is predicted that phosphorylated TarP acts as a scaffolding protein where multiple host signaling proteins containing Src homology 2 (SH2) domains can localize. For example, *in vitro* TarP has been shown to bind the E3 ligase Cbl; the Rac1 exchange factor Vav2; the p85

regulatory subunit of phosphoinositide 3-kinase (PI3K); and the signaling adaptors Shc1, Nck2, and CrkL (127).

GEF-TarP interactions stimulate Rac1-dependent signaling for actin reorganization (119, 128). Rac1-dependent activation of WAVE2 and Abi1 during chlamydial invasion leads to downstream activation of the Arp2/3 complex, a key player in actin polymerization dynamics (129, 130). At least two models of TarP mediated Rac activation exist. One study suggests that phosphorylated TarP, through the Src-homology 2 domain (Sb), directly or indirectly activates the Sos1/Eps8/Abi1 complex and Vav2, two Rac activating GEFs (128). Alternatively, the p85 subunit of PI3K is also recruited to the Sb domain of phosphorylated TarP and activated to produce phosphatidylinositol-3,4,5-triphosphate [PI(3,4,5)P3], which subsequently may activate Vav2. The redundancy of GEF activation may represent multiple mechanisms to promote Rac activation with variable levels of PI(3,4,5)P3 availability (128).

Independent of phosphorylation, TarP can also directly nucleate and bundle actin through its G-actin and F-actin domains, respectively (121, 131). When treated with PP2, a kinase inhibitor, TarP phosphorylation was reduced to levels below detection; however, Chlamydial invasion was not reduced, indicating that TarP phosphorylation is not essential for invasion (123). *C. trachomatis* strains containing *tarp* gene deletions are significantly inhibited during invasion, highlighting TarP as a critical invasion-related effector (132). TarP may also be important for promoting host cell survival since the Sb domain of TarP interacts with SHC1, which is important for preventing early apoptosis (127)

### 1.5.2. TepP

TepP is one of the most abundant effector proteins found within EBs (118) and is secreted during EB invasion. After secretion, TepP is phosphorylated by host kinases at tyrosine and serine residues, yet phosphorylation occurs later than TarP (111). Similar to TarP, TepP also contains binding domains for SH2-containing proteins. For example, TepP engages both splice variants of Crk (Crk I/II), a signaling adapter protein, and is recruited to early inclusions in a TepP-dependent manner (111). Crk activation has been linked to Rac1-dependent cytoskeletal reorganization in other cell types where ITG $\beta$ 1 activation leads to Crk docking at the plasma membrane with DOCK180, a Rac1 specific activator (133, 134); however, the loss of TepP does not impact chlamydial invasion (135). Transcriptional comparison of epithelial cell responses to infection with TepP-deficient or TepP-overexpressing strains also revealed a role for TepP in the induction of type 1 interferon responses (111). TepP was also shown to colocalize with class I phosphoinositide 3-kinases (PI3K) and CrkL. TepP induces PI3K activation on the cytosolic face of the cell membrane and early inclusions to generate phosphoinositide-(3,4,5)-triphosphate (PIP3) without activating the canonical PI3K pathways at the plasma membrane (136). Taken together, TepP may function to regulate the innate immune response targeted at *Chlamydia* infection and may promote host cell survival

### 1.5.3. TmeA and TmeB

TmeA and TmeB (alternative names CT\_694 and CT\_695, respectively) are encoded within a bicistronic operon, are secreted during chlamydial invasion, and associate with the host plasma and inclusion membrane, respectively, later during infection (137-142). TmeA is 323 aa (uniprot accession number: O84700) and TmeB is 398 aa (uniprot

accession number: O84701). TmeA is essential for efficient chlamydial invasion; however, TmeB is dispensable for invasion (143). TmeA has been implicated in actin reorganization (137, 138) and has been shown to disrupt the actin-bundling activity of AHNAK, a large host scaffolding protein (143). A *C. trachomatis* strain harboring a *tmeA* gene deletion is defective for invasion (143) and displays a phenotype similar to a *tarp* null strain (132). The TmeA interaction with AHNAK is not required for invasion, and TmeA induces host cell morphology changes independent of the AHNAK binding domain (137). The molecular mechanism governing TmeA's activity is an open question. The function of TmeB is unknown.

### **1.6. Actin Dynamics and Cytoskeletal Response to *C. trachomatis* Invasion**

The actin cytoskeleton of eukaryotic cells is essential for maintaining cell morphology and is important for many cellular activities, including motility, division, endocytosis, and vesicular trafficking. Cellular actin includes two forms: monomeric globular actin (G-actin) and filamentous actin (F-actin). Actin structures are closely involved in microbial infection. The cortical actin network that resides beneath the plasma membrane and around intracellular organelles provides a physical barrier against invasive pathogens and endocytic vesicles, respectively (144). Invasive bacteria must overcome these barriers to gain entry and for intracellular transport. Furthermore, these barriers must also be circumvented for bacterial escape and spread.

The Rho-family proteins Rho, Rac, and Cdc42 are small G-proteins that act as molecular switches and regulate actin stress fiber, lamellipodia, and filopodia formation,

respectively, at the periphery of the cell (145). Actin cytoskeleton remodeling through Rho-family proteins is known to be a target of numerous extra- and intracellular bacteria to facilitate invasion of non-phagocytic cells (146), move within the cytosol or from cell to cell (147), and surround the phagocytic vacuole with a polymerized actin meshwork (148).

*C. trachomatis* appear to utilize redundant paths for entry into non-phagocytic cells employing facets of both the “zipper” and “trigger” mechanisms (146). The “zipper” mechanism entails bacterial adherence to cell surface receptors leading to receptor clustering, signaling, and phagocytic cup formation. EB binding to host surface receptors has been shown to initiate receptor clustering and downstream signaling events for actin remodeling (119, 126, 129, 149, 150). Examples include *C. trachomatis* CT017 binding to integrin  $\beta 1$  (ITG $\beta 1$ ) and *C. pneumoniae* Pmp21 binding to EGFR promoting host-cell invasion (84, 85). EGFR phosphorylation is increased during *C. trachomatis* infection, is required for intracellular development, and re-localizes to the periphery of the inclusion; however, no direct interactions between EGFR and *C. trachomatis* outer membrane proteins have been identified (151).

*C. trachomatis* entry also resembles the “trigger” mechanism where bacterial effector proteins are secreted through the T3SS and directly manipulate actin signaling (119, 121, 138). Examples of this are the T3SEs TarP, which promotes RAS-related C3 botulinum toxin substrate 1 (Rac1) activation and directly nucleates actin, and TmeA, which inhibits the actin-bundling activity of AHNAK. Beyond invasion, the actin-based cytoskeleton maintains inclusion integrity during intracellular development (152) and host cell exit by exocytosis (99).

In either case, actin is rapidly recruited to the chlamydial attachment site (120), and *in vitro* studies demonstrate that *C. trachomatis* invasion is impaired when actin polymerization or depolymerization are disrupted with either cytochalasin D or Jasplankinolide, respectively (reviewed in (120)). Prominent host factors, including the Rac1, Wiskott-Aldrich syndrome protein family member 2 (WAVE2), and the Arp2/3 complex, are all vital during *C. trachomatis* internalization (reviewed in (120)).

### **1.7. *Chlamydia* Genetics.**

Due to genetic intractability, it was historically difficult to provide definitive evidence regarding how chlamydial gene products contribute to development and pathogenesis; however, the acquisition of tools to genetically manipulate chlamydiae now offers more efficient opportunities to reveal aspects of infection biology (153-155). Unlike *E. coli*, many classical cloning techniques do not apply to *Chlamydia*. A few significant limitations involve transformation efficiency, lack of counterselection reporters, and plasmid maintenance. *E. coli* plasmids can generally be maintained indefinitely with an origin of replication and appropriate selective pressure; however, *C. trachomatis* plasmids require an additional eight open reading frames (*pgp1-8*) for maintenance that are found on the native pL2 plasmid within the L2 serovar (156-158).

Early genetic advances relied on forward and reverse genetic mutagenesis approaches to associate genes with particular phenotypes. The ability to coinfect chlamydial strains for DNA exchange via lateral gene transfer (LGT) was exploited for gene association studies in heavily chemically mutagenized genomes (159). There have

been multiple genetic tools generated that accommodate *Chlamydia*'s unique biology in recent years, yet there are still limitations (153-155). Chemical mutagenesis by ethyl methanesulfonate (EMS) treatment can introduce missense mutations or (less frequently) can result in nucleotide transitions introducing a premature stop codon to yield a nonsense mutation (160). Transposon insertion is efficient for gene disruption, but currently, this technology in *Chlamydia* research is laborious and time-consuming due to low transformation efficiency (161). Both EMS treatment and transposon mutagenesis techniques generate random mutations and require rigorous screening methods to isolate mutant strains. CaCl<sub>2</sub> chemical transformation of *C. trachomatis* (156) with exogenous plasmid DNA has led to the development of more targeted strategies, including the use of the TargeTron system (162) and fluorescence-reported allelic exchange mutagenesis (FRAEM) (163). TargeTron is a method to disrupt genes by insertion of group II introns; however, this method is limited by efficiency, and the insertion site requires trial and error (162). FRAEM is a strategy used for targeted gene deletion coupled with the insertion of a selection cassette providing antibiotic resistance and a fluorescence reporter (163). Ectopic expression of epitope-tagged gene products has also been employed to study effector localization and function (164-166). Most recently, the expression of enzymatically dead Cas9 was leveraged for conditional knockdown of targeted messages (167).

The FRAEM method was initially developed in the Fields' Lab (163) and utilizes the pSUMC 4.0 suicide vector, which can be conditionally maintained through the inducible expression of *pgp6*. Expression of *pgp6* has previously been shown to be necessary for plasmid retention and is therefore leveraged to control plasmid maintenance (163, 168). When *C. trachomatis* is grown in media supplemented with anhydrous

tetracycline (aTc) to induce *pgp6* expression, the vector is maintained. In the absence of aTc, the vector is lost. Targeted gene deletion is achieved through allelic exchange of the gene for the selection cassette. The 3 kb regions directly upstream and downstream of the targeted gene serve as homology arms for recombination. These arms are cloned into the pSUmC 4.0 vector flanking the selection cassette. Successful *C. trachomatis* transformation and recombination events are observed through fluorescence reporting. Expression of *mCherry* on the vector backbone and *gfp* within the selection cassette yield red and green fluorescent inclusions. Once aTc is removed from culture media, green-only inclusions indicate successful recombination events with the loss of the suicide vector and integration of the selection cassette into the bacterial genome.

## **1.8. Overall Hypothesis**

I hypothesize that the type III secreted effectors TmeA and TmeB are important for the formation and maintenance of the *C. trachomatis* inclusion and that they are functionally linked through similar host target proteins or pathways.

## CHAPTER 2: METHODS

A complete list of materials can be found in Appendix 2, and detailed protocols for selected methods can be found in Appendix 3.

### 2.1. Organisms

*C. trachomatis* serovar L2 (LGV 434) and derivative strains were used in these studies (Table 1). Chlamydiae were routinely maintained in either HeLa 229 epithelial cell monolayers (CCL-1.2; ATCC) or McCoy cell monolayers (CRL-1696; ATCC). Vero Cells (CCL-81; ATCC) were used in plaquing assays. Unless otherwise indicated, all cultures were grown in RPMI 1640 medium containing 2 mM L-glutamine (Life Technologies) supplemented with 10% (vol/vol) heat-inactivated fetal bovine serum (FBS; Sigma) at 37 °C in an environment with 5% CO<sub>2</sub> and 95% humidified air. For transformation and FRAEM protocols, chlamydiae were cultivated in the presence of 600 ng/mL penicillin G (PenG; Sigma), 500 µg/mL spectinomycin (Spec; AlfaAesar), and 1 µg/mL cycloheximide (Sigma), in addition to 50 ng/mL anhydrotetracycline (aTc) where appropriate. Rifampin (Rif)-resistant strains were generated as described previously (169) by cultivation for four passages in 2.5 ng/mL Rif, followed by four passages in 5 ng/mL Rif. Clonal isolates for all final *Chlamydia* strains were obtained as described by two sequential limiting dilution passages in 384-well plates (170). *Escherichia coli* NEB-10 (New England Biolabs) was utilized for cloning procedures and verification of Cre activity. An *E. coli* *dam*<sup>-</sup>/*dcm*<sup>-</sup> deletion mutant (New England Biolabs) was used as a host to generate unmethylated

plasmid DNA used to transform *Chlamydia* species. *E. coli* strains were routinely grown at 37 °C in Luria-Bertani broth (Amresco), or on LB agar plates supplemented with 50 µg/mL carbenicillin (Teknova) or 100 µg/mL spectinomycin (Alfa Aesar), as appropriate.

**Table 1: *C. trachomatis* Strains**

Strain Designation	Plasmid, Relevant genotype, Antibiotic Resistance	Reference or Source
<b>WT L2</b>		ATCC
<b>WT<sup>Rif</sup></b>	Rif <sup>r</sup>	This Study
<b>L2R</b>	pL2-	(171)
<b>WT+pSU-CRE</b>	<i>cre</i> <sup>+</sup> , <i>mCherry</i> <sup>+</sup> , Spec <sup>r</sup>	This Study
<b>WT<sup>Rif</sup>+pCompAII</b>	pL2-, <i>gfp</i> <sup>+</sup> , <i>mCherry</i> <sup>+</sup> , Rif <sup>r</sup> , Spec <sup>r</sup>	This Study
<b><math>\Delta</math>tmeA</b>	<i>tmeA</i> -, <i>gfp</i> <sup>+</sup> , Pen <sup>r</sup>	(163)
<b><math>\Delta</math>tmeA-lx-gfp-bla</b>	<i>tmeA</i> -, <i>loxP</i> <sup>+</sup> , <i>gfp</i> <sup>+</sup> , Rif <sup>r</sup> , Pen <sup>r</sup>	This Study
<b><math>\Delta</math>tmeA-lx</b>	<i>tmeA</i> -, <i>loxP</i> <sup>+</sup> , Rif <sup>r</sup>	This Study
<b>L2R<sup>Rif</sup> <math>\Delta</math>tmeA-lx</b>	pL2-, <i>tmeA</i> -, <i>loxP</i> <sup>+</sup> , Rif <sup>r</sup>	This Study
<b><math>\Delta</math>tmeA-lx+pCompAII</b>	pL2-, <i>tmeA</i> -, <i>loxP</i> <sup>+</sup> , <i>gfp</i> <sup>+</sup> , <i>mCherry</i> <sup>+</sup> ; Rif <sup>r</sup> , Spec <sup>r</sup>	This Study
<b><math>\Delta</math>tmeA-lx+pTmeA</b>	pL2-, <i>loxP</i> <sup>+</sup> , <i>mCherry</i> <sup>+</sup> ; Rif <sup>r</sup> , Spec <sup>r</sup>	This Study
<b><math>\Delta</math>tmeB</b>	<i>tmeB</i> -, <i>gfp</i> <sup>+</sup> , Pen <sup>r</sup>	(163)
<b><math>\Delta</math>tmeB+pTmeB</b>	pL2-, <i>gfp</i> <sup>+</sup> , <i>mCherry</i> <sup>+</sup> ; Pen <sup>r</sup> , Spec <sup>r</sup>	This Study
<b>WT+pTmeB</b>	pL2-, <i>mCherry</i> <sup>+</sup> , Spec <sup>r</sup>	This Study
<b>WT+pTmeA/TmeB</b>	pL2-, <i>mCherry</i> <sup>+</sup> , Spec <sup>r</sup>	This Study
<b><math>\Delta</math>tmeA/tmeB</b>	<i>tmeA</i> -, <i>tmeB</i> -, <i>gfp</i> <sup>+</sup> , Pen <sup>r</sup>	This Study
<b><math>\Delta</math>tarp</b>	<i>tarp</i> -, <i>gfp</i> <sup>+</sup> , Pen <sup>r</sup>	(132)
<b><math>\Delta</math>tmeA/tarp</b>	<i>tmeA</i> -, <i>tarp</i> -, <i>gfp</i> <sup>+</sup> , Pen <sup>r</sup>	This Study
<b>Cis-tmeA</b>	Spec <sup>r</sup>	This Study
<b>Cis-tmeB</b>	Spec <sup>r</sup>	This Study
<b><math>\Delta</math>tmeA-lx+pTmeA-APEX</b>	pL2-, <i>loxP</i> <sup>+</sup> , <i>APEX</i> <sup>+</sup> , Rif <sup>r</sup> , Spec <sup>r</sup>	This Study
<b><math>\Delta</math>tmeB+pTmeB-APEX</b>	pL2-, <i>loxP</i> <sup>+</sup> , <i>APEX</i> <sup>+</sup> , Rif <sup>r</sup> , Spec <sup>r</sup>	This Study
<b><math>\Delta</math>tmeB+pTmeB-FT</b>	pL2-, <i>tmeA</i> <sup>+</sup> , <i>tmeB</i> <sup>+</sup> ; Spec <sup>r</sup> , Pen <sup>r</sup>	This Study

\*pL2- refers to the absence of the endogenous *C. trachomatis* plasmid. The coding sequences for Pgp1 to -8 are present on the engineered plasmids pCompAII, pSU-CRE, pTmeA, and pTmeB.

## 2.2. DNA Methods

### 2.2.1. Cloning

All PCR-based amplifications for cloning were performed using Q5 high-fidelity DNA polymerase (New England Biolabs) from plasmid purified from *E. coli* using the Monarch plasmid miniprep kit (New England Biolabs). All primers were custom DNA oligonucleotides purchased from Integrated DNA Technologies (Table 2), and final constructs were confirmed by DNA sequencing of engineered regions (ACGT, Inc).

The allelic exchange plasmid pSU- $\Delta$ *tmeA-lox-gfp-bla* was generated by the addition of *loxP* sites flanking the *bla-gfp* cassette. Flanking *loxP* sites were added via insertion PCR (iPCR) by amplifying the previously described pUC18 $\Delta$ ctl0063 (163) using the *loxP*-*blagfp*-F and *loxP*-*blagfp*-R primers. DNA containing the floxed *gfp-bla* cassette flanked by chlamydial DNA 3 kb up- and downstream of the deleted *tmeA* sequence was amplified with HOMRR@pSUMC-F and HOMRR@pSUMC-R primers. The amplicon was then used in iPCR with pSUMC (163) to yield pSUMC-*tmeA-loxP*.

A plasmid for creating a double deletion of *tmeA* and *tmeB* in *C. trachomatis* was generated using pSUMC-4.0 with *loxP* sites as described above. The 5' and 3' homology regions of the *tmeA/tmeB* locus were amplified from WT L2 DNA using custom primers ctl0063-SalI-S, ctl0063-SalI-AS, ctl0064-SbfI-S, and ctl0064-SbfI-AS, respectively. The amplicons were inserted into the SalI and SbfI restriction enzyme sites, respectively.

pSU-CRE was constructed first by PCR amplifying the complete CRE coding sequence from pSF-CMV-CRE (Sigma) using primers CRE@pUC18A-F and CRE@pUC18A-R. The amplicon was used in an iPCR reaction to replace *bla* in pUC18A (170) with the CRE-encoding DNA. *cre* and upstream *aadA* were then PCR amplified using

**Table 2: Oligonucleotide Primer Sets**

Target	Primer Name	Primer Sequence (5'→3')
<b><u>Cloning Primers</u></b>		
<i>cre</i>		
	CRE@pUC18A-F	5'-GGTCTGACGCTCAGTGG AACGGCAGAGGCCTG CGGATCC-3'
	CRE@pUC18-R	5'-CTGGCGTTACCCA ACTTAATCGCCGGAGGACA CCATGTCCAATTTACTGACCGTACACC-3'
	CRE-aadA@pSUMC-F	5'-CTGCAGGTACCGGTTCGACCATTGCAAGCTTA TCATCATGCCTCC-3'
	CRE-aadA@pSUMC-R	5'-GATCTTTCTACGGGGTCTGACGCTCGCAGAGG CCTGCGGATCC-3'
	CRE+Pbla-F	5'-AGGGTTATTGTCTCATGAGCGGATACATATTT GAAGTCACGACGTTGTA AACGACGGC-3'
	CRE+Pbla-R	5'-GATAAATGCTTCAATAATATTGAAAAAGGAA GAGTATGTCCAATTTACTGACCGTACACC-3'
<i>imeA</i>		
	LoxP-blagfp-F	5'-CTACTTCGTATAGCATA CATTATACGAAGTTA TGGAAATGTGCGCGGAACCC-3'
	LoxP-blagfp-R	5'-ATAACTTCGTATAATGTATGCTATACGAAGTT ATTTACTTGTATAGTTCATCCATGCCAT-3'
	HomRR@pSUMC-F	5'-CTGCAGGTACCGGTTCGACCATTGCGTCTGACG CTCAGTGGAACG-3'
	HomRR@pSUMC-R	5'-GATCTTTCTACGGGGTCTGACGCTCCTGGCGT TACCCA ACTTAATCGCC-3'
	694pro@NmPgf F	5'-CGGTTCTGGCCTTTTGCTGGGTACGGAAA TACTATCTCCAGCTCAAAGC-3'
	694@NmPgf R	5'-GCCCCGCCCTGCCACTCATCGGGACCGAA CACCGTATACCT
Cis Constructs		
	695Cis5armF2	5'-GTCACTGCAGGTACCGGGACTCTATCCCCA AAGTTATTCTTCAA AAGTTCT-3'
	695Cis5armR2	5'-AGGCATGATGATGAATGGTTCGATTAGATATTC CCAACCGAAGAAGGATC-3'
	695 cis 3armF	5'-CTCACTGATTAAGCATTGGTAACCTGGGTCC GCGCACATTTCC-3'
	695 cis 3armR	5'-CTTTCTACGGGGTCTGACCTTTGCTTGCTCCCA AATTGTA AACGC-3'
BirA		
	BirA-TmeA-F	5'-CCGGTACCGAGTATTCGACCTACTAATGGG AGTGGAATG-3'
	BirA-TmeA-R	5'-GGGGGTACCTTAGTCTAAGAAAACAGAAG AAGTTATGACAGTTAGTGTGG-3'
	BirA-TmeB-F	5'-CCCGGTACCGAGTAGCATAAGCCCTAT AGGGGGG-3'
	BirA-TmeB-R	5'-GGGGGTACCTTAGATATTTCCCAACCGAAG AAGGATCTTCCTC-3'

**Table 2:** Continued

APEX		
	APEX2-0884-S	5'-GACTACAAGGATGACGACGATAAGGGAAAGT-3'
	APEX2-0884-AS	5'-CCCTCTAGATGCATGCTCGAGCTATTAG-3'
	pBomb-694-S	5'-GAAAGGATCTGCGGCCGCATGAGTATTCGAC CTACTAATGGGAGTGGAAATG-3'
	pBomb-Apex-694-AS	5'-CTTTCCCTTATCGTCATCCTTGTAGTCGTCTAA GAAAACAGAAGAAGTTATGACAGTTAGTGTGG-3'
	iPCR pBomb-695 F	5'-GATCTGCGGCCGCATGAGTAGCATAAGCCC TATAG-3'
	Gib APEX-695 REV	5'-CTTTCCCTTATCGTCGTCATCCTTGTAGTCGAT ATTCCAACCGAAGAAGGAT-3'
TmeB- FT		
	695FLAG-F	5'-AGAAAGGATCTGCGGCCGCAACTATTA AGAGGAAGTAGTAGTGAGTAGCATAAGC-3'
	695FLAG-R	5'-GGTCGACCGGTACCTGCAGTTACTTGTTCATCG TCGTCCTTGTAGTCGATATTCCAACCGAAGAAGGAT CTTCC-3'
pTmeA/TmeB		
	694695compAII-F	5'-AGGTACCGGTCGACCAGAACTAATTTTCGTTCCG TTTAAAAACAGAACAATTG-3'
	694695compAII-R	5'- CCTTTGATCTTTCTACGGGGTTACGGTCCGA TTAGATATTCCAACCGAAGAA-3'
<i>ΔtmeA/tmeB</i>		
	ctl0063-SalI-S	5'-GCAAAAGAGCTGATCCTCCGTCCTGCAGGTACC GCTCCAGCGTTGCGTATTGTTTGTGG-3'
	ctl0063-SalI-AS	5'-CGTATAATGTATGCTATACGAAGTAGGAAT GCCTCCGCCGAAGCAATAACTTTTAATTCC-3'
	ctl0064-SbfI-S	5'- GTATAGCATAATTATAACGAAGTTATGCA TTTTCTAATAGGGAAGAGGATAAATAGCGTG-3'
	ctl0064-SbfI-AS	5'-CTTTGATCTTTCTACGGGGTCTGACGCCC GACCATTTACTTTGGAATAAGTGTGATATC-3'
<b><u>Screening Primers for <i>gfp-bla</i></u></b>		
ploxP-GFP - bla	Screen-S	5'-CTTAGCCGTGAAAGTACACA ACTATTG-3'
	Screen-AS	5'-GAGAAGCGACATCTTTACGTTCCGCC-3'
<i>tmeA</i> locus	Surroundctl0063-F	5'-TAGTAGCTCTTGCAGGGTGTACTT-3'
	Surroundctl0063-R	5'-TACTACTTCCTCTTAATAGTTGAAAGGACCG-3'
<b><u>qPCR Primers</u></b>		
<i>16S</i>		
	Fwd	5'-CCTGGTAGTCCTTGCCGTAAAC-3'

**Table 2:** Continued

---

<i>16S</i>	Rev	5'-TACTCCTCAGGCGGCATACTTA-3'
<i>tmeA</i>	Fwd	5'-TAACCTATCTGTGGGAGGGAAG-3'
	Rev	5'-GGCATCTACCGTAGGATCTGTA-3'
<i>tmeB</i>	Fwd	5'-TTCGGAGCTCATAGGAGAACT-3'
	Rev	5'-GCTCATTACAGGAGGGAATAC-3'
<i>tarp</i>	Fwd	5'-ACACTACTGCCTTCACCACCTC-3'
	Rev	5'-TCCTCCCATCATCAAGGATGTGG-3'
<i>gfp</i>	Fwd	5'-GTGCCATGCCCCGAAGGTTAT-3'
	Rev	CTTCAGCACGTGTCTTGTAGTTCC-3'
<i>cre</i>	Fwd	5'-TGCAAGTTGAATAACCGGAAATG-3'
	Rev	5'-GGGCCTGAAGATATAGAAGATAATCG-3'
<i>rpoD</i>	Fwd	5'-GCGGTGTTTCCATTGTCGTCATA-3'
	Rev	5'-ATTTCTCTCAGCTCGCGCTTTC-3'
<i>Ct696</i>	Fwd	5'-TCGTAGAGGTTCTGCTAGCCTTT-3'
	Rev	5'-TCGGTAATCACGCCTCCGATAA-3'
pL2	Fwd	5'-GACAACGCTTCAAAGAAGATGGCTCTA-3'
	Rev	5'-CCTCTAGTACAAACACCCCAATATTGTG-3'

---

CRE-aadA@pSUMC-F and CRE-aadA@pSUMC-R and mobilized into pSUMC via iPCR. A bla promoter ( $P_{bla}$ ) was inserted upstream of *cre* via iPCR amplification of pSU-*aadA-CRE* with primers loxP-blagfp-F and loxP-blagfp-R. The resulting amplicon was kinased (New England Biolabs), blunt-end ligated (New England Biolabs), and transformed into *E. coli* to yield pSU-CRE.

Strains with complementation in trans and for overexpression experiments were previously generated (143) by mobilizing *tmeA* or *tmeB* with the endogenous promoter into pCompAII (163) using gene-specific primers (694pro@NmPgfpF, 694@NmPgfp R; Ken Fields, unpublished). pSUMC was used to generate the construct for *tmeA* and *tmeB* cis-complemented strains. The construct was assembled via Gibson assembly using HiFi DNA assembly master mix (New England Biolabs). A two-step process was employed where an ca. 5.5 kb fragment containing *tmeA*, *tmeB*, and ca. 2 kb upstream of *tmeA* was amplified from WT L2 *C. trachomatis* via PCR using primers 695Cis5armF2 and 695Cis5armR2 and was mobilized into the Sall site of pSUMC-*aadA* (172) such that the chlamydial DNA was positioned immediately upstream of the *aadA* promoter. Then, 3 kb of DNA downstream of *tmeB* was amplified from WT L2 *C. trachomatis* via PCR using primers 695 cis 3armF and 695 cis 3armR. A Gibson reaction was used to mobilize this element into the SbfI site immediately downstream of *aadA*.

The overexpression construct, pTmeA/TmeB, was generated by amplifying the *tmeA/tmeB* locus, including the native upstream promoter region, with 694695compAII-F and 694695compAII-R custom primers (Table 2). The fragment was then mobilized into pCompAII downstream of *aadA* via Gibson Assembly.

The ectopically expressed 3x FLAG® pTmeA-FLAG and pTmeB-FLAG constructs were generated as previously described using a mammalian expression vector (138). The 1x FLAG vector for chlamydial expression, TmeB-FT, was developed by mobilizing *tmeB* into pBOMB-4 (166) immediately downstream of the *tet* promoter. 1x FLAG was added to the C-terminal end of TmeB before the stop codon using gene-specific primers 695FLAG-F and 659FLAG-R via divergent PCR.

BirA-containing expression constructs were generated by mobilizing full-length *C. trachomatis* L2 *tmeA* or *tmeB* and recombinant *tmeA*Δ*mld* (137) into pcDNA3.1 mycBioID (173). Custom primers containing engineered flanking KpnI sites were used to amplify *tmeA* or *tmeB*. Amplification of *tmeA* sequences was accomplished using BirA-TmeA-F and -R primers, whereas *tmeB* was amplified with BirA-TmeB-F and -R primers. Standard cloning procedures were employed to insert chlamydial genes into the KpnI site of pcDNA3.1 mycBioID to yield chimeric sequences encoding N-terminally tagged TmeA, TmeAΔ*mld*, or TmeB.

APEX2-containing constructs were generated by first amplifying APEX2 from pcDNA3 APEX2-NES (174) using custom primers APEX2-0884-S and APEX2-0884-AS and mobilizing the fragment into pBOMB-4 (166) between the *mCherry* and *aadA* sequences. Next, full-length *tmeA* or *tmeB*, excluding the stop codon, was amplified from the *C. trachomatis* L2 genome and mobilized into pBomb-APEX immediately upstream of *APEX* and replacing *mCherry* via iPCR. *tmeA* was amplified using pBomb-694-S and pBomb-Apex-694-AS custom primers. *tmeB* was amplified using iPCR pBomb-695 F and Gib APEX-695 REV custom primers.

### 2.2.2. PCR Screening

Cre activity in *E. coli* was assessed by cotransformation of *E. coli* with pUC18 containing a floxed *gfp* cassette and pSUmC or pSU-CRE. Transformants were screened by fluorescence and PCR with Screen-S and Screen-AS primers (Table 2).

PCR screening of chlamydial loci with Surroundctl0063-F and Surroundctl0063-R primers was accomplished by harvesting whole-culture DNA using 0.5 N NaOH-mediated lysis, as described previously (160).

### 2.2.3. Quantitative PCR Screening and RNA detection

For quantitative PCR (qPCR), DNA from McCoy cell monolayers infected at a multiplicity of infection (MOI) of 1 was harvested by 0.5 N NaOH extraction. iTaq Universal SYBR green supermix (Bio-Rad) and gene-specific primers (Table 2) were used for amplification. To assess gene expression, the Aurum total RNA mini kit (Bio-Rad) was used to isolate RNA from McCoy cell monolayers infected at an MOI of 1. The subsequent generation of cDNA was achieved using the QuantiTect reverse transcription kit (Qiagen), and cDNAs were amplified with iTaq Universal SYBR green supermix (Bio-Rad) and gene-specific primers.

### 2.3. Genetic manipulation of chlamydiae

CaCl<sub>2</sub>-mediated chemical transformation (156) was used to mobilize respective plasmids into *C. trachomatis* L2. Subsequent manipulations leveraging fluorescence reporting to yield *trans*-expression or allelic replacement were accomplished according to established protocols (132, 170, 172, 175). 2 µg of unmethylated DNA per well of a 6-well plate was used to transform WT *C. trachomatis* L2, and transformants were selected with Spec or Pen as appropriate.  $\Delta tmeA$ ,  $\Delta tmeB$ ,  $\Delta tepp$ , and  $\Delta tarp$  were generated using fluorescence-reported allelic exchange mutagenesis (FRAEM) (163).

Generation of the *tmeA-lx* mutant via floxed-cassette allelic exchange mutagenesis (FLAEM) was accomplished by first cultivating pSUmC-*tmeA-lox-gfp-bla* transformants in the absence of aTc for multiple passages, followed by clonal isolation of Pen-resistant GFP-expressing chlamydiae. The intermediate strain, L2  $\Delta tmeA-lox-gfp-bla$ , was grown in the presence of Rif, and spontaneous Rif-resistant chlamydiae were isolated. pSU-CRE was mobilized into these chlamydiae by lateral gene transfer. L2<sup>Rif</sup> *tmeA-lox-gfp-bla* chlamydiae were used with WT expressing pSU-CRE to coinfect McCoy cells at a 10:1 ratio. Cultures were maintained for two 48 hr passages in the presence of aTc and cycloheximide but in the absence of antibiotic selection. Five serial passages (48 hrs each) were then performed in the presence of Rif, Spec, aTc, and cycloheximide. Rif- and Spec-resistant chlamydiae expressing mCherry, but not GFP, were isolated by limiting dilution. Strains were cultivated for five serial passages in Rif and cycloheximide, followed by clonal isolation of Rif-resistant chlamydiae lacking mCherry. The absence of *gfp* and *bla* was confirmed via PCR and penicillin sensitivity assays, respectively. The absence of *tmeA* was confirmed as described above via PCR and DNA sequencing. Endogenous pL2 was

restored via lateral gene transfer by coinfection with *C. trachomatis* L2 *tmeA* (163) and L2R<sup>Rif</sup> *tmeA-lx*. The final L2R<sup>Rif</sup> *tmeA-lx* strain was isolated by limiting dilution from cultures exposed to Rif. A spontaneously Rif-resistant WT strain was also isolated and, along with the *tmeA-lx* mutant, was transformed with pCompAII (163) using Spec selection to produce vector-only controls. Cis complementation of the *tmeA* and *tmeB* was accomplished by transforming  $\Delta tmeA-lx$  or  $\Delta tmeB$  with pSU-CisA/B and following the established FRAEM protocol (163). Generation of  $\Delta tmeA/tarp$  and  $\Delta tmeA/tmeB$  was accomplished using FLAEM (175) as described above and is further detailed in the text.

#### **2.4. Chlamydia Fitness Models**

All infections were accomplished using Hanks Balanced Salt Solution (HBSS; Gibco) and density gradient-purified EBs (176). EBs were centrifuged onto cell monolayers at 20 °C for 1 hr at 900 xg or rocking on ice at 4 °C when appropriate. Incubations were carried out at 37 °C in an environment with 5% CO<sub>2</sub>.

Chlamydial fitness was assessed by (i) enumerating inclusions in primary infections (Direct counts), (ii) enumerating infectious progeny (Progeny IFUs), (iii) quantifying genomes over multiple passages, and (iv) quantifying inclusion area.

##### **2.4.1. Direct IFU Counts**

The EB concentration of laboratory stocks was quantified using acridine orange stain and fluorescent microscopy. Equal EBs were used to infect confluent HeLa monolayers in triplicate at a multiplicity of infection (MOI) 0.1-0.5 by centrifugation. Infected cultures were incubated at 37 °C for 24 hrs. Then, monolayers were fixed with

methanol, and inclusions were labeled with anti-HSP60 (Santa Cruz Biotechnology) primary antibody and anti-mouse secondary antibody conjugated to AlexaFluor-594 (Invitrogen). Stained inclusions were counted for the entire well using the Cell Insight CX5 High-Content Screening platform (ThermoFisher Scientific). Counts were adjusted for dilution when appropriate.

#### 2.4.2. Progeny IFU Enumeration

Approximately equal inclusion forming units (IFUs) for each chlamydial strain were used to infect duplicate sets of confluent HeLa monolayers at an MOI of 0.1-0.5 by centrifugation. 24 hrs post-infection (hpi), one of the duplicate infected monolayers was fixed and stained for inclusions as described (2.4.1. Direct IFU Counts). This set of wells served as a reference for starting IFUs and was used later for progeny normalization if necessary. The remaining monolayers were harvested for progeny EBs by mechanically scraping, and HeLa cell debris was reduced through centrifugation steps. Harvested progeny were serially diluted and used to infect fresh HeLa cell monolayers by centrifugation. The progeny infected monolayers were fixed 24 hpi, and inclusions were stained and enumerated as described (2.4.1. Direct IFU Counts).

#### 2.4.3. Genome Quantity over Multiple Passages and Penicillin Sensitivity Assay

HeLa monolayers were infected with approximately equal IFUs by centrifugation at an MOI of 0.5. At 24 hpi, monolayers were mechanically harvested, and HeLa cell debris was reduced through centrifugation steps. Equal portions of the harvested material were

saved for 0.5 N NaOH DNA extraction. The remaining portion of the harvested material was diluted equally for all strains and used to infect fresh HeLa monolayers. This process was repeated every 24 hrs for multiple passages. DNA was quantified by qPCR with iTaq Universal SYBR green supermix (Bio-Rad) and 16S specific primers (Table 2). Penicillin sensitivity assays were done in the same manner; however, McCoy cells were used instead of HeLa cells, and RPMI growth media was supplemented with 0.6 µg/mL penicillin. Fold change was calculated using the  $\Delta\Delta C_t$  method.

#### 2.4.4. Quantifying Inclusion Area

The areas of 50 inclusions per chlamydial strain were quantified from HeLa infected cultures, fixed, and stained for inclusions (2.4.1 Direct Counts), using the Cell Insight CX5 High-Content Screening platform (ThermoFisher Scientific) and HSC Studio version 6.6 (ThermoFisher Scientific).

### 2.5. Immunoblotting

Density gradient purified EBs or whole-culture material was harvested 24 hpi. Proteins were precipitated in 10% (vol/vol) trichloroacetic acid in PBS and solubilized using 3x Complete Solubilization Solution (CSS; Appendix 2). Proteins were then resolved using 4 to 15% (vol/vol) SDS-PAGE gels and transferred to Immobilon-P membranes (Millipore). Appropriate primary antibodies and horseradish peroxidase-conjugated secondary antibodies (Table 3) were used for detection via chemiluminescence using Amersham ECL Plus (GE Healthcare UK Limited) reagent.

**Table 3:** List of Antibodies Used

Target	Company or Reference	Catalog Number	Details*
<b><u>Primary Antibodies and Probes</u></b>			
Alpha.beta-Tubulin	Cell Signaling	2148S	Rabbit pAb
Annexin A2, clone D11G2	Cell Signaling	8235S	Rabbit mAb
ANHNAK	(138)		Rabbit pAb
Arp2	Cell Signaling	3128S	Rabbit pAb
Arp3	Cell Signaling	4738S	Rabbit pAb
Arp2/3 Complex, clone 13C9	Millipore	MABT95	Mouse mAb
ASCT2 (SLC1A5), clone D7C12	Cell Signaling	8057S	Rabbit mAb
Avidin, NeutrAvidin™, Horseradish peroxidase conjugate	Invitrogen	A2664	
CD44, clone 8E2	Cell Signaling	5640S	Mouse mAb
CD98 (SLC3A2)	Invitrogen	PA5-23661	Rabbit pAb
Cofilin, clone D3F9	Cell Signaling	5175S	Rabbit mAb
Cre Recombinase, clone D3U7F	Cell Signaling	12830S	Rabbit mAb
EGFR	Santa Cruz Biotechnology	SC-03	Rabbit pAb
EphA2, clone D4A2	Cell Signaling	6997S	Rabbit mAb
FLAG, clone M2	Sigma	F1804	Mouse mAb
FNBP1	Invitrogen	PA5-28626	Rabbit pAb
GAPDH, clone D16H11	Cell Signaling	5174S	Rabbit mAb
HSP-60, clone A57-B9	Santa Cruz Biotechnology	Sc-57840	Mouse mAb
ITGβ1, clone D6S1W	Cell Signaling	34971S	Rabbit mAb
IQGAP1, clone D8K4X	Cell Signaling	20648S	Rabbit mAb
LAT1 (SLC7A5)	Cell Signaling	5347S	Rabbit pAb
LimK1	Cell Signaling	3842S	Rabbit pAb

**Table 3: Continued**

LPS (Chlamydial), clone 512F	Novus	NB100-62449	Mouse mAb
MOMP	(138)		
N-WASP, clone 30D10	Cell Signaling	4848S	Rabbit mAb
P-Cofilin, clone 77G2	Cell Signaling	3313S	Rabbit mAb
P-EGFR (Y845), clone D63B4	Cell Signaling	6963S	Rabbit mAb
P-EphA2 (S897), clone D9A1	Cell Signaling	6347S	Rabbit mAb
Phospho-tyrosine, clone 4G10	Millipore	05-321	Mouse mAb
PODXL	Invitrogen	PA5-28116	Mouse pAb
Scc2	(103)		
SNX9, clone G-5	Santa Cruz Biotechnology	Sc-166863	Mouse mAb
TarP	(119)		
TepP	(177)		
TmeA	(138)		
TmeB	(139)		
<b><u>Secondary Antibodies</u></b>			
AlexaFluor-488 (anti-Rabbit)	Invitrogen	A11034	
AlexaFluor-488 (anti-Mouse)	Invitrogen	A11029	
AlexaFluor-594 (anti-Rabbit)	Invitrogen	A11037	
AlexaFluor-594 (anti-Mouse)	Invitrogen	A11005	
Anti-Mouse Horseradish peroxidase	Sigma	A6154	
Anti-Rabbit Horseradish peroxidase	Sigma	A0168	

\* mAb: monoclonal antibody; pAb: polyclonal antibody

## **2.6. Plaque Assay**

Confluent monolayers of Vero cells were infected with approximately 100 IFUs per well of a 6-well plate by centrifugation at 900 xg for 1 hr at 20 °C. Infected cells were overlaid with 0.5% LE Quick Dissolve agarose (Genemate) dissolved in water and 90 % (v/v) RPMI + 10% RPMI. Once the agarose was solidified, the cultures were incubated at 37 °C for 7 days. Next, 1% (w/v) agarose containing 0.06% (w/v) neutral red (VWR Life Sciences) was overlaid on the existing agarose, and the plates were incubated for 3 hrs at 37 °C. Both layers of solidified agarose were carefully removed, and the stained monolayers were imaged using the Cell Insight CX5 High-Content Screening platform (ThermoFisher Scientific). Plaque areas were calculated by arbitrary units using FIJI image processing software.

## **2.7. Rifampin Resistance Co-infections**

Confluent HeLa cultures were infected by centrifugation at 900 xg for 1 hr at 20 °C with an MOI of 1 for both chlamydial strains achieving a final MOI of 2. Cultures were incubated at 37 °C for 24 hrs. Then monolayers were mechanically harvested, and chlamydial debris was reduced by centrifugation. The harvested material was diluted and passed onto fresh HeLa cultures with 5 ng/mL Rif media. After 24 hrs, cultures were fixed, and Rif resistant IFUs were enumerated by fluorescent staining (2.4.1. Direct IFU Counts).

## 2.8. Microscopy

### 2.8.1. *E. coli* Colonies

*E. coli* colonies were imaged at 20x magnification using bright-field or epifluorescence microscopy. 100 plated colonies were visualized for each strain.

### 2.8.2. N-WASP Localization

Localization of EBs and N-WASP via microscopy was accomplished using direct fluorescence of HeLa cells expressing GFP-N-WASP (178) for 30 hrs prior to infection or by indirect immunofluorescence using primary antibodies specific to MOMP (Novus Biologicals) or N-WASP (Cell Signaling). The same infection strategy was used for both approaches. HeLa cells were infected at an MOI of 20 with EBs on ice with rocking for 1 hr then shifted to 37 °C for 20 min. Cells were fixed with 4% paraformaldehyde and permeabilized with 0.1% Triton X-100 for 20 min. EBs were labeled with rabbit anti-MOMP-specific antibodies in both approaches, and N-WASP was labeled with mouse anti-N-WASP-specific antibodies for non-transfected cells. Appropriate rabbit or mouse secondary antibodies conjugated to AlexaFluor-594 or -488 (Invitrogen) were used for detection. Cells were examined via epifluorescence microscopy, and images were acquired using a 100x oil-immersion objective. Images were processed equivalently using Adobe Photoshop 6.0 (Adobe Systems). Samples were blinded then localization was scored by viewing red fluorescent EBs, and localized green fluorescence above background in the exact location. 100 EBs per strain were scored.

## **2.9. Percent Invasion Assay**

HeLa cells were prepared in 24-well plates with 12 mm coverslips, and invasion assays were performed essentially as described (129). Density gradient purified EBs were used at an MOI of 20. Infections were done on ice with rocking for 1 hr to allow attachment, then shifted to 37 °C to promote invasion for 30 min or otherwise noted. The cultures were fixed with 4% paraformaldehyde, and extracellular EBs were labeled with chlamydial LPS-specific (mouse). Cultures were then permeabilized with 0.1% Triton X-100 for 20 min and total EBs were labeled with MOMP-specific (rabbit) antibodies. Detection was accomplished with secondary antibody conjugated to AlexaFluor-594 (anti-mouse) or AlexaFluor-488 (anti-rabbit). Percentages of invaded chlamydiae were computed by enumeration of internal and external chlamydiae in 10 fields of view. The percentage EB internalization was calculated via the formula  $([\text{total EBs} - \text{external EBs}] / \text{total EBs}) \times 100 = \text{percent (\%)} \text{ invasion}$ .

## **2.10. Inhibitor Assays**

### **2.10.1. Percent Invasion**

HeLa cells were prepared in 24-well plates with 12 mm coverslips, and invasion assays were performed essentially as described (129). Density gradient purified EBs were used at an MOI of 20. Where appropriate, host cells were treated with medium containing 100 μM EIPA, 20 μM casin, 25 μM wiskostatin, 25 μM Ehop-016, or 200 μM CK666 (all purchased from Sigma-Aldrich) final concentration for 15 min before infection. Cultures were either mock-treated with media only or maintained with inhibitors during infection

and the subsequent incubation. Infections were done on ice with rocking for 1 hr and then shifted to 37 °C for 45 min. The cultures were fixed with 4% paraformaldehyde, and extracellular or intracellular EBs were differentially labeled with chlamydial LPS-specific (mouse) or MOMP-specific (rabbit) antibodies, respectively (Table 3). Detection was accomplished with secondary antibody conjugated to AlexaFluor-594 (anti-mouse) or AlexaFluor-488 (anti-rabbit) (Invitrogen). Percentages of invaded chlamydiae were computed by enumeration of internal and external chlamydiae in 10 fields of view. The percentage EB internalization was calculated via the formula  $([\text{total EBs} - \text{external EBs}] / \text{total red EBs}) \times 100 = \text{percent (\%)} \text{ invasion}$ .

#### 2.10.2. Percent IFU Recovery

Approximately equal IFUs for each chlamydial strain were used to infect duplicate sets of confluent HeLa monolayers at an MOI of 0.1-0.5 by rocking. HeLa monolayers were either mock-treated or treated with 1 µg/mL Cytochalasin D, 50 µM NSC, 7.5 mM Wiskostatin, or 40 µM CK-636 (all purchased from Sigma-Aldrich) 15 min before infection. Inhibitors were maintained during infection and subsequently for 2 hrs. The monolayers were fixed and stained for inclusions 24 hpi as described (2.4.1. Direct IFU Counts). Percent recovery was calculated by  $(\text{inclusions in treated cultures} / \text{inclusions in untreated cultures}) \times 100 = \text{percent recovered IFUs}$ .

#### 2.11. BirA Biotinylation

BirA-mediated biotinylation of host proteins was accomplished according to established protocols (179). HeLa cells were nucleofected with empty pcDNA3.1

mycBioID as a BirA-only control or with TmeA- and TmeB-containing constructs. For control experiments, parallel cultures were cultivated in RPMI supplemented with dialyzed FBS with or without 50 mM biotin. Cultures were maintained for 24 hrs.

### **2.12. Apex Biotinylation**

The apex biotinylation procedure is described in detail by Olsen et al. (180). Briefly, HeLa cells were cultivated in one 6-well plate per experimental condition and Dulbecco modified Eagle medium (DMEM) + 10% FBS. Once confluent, monolayers were either mock-infected or infected with WT, TmeA-APEX, or TmeB-APEX by spinning at 900 xg for 60 min to reach an MOI of 2. EBs used for infection were previously cultivated in the presence of 50 ng/mL aTc for expression of TmeA-APEX and TmeB-APEX before invasion. After incubating infected cultures at 37 °C for 24 h in growth medium supplemented with 50 ng/ml aTc, 1.5 mM final concentration Biotin-phenol was added to medium and incubated for 30 min. Biotinylation was catalyzed by replacing the medium with 3 mM H<sub>2</sub>O<sub>2</sub> in phosphate-buffered saline (PBS) for 1 min and then washing cultures 3 times with quenching solution.

### **2.13. Mass Spectrometry Based Protein Identification**

BirA or APEX cultures were harvested into RIPA buffer (Appendix 2) supplemented with Halt Protease Inhibitor Cocktail (ThermoFisher Scientific) and incubated on ice for 1 hr. The insoluble fraction was separated by spinning at 17,000 xg for 3 min, and then the soluble fraction was applied to equilibrated high-capacity

NeutrAvidin Agarose (Thermo Scientific) and rocked overnight at 4 °C. The resin was washed 3 times, and biotinylated proteins were eluted in 40 µl 3x CSS (Appendix 2) at 95 °C for 4 min. To identify biotinylated proteins using mass spectrometry, proteins were run into a 12% SDS-PAGE gel for 15 min at 200 V and then stained with Sypro Ruby protein blot stain (Lonza) and cut into lanes. The University of Kentucky Proteomics Core performed digestion and preparation of samples. A TSQ Vantage triple quadrupole mass spectrometer was used for liquid chromatography with tandem mass spectrometry (LC-MS/MS) protein identification. Analysis of samples was done using Mascot data analysis software.

#### **2.14. FLAG-Tag Immunoprecipitations**

FLAG-tagged proteins were ectopically expressed in HeLa cells or expressed and secreted from *C. trachomatis* during infection. HeLa cells were lysed using ice-cold 0.5% NP-40 buffer (Appendix 2) containing Halt Protease Inhibitor Cocktail (ThermoFisher Scientific). After removing the insoluble fraction, the lysate was pre-cleared with Sepharose 4B beads (Sigma), then applied to anti-FLAG M2 resin and incubated with rocking at 4 °C overnight. The resin was washed 4 times with 0.05% NP-40 buffer (Appendix 2), and bound proteins were eluted into 30 µL 6 x Laemmli buffer (Appendix 2) by heating at 95 °C for 5 minutes. The eluted proteins were then analyzed by immunoblotting (2.5. Immunoblotting).

### 2.15. Pyrene Assay

Pyrene actin polymerization assays were performed as previously described (121). Briefly, monomeric pyrene-labeled actin was prepared by diluting lyophilized pyrene actin (Cytoskeleton) in 5 mM Tris (pH 8.0), 0.2 mM CaCl<sub>2</sub>, 0.2 mM ATP (G buffer) and incubating on ice for 1 hr. Monomeric pyrene actin was obtained by collecting the supernatant after centrifuging for 90 min, at 100,000 xg and 4 °C in a Beckman Optima MAX TL ultracentrifuge using a TLA 55 rotor (Beckman Coulter). N-WASP $\Delta$ EVH1 (NWASP<sup>151-501</sup>) was employed as previously reported to facilitate purification from *E. coli* (181). Approximately 30  $\mu$ g of pyrene-labeled actin was mixed with 1 to 2  $\mu$ g of the indicated proteins (TmeA, N-WASP<sup>151-501</sup>, Arp2/3, TarP, or VCA) in a volume of 500  $\mu$ l for 5 min before the addition of 1/20th volume of polymerization buffer (500 mM KCl, 20 mM MgCl<sub>2</sub>, 10 mM ATP). The reaction (contained in a semi-microcuvette and holder assembly) was monitored for 30 min with an LS 55 luminescence spectrophotometer equipped with the biokinetic accessory and directed by FL Winlab software version 4.0 (Perkin-Elmer, Beaconsfield, Bucks, United Kingdom) with 2.5-nm bandwidth at 365-nm excitation wavelength and a 2.5-nm bandwidth at 407-nm emission wavelength.

### 2.16. 2D Gels

Duplicate HeLa monolayers were infected at an MOI of 1000 with density gradient (DG) purified EBs in 24-well plates by rocking at 37 °C for 20 min. Two wells per sample were lysed in ice-cold water containing Halt Protease Inhibitor Cocktail (ThermoFisher Scientific). Excess salts and lipids were removed from samples by Chloroform-methanol extraction, and proteins were resuspended with 2-D Ready Prep Resuspension Buffer

(BioRad). Proteins were separated in the first dimension on 11 cm IPG strips pH 4-7 (BioRad) by isoelectric point. Proteins were separated in the second dimension on 4-15% SDS-PAGE gels (BioRad). Phosphorylated proteins were detected using phosphotyrosine-specific primary antibodies after being transferred to Immobilon-P membranes (Millipore) or detected within the gel using Pro-Q Diamond Phosphoprotein Gel Stain (ThermoFisher Scientific) prior to mass spectrometry.

### **2.17. Mouse Infections**

Groups of 5 female C3H/HeJ mice 6 to 8 weeks old purchased from Jackson Laboratory were used for these studies. Mice were given food and water ad libitum in a controlled environment with 14 hr light and 10 hr darkness cycles. Mice were pretreated with 2.5 mg medroxyprogesterone (Depo-Provera) subcutaneously 5 days before infection. Mice were infected by depositing  $5 \times 10^5$  IFUs, diluted to 5  $\mu$ l in SPG buffer (Appendix 2), into the vaginal vault. Vaginal shedding was monitored by vaginal vault swabs (Calgiswab; 7 turns to the left, 7 turns to the right) beginning on day 3 and then every 4 days. Sheds IFUs were extracted from swabs by vortexing and were used to infect fresh McCoy cells. RPMI + 10% FBS media was supplemented with 10  $\mu$ g/mL gentamicin (Gibco). IFUs were enumerated by fluorescent staining 24 hpi (2.4.1. Direct IFU Counts). All manipulations were reviewed and approved by the University of Kentucky Institutional Animal Care and Use Committee.

## **2.18. Statistical Analysis**

Data are representative of a minimum of three experiments. Unless otherwise noted, quantitative data were generated from experiments containing triplicate biological samples. Calculation of standard deviation of the mean and assessment of statistical significance by Student's t-test with Welch's correction, Mann-Whitney U-test, or linear regression was performed using Prism 6, version 6.04 (GraphPad Software, Inc., La Jolla, CA).

## **2.19. Image Creation**

Schematic representations were generated using PowerPoint (Microsoft Office) and BioRender.com.

## **CHAPTER 3: Floxed-Cassette Allelic Exchange Mutagenesis Enables Markerless Gene Deletion in *Chlamydia trachomatis* and Can Reverse Cassette-Induced Polar Effects**

Some of the data presented here have been previously published in, “Keb G, Hayman R, and Fields KA. (2018). Floxed-Cassette Allelic Exchange Mutagenesis Enables Markerless Gene Deletion in *Chlamydia trachomatis* and Can Reverse Cassette-Induced Polar Effects. *Journal of bacteriology*, 200(24), e00479-18. PMID: 30224436.”

Contributions: Dr. Fields proposed the genetic strategies and performed the lateral gene transfer methods. Robert Hayman performed inclusion size analysis and high throughput platform screening of chlamydial mutants. I did all other experiments. Dr. Fields and I authored the original paper collaboratively.

### **3.1. Summary**

The goal of the work presented herein was to develop a mutagenesis strategy for generating markerless gene deletions in *C. trachomatis*. This new strategy aimed to alleviate the cassette-induced polar effects previously observed with the fluorescence-reported allelic exchange mutagenesis (FRAEM) method. The FRAEM selection cassette, encoding green fluorescent protein (GFP) and antibiotic resistance, was re-engineered to contain flanking *loxP* sites. In the presence of Cre recombinase, the *loxP* sites recombine and result in the excision of the cassette from the genome. When *C. trachomatis tmeA* was targeted for deletion by allelic replacement with the FRAEM *gfp-bla* selection cassette,

downstream expression of *tmeB* was negatively impacted. Here, *C. trachomatis tmeA* was targeted for deletion using the re-engineered floxed cassette, and Cre-*loxP* genome editing was employed to remove the cassette. This strategy, floxed-cassette allelic exchange mutagenesis (FLAEM), successfully generated a markerless *C. trachomatis tmeA* deletion mutant and restored expression of downstream *tmeB*.

### 3.2. Introduction

The ability to genetically manipulate *Chlamydia* spp. has historically impeded rapid progress in understanding the function of specific chlamydial virulence factors and their contributions during infection. Early genetic strategies relied on chemical mutagenesis with forward and reverse approaches to associate genes with phenotypes. Coinfection of chlamydial strains to exchange DNA via lateral gene transfer (LGT) has been exploited for gene association studies in heavily mutagenized genomes (159). Successful CaCl<sub>2</sub> chemical transformation of *C. trachomatis* (156) with exogenous plasmid DNA has opened the door to more targeted strategies like the TargeTron system (162) and fluorescence-reported allelic exchange mutagenesis (FRAEM) (163). The TargeTron system enables site-specific gene inactivation by inserting a group II intron, whereas FRAEM replaces entire gene sequences with a selection cassette, encoding green fluorescent protein and antibiotic resistance, via allelic recombination.

Consistent with a reductionist genome, many *C. trachomatis* genes are likely arranged in operons. For example, the genes encoding the basal apparatus of the T3SS exist within ten different operons (182). Insertion mutagenesis approaches targeted at genes

within operons have the potential to alter the expression of downstream genes. FRAEM was previously used to target *C. trachomatis tmeA*, a significant invasion-related effector, for deletion (143). The  $\Delta tmeA$  strain revealed a functional requirement for TmeA during invasion *in vitro* and intravaginal infection of mice; however, the FRAEM-generated  $\Delta tmeA$  strain had decreased expression of downstream *tmeB* (143).

Bacteriophage Cre recombinase has been used effectively for genome editing of DNA flanked by *loxP* recognition sequences (183). In particular, the Cre-*lox* system has been applied successfully in genetically tractable bacteria (184), including the intracellular pathogen *Coxiella burnetii* (185). Although the obligate intracellular nature and comparatively limited malleability of *Chlamydia* spp. presents challenges, the broadly efficacious Cre-*lox* approach represents a promising strategy for genome editing in *Chlamydia* spp.

Floxed-cassette allelic exchange mutagenesis (FLAEM) was developed using the Cre-*loxP* system to overcome the obstacle of cassette-induced polar effects. FLAEM is essentially an extension of the original FRAEM method. Here, the FRAEM selection cassette is re-engineered with flanking *loxP* sites for recombination in the presence of Cre recombinase. Using a stepwise transformation approach, *tmeA* was successfully deleted and replaced with the *loxP*-flanked selection cassette; then, the cassette was targeted by transiently expressed Cre recombinase. Indeed, this process successfully removed the selection cassette, restored the expression of *tmeB*, and generated the first markerless gene deletion in *C. trachomatis*. In a broader sense, this technique allows a more direct assessment of specific gene functions and provides the greater *Chlamydia* research community a tool for deleting genes within operons.

### 3.3. Results

**Excision strategy and Cre activity.** The lack of TmeB in the *C. trachomatis* L2  $\Delta tmeA$  strain was hypothesized to be directly due to the replacement of *tmeA* with the 2.1-kb *gfp-bla* selection marker. Cre-*loxP* genome editing was chosen to investigate this hypothesis and determine whether removing the selection cassette would restore *tmeB* expression. This strategy requires a *tmeA* deletion strain where the pSUMC suicide plasmid (Figure 1A) *gfp-bla* cassette, with flanking 34 bp *loxP* sites, replaces the target gene. The mutant is then transformed with a Cre-expressing suicide plasmid, pSU-Cre (Figure 1B). The pSU-CRE plasmid also encodes *aadA* and *mCherry* for selection and fluorescence reporting, respectively. Expression of Cre is maintained until excision of the chromosomal cassette is achieved, yielding a single *loxP* scar sequence in the genome (Figure 1C).

To determine the functionality of this mutagenesis strategy, I utilized *E. coli* to confirm the system's overall efficiency. *E. coli* was co-transformed with ploxP-GFP, which contains *loxP* sites flanking *gfp* and encodes *blaM* on the backbone, and either pSU-Cre or empty vector pSUMC (negative control). 100 plated colonies were examined by direct fluorescence 24 hrs after transformation. No green fluorescent colonies were observed in the presence of pSU-CRE, whereas all the colonies were both red and green fluorescent in the presence of empty pSUMC (Figure 2A). To further confirm the removal of the *gfp*-cassette from ploxP-GFP, plasmid DNA from multiple *E. coli* isolates was harvested, and the cassette locus was PCR amplified using primers annealing to regions flanking the *loxP* sites. All amplicons from *E. coli* strains cotransformed with pSU-CRE migrated at a smaller size, corresponding to the loss of the *gfp*-containing DNA, compared to the empty

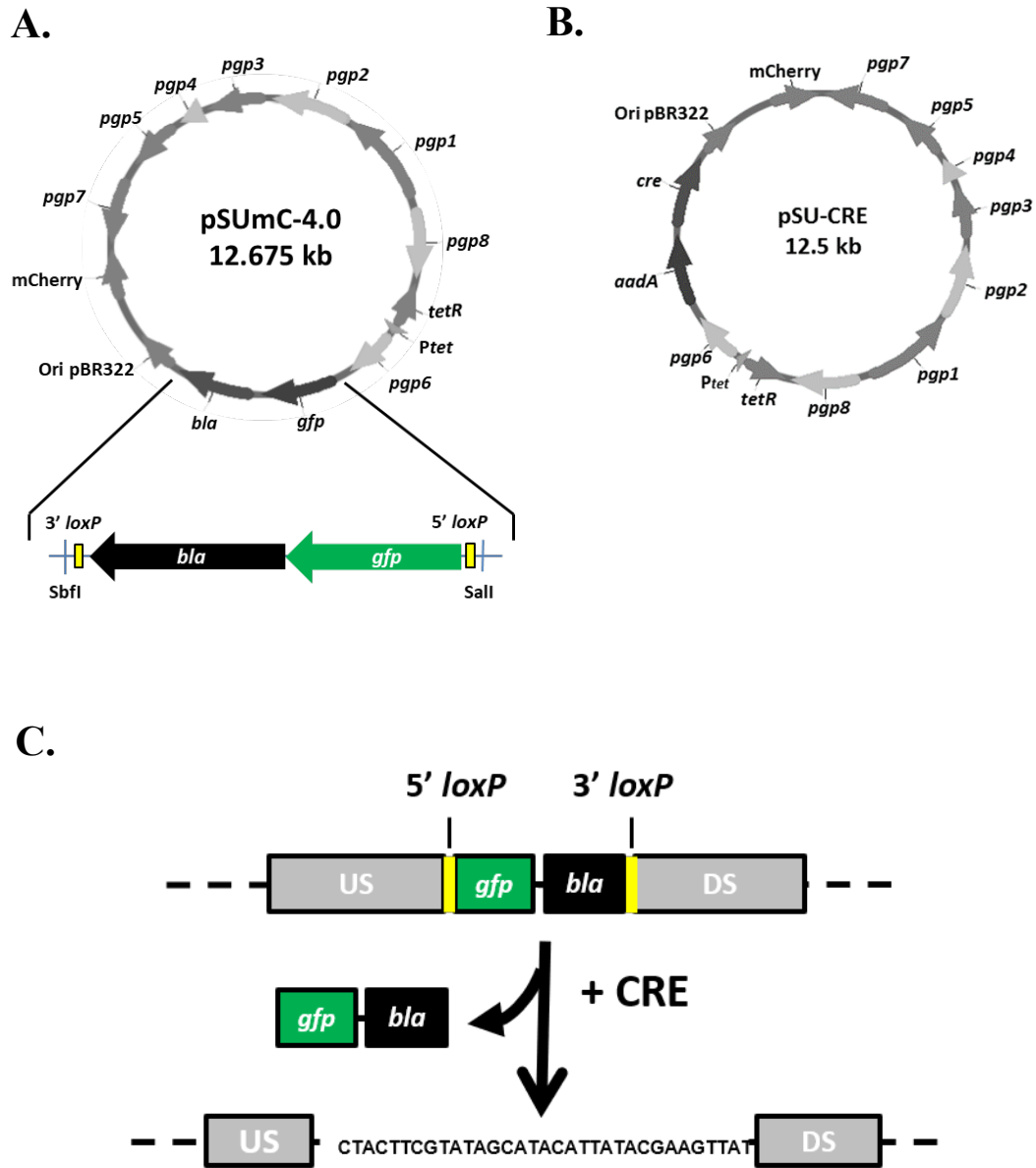
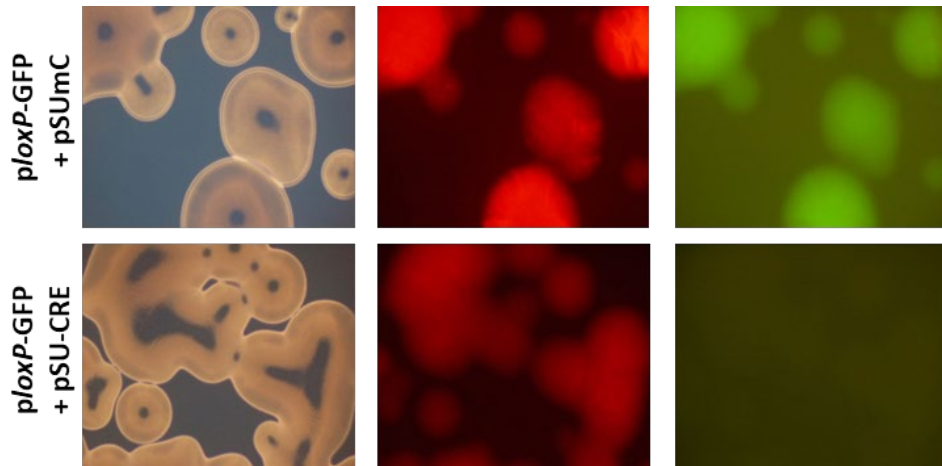


**Figure 1: Vector maps and mutagenesis strategy.**

(A) Schematic of the pSUmC-4.0 plasmid containing the *gfp-bla* selection cassette flanked by *loxP* sites. (B) Schematic of pSU-CRE plasmid for conditional expression of Cre in *C. trachomatis*. (C) Schematic representation of Cre recombinase strategy for use in *Chlamydia* spp. Cre expression is used to excise the *gfp* and  $\beta$ -lactamase resistance (*bla*) reporter genes when flanked by upstream (US) and downstream (DS) *loxP* sites, leaving behind a *loxP* scar sequence. The resulting locus is shown and contains one remaining *loxP* site.

A.



B.

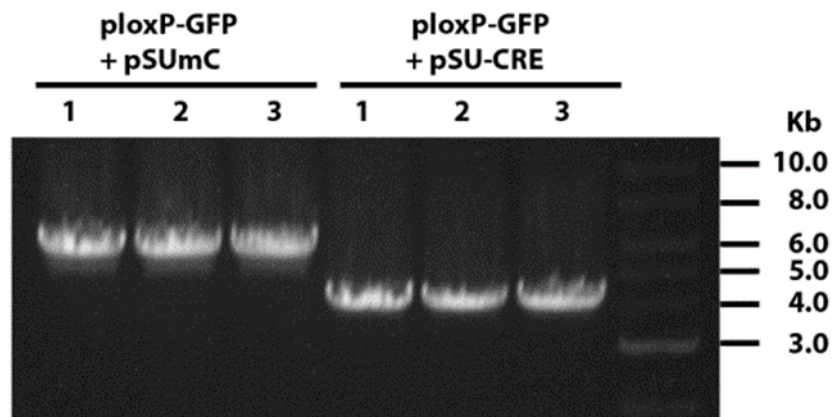


**Figure 2. Cre recombinase excises a fluorescence cassette in *E. coli*.**

(A) *E. coli* colonies expressing ploxP-GFP and lacking (pSUMC) or expressing (pSU-CRE) Cre recombinase. Colonies were imaged with bright-field and fluorescence microscopy. (B) Excision of the reporter cassette was confirmed for three different transformants (1 to 3) by PCR amplification of the locus with primers annealing within the upstream and downstream flanking regions

pSUmC control (Figure 2B). These data indicated that the Cre recombinase encoded by pSU-CRE was functional and that removal of the selection cassette was efficient in *E. coli*.

Next, I wanted to determine if Cre recombinase could be efficiently expressed in *C. trachomatis* and whether it would negatively impact chlamydial development. *C. trachomatis* L2 was transformed with pSU-CRE, using standard CaCl<sub>2</sub> methods, and protein samples were harvested from monolayers infected with either wild-type (WT) or *C. trachomatis*-pSU-CRE 24 hours post-infection (hpi). Cre recombinase was detected via immunoblotting only in the *C. trachomatis*-pSU-CRE cultures (Figure 3A). Although the inclusions formed by pSU-CRE-expressing chlamydiae appeared to have normal morphology (not shown), I investigated the impact of Cre expression on overall chlamydial fitness. *C. trachomatis* expressing or lacking Cre was used to infect HeLa cells. 24 hpi cultures were then either methanol fixed and stained for inclusions or harvested for enumeration of progeny inclusion-forming units (IFU). As expected, there was no significant difference in inclusion areas (analysis done by Robert Hayman) (Figure 3B), and there was no difference in the production of progeny IFUs (Figure 3C). Therefore, Cre is efficiently expressed in *C. trachomatis* and does not overtly impact chlamydial development.

**Generation of a markerless *tmeA* mutant.** The Cre-*lox* approach, to create a  $\Delta tmeA$  strain lacking the selection cassette, began by creating a new *tmeA* mutant with *loxP* sites. WT *C. trachomatis* L2 was transformed with pSUmC-*tmeA-lox-gfp-bla*, where *loxP* sites flanked *gfp-bla*, and *tmeA* was targeted for deletion using the FRAEM method, as previously described (163, 170). The resulting mutants of this initial step, containing a floxed *gfp-bla* cassette in place of *tmeA* in the chromosome, were isolated in the presence

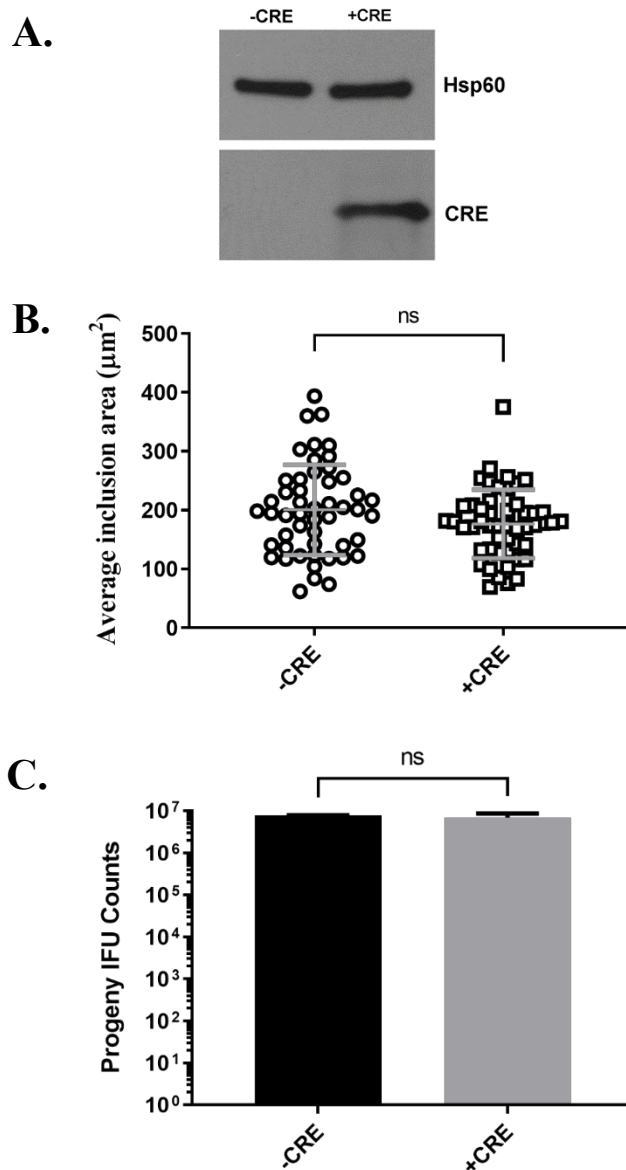


**Figure 3. Cre is expressed in *Chlamydia* spp. and does not impact development.**

HeLa cells were infected for 24 hrs with equivalent IFUs of *C. trachomatis* expressing (+CRE) or lacking (-CRE) pSU-CRE. (A) Whole-culture material was probed in immunoblots with Cre-specific antibodies or anti-Hsp60 as the loading control and visualized via chemiluminescence. (B) Cultures were methanol fixed and stained for inclusion visualization using indirect immunofluorescence. Areas of 50 representative inclusions were measured and plotted individually, with the means  $\pm$  one standard deviation shown. (C) Primary cultures were harvested, and progeny *Chlamydia* spp. were enumerated after secondary passage onto fresh HeLa cells. Error bars represent one standard deviation. Statistical significance was addressed using a Student's t-test with Welch's correction.

of rifampin (Rif) to select Rif-resistant chlamydiae, and a clonal strain was derived by limiting dilution. This clonal population of L2<sup>Rif</sup> *tmeA-lx-gfp-bla* served as the progenitor strain for downstream genome editing (Figure 4A). I was unable to transform this strain with pSU-CRE after several attempts; therefore, lateral gene transfer (LGT) (performed by Dr. Fields) was leveraged to mobilize pSU-CRE from L2-pSU-CRE to L2<sup>Rif</sup> *tmeA-lx-gfp-bla* by co-infecting and selecting for red and green inclusions that were resistant to Rif, penicillin G (PenG), and spectinomycin (Spec). Cultures were maintained in the presence of anhydrotetracycline (aTc) to promote retention of the pSU-CRE vector, and PenG selection was removed to allow loss of the cassette. Red-only inclusions were observed after one passage suggesting successful excision of the *gfp-bla* cassette. This process yields a mixed population of mutants (lacking or still containing the *gfp-bla* cassette); thus, Rif- and Spec-resistant red-only bacterial were clonally isolated by limiting dilution. The isolated bacteria were then cultivated for multiple passages without Spec selection and aTc to promote the curing of the pSU-Cre plasmid. This process resulted in non-fluorescent mutant bacteria, which were again clonally isolated by limiting dilution and termed L2R<sup>Rif</sup>  $\Delta$ *tmeA-lx*. A common phenomenon when cultivating pSUMC transformed *C. trachomatis* for multiple passages is that the endogenous pL2 plasmid is cured (163). PCR analysis (not shown) confirmed that the isolated L2R<sup>Rif</sup>  $\Delta$ *tmeA-lx* non-fluorescent strain had been cured of the pL2 plasmid. Because the pL2 plasmid is required for chlamydial fitness, LGT was again utilized to reintroduce the pL2 plasmid by coinfecting WT L2 with L2R<sup>Rif</sup>  $\Delta$ *tmeA-lx* and selecting for Rif resistance. This strategy yielded L2R<sup>Rif</sup>  $\Delta$ *tmeA-lx*, and qPCR analysis confirmed that the levels of pL2 plasmid were comparable to the WT, indicating successful restoration of the endogenous plasmid (Figure 4B).

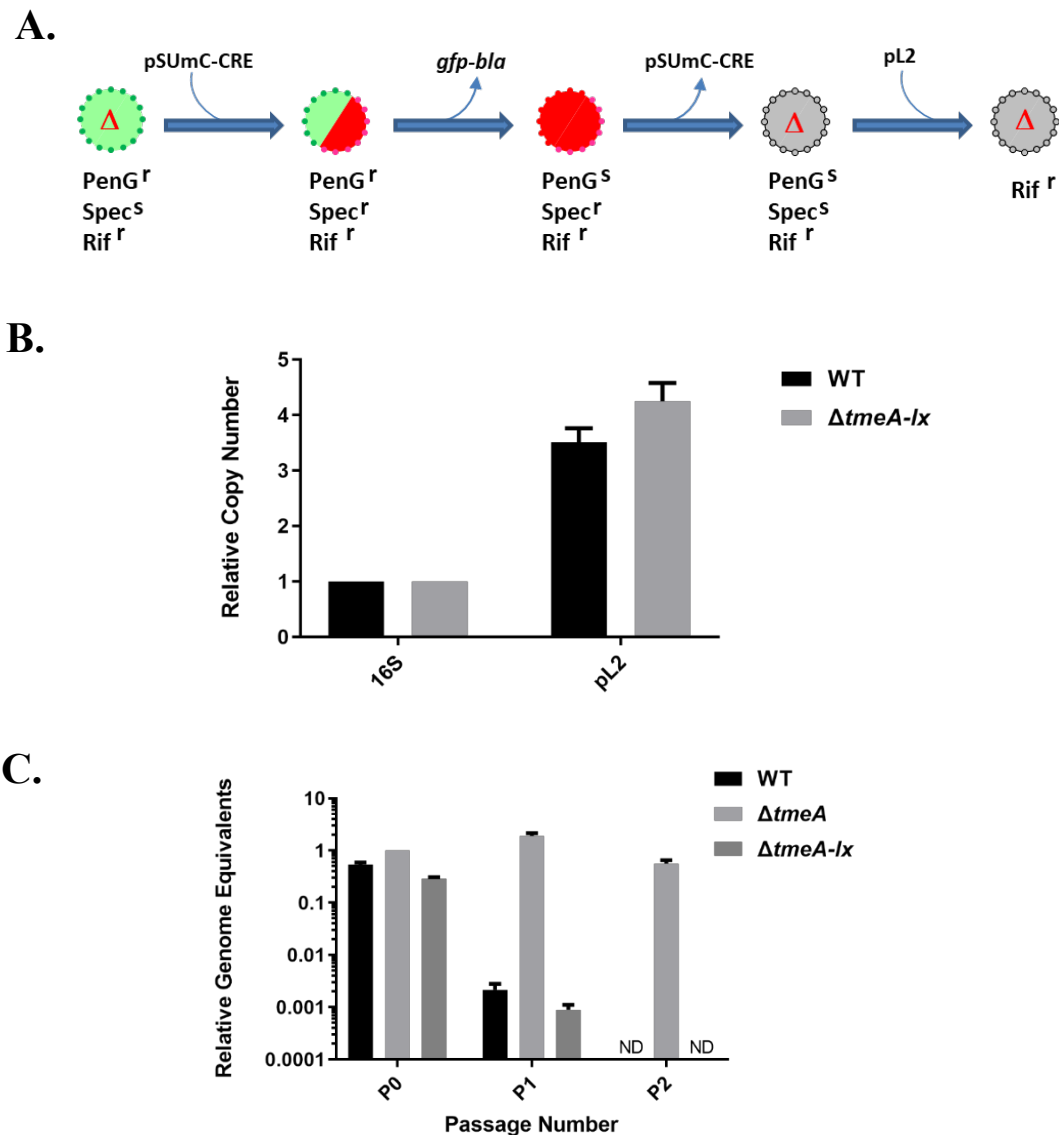


**Figure 4. Construction of a markerless *C. trachomatis tmeA* mutant.**

(A) Schematic representation of the strategy used to create a markerless *tmeA* mutant. Each intermediate is depicted with fluorescent qualities (green, GFP<sup>+</sup>; red, mCherry<sup>+</sup>; gray, no fluorescence) and antibiotic sensitivities (PenG<sup>r</sup>, penicillin G resistant; PenG<sup>s</sup>, penicillin-susceptible; Rif<sup>r</sup>, rifampin-resistant; Spec<sup>s</sup>, spectinomycin-susceptible; Spec<sup>r</sup>, spectinomycin-resistant). (B) qPCR-based comparison of endogenous pL2 (plasmid) copy number in WT or  $\Delta tmeA-lx$  mutant chlamydiae relative to chlamydial 16S rRNA. DNA was harvested from infected McCoy cells at 24 hpi. (C) McCoy cell cultures were infected with equal IFUs of WT,  $\Delta tmeA$ , or  $\Delta tmeA-lx$  and serially passaged every 24 hrs in media containing PenG. At each passage, DNA was harvested for quantitative real-time PCR to determine genome equivalents based on chlamydial 16S rRNA.

Sensitivity to PenG was assayed as an indicator for the loss of the *gfp-bla* cassette (Figure 4C). *C. trachomatis* infected HeLa cultures were grown in antibiotic-supplemented media, and *C. trachomatis* genomes were enumerated by detecting chlamydial 16S via quantitative PCR (qPCR) over three passages. In contrast to  $\Delta tmeA$  (retaining *gfp-bla* cassette), the WT and  $\Delta tmeA-lx$  genome levels dropped below detection by the third passage in the presence of PenG. Overall, these data support that our strategy resulted in the generation of a markerless *tmeA* deletion strain.

Next, I directly focused on the *tmeA* locus to verify that Cre-*lox* genome editing occurred by our design. Genomic DNA was harvested from *C. trachomatis* WT,  $\Delta tmeA$ , or  $\Delta tmeA-lx$  infected HeLa cultures 24 hpi. PCR amplicons using primers flanking the *tmeA* locus should yield a 2.1 kb reduction, compared to  $\Delta tmeA$  if the *gfp-bla* cassette was successfully removed. The amplicons from WT and  $\Delta tmeA$  migrated as expected at 1.4 and 2.9 kb, respectively, while the amplicon from  $\Delta tmeA-lx$  migrated at approximately 0.5 kb indicating the loss of the cassette (Figure 5A). Amplicons for *tmeA* and *tmeB* were also detected by qPCR and confirmed the absence of *tmeA* and retention of *tmeB* in  $\Delta tmeA-lx$  (Figure 5B). A *gfp*-specific signal was only detected for the  $\Delta tmeA-polar$  strain, and a *cre*-specific signal was not detected for any of the strains. These data confirm the complete loss of both the *gfp-bla* selection cassette and *cre* in the isolated  $\Delta tmeA-lx$  mutant.

Furthermore, the locus was directly sequenced and revealed a single *loxP* scar sequence immediately following the *tmeA* start codon and prior to the stop codon (Figure 5C). The intervening upstream region of *tmeB* and the GTG start codon were not disrupted.

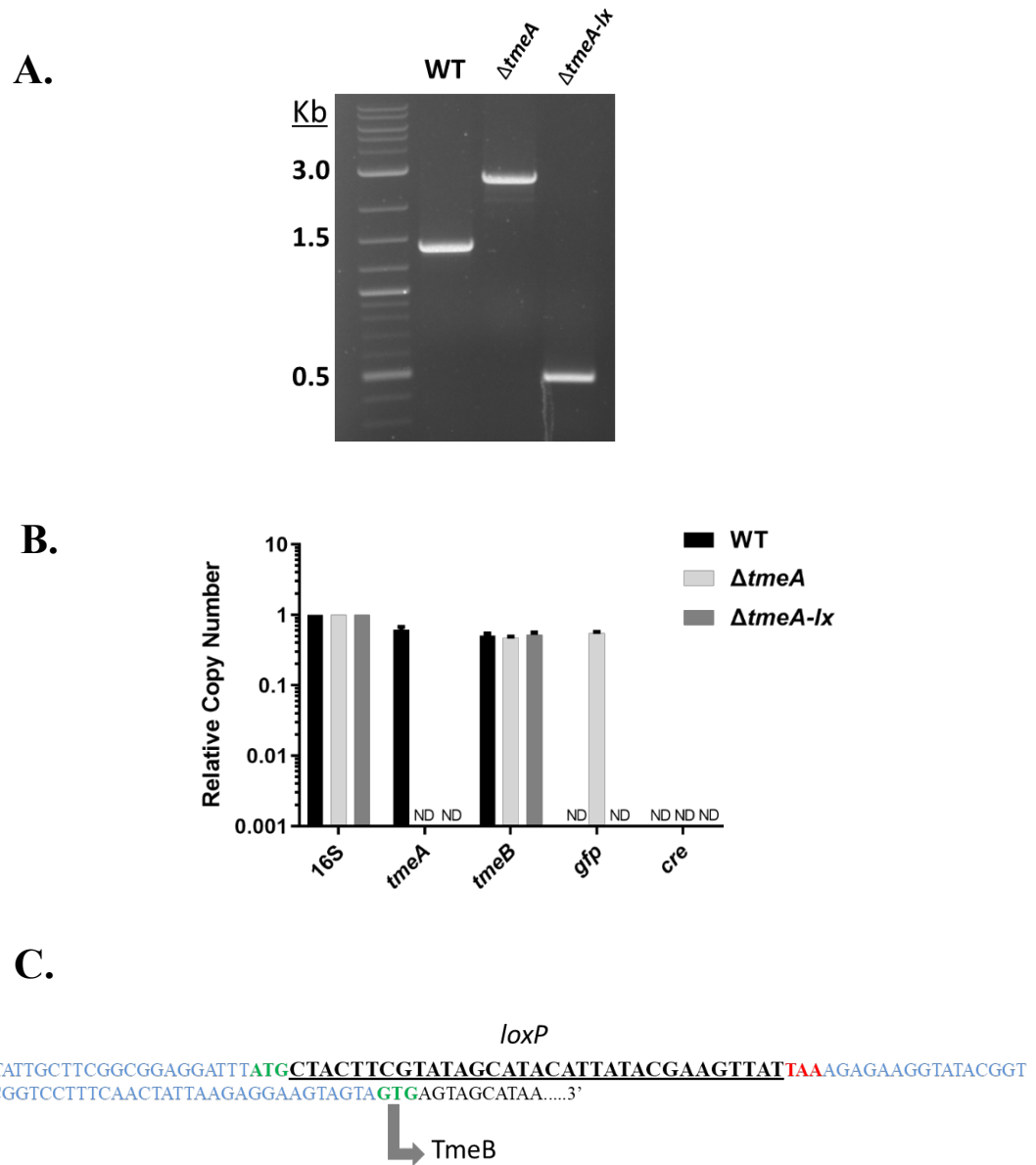


**Figure 5. Direct evidence of *gfp-bla* excision.**

(A) Excision of the reporter cassette confirmed by PCR by amplifying the *tmeA* locus with primers in the surrounding upstream and downstream regions. Products are shown resolved in a 1.0% agarose gel. (B) McCoy cells infected with equal IFUs of *C. trachomatis* WT,  $\Delta tmeA$ , or  $\Delta tmeA-lx$  were harvested at 24 hpi, and DNA was extracted for qPCR. Relative copy numbers for *tmeA*, *tmeB*, *gfp*, and *cre* were assessed by signal normalized to chlamydial 16S rRNA. ND, none detected. (C) The sequenced *tmeAB* locus from  $\Delta tmeA-lx$  indicating the remaining *loxP* scar sequence (underlined). Flanking DNA appears in blue, while start codons are in green, and the TmeA stop is highlighted in red. The noncanonical start codon for TmeB is also depicted.

In aggregate, these data support that the Cre-*lox* genome editing strategy was targeted and effective in creating the markerless *C. trachomatis*  $\Delta tmeA$ -*lx* strain.

**Excision of the *gfp-bla* cassette reverses polar disruption of *tmeB* expression.**

Having confirmed the successful removal of the *gfp-bla* selection cassette, I next wanted to determine whether this method alleviated the polar effects on *tmeB* expression. RNA and protein were extracted from infected HeLa cultures 24 hpi to examine *tmeB*-specific products. RNA levels were enumerated by quantitative reverse transcriptase PCR (qRT-PCR) and normalized to *rpoD* levels, a *C. trachomatis* housekeeping gene (Figure 6A). Similar levels of *tmeA*- and *tmeB*-specific amplicons were detected in WT infected cultures, whereas no signal was detected for *tmeA* and *tmeB* in the respective null mutant strains. As expected, the  $\Delta tmeA$  mutant containing the *gfp-bla* cassette had reduced *tmeB* signal; however, the newly isolated  $\Delta tmeA$ -*lx* mutant had restored levels of *tmeB*; thus, the *loxP* scar sequence did not inhibit *tmeB* expression. Previous work has indicated that *ct696*, located downstream of the *tmeA* operon, is independently transcribed and was included as an additional downstream control (139). Message levels for *ct696* were comparable to WT for all tested strains.

Protein levels, detected by western blot using TmeA and TmeB specific antibodies, were consistent with qRT-PCR results (Figure 6B). TmeB was not detected in lysates from  $\Delta tmeA$  cultures but was present in  $\Delta tmeA$ -*lx* cultures. Interestingly, TmeB appeared to be more abundant in the  $\Delta tmeA$ -*lx* and *tmeA* trans-complemented strains as compared to WT.

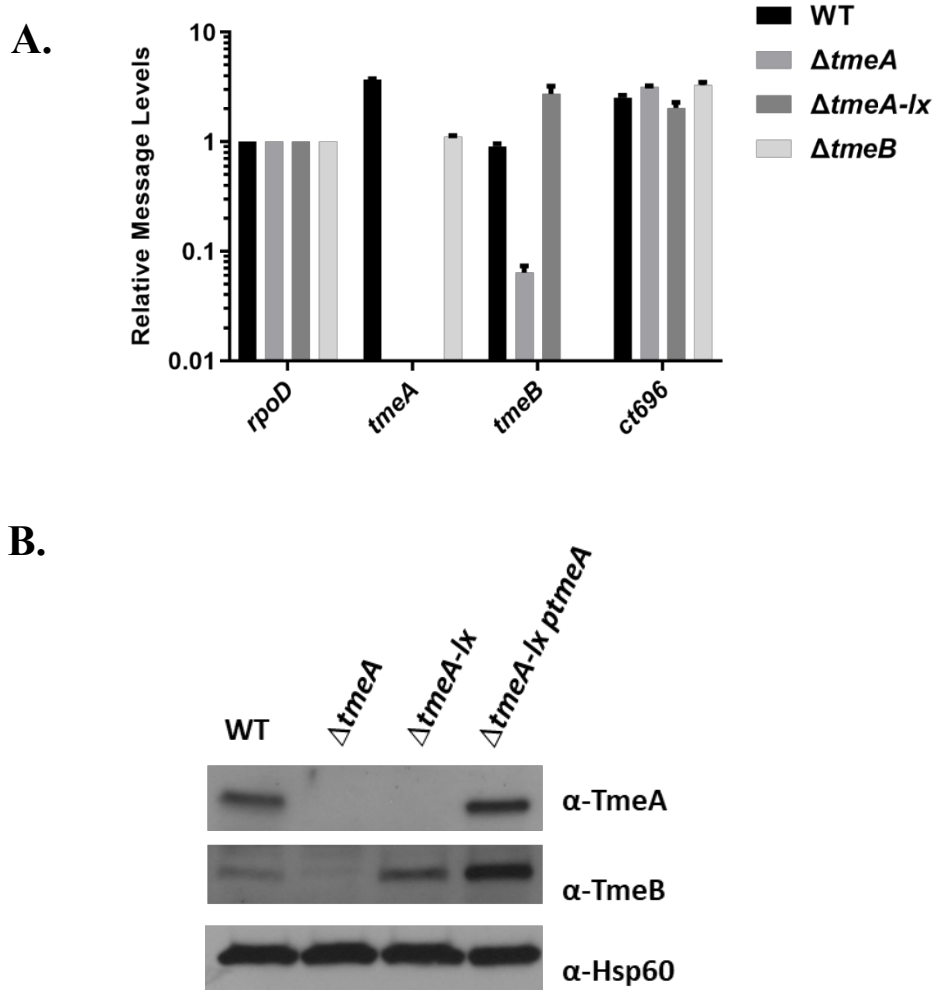


**Figure 6. Removal of the reporter cassette relieves polar effects on *tmeB*.**

(A) The presence of transcripts downstream of *tmeA* was determined by reverse transcriptase (RT) quantitative PCR. Total RNA was isolated at 24 hpi from McCoy cells infected at an MOI of 1 with WT,  $\Delta tmeA$ ,  $\Delta tmeB$ , or  $\Delta tmeA-lx$ . Transcripts for *tmeA*, *tmeB*, and *ct696* were detected by qRT-PCR, and signals are presented after normalization to *rpoD*. ND, none detected. (B) Equal quantities of whole-culture material from 24-h cultures infected with equal IFUs of WT,  $\Delta tmeA$ ,  $\Delta tmeA-lx$ , or  $\Delta tmeA-lxptmeA$  were probed in immunoblots for TmeA and TmeB. Hsp60 was used as a loading control, and proteins were visualized by chemiluminescence.

### 3.4. Discussion

An obligate intracellular existence presents obvious barriers to direct genetic manipulation of bacteria. As with *Coxiella*, *Anaplasma*, and *Ehrlichia* spp., the addition of a biphasic developmental cycle has further complicated progress in *Chlamydia* spp. (186). The ability to transform *Chlamydia* spp. with a stably maintained shuttle vector has ushered in the ability to inactivate targeted chromosomal genes via insertion with group II introns or complete gene deletion using FRAEM (154). Both processes require integrating a selectable marker to recover desired strains due to the numerical confines imposed by the requirement of host cell culture and low-frequency mutagenic events. These insertion elements can disrupt the processivity of RNA polymerase and translating ribosomes, thereby impacting *the expression* of downstream genes. Insertion-induced disruption to downstream genes is an important issue given the propensity of bacteria to have genes organized in polycistronic operons (187). While promoter and operon structures have not been well characterized in *Chlamydia* spp. (188), transcriptome studies indicate the presence of polycistronic messages. Deep sequencing of the *C. trachomatis* L2b transcriptome was not sufficient to identify all transcription start sites (189), yet at least 246 polycistronic transcripts were detected using a similar approach with closely related *Chlamydia pneumoniae* (190). Therefore, overcoming the possibility of polar effects in applying current gene inactivation technologies in *Chlamydia* spp. is a valuable tool.

*C. trachomatis tmeA* and *tmeB* represent invasion-related T3SEs cotranscribed as a bicistronic operon (139). TmeB levels were significantly reduced when *tmeA* was replaced with a *gfp-bla* cassette via FRAEM (163), raising the possibility of cassette-dependent polar inactivation. In this study, an approach that sequentially couples FRAEM-mediated

gene deletion with Cre-*lox*-mediated excision of the resulting selection cassette was created. This approach was applied successfully to generate a markerless deletion of *tmeA* that did not negatively impact *tmeB* expression. Although the Cre-*lox* system has been used in *Coxiella* spp. with a two-step gene deletion strategy, mutagenesis was accomplished with the benefit of an axenic medium, and the resulting deletion strains retained a drug resistance cassette (185). This work represents the first application of Cre-*lox* technology for markerless gene deletion in an obligate intracellular bacterium during host cell infection.

Cre recombinase mediates the conversion of bacteriophage P1 dimers to monomers through recognition and binding to 34 bp direct repeats termed *loxP* sites (191). The Cre-*lox* system has been adapted to successfully manipulate a wide diversity of genomes, including removing selection markers from bacteria (192). Cre must be present and active to remove the floxed selection cassette and then be eliminated from the bacteria. One strategy developed for *Mycoplasma* spp. relied on conditional expression of Cre using a tet-inducible promoter (193). Cre was encoded within the selection cassette such that it was lost in tandem with the excision event. Notably, the *loxP* scar sequence that remains after marker excision has not been observed to exert adverse effects on downstream genes (185, 194). FLAEM relies on the expression of Cre in *C. trachomatis* using the conditionally replicating pSUMC plasmid (170). Cre is constitutively expressed from pSU-CRE via a *blaM* promoter, and the plasmid is maintained via selection with Spec and aTc to induce the expression of *pgp6*. The backbone of the plasmid also encodes *mCherry* as a fluorescence marker. Given the labor-intensive requirements for genetically manipulating *C. trachomatis*, the first step of this study was to ensure that the pSU-CRE-encoded

recombinase was active in *E. coli* and adequately expressed in WT *C. trachomatis* without interfering with development.

Generation of a markerless deletion mutant began with a *Chlamydia* strain where *tmeA* had been replaced with a *gfp-bla* cassette flanked by *loxP* sites. pSU-CRE was then mobilized into this strain. Neither Dr. Fields nor I are sure why the strain could not be transformed with pSU-CRE using the conventional CaCl<sub>2</sub> method, but we suspect general low transformation efficiency in *Chlamydia* may be the culprit. LGT can be efficiently leveraged to mobilize engineered plasmids among chlamydial strains. The exchange of genomic DNA via LGT occurs at a frequency of 10<sup>-3</sup> to 10<sup>-4</sup> (195), yet plasmid DNA can be transferred 10- to 100-fold more efficiently (Ken Fields, data not shown). A spontaneous Rif-resistant strain, L2<sup>Rif</sup>  $\Delta$ *tmeA-gfp-bla*, was generated to allow selective recovery after coinfection with L2 pSU-CRE. Experiments in *E. coli* (Figure 2) were consistent with Cre-mediated excision of the marker cassette being highly efficient, which was important since there was no selective pressure for excision of the cassette in *C. trachomatis*. Although there was no selection to recover markerless mutants, we leveraged the fluorescence reporting of our constructs to monitor excision and recover appropriate strains. Indeed, I could readily visualize a minor population of red-only inclusions after a single passage of L2<sup>Rif</sup>  $\Delta$ *tmeA-gfp-bla* and pSU-CRE co-infection. Consistent with previous observations, selective maintenance of an engineered plasmid in *C. trachomatis* results in the eventual loss of endogenous pL2 during this process (163). Therefore, LGT was leveraged a second time to restore endogenous pL2 after curing pSU-CRE. The final strain, L2<sup>Rif</sup>  $\Delta$ *tmeA-lx*, was isolated and will be described phenotypically in subsequent chapters.

Overall, these data are consistent with the marker cassette exerting a polar effect on *tmeB* in L2  $\Delta tmeA$  that was alleviated by excision of the *gfp-bla* cassette. Both message and protein levels for *tmeB* were decreased relative to the WT in L2  $\Delta tmeA$ , raising the possibility that the presence of *gfp-bla* interfered with mRNA stability or translation. These data also provide proof of concept that Cre-*lox*-mediated recombination is an effective technique for manipulation of the chlamydial genome. Due to limitations imposed by host cell culture and genetic manipulation of *Chlamydia* spp., this method is somewhat laborious. It is perhaps most appropriate for instances when operon-localized genes are targeted for inactivation. Other applications are possible as well. Alternative antibiotic resistance genes have been used to sequentially engineer a chlamydial strain harboring two inactivated genes (143). Given the limited number of effective antibiotics available for positive selection in *Chlamydia* spp., the Cre-*lox* system could be exploited as a mechanism to generate multigene mutant strains. Group II introns have been widely used to disrupt chlamydial genes (154), and Cre-*lox* has been used to excise group II introns in other bacteria (192). However, the lack of a fluorescence reporter in group II introns would likely complicate strain recovery for *Chlamydia* species. Cre-*lox* is, therefore, most appropriate for use with FRAEM. Based on the wide variety of manipulations that have been accomplished in other genomes, it is also possible that more generalized engineering of the *C. trachomatis* chromosome can be performed using Cre-*lox*. Inversions, insertions, and gene deletions may become possible as the chlamydial system becomes more tractable.

## CHAPTER 4: Non-physiological Levels of TmeB Impacts Intracellular *C. trachomatis* Development

Parts of this chapter have been previously published in, “Keb G, Hayman R, and Fields KA. (2018). Floxed-Cassette Allelic Exchange Mutagenesis Enables Markerless Gene Deletion in *Chlamydia trachomatis* and Can Reverse Cassette-Induced Polar Effects. *Journal of Bacteriology*, 200(24), e00479-18. PMID: 30224436”

Contributions: Dr. Ken Fields performed the percent invasion assays. Dr. Kate Wolf generated the pSUMC construct used to delete the *tmeA/B* operon and transformed *C. trachomatis* to yield the L2 $\Delta$ *tmeA/B-gfp-aadA* strain. Dr. Ken Fields transformed L2 $\Delta$ *tmeA/B-gfp-aadA* with pSU-Cre-bla and developed the L2 $\Delta$ *tmeA/B* double mutant strain. Maria Clouse generated the pCompTmeA/TmeB construct and transformed *C. trachomatis*. I conducted all other experiments.

### 4.1. Summary

The goal of the work presented here was to determine if the FLAEM-generated *C. trachomatis*  $\Delta$ *tmeA-lx* strain manifests the same invasion defect as was previously observed for the  $\Delta$ *tmeA* strain, which contained the FRAEM selection cassette and had decreased expression of *tmeB*. This study found that the “non-polar” *C. trachomatis*  $\Delta$ *tmeA-lx* strain had reduced fitness compared to  $\Delta$ *tmeA* and that non-physiological levels of TmeB impact chlamydial development. FLAEM mutagenesis was also utilized to generate one of the first

markerless double deletion mutants in *C. trachomatis*. This strain was used to further investigate the contributions of TmeA and TmeB during *C. trachomatis* development.

#### 4.2. Introduction:

Invasion of bacteria into non-phagocytic cells requires considerable reorganization of the actin cytoskeleton. *C. trachomatis* hijacks host actin polymerization pathways by secreting effectors into the host cytosol through a T3SS. For example, *C. trachomatis* secretes the effector TarP to nucleate actin directly. TarP is secreted during invasion and shares the chaperone, Slc1, with *C. trachomatis* TmeA and TmeB. Previous studies have shown that TmeA is important for *C. trachomatis* invasion into host cells and plays a role during infection of a mammalian host (143). Initial investigations into the function of TmeA were complicated because the *C. trachomatis*  $\Delta tmeA$  deletion strain had cassette-induced decreased expression of the downstream gene *tmeB*. My collaborators and I generated the  $\Delta tmeA-lx$  strain using the Cre-*loxP* system to remove the *gfp-bla* selection cassette, which restores expression of *tmeB* (Chapter 3), although the abundance of TmeB was increased to non-physiological levels.

This chapter aimed to investigate whether the newly generated  $\Delta tmeA-lx$  strain maintained similar phenotypes to  $\Delta tmeA$  and further explore the contributions of TmeA and TmeB on *C. trachomatis* invasion and intracellular development. While investigating the developmental phenotypes of  $\Delta tmeA-lx$ , I found that increased expression of TmeB negatively impacts *C. trachomatis* invasion and development. Furthermore, I present data that supports the absence of TmeB improves *C. trachomatis* ability to produce infectious

progeny and spread cell-to-cell in plaquing assays compared to WT strains. These findings are novel since previous studies have suggested that TmeB is dispensable for efficiently producing infectious progeny (143). Collectively, the data presented here also support the hypothesis that TmeA and TmeB are functionally related and have antagonistic functions.

#### 4.3. Results:

**Rif resistance does not impact chlamydial development.** Previous studies have shown that the elimination of *tmeA* manifests as a defect in invasion efficiency that correlates with a reduction in inclusion numbers in primary and secondary cultures (143). Since this strain also lacked TmeB, studies could not formally exclude the possibility that the loss of TmeB contributed to the observed phenotypes. With the newly generated L2<sup>Rif</sup> $\Delta$ *tmeA-lx* strain ( $\Delta$ *tmeA-lx*), I wanted to compare the infectivity and developmental phenotypes of  $\Delta$ *tmeA-lx* to WT and determine if the absence of *tmeA* still manifests as an infectivity defect.

To ensure valid phenotypic comparisons, I utilized a Rif-resistant WT strain (WT<sup>Rif</sup>, generated by K. Fields) and produced a WT<sup>Rif</sup> strain containing empty vector pCompAII (WT+pCompAII) using CaCl<sub>2</sub> transformation. To determine if the Rif resistant background impacted *C. trachomatis* development, HeLa cells were infected with *C. trachomatis* WT, WT<sup>Rif</sup>, or WT<sup>Rif</sup>+pCompAII (Figure 7). At time points corresponding to *C. trachomatis* early-(1 & 6 hpi), mid-(12 hpi), and late-(24 & 48 hpi) cycle development, cultures were harvested for infectious progeny and passaged onto fresh HeLa monolayers.

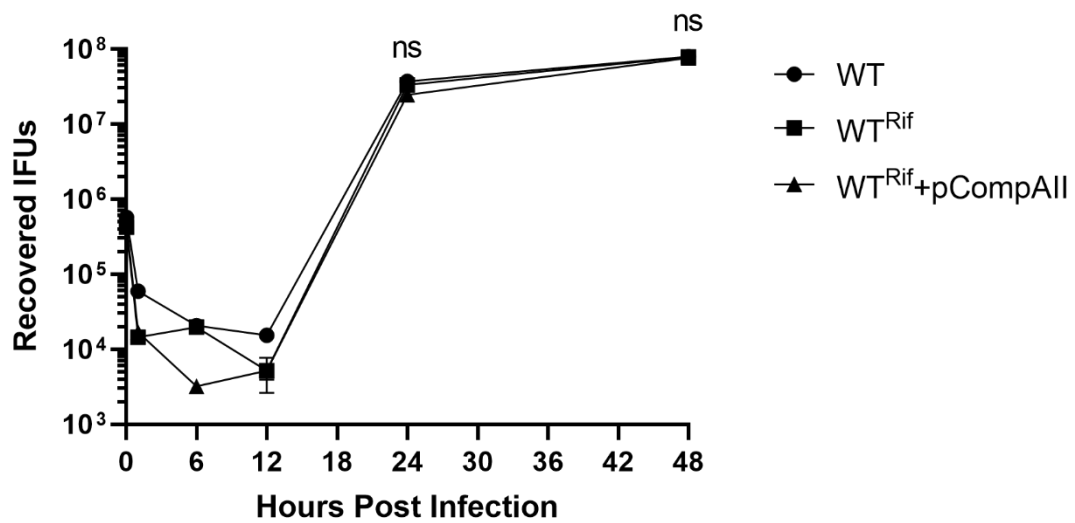


**Figure 7. Rif resistance does not negatively affect *C. trachomatis* L2 development.**

HeLa cultures were infected in triplicate with equal inclusion forming units (IFUs) of WT, WT<sup>Rif</sup>, or WT<sup>Rif</sup>+pCompAll (empty vector) at an MOI of 0.5. Cultures were harvested at 1, 6, 12, 24, and 48 hpi. Then chlamydiae were passaged onto fresh monolayers for enumeration of recovered IFUs by fluorescence staining of chlamydiae in fixed samples. Data are represented by the mean  $\pm$  one standard deviation of triplicate samples. Statistical significance was assessed using a Student's t-test with Welch's correction at times 24 and 48 hpi (ns; not significant).

Inclusions were enumerated by fluorescent staining of fixed cultures. Recovered IFUs were normalized to WT for starting IFUs. During early-cycle development, EBs differentiate into RBs, non-infections, and asynchronously transition back into EBs mid-cycle; thus, it is not unusual that recovered IFUs vary during these time points. By 24 and 48 hpi, there was no significant difference in infectious progeny for WT<sup>Rif</sup> or WT<sup>Rif</sup>+pCompAII compared to WT.

**L2<sup>Rif</sup> $\Delta tmeA$ -lx manifests a developmental defect in tissue culture.** I wanted to directly investigate the infectivity of the  $\Delta tmeA$ -lx strain by quantifying direct IFUs (Figure 8A) and progeny IFUs (Figure 8B). When cultures are infected with particle-normalized infectious EBs, this assay can be used as an indicator of defects during early infection (143). I generated a L2<sup>Rif</sup> $\Delta tmeA$ -lx+pCompAII ( $\Delta tmeA$ -lx+pCompAII) mutant to use as an isogenic control for the L2<sup>Rif</sup> $\Delta tmeA$ -lx+pCompTmeA ( $\Delta tmeA$ -lx+pCompTmeA) mutant. HeLa cell cultures were infected with chlamydial strains normalized for particles (Figure 8A) or IFUs (Figure 8B). Inclusions were enumerated in particle-normalized cultures at 24 hpi, whereas IFU-normalized cultures were harvested and passaged onto fresh cells to enumerate progeny IFUs. In both cases, infection was significantly reduced for the  $\Delta tmeA$ -lx+pCompAII mutant with  $3.45 \times 10^6$  direct IFUs and  $1.39 \times 10^6$  progeny IFUs compared to WT+pCompAII with  $8.91 \times 10^6$  direct IFUs and  $3.79 \times 10^6$  progeny IFUs. This deficiency was reversed by complementation in direct counts; however, restoration of progeny yields was not as robust. These data are consistent with previous findings that TmeA is important for chlamydial development, however, does not rule out the possibility of a TmeB effect.

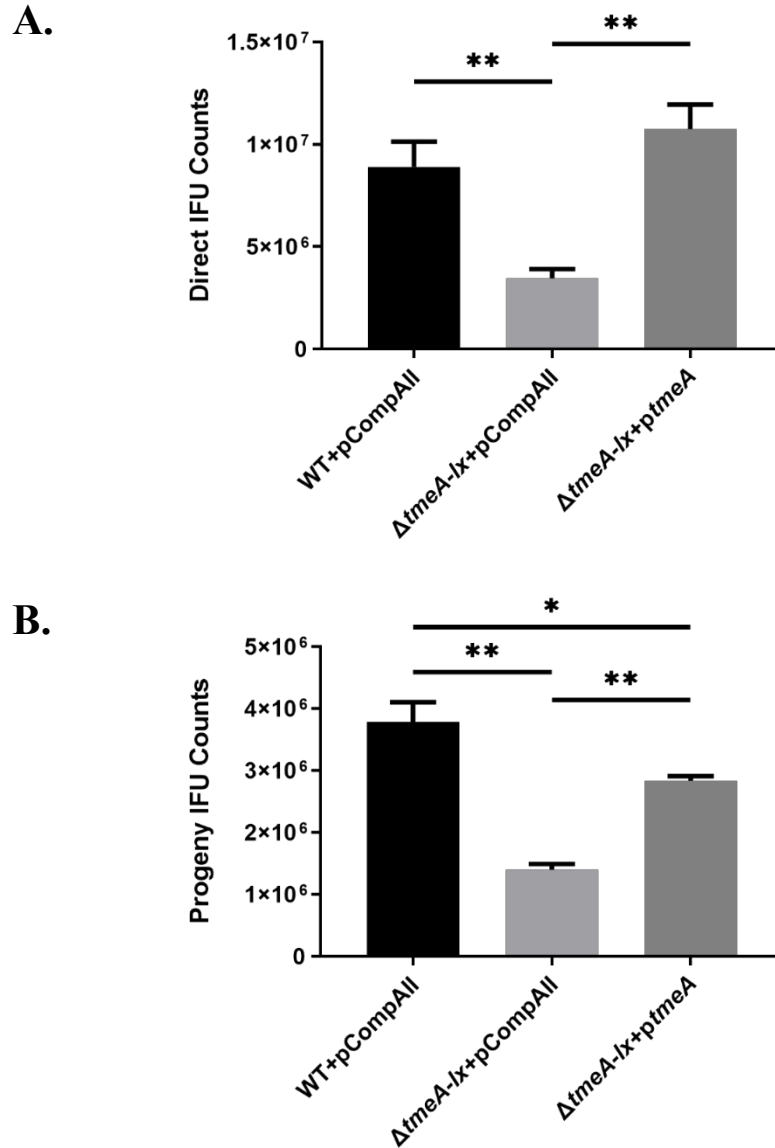


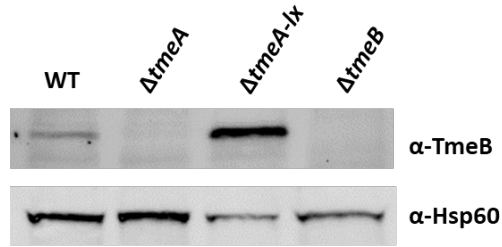
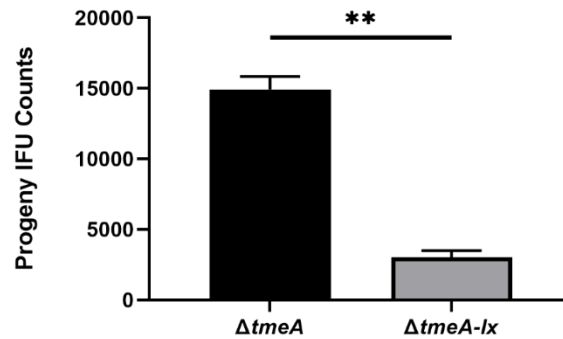
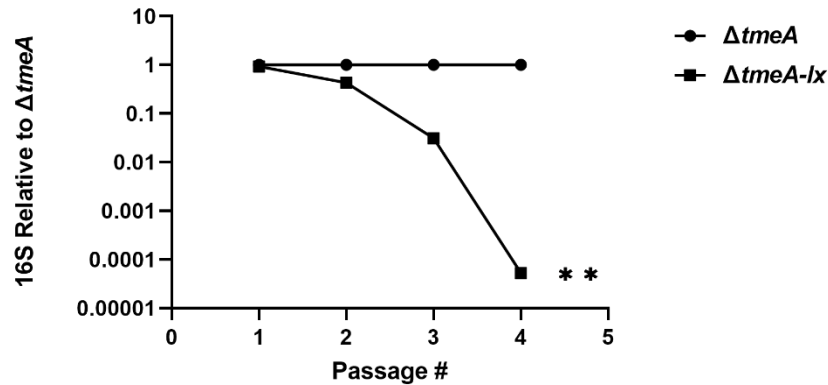
**Figure 8. *C. trachomatis* L2  $\Delta tmeA-lx$  manifests a developmental defect in tissue culture.**

(A) HeLa cultures were infected in triplicate with equal numbers of WT+pCompAll,  $\Delta tmeA-lx$ +pCompAll, or  $\Delta tmeA-lx$ +ptmeA (A) EBs or (B) IFUs to achieve an approximate MOI of 0.1. Cultures were methanol fixed and stained for inclusions (A) or processed for enumeration of progeny IFUs (B) at 24 hpi. All inclusions were enumerated by fluorescence staining of chlamydiae in fixed samples, and data for direct and progeny IFUs counts are represented as mean with error bars at one standard deviation of triplicate samples. A Student's t-test with Welch's correction was used to address significance (\*,  $P < 0.02$ ; \*\*,  $P < 0.005$ ).

Although the  $\Delta tmeA-lx$  strain (non-polar) has restored expression of TmeB compared to  $\Delta tmeA$  (polar), TmeB levels appear to be more abundant in  $\Delta tmeA-lx$  compared to WT when detected via immunoblot (Figure 9A). I wanted to investigate whether this increase affected  $\Delta tmeA-lx$  development compared to  $\Delta tmeA$ . I started by comparing the ability of either strain to produce infectious progeny (Figure 9B). HeLa cell cultures were infected with equal IFUs, then harvested 24 hpi and passaged onto fresh monolayers. IFUs were fluorescently stained in fixed cultures and enumerated. The  $\Delta tmeA-lx$  strain produced significantly fewer IFUs ( $3.02 \times 10^3$  IFUs) as compared to  $\Delta tmeA$  ( $1.49 \times 10^4$  IFUs). To better observe this phenotype, I quantified progeny genomes for each strain from infected cultures across several passages by qPCR (Figure 9C). The  $\Delta tmeA-lx$  strain had significantly fewer genomes after as few as three passages. Together these data indicate *C. trachomatis*  $\Delta tmeA-lx$  are more attenuated compared to WT.

**Overexpression of *tmeB* negatively impacts *C. trachomatis* development.** To further examine the effect of non-physiological levels of TmeB and determine if TmeB levels contributed to the decreased fitness of the  $\Delta tmeA-lx$  strain, I generated *C. trachomatis* WT and  $\Delta tmeB$  strains that expressed *tmeB* under its native promoter using the pCompAII vector (pTmeB) and CaCl<sub>2</sub> transformation. The increased expression of TmeB in WT+pTmeB and  $\Delta tmeB$ +pTmeB strains was confirmed by immunoblot with TmeB-specific antibodies (Figure 10A). Both WT+pTmeB and  $\Delta tmeB$ +pTmeB had increased TmeB-specific signal compared to WT, whereas no signal was detected for  $\Delta tmeB$ .

Progeny IFUs were then enumerated from HeLa cultures infected with WT+pCompAII, WT+pTmeB,  $\Delta tmeB$ +pCompAII, and  $\Delta tmeB$ +pTmeB (Figure 10B).

**A.****B.****C.**

**Figure 9. *C. trachomatis* L2  $\Delta tmeA-lx$  manifests a greater developmental defect in tissue culture as compared to  $\Delta tmeA$ .**

(A) Equal quantities of whole-culture material from 24 hr cultures infected with equal IFUs of WT,  $\Delta tmeA$ ,  $\Delta tmeA-lx$ , or  $\Delta tmeB$  were probed in immunoblots with TmeB-specific antibody. Hsp60 was used as a chlamydial loading control, and proteins were visualized by chemiluminescence. (B & C) HeLa cultures were infected in triplicate with equal IFUs of  $\Delta tmeA$  or  $\Delta tmeA-lx$  to achieve an approximate MOI of 0.1. (B) Cultures were methanol fixed and stained for chlamydiae 24 hpi. Progeny IFUs are represented as mean with error bars at one standard deviation of triplicate samples. A Student's t-test with Welch's correction was used to address significance (\*\*,  $P < 0.005$ ). (C) Infected cultures were harvested and passaged onto fresh HeLa monolayers. A portion of harvested material was used for DNA extraction and quantification by qPCR detecting chlamydial 16S from triplicate biological and technical samples. Linear regression was used to address statistical significance (\*\*,  $P < 0.005$ ).

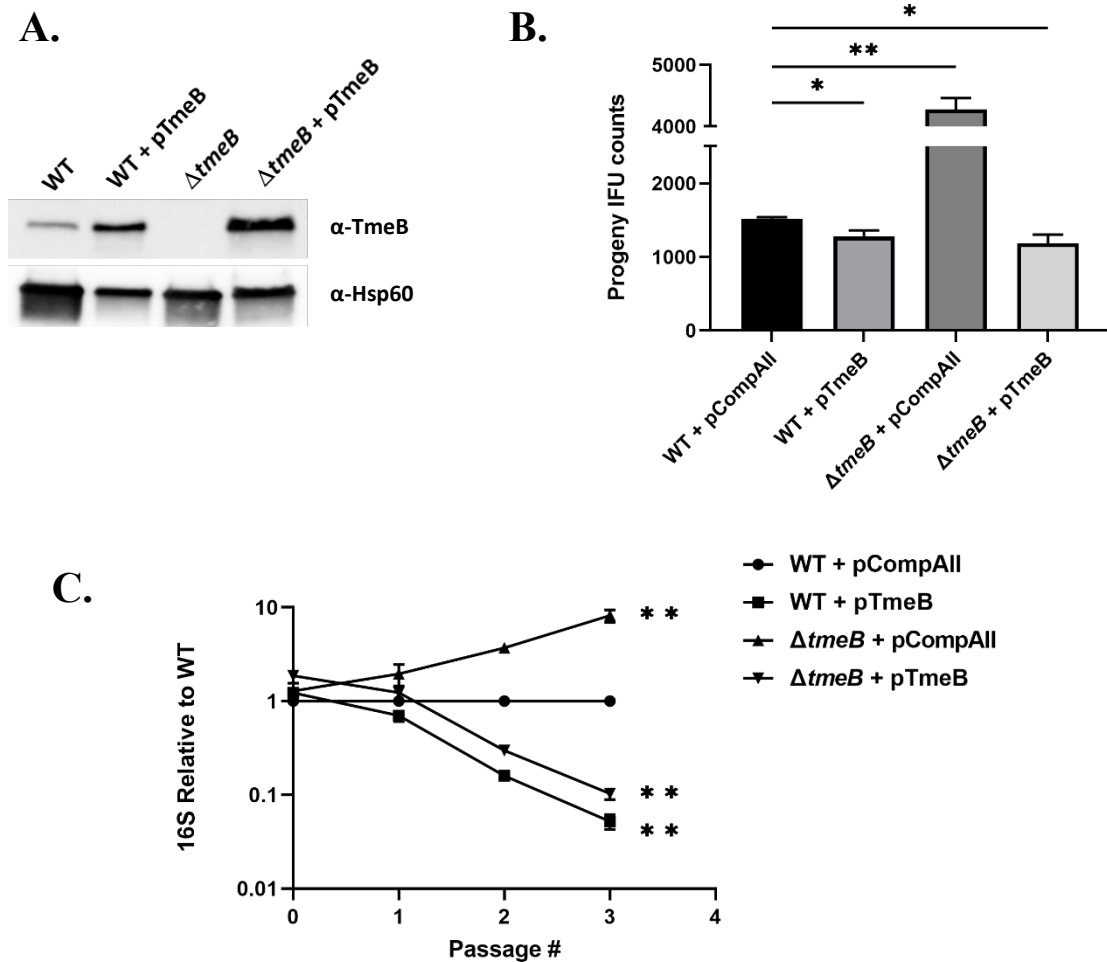


**Figure 10. Overexpression of *tmeB* negatively impacts *C. trachomatis* L2 development.**

(A) Equal quantities of material harvested from WT+pCompAll, WT+pTmeB,  $\Delta tmeB$ , or  $\Delta tmeB$ +pTmeB density gradient purified EBs were probed in immunoblots with TmeB-specific antibody. Hsp60 was used as a chlamydial loading control, and proteins were visualized by chemiluminescence. (B & C) HeLa cultures were infected in triplicate with equal IFUs of *C. trachomatis* L2 WT+pCompAll, WT+pTmeB,  $\Delta tmeB$ +pCompAll, or  $\Delta tmeB$ +pTmeB to achieve an approximate MOI of 0.1. (B) Cultures were harvested for enumeration of progeny IFUs at 24 hpi. All inclusions were enumerated by fluorescent staining of chlamydiae in fixed samples, and data are represented as mean with error bars at one standard deviation of triplicate samples. A Student's t-test with Welch's correction was used to address significance (\*, P<0.05; \*\*, P<0.005). (C) Infected cultures were harvested and passaged onto fresh HeLa monolayers every 24 hrs. A portion of the harvested material was used for DNA extraction and quantification by qPCR detecting chlamydial 16S. Data are represented by mean fold change  $\pm$  one standard deviation. Linear regression was used to address statistical significance (\*\*, P<0.0001).

Both WT+pTmeB ( $1.29 \times 10^3$  IFUs) and  $\Delta tmeB$ +pTmeB ( $1.19 \times 10^3$  IFUs) strains had fewer progeny IFUs than WT+pCompAII ( $1.52 \times 10^3$  IFUs); however, *C. trachomatis*  $\Delta tmeB$ +pCompAII ( $4.28 \times 10^3$  IFUs) had significantly more infectious progeny than WT+pCompAII. Next, I collected chlamydial genomes for each strain from infected cultures at 24 hpi across multiple passages (Figure 10C). Chlamydial genomes were quantified by detecting 16S via qPCR. Both strains with increased levels of TmeB had significantly fewer genomes after numerous passages compared to WT+pCompAII. Conversely,  $\Delta tmeB$ +pCompAII produced significantly more genomes compared to WT. These data suggest that TmeB levels correlate with increased or decreased *C. trachomatis* fitness for  $\Delta tmeB$ +pCompAII or WT+TmeB and  $\Delta tmeB$ +pTmeB strains, respectively.

**Overexpression of *tmeB* negatively impacts *C. trachomatis* invasion.** Similar to the role of TmeA, one explanation for the TmeB-related fitness may be that TmeB has a role during invasion. Invasion efficiency was directly examined for WT,  $\Delta tmeB$ , and WT+pTmeB strains. Hela monolayers were infected with equal IFUs by rocking at 4 °C to allow chlamydial attachment, then shifted to 37 °C for 30 min to synchronize invasion. Infections were fixed and differentially stained for internalized or extracellular bacteria. There was no difference between *C. trachomatis* WT (79%) and  $\Delta tmeB$  (80%) invasion efficiency (Figure 11A); however, WT+pTmeB had significantly decreased invasion efficiency (36.8%) compared to WT (73.5%) (Figure 11B) indicating the overabundance, but not absence, of TmeB impacts invasion.

***C. trachomatis*  $\Delta tmeB$  form larger plaques compared to WT.** I next investigated the impact of TmeB on overall chlamydial infectivity *in vitro*. I compared the ability of WT,  $\Delta tmeA-lx$ ,  $\Delta tmeA-lx$ +pTmeA,  $\Delta tmeB$ , and  $\Delta tmeB$ +pTmeB to form plaques in Vero

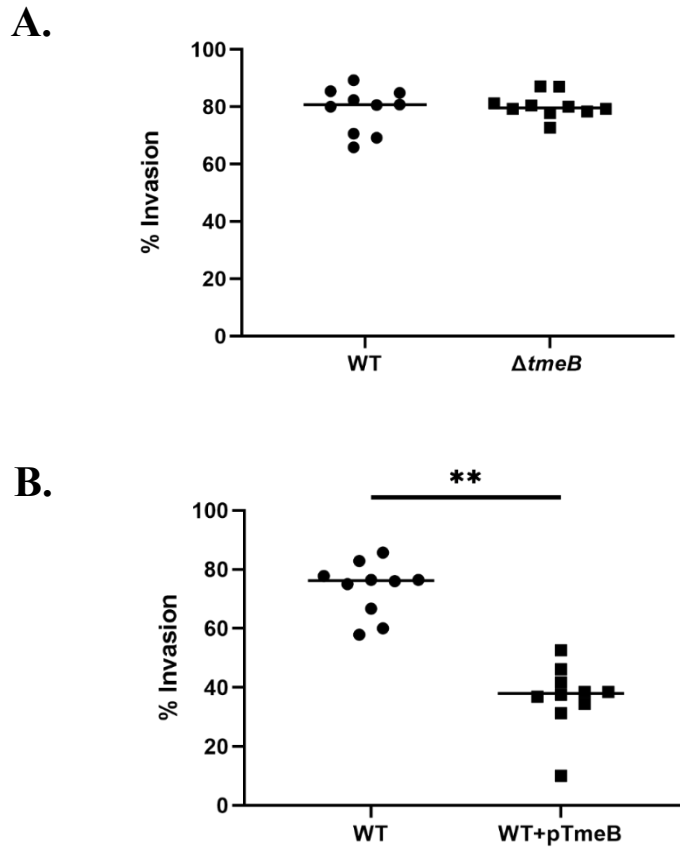


**Figure 11. Increased TmeB levels negatively impact *C. trachomatis* L2 invasion.**

HeLa monolayers were infected for 1 hr at 4 °C with *C. trachomatis* L2 WT and (A)  $\Delta tmeB$  or (B) WT+pTmeB at an MOI of 20. Cultures were shifted to 37 °C for 30 min and then paraformaldehyde-fixed. Inside-out staining was used to determine invasion where external EBs were labeled with MOMP-specific antibodies, and internalized bacteria were labeled using *Chlamydia* LPS-specific antibodies in subsequently permeabilized cultures. Data are represented as the percentage of internalized chlamydiae for 10 fields of view with means represented. Statistical significance was computed using Student's t-test with Welch's correction (\*\*,  $P < 0.0001$ ).

cell monolayers. Cell cultures were infected with equal IFUs and overlaid with an agarose media. In plaquing assays, clearings form in the monolayer from host cell death, and larger clearings are associated with increased infectivity (196). On day 7 post-infection, I stained the monolayers with neutral red solution (Figure 12A) and quantified the area of each plaque (Figure 12B). *C. trachomatis* L2R lacks the native pL2 plasmid rendering it avirulent. This strain was included as a negative control for cell-to-cell spread. Although increased TmeB levels were associated with decreased invasion efficiency, the median area of plaques formed by the  $\Delta tmeA-lx$  strain was 364 au and was similar to the median area of WT plaques at 385 au. The  $\Delta tmeA-lx+pTmeA$  and  $\Delta tmeB+pTmeB$  strains did form slightly smaller plaques compared to WT with median areas of 330 au and 348 au, respectively; however, the  $\Delta tmeB$  strain formed significantly larger plaques with a median area of 541 au.

***C. trachomatis* WT<sup>Rif</sup> outcompetes WT+pTmeB compared to WT.** I also investigated TmeB's impact on chlamydial development using a co-infection assay. I infected HeLa monolayers with equal IFUs of WT<sup>Rif</sup> and WT strains or WT<sup>Rif</sup> and WT+pTmeB strains, each at an MOI of 1 to promote inclusion fusion between the two strains. 24 hpi, I harvested the cultures and enumerated Rif-resistant progeny (Figure 13). When WT<sup>Rif</sup> was co-infected with WT+pTmeB, there were significantly more recovered Rif-resistant progeny than co-infection with WT ( $2.17 \times 10^7$  and  $1.2 \times 10^7$  Rif-resistant IFUs, respectively). These data suggest that *C. trachomatis* WT<sup>Rif</sup> could survive more efficiently with WT+pTmeB than WT, indicating WT<sup>Rif</sup> may outcompete WT+pTmeB better than WT.

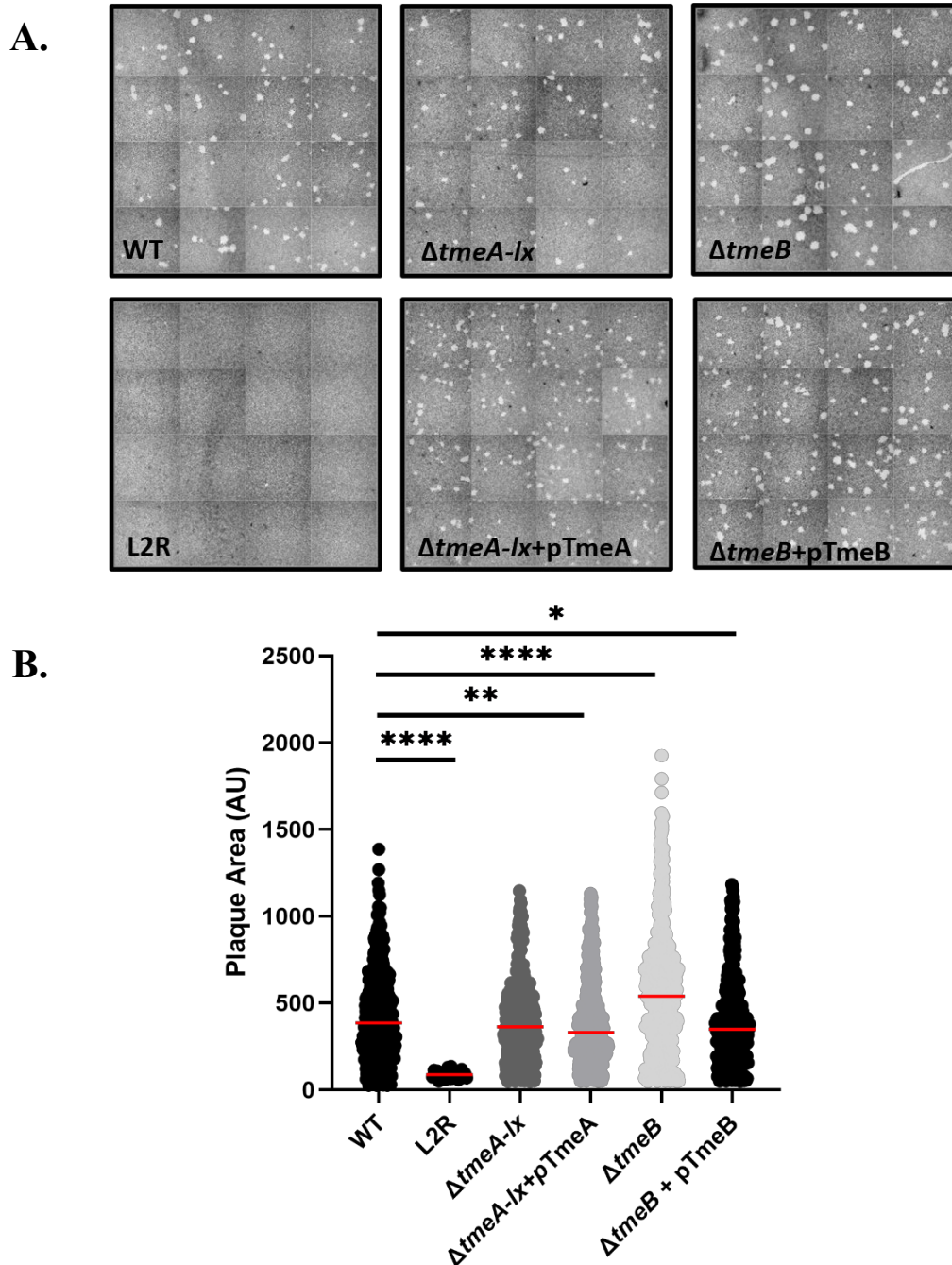


**Figure 12. *C. trachomatis* L2  $\Delta tmeB$  form larger plaques compared to WT.**

(A) Vero cell monolayers were infected with equal IFUs of WT, L2R,  $\Delta tmeA$ ,  $\Delta tmeA+pTmeA$ ,  $\Delta tmeB$ , or  $\Delta tmeB+pTmeB$  in triplicate. The cultures were stained with neutral red 7 days post-infection and imaged by brightfield microscopy. (B) Plaque areas were quantified as arbitrary units (AU) for each strain using Image J analysis software (n=446; L2R, n=25). Medians are represented by red bars. Statistical significance was addressed using a Mann-Whitney U-test (\*, p<0.05; \*\*, p<0.01; \*\*\*\*, p<0.0001) and outliers were removed according to ROUT analysis Q=1%.

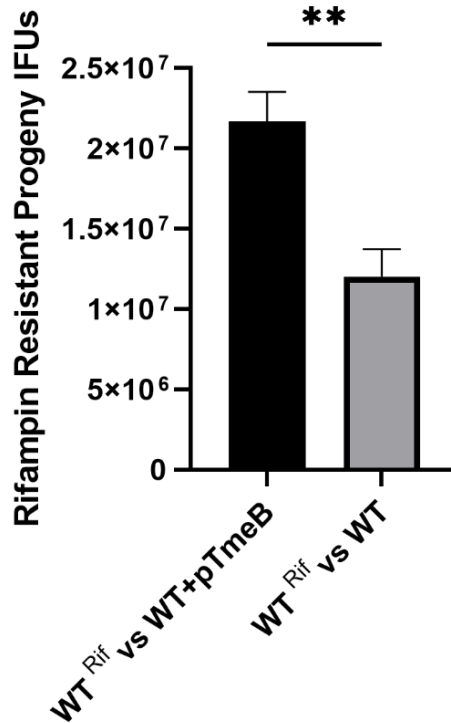


**Figure 13. *C. trachomatis* L2 WT<sup>Rif</sup> outcompetes WT+pTmeB compared to WT.**

HeLa cultures were infected in triplicate at an MOI of 1 for each strain with equal IFUs of WT<sup>Rif</sup> and WT+pTmeB or WT<sup>Rif</sup> and WT. Cultures were harvested 24 hpi and passaged onto fresh monolayers in the presence of rifampin (5 ng/mL). Rifampin-resistant progeny were enumerated by fluorescence staining of chlamydiae in fixed samples. Data are represented as means with error bars at one standard deviation. Statistical analysis was addressed using a Student's t-test with Welch's correction (\*\*, p<0.002).

***C. trachomatis* lacking both *tmeA* and *tmeB* produce a similar amount of infectious progeny as WT.** The lack of TmeA and the over-expression of TmeB are associated with negative chlamydial development phenotypes. I wanted to investigate the impact of deleting both effectors on chlamydial development. Dr. Wolf and Dr. Fields successfully generated a double mutant strain,  $\Delta tmeA/tmeB$ , using FLAEM to target the entire TmeA/B operon for deletion. Immunoblot (Figure 14A) and qPCR (Figure 14B) analysis confirm the absence of TmeA and TmeB in the  $\Delta tmeA/B$  strain. A cross-reactive band is detected at a slightly greater molecular weight than TmeB with TmeB specific antibodies in immunoblots. This band likely represents a HeLa protein and varies in intensity depending on the purity of the EB stock. Next, I compared progeny IFUs for *C. trachomatis* WT,  $\Delta tmeA-lx$ ,  $\Delta tmeB$ , and  $\Delta tmeA/B$  strains (Figure 14C). As previously observed, the  $\Delta tmeA-lx$  ( $1.01 \times 10^5$  IFUs) and  $\Delta tmeB$  ( $3.08 \times 10^6$  IFUs) strains had decreased and increased progeny, respectively, compared to WT ( $1.67 \times 10^6$  IFUs). The  $\Delta tmeA/B$  ( $1.91 \times 10^6$  IFUs) strain had similar progeny as compared to WT.

***C. trachomatis* strains lacking both *tmeA* and *tmeB* or over-expressing *tmeA* and *tmeB* produce fewer progeny genomes than WT.** I quantified genomes across multiple passages to more closely investigate the ability of  $\Delta tmeA/tmeB$  double mutant to produce progeny (Figure 15A). By passage four, the  $\Delta tmeA-lx$  and  $\Delta tmeA/B$  strains had significantly fewer genomes as compared to WT.  $\Delta tmeB$  did not have significantly different genomes compared to WT.

Genomes were also quantified across multiple passages from infected cultures for a WT strain expressing additional TmeA and TmeB, WT+pTmeA/TmeB, to investigate

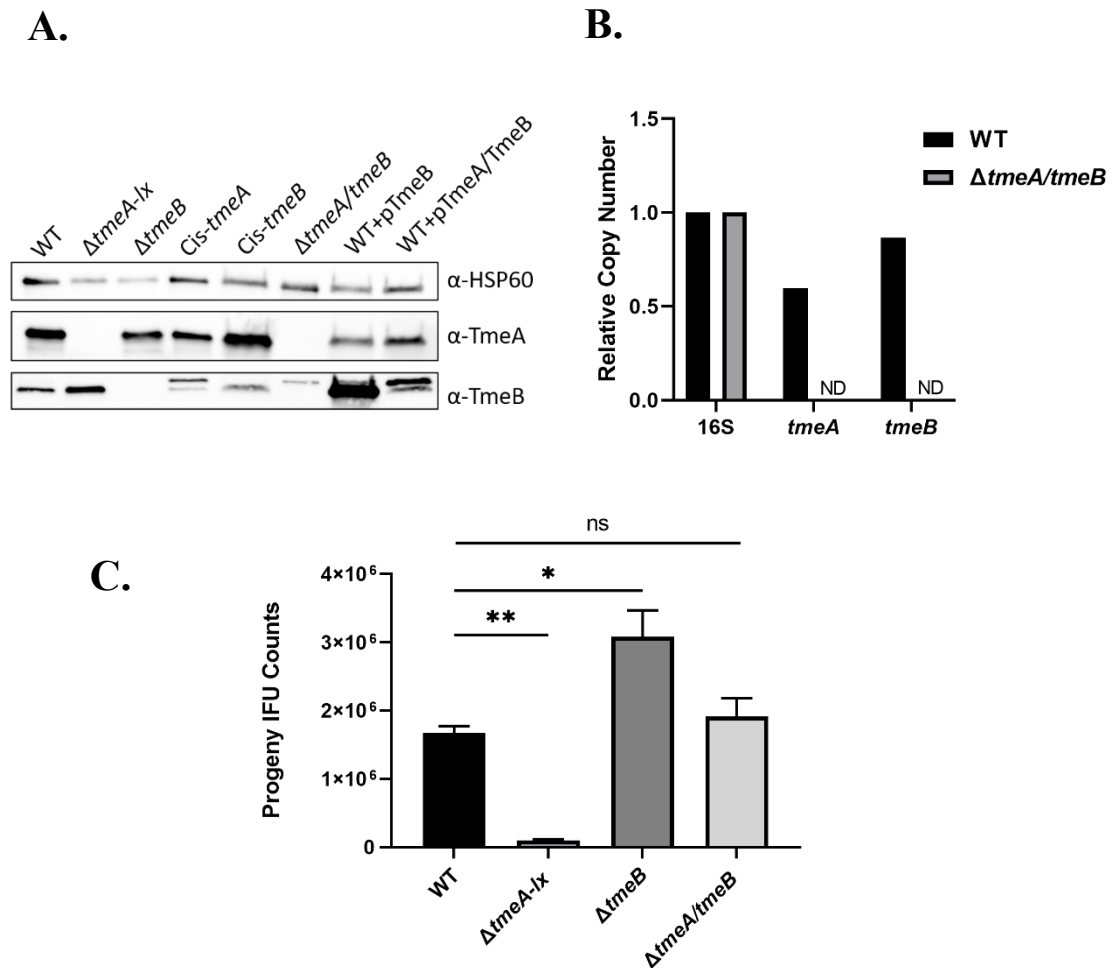


**Figure 14. *C. trachomatis* L2 lacking both *tmeA* and *tmeB* are not deficient in producing infectious progeny.**

(A) Equal quantities of material harvested from EBs was probed in immunoblots with antibodies specific to TmeA and TmeB. HSP60 was used as a loading control for chlamydiae, and proteins were visualized by chemiluminescence. (B) McCoy cells infected in triplicate with equal IFUs of *C. trachomatis* L2 WT or  $\Delta tmeA/tmeB$  were harvested at 24 hpi, and DNA was extracted for qPCR. Relative copy numbers for *tmeA* and *tmeB* were assessed by signal normalized to chlamydial 16S (ND, none detected). (C) HeLa cultures were infected in triplicate with equal IFUs of *C. trachomatis* L2 WT,  $\Delta tmeA-lx$ ,  $\Delta tmeB$ , or  $\Delta tmeA/tmeB$  to achieve an MOI of 0.1. Cultures were harvested for enumeration of progeny EBs at 24 hpi. All inclusions were enumerated by fluorescence staining of chlamydiae in fixed samples, and data are represented as mean with error bars at one standard deviation of triplicate samples. Statistical analysis was addressed using a Student's t-test with Welch's correction (\*,  $p < 0.02$ ; \*\*,  $p < 0.001$ ; ns, not significant).

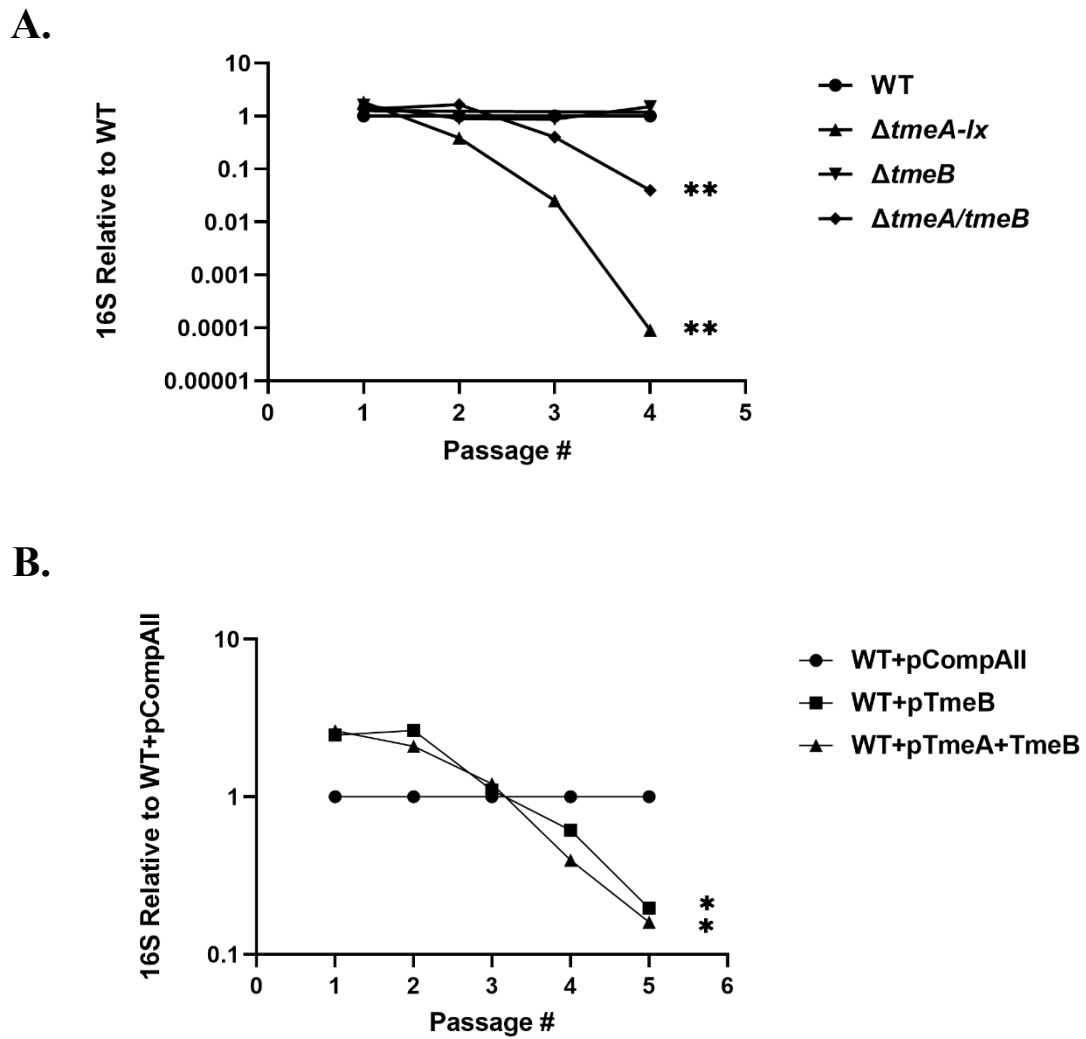


**Figure 15. *C. trachomatis* L2 strains lacking both TmeA and TmeB or over-expressing TmeA and TmeB produce fewer progeny genomes over multiple passages than WT.**

HeLa monolayers were infected with *C. trachomatis* L2 (A) WT,  $\Delta tmeA-lx$ ,  $\Delta tmeB$ , or  $\Delta tmeA/tmeB$ ; or (B) WT+pCompAll, WT+pTmeB, or WT+pTmeA+TmeB. Infected cultures were harvested and passaged onto fresh HeLa monolayers every 24 hrs. A portion of the harvested material was used for DNA extraction and quantification by qPCR detecting chlamydial 16S. Data are represented as fold change from triplicate biological and technical samples. Linear regression was used to assess statistical significance (\*,  $p < 0.02$ ; \*\*,  $P < 0.0001$ ).

whether increased TmeA would negate the effects of increased TmeB. This strain contains the pCompAII plasmid with the *tmeA/tmeB* locus under its native promoter (generated by Maria Boderó). Although WT+pTmeB and WT+pTmeA/TmeB were infected with 2.5 times the starting inoculum as WT, after 5 passages, there were significantly fewer genomes (Figure 15B). These data indicate that increased TmeA does not rescue the defect associated with increased TmeB expression.

#### 4.4. Discussion

The lack of physiological TmeB levels in the  $\Delta tmeA$  (“polar”) strain made it challenging to identify specific contributions of TmeA independent of TmeB. The  $\Delta tmeA-lx$  (“non-polar”) strain was generated by removing the FRAEM-associated selection cassette via *Cre-loxP* genome editing and resulted in increased expression of TmeB. Using this newly generated strain, I investigated whether the previously observed direct and progeny IFU defects for  $\Delta tmeA$  (143) remained consistent for  $\Delta tmeA-lx$ . The data presented here indicate that  $\Delta tmeA-lx$  is more attenuated during development than  $\Delta tmeA$  and suggest that TmeA and TmeB have an inverse relationship since the lack of TmeA and excess TmeB both negatively correlate with chlamydial fitness.

To ensure appropriate controls throughout the study, I first wanted to determine whether Rif resistance or transformation with an empty pCompAII vector affected the growth of *C. trachomatis*. Neither control strain impacted chlamydial development, indicating that they would be suitable controls. Vector-only controls are also important to use given the contributions of genes encoded by pL2 during chlamydial infection (197) and

observations that ectopic expression of fluorescent proteins can impact fitness in some bacteria (198).

Similar to  $\Delta tmeA$ , the  $\Delta tmeA-lx$  strain also manifested a decrease in chlamydial infectivity. These data are therefore consistent with the proposed role of TmeA in chlamydial invasion. Although complementation was achieved when assessing direct IFUs for  $\Delta tmeA-lx$ , progeny IFUs were not fully restored for the complementing strain (Figure 8B), unlike the  $\Delta tmeA$  strain where complementation was achieved with both direct and progeny IFUs (143). The  $\Delta tmeA-lx$  strain restored expression of *tmeB*; however, TmeB levels were increased compared to WT (Figure 9A). Therefore, I wondered if the increased expression of TmeB was causing adverse effects on chlamydial development and if this was the reason the *tmeA* complementing strain did not rescue the defect in progeny IFUs for  $\Delta tmeA-lx$ . Direct comparison between the  $\Delta tmeA$  and  $\Delta tmeA-lx$  strains for progeny IFUs after a single or multiple 24 hr passages revealed that  $\Delta tmeA-lx$  had an increased defect for production of infectious progeny (Figure 9B&C). These data suggest that non-physiological levels of TmeB may be impacting *C. trachomatis* development.

To directly test the impact of non-physiological levels of TmeB, I generated WT and  $\Delta tmeB$  strains that expressed TmeB in excess using the pCompTmeB vector. In experiments comparing progeny IFUs and progeny genomes over time, strains with increased TmeB abundance had significantly decreased progeny, whereas the  $\Delta tmeB$  strain had significantly increased progeny compared to WT (Figure 14C). Interestingly,  $\Delta tmeB$  did not have increased genomes compared to WT across multiple passages (Figure 15A). These data may suggest that  $\Delta tmeB$  strains produce more EBs by 24hpi, but do not have more overall progeny (RBs +EBs) compared to WT. Taken together, these data are

consistent with TmeB levels inversely correlating with *C. trachomatis* fitness, where increased TmeB has a negative effect.

Because TmeA is implicated in actin reorganization during invasion, I wanted to determine the impact of TmeB on *C. trachomatis* invasion. Percent invasion assays revealed that excess TmeB decreased *C. trachomatis* invasion; however, the deletion of *tmeB* had no effect. One possible explanation for this effect is that excess TmeB is blocking the secretion of other invasion-related effectors; however, the Slc1 chaperoned effector, TepP, is still secreted and phosphorylated by host kinases in the presence of excess TmeB (Appendix 4). Although this does not rule out the possibility that the secretion of other effectors is being blocked or altered, TmeB may likely be hindering an important invasion-related event, such as actin reorganization. The  $\Delta tmeB$  strain did not have a defect or advantage during invasion; however, progeny IFUs relative to WT were increased, indicating a developmental advantage. These data may indicate a role for TmeB after invasion and during development by 24 hrs.

To look at the influence of TmeA and TmeB on overall *C. trachomatis* development, including host cell exit, I utilized a plaquing assay. *C. trachomatis* exit cells by host cell lysis or by extrusion. Larger plaques indicate greater cell to cell spread and overall infectivity. Interestingly,  $\Delta tmeB+pTmeB$ , with increased levels of TmeB, only had a mild decrease in plaque area relative to WT (385 au and 348 au, respectively). Therefore, unlike invasion, increased TmeB may provide an advantage late in development or increase the occurrence of host cell exit by lysis. In contrast, the absence of *tmeB* was associated with increased plaque area (541 au), which agrees with increased progeny IFU and genome data (Figure 10B&C).

When two or more EBs co-infect the same host cell, their inclusions fuse, and the bacteria maintain the same intracellular environment (199). Homotypic fusion between inclusions requires *C. trachomatis* IncA, which is expressed mid-cycle ca. 10 hpi (200). When WT<sup>Rif</sup> chlamydiae were co-infected with either WT+pTmeB or WT, more Rif resistant progeny were recovered from WT+pTmeB co-infections. These data suggest that WT<sup>Rif</sup> chlamydiae outcompete WT+pTmeB chlamydiae, which supports that an excess of TmeB is associated with a developmental defect before host cell escape. These data may also suggest that the effect of excess TmeB is specific to the chlamydiae and not to the fused inclusion. If TmeB functions within the host cytosol, as predicted based on secretion, I would expect WT<sup>Rif</sup> to be attenuated during development when infected with WT+pTmeB raising the possibility that TmeB may function before inclusion fusion. The inclusion becomes fusogenic with exocytic vesicles carrying nutrients like sphingomyelin as early as 2 hpi (91, 92); therefore, TmeB may be disrupting similar early cycle events like nutrient acquisition that require actin reorganization.

Collectively, these data indicate that TmeA and TmeB have an inverse relationship, where *C. trachomatis* manifest defects in the absence of TmeA or the abundance of TmeB. Therefore, I investigated *C. trachomatis* fitness when both effectors were deleted or over-expressed. FLAEM was again utilized to delete the entire TmeA/B operon from *C. trachomatis*. This double deletion strain represents one of the first double deletion mutants in *Chlamydia* (in addition to  $\Delta tmeA-lx/tarp$  detailed in Chapter 5). Additionally, the pCompAII plasmid was engineered to express both *tmeA* and *tmeB* by their native promoter. The  $\Delta tmeA/tmeB$  strain produced similar progeny IFUs to WT chlamydiae at 24 hpi for a singular passage (Figure 14C). This is likely due to a culmination of the invasion

defect associated with the loss of *tmeA* and an increase in progeny related to the loss of *tmeB*; however, when progeny genomes were collected every 24 hrs across multiple passages (Figure 15A), there were significantly fewer genomes by day four relative to WT. These data may indicate a subtle defect during the first 24 hrs of development that is not fully captured by a progeny comparison of a single passage. When progeny genomes were collected for *C. trachomatis* WT+pTmeA+TmeB, there were also significantly fewer genomes relative to WT, suggesting that TmeB has a dominant-negative effect on development and is not negated by increased TmeA production.

Genes within operons are often functionally related (201); therefore, I hypothesized that TmeA and TmeB were functionally related. Taken together, the data presented here support this hypothesis and are consistent with *C. trachomatis* TmeA and TmeB being inversely related. TmeA has been described as an important effector for *C. trachomatis* invasion, and I have provided evidence here that TmeB is also involved in invasion since abundant non-physiological levels of TmeB negatively impact invasion. TmeA and TmeB are secreted during and after invasion and remain localized to plasma and inclusion membranes, respectively, at 24 hpi.  $\Delta tmeB$  strains invaded host cells as efficiently as WT at 30 min pi; however,  $\Delta tmeB$  strains repeatedly manifested an increase in production of infectious progeny and formed larger plaques, supporting a role for TmeB beyond invasion.

I predict TmeB has a dominant-negative effect when expressed at high levels because it functions to counteract the TmeA-mediated actin reorganization within the host cytosol. With the surplus of TmeB, the invasion-promoting functions of TmeA may be negated, and invasion efficiency is negatively affected. At native levels of expression, the functions of TmeA and TmeB are likely finely balanced. TmeA promotes host actin

remodeling during invasion, whereas TmeB may function to reverse signaling cascades, thereby preventing spurious signaling in the host. A similar relationship has been found between *Salmonella* effectors SopE2 and SptP. SopE2 promotes host actin remodeling by activating the Rho-family GTPase Cdc42 (202), and SptP is a tyrosine phosphatase that inhibits GTPase activity (146, 203). These effectors, along with others, work in concert to promote *Salmonella* invasion and modulate host immune responses triggered by hijacked cellular signaling pathways (204-206).

## **CHAPTER 5: *Chlamydia trachomatis* TmeA Directly Activates N-WASP to Promote Actin Polymerization and Functions Synergistically with TarP during Invasion**

This chapter has been adapted from previously published work “Keb, G., Ferrell, J., Scanlon, K. R., Jewett, T. J., & Fields, K. A. (2021). *Chlamydia trachomatis* TmeA Directly Activates N-WASP to Promote Actin Polymerization and Functions Synergistically with TarP during Invasion. *mBio*, 12(1), e02861-20. PMID: 33468693”

Contributions: Dr. Fields established the  $\Delta tmeA-lx/tarp$  deletion strain, performed the invasion efficiency assays and the BirA immunoblot analyses. J. Ferrell conducted the BirA biotinylation experiments. K.R. Scanlon and K.R. Jewett performed the pyrene assays. I conducted the progeny IFU comparisons, immunoprecipitations, APEX biotinylation cloning and subsequent experiments, immunoblot analysis, and transformation of cis-complementing *C. trachomatis* strains. Maria Boderó generated the plasmid used for cis complementation in *E. coli*. Dr. Fields and I conceptualized and authored the original manuscript collaboratively.

### **5.1. Summary**

*C. trachomatis* TarP and TmeA are both implicated in host actin reorganization and EB invasion. The high degree of redundancy in host actin cytoskeletal rearrangement pathways makes it difficult to identify specific and collective roles of T3SS effectors during host cell invasion. Using FRAEM and FLAEM, single deletions have been made for both *tarp* and *tmeA*, yielding *C. trachomatis*  $\Delta tarp$  and  $\Delta tmeA-lx$  single deletion strains. This

study further expands the FLAEM technique and has generated a double *tarp* and *tmeA* deletion strain,  $\Delta tmeA-lx/tarp$ . Here I present data using the single and double deletion strains for fitness comparisons and other biochemical approaches. These data provide evidence that the individual functions of TmeA and TarP impact separate pathways yet converge to promote Arp2/3-mediated actin polymerization essential for efficient chlamydial invasion. I also present evidence that TmeA is required for localization of N-WASP to the site of EB entry into host cells and that TmeA directly binds and activates N-WASP to promote actin polymerization. In a broader sense, identifying the role of TmeA also narrows the scope of potential interacting partners for TmeB since I hypothesize the function of TmeB is intimately linked to the role of TmeA (Chapter 4).

## 5.2. Introduction

*Chlamydia trachomatis* preferentially infects columnar epithelial cells and is dependent upon invasion for intracellular survival. Entry into nonprofessional phagocytes likely requires multiple and redundant entry mechanisms with active and inherent manipulation of the host actin cytoskeletal network. Although manipulation of the cytoskeleton plays an essential role during invasion and throughout chlamydial development, the mechanisms initiating and maintaining these events are poorly understood in the context of *C. trachomatis* infection. Previous studies have primarily leveraged inhibitors to target host proteins during invasion, which has made it challenging to identify the roles of individual effectors.

Actin is rapidly recruited to the site of chlamydial attachment (129), and *in vitro* studies have shown that invasion of *C. trachomatis* is significantly impaired when actin

polymerization or depolymerization is disrupted with either cytochalasin D or jasplakinolide, respectively (reviewed in reference (120)). It has also been well established that central host factors responsible for manipulating actin dynamics, such as Ras-related C3 botulinum toxin substrate 1 (Rac1), Wiskott-Aldrich syndrome protein family member 2 (WAVE2), and the Arp2/3 complex, play important roles during *C. trachomatis* internalization (reviewed in reference (120)). Beyond invasion, the actin-based cytoskeleton maintains chlamydial inclusion integrity during intracellular development (152) and host cell exit (99).

*Chlamydia* initially adheres to the host plasma membranes via low-affinity interactions such as those manifested between heparan sulfate proteoglycans and *C. trachomatis* outer membrane proteins, such as OmcB (83). Subsequent high-affinity interactions are established between chlamydial outer membrane proteins and host receptors, such as integrin  $\beta$ -1 (ITG $\beta$ 1) (84), epidermal growth factor receptor (EGFR) (85), ephrin receptor A2 (EPHA2)(86), or platelet-derived growth factor receptor b (PDGFRb)(124). These high-affinity interactions can mediate chlamydial attachment leading to receptor clustering and downstream actin remodeling, culminating in invasion (86, 119, 129, 149). For example, *C. trachomatis* Ctad1 binds to ITG $\beta$ 1 and induces receptor clustering, activation of Erk1/2, and chlamydial internalization (84). The individual activities of both EGFR (151) and EPHA2 (86) also contribute to chlamydial entry. These receptors presumably represent separate, redundant doorways for *Chlamydia* to cross the host's plasma membrane barrier.

In addition to receptor-mediated endocytosis, actin-containing filopodia that form distinct cup, tail, and ruffle structures have been noted during chlamydial invasion (88,

129). Detailed structural and biochemical analyses have recently revealed that these structures correspond to events associated with macropinocytosis-mediated entry and have implicated novel contributions of the Bin/amphiphysin/Rvs (BAR) domain protein sorting nexin 9 (SNX9), cell division control protein 42 (Cdc42), and neural Wiskott-Aldrich syndrome protein (N-WASP) during chlamydial infection. Macropinocytosis is an actin-dependent process where extended filopodia fuse with the plasma membrane to form fluid-phase endocytic compartments termed macropinosomes (207). SNX9 contributes to membrane curvature and can impact actin dynamics by recruiting Cdc42 and N-WASP (208). All three host proteins are recruited to EB attachment sites, and infection of SNX9<sup>-/-</sup> cells or pharmacologic inhibition of Cdc42 or N-WASP negatively impacts invasion (88). These data indicate that *Chlamydia* may deploy effector proteins that manipulate macropinocytosis to effect entry. In support of this notion, *C. pneumoniae* Cpn0678, a *C. trachomatis* TmeA ortholog, binds directly to SNX9 to effect membrane curvature associated with entry events (209).

The effectors TarP and TmeA are chaperoned by the same chlamydial protein, Slc1, before secretion. These effectors are secreted during invasion and early entry events through the T3SS. TarP has been well established as an effector capable of directly and indirectly manipulating actin. TarP contains both globular- (G) and filamentous- (F) actin-binding domains and can directly nucleate actin. Through interactions with the signaling proteins Src and WAVE, TarP also leads to indirect actin polymerization by Rac1 activation. *C. trachomatis*  $\Delta tarp$  mutants have decreased levels of invasion-related infectivity as compared to WT (132); thus, TarP plays an important role in early entry events. Similarly, *C. trachomatis* deletion strains lacking *tmeA* also have decreased

invasion-related infectivity. Previous studies have shown that TmeA interacts with AHNAK, a large host scaffolding protein, and inhibits actin bundling (143). However, TmeA strains lacking the AHNAK binding domain still cause morphological changes in host cells (137), raising the possibility of interacting partners in addition to AHNAK.

Because TarP and TmeA both play a role in manipulating the actin network, my collaborators and I sought to further understand their mechanism(s) of action by investigating whether they function independently from one another along separate pathways or whether they functioned synergistically along a similar path. Here, we utilize *C. trachomatis* mutant strains containing null deletions of *tarp* and *tmeA* to investigate the contributions of individual effectors on these processes; furthermore, we use a mutant strain containing gene deletions of both effectors simultaneously to analyze their collective impact. The work presented herein provides evidence that TmeA and TarP have distinct functions and ultimately work on separate pathways that converge in the activation of Arp2/3 for actin polymerization. I also present data that support a role for TmeA in recruiting N-WASP to the site of EB invasion and directly binding and activating N-WASP to promote Arp2/3 complex activation. Taken together, these data support an appreciation for the number of resources a pathogen with a minimal genome dedicates to overcome critical obstacles for survival.

### 5.3. Results

**Generation of a *C. trachomatis*  $\Delta tmeA-lx/tarp$  double deletion mutant.** To begin investigating the individual and cumulative effects of TarP and TmeA on invasion, Dr. Fields generated a *C. trachomatis* deletion mutant lacking both effectors. Lateral gene

transfer was used to introduce a *tarP* deletion into the  $\Delta tmeA-lx$  strain. This was achieved by coinfecting  $\Delta tarP$ , expressing penicillin G (PenG) resistance, and  $\Delta tmeA-lx$ , expressing rifampin resistance (Rif). Cocultures were serially passaged without antibiotic selection initially to allow adequate time for LGT to occur; then, selection was introduced to isolate a mutant resistant to both PenG and Rif (Figure 16A). The isolated strain was deficient in both *tmeA* and *tarP*, confirmed by qPCR (Figure 16B) and immunoblot analysis (Figure 16C). Notably, the deletion of TmeA and TarP did not affect the expression of the other Slc1 chaperoned effectors, TmeB and TepP (Appendix 4).

***C. trachomatis* lacking *tmeA* and *tarP* are attenuated during development.** To compare the fitness of the double mutant strain to single mutants and WT, I utilized a direct inclusion-forming unit assay. HeLa cells were infected with equal numbers of EBs for each strain. 24 hpi inclusions were enumerated by fixing and staining the cultures (Figure 17A). The  $\Delta tmeA-lx/tarP$  double mutant strain was significantly attenuated compared to WT and the single mutant strains.

The areas of stained inclusions from infected cultures were quantified. Both  $\Delta tmeA-lx$  and  $\Delta tmeA-lx/tarP$  formed smaller inclusions (median = 139  $\mu\text{m}^2$  and 109  $\mu\text{m}^2$ , respectively) and while  $\Delta tarP$  formed larger inclusions (median = 206  $\mu\text{m}^2$ ) relative to WT (median = 180  $\mu\text{m}^2$ ) (Figure 17B). I next enumerated infectious progeny from cultures infected with equal IFUs 24 hpi.  $\Delta tmeA-lx$  ( $3.22 \times 10^6$  IFUs) and  $\Delta tmeA-lx/tarP$  ( $3.38 \times 10^6$  IFUs) produced significantly fewer progeny relative to WT ( $1.56 \times 10^7$  IFUs), whereas  $\Delta tarP$  ( $1.68 \times 10^7$  IFUs) produced a similar amount to WT (Figure 17C).

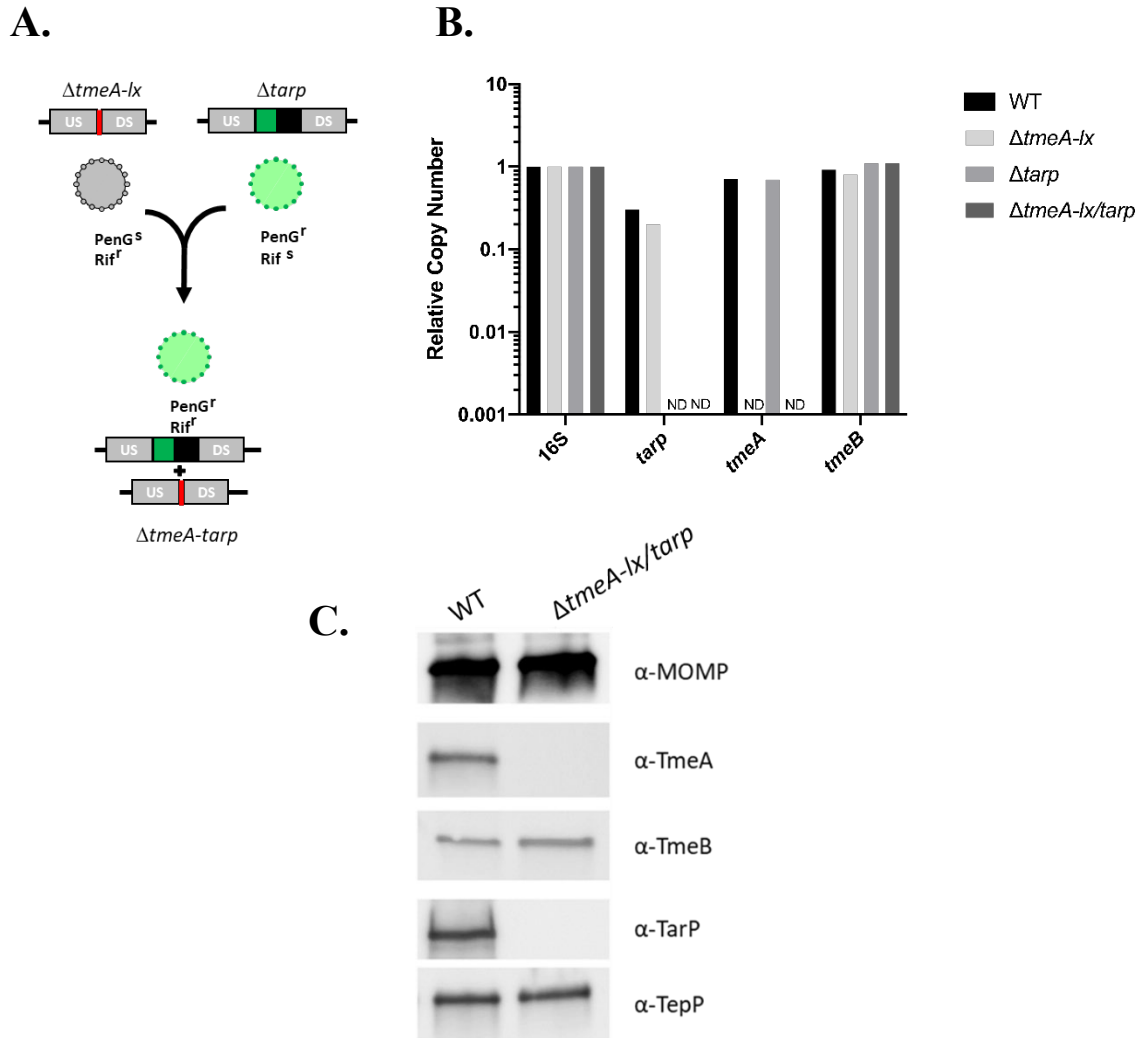


**Figure 16. Conformation of *tarp tmeA* double deletion mutant.**

(A). Schematic for application of lateral gene transfer to generate  $\Delta tmeA-lx/tarp$  from single mutant strains. Rifampin-resistant (Rif<sup>r</sup>), penicillin-sensitive (PenG<sup>s</sup>)  $\Delta tmeA-lx$  lacking GFP was cocultured with penicillin-resistant (PenG<sup>r</sup>), rifampin-sensitive (Rif<sup>s</sup>)  $\Delta tarp$  to allow lateral gene transfer between strains. Both PenG and Rif selection was applied to isolate a GFP<sup>+</sup> strain lacking *tmeA* and *tarp*. *LoxP* sites are represented by red bars, *bla* by black bars, and *gfp* by green bars. (B) McCoy cells were infected in triplicate with equal IFUs of WT,  $\Delta tmeA-lx$ ,  $\Delta tarp$ , or  $\Delta tmeA-lx/tarp$ . *C. trachomatis* were harvested 24 hpi, and DNA was extracted for qPCR. Relative copy numbers of *tarp*, *tmeA*, and *tmeB*, with technical triplicates, was assessed by signal normalized to 16S (ND, none detected). (C) Immunoblot analysis of material from DG-purified WT or  $\Delta tmeA-lx/tarp$  EBs. SDS-PAGE-resolved material was probed with antibodies specific for effectors TmeA, TmeB, TarP, and TepP. MOMP was used as a chlamydial loading control, and proteins were detected by chemiluminescence.

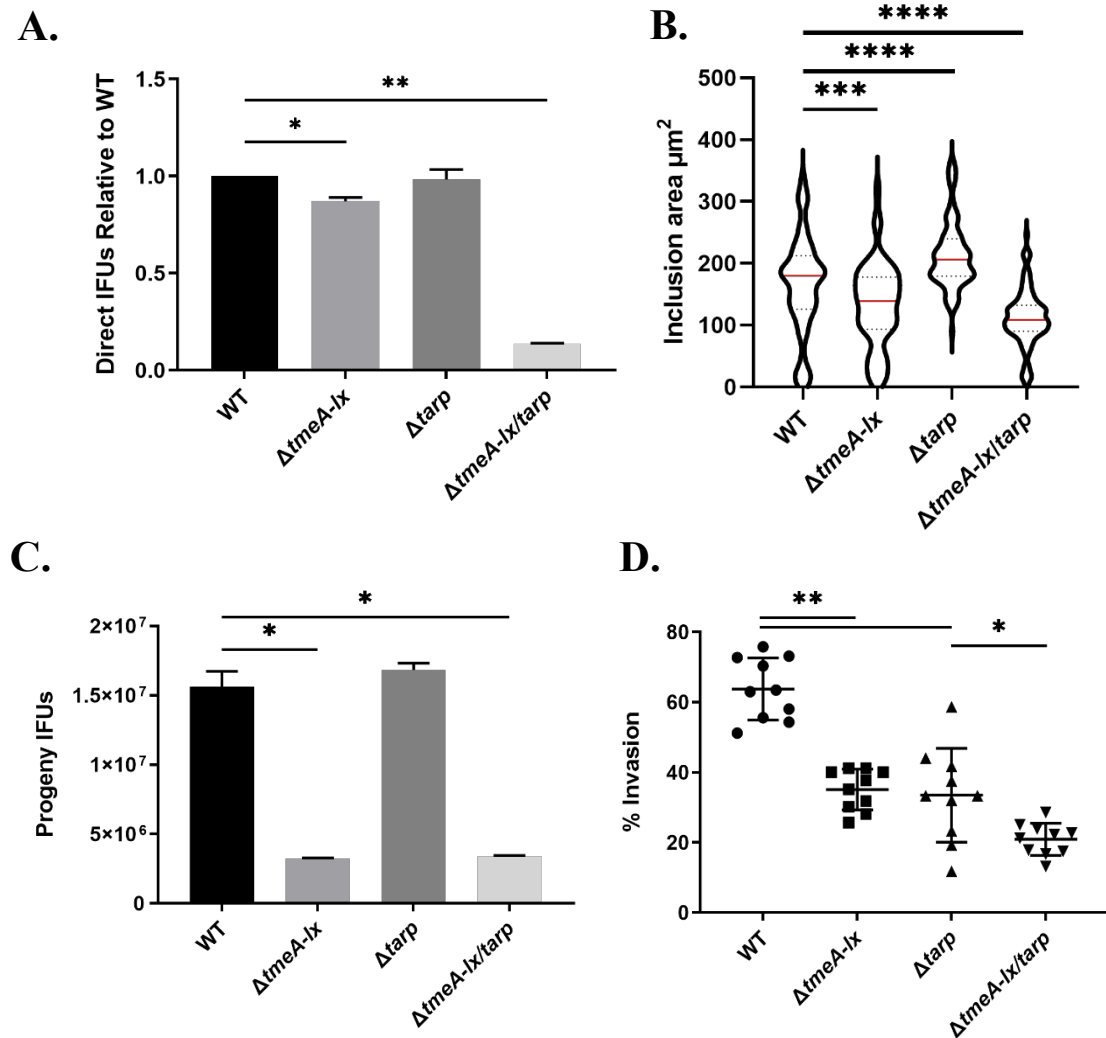


**Figure 17. *C. trachomatis* lacking *tmeA* and *tarp* are attenuated during development.**

HeLa cells were infected using equivalent numbers of WT,  $\Delta tmeA-lx$ ,  $\Delta tarp$ , or  $\Delta tmeA-lx/tarp$  strains at an approximate MOI of 0.1. At 24 hpi, cultures were methanol fixed and stained to enumerate (A) chlamydial inclusions and (B) inclusion areas or (C) harvested and passaged to enumerate progeny IFUs by fluorescent staining in fixed cultures 24 hpi. (A&C) Data from mutant strains are represented as the mean  $\pm$  one standard deviation of triplicate samples. Statistical significance was addressed using Student's t-test with Welch's correction (\*,  $p < 0.05$ ; \*\*,  $p < 0.005$ ). (B) Median areas are represented by red bars (N=100) and statistical significance was assessed using a Mann-Whitney U-test (\*\*\*,  $P < 0.0007$ ; \*\*\*\*,  $P < 0.0001$ ). Outliers were removed using ROUT analysis with Q= 1%. (D) HeLa monolayers were infected for 1 hr at 4 °C with WT or mutant strains at an MOI of 10. Cultures were shifted to 37 °C for 30 min and then paraformaldehyde-fixed and processed for inside-out staining to assess invasion efficiency. Data are represented as mean values for the percentage of internalized chlamydiae for 10 fields of view and are shown with error bars at one standard deviation. Statistical significance was addressed using Student's t-test with Welch's correction (\*,  $p < 0.05$ ; \*\*,  $p < 0.005$ ).

Next, the mutant strains were compared for their ability to invade host cells within 30 min (Figure 17D). Typically, at this time point, 50-80% of WT bacteria will successfully invade. The infections were synchronized by infecting HeLa cells at 4 °C, which allows attachment, then shifting the cultures to 37 °C for 30 min to allow invasion. Cultures were then fixed and differentially stained for extracellular vs. intracellular bacteria. 63.7% ( $\pm$  8.8%) of WT EBs were intracellular by 30 min. Consistent with previous findings, the invasion efficiency of the single mutant strains was 35% ( $\pm$  5.7%) for  $\Delta tmeA-lx$  and 33.5% ( $\pm$  13.3%) for  $\Delta tarp$ . In the absence of both TmeA and TarP, the invasion defect was exacerbated where only 20% ( $\pm$  4.5%) of bacteria successfully invaded at 30 min. These data indicate that TmeA and TarP function in an additive fashion to promote efficient uptake of *Chlamydia*.

**Proximity labeling identifies several proximal proteins to TmeA.** Previous studies have shown that the interaction of TmeA with AHNAK is not solely responsible for TmeA's effect on the actin cytoskeleton. When the AHNAK binding domain of TmeA is deleted, ectopic expression of the truncated protein in HeLa cells still causes morphological changes (137). Therefore, it is likely that TmeA has multiple functional domains capable of manipulating the host actin network.

J. Ferrell has previously identified potential binding partners using BirA proximity labeling (210). Proximity labeling has emerged as an efficacious approach for delineating potential interacting partners of chlamydial effectors (180, 211, 212). He reasoned that ectopic expression of a TmeA-containing chimeric protein in HeLa cells would provide a nonbiased indication of potential interacting host proteins. TmeA was fused to the promiscuous biotin ligase, BirA, and a similar fusion was created using TmeA lacking the

membrane-localization domain (MLD) as a nonspecific control. Duplicate experiments were performed where HeLa cells were transiently transfected via nucleofection with BirA only, TmeA-BirA, or TmeA $\Delta$ mld-BirA and cultured in the presence of exogenous biotin for 24 hrs. A portion of each sample was resolved via SDS-PAGE followed by probing with streptavidin-horseradish peroxidase (HRP) in immunoblots to confirm ligase activity. Nucleofection efficiency and localization of TmeA-containing fusion proteins were confirmed by parallel staining of fixed cells with c-myc antibodies.

Purified biotinylated proteins were identified by mass spectrometry (MS). Common contaminants such as keratin, heat shock proteins, and endogenously biotinylated proteins were excluded from the results. Proteins identified in TmeA-BirA samples were designated unique if they were also absent in BirA-only and TmeA $\Delta$ mld-BirA samples. A total of 12 unique host proteins were identified for TmeA-BirA samples (Table 4). As expected, AHNAK and AHNAK2 were detected. Additional host proteins previously implicated during *C. trachomatis* attachment or invasion, including ITG $\beta$ 1 (84), WASL/N-WASP (88), EphA2 (86), and EGFR (85). Additional proteins included the amino acid transporters SLC3A2 (CD98hc), SLC7A5 (LAT1), and SLC1A5 (ASCT2); cytoskeleton-associated factors formin BP1 (FNBP1) and podocalyxin-like protein (PODXL); and the surface receptor CD44.

To confirm the identified hits were specific to the TmeA-BirA samples and were not background contaminants from MS, protein material was directly analyzed from replicate BioID experiments by immunoblotting with antibodies specific for each of these hits (K. Fields). These analyses confirmed reproducible TmeA-dependent biotinylation of receptors CD44, EphA2, EGFR, and the actin-associated proteins AHANK and N-WASP

**Table 4.** MS Identification of Host Proteins Uniquely Proximal to TmeA-BirA

Uniprot accession no.	Description <sup>a</sup>	Score <sup>b</sup>	Coverage <sup>c</sup>	Unique peptides <sup>d</sup>	Total peptides <sup>e</sup>	AA <sup>f</sup>	Mol wt (kDa)
Q09666	AHNAK GN=AHNAK	6,349.70	72.41	209	302	5,890	628.7
Q8IVF2	AHNAK2 GN=AHNK2	1,610.09	36.15	50	81	5,795	616.2
P08195	CD98 GN=SLC3A2	309.22	23.81	9	13	630	68.0
P05556	Integrinb1 GN=ITGB1	123.99	8.52	5	5	798	88.4
P16070	CD44 GN=CD44	73.46	4.99	2	3	742	81.5
Q01650	LAT1 GN=SLC7A5	63.96	7.69	1	3	507	55.0
Q15758	ASCT2 GN=SLC1A5	60.98	4.44	2	2	541	56.6
P00533	EGFR GN=EGFR	46.38	0.83	1	1	1,210	134.2
O00592	Podocalyxin GN=PODXL	41.67	4.66	2	2	558	58.6
P29317	EphA2 GN=EPHA2	40.11	1.02	1	1	976	108.2
Q96RU3	Formin BP1 GN=FBNBP1	39.77	1.62	1	1	617	71.3
O00401	NWASP GN=WASL	34.67	7.72	1	3	505	54.8

<sup>a</sup>Uniprot gene names are provided as a common designation followed by the acronym

<sup>b</sup>Confidence score expressed as cumulative mass spectra for detected peptides.

<sup>c</sup>Percentage of respective protein represented by cumulative detected peptides.

<sup>d</sup>Values correspond to the number of high-confidence peptides detected.

<sup>e</sup>Numbers correspond to the total number of peptides detected.

<sup>f</sup>Numbers correspond to the total number of amino acids in the respective proteins.

(Figure 18A). N-WASP has been implicated in association with sorting nexin 9 (SNX9) during *C. trachomatis* invasion (88). SNX9 was also detected via immunoblot as selectively biotinylated in the presence of TmeA-BirA. MS identified proteins that were not confirmed by immunoblot include ITG $\beta$ 1, solute transporters SLC3A2, SLC7A5, and SLC1A5, PODXL, and FNBP1.

Based on gene ontology (Table 5) and STRING (Figure 18B) (<http://www.string-db.org>; 41) analyses, the identified proteins were clustered into functional classes relating to amino acid transport or processes pertaining to cytoskeletal manipulations. SLC1A5, SLC7A5, and SLC3A2 are membrane-associated solute transporters; thus, they appear in multiple ontology categories. Collectively, the functional classes of these TmeA target proteins suggest an impact on the host actin network.

The BirA BioID method relies on ectopic expression of TmeA and identifies proximal proteins over 24 hrs; therefore, I sought to identify TmeA targets in the context of infection. I utilized the engineered ascorbate peroxidase, APEX2, which biotinylates proximal proteins in the presence of biotin-phenol and hydrogen peroxide. Unlike BirA, APEX2 is readily secreted through the T3SS and rapidly biotinylates proteins within seconds once the reaction is catalyzed with hydrogen peroxide (180). I generated expression plasmids for both TmeA-APEX and TmeB-APEX chimeric proteins and introduced them into the respective null *C. trachomatis* strains. The established invasion defect of  $\Delta tmeA-lx$  was utilized to determine whether TmeA-APEX was functional (Figure 19A). HeLa cells were synchronously infected with either the WT,  $\Delta tmeA-lx$ , or  $\Delta tmeA+tmeA-APEX$ , and the invasion percentage was quantified for each strain using differential inside-out fluorescence staining 45 min post-infection.

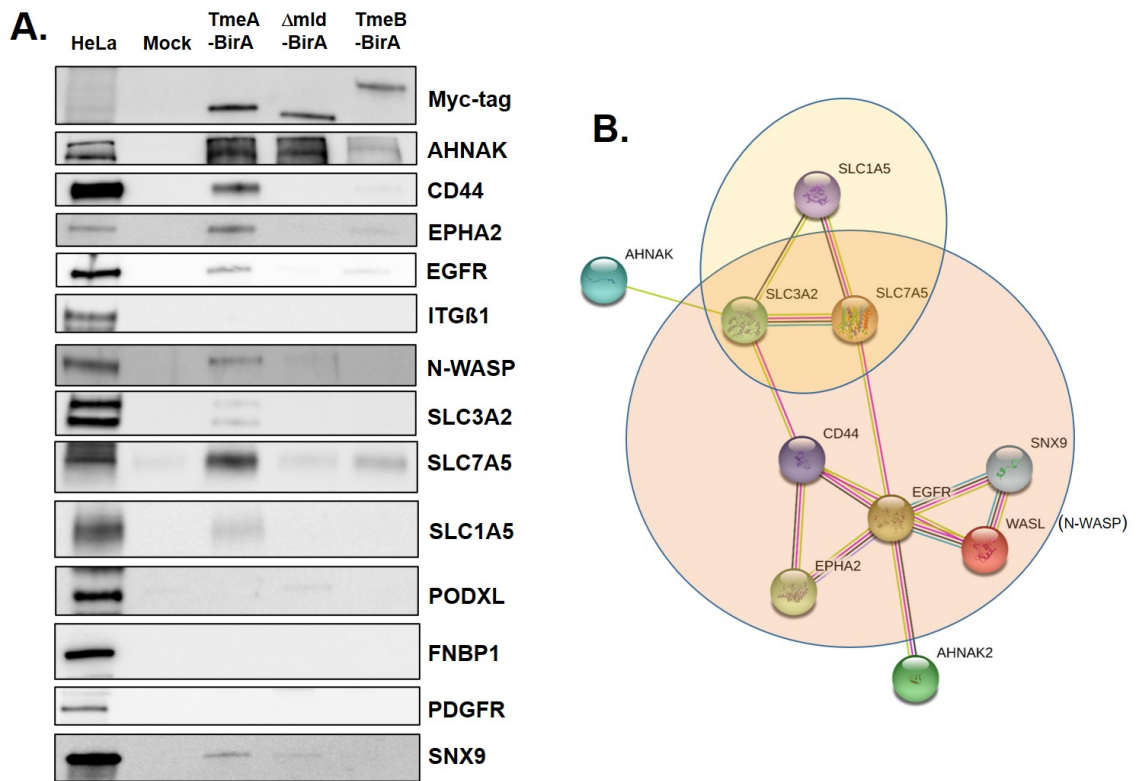


**Figure 18. Detection of biotinylated host proteins via immunoblot.**

(A) HeLa cells were mock-treated or nucleofected with TmeA-BirA,  $\Delta$ mldTmeA-BirA, or TmeB-BirA and cultivated for 24 hrs in the presence of biotin. Whole-culture material was harvested, biotinylated proteins were isolated with Avidin beads, and eluates were subjected to immunoblot analysis. HeLa lysate was also loaded as a control for antibody specificity. Representative images from a single experiment are shown. BirA-containing fusion proteins were detected with cMyc-specific antibodies. Host proteins were detected using antibodies indicated (Table 3). (B) Reproducibly detected host proteins were examined via STRING analysis and grouped according to ontology analysis. Yellow corresponds to transmembrane transport, whereas the orange sphere reflects proteins involved in cell movement.

**Table 5.** Selected Enriched Gene Ontology (GO) Molecular Functions Identified Among Host Proteins Targeted by TmeA-BirA

Term	<i>P</i> -value <sup>a</sup>	Specific targets
Amino acid transport	2.88e-05	SLC7A5, SLC3A2, SLC1A5
Organic acid transmembrane transport	2.69e-05	SLC7A5, SLC3A2, SLC1A5
Viral entry into host	1.11e-05	EphA2, EGFR, SLC1A5
Cell migration	4.28e-05	EphA2, SLC7A5, EGFR, CD44, SLC3A2
Movement of cell or subcellular component	2.97e-05	EphA2, SLC7A5, N-WASP, EGFR, CD44, SLC3A2

<sup>a</sup>Calculated *P*-value using Fisher's exact test and setting the false-discovery rate at <0.05.

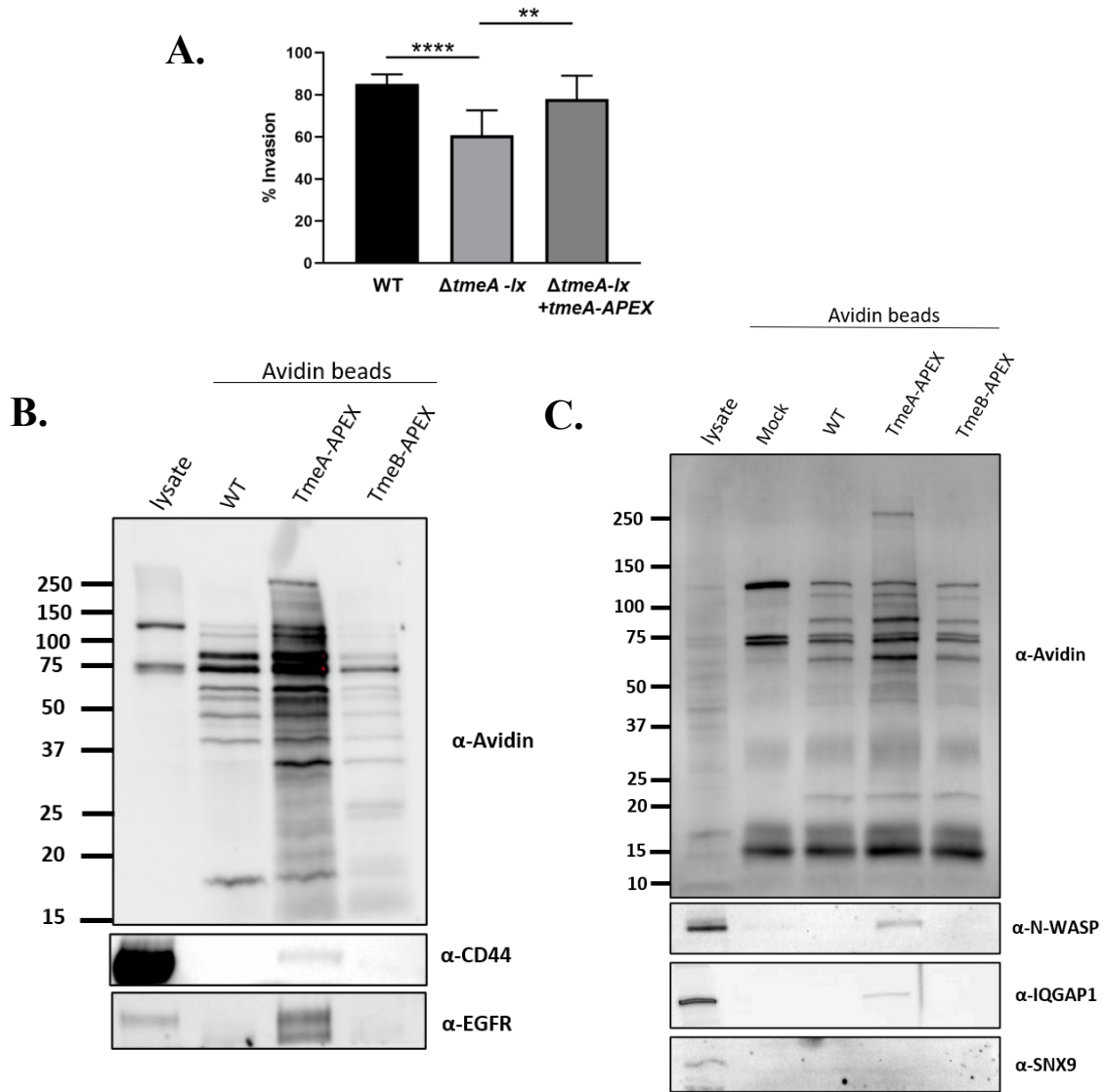


**Figure 19. A TmeA-APEX fusion is functional when expressed in *C. trachomatis* and biotinylates proximal proteins.**

(A) The ability of TmeA-APEX to complement  $\Delta tmeA-lx$  invasion was tested by infecting HeLa monolayers for 1 hr at 4 °C with WT,  $\Delta tmeA-lx$ , or  $\Delta tmeA-lx$  expressing TmeA-APEX at an MOI of 10. Cultures were shifted to 37 °C for 45 min, paraformaldehyde-fixed, then stained to assess invasion efficiency. Data are represented as the mean percentage of internalized chlamydiae with error bars at one standard deviation. Statistical significance was computed using Student's t-test with Welch's correction (\*,  $P < 0.003$ ; \*\*,  $P < 0.0001$ ). (B) HeLa monolayers were mock-treated or infected for 24 hrs with WT and  $\Delta tmeA-lx$  or  $\Delta tmeB$  strains expressing TmeA-APEX or TmeB-APEX, respectively. Biotinylation was catalyzed, then whole-culture material was harvested, biotinylated proteins were isolated with Avidin beads, and eluates were subjected to immunoblot analysis. HeLa lysates were loaded as a control for antibody specificity. Total biotin content was probed using HRP-conjugated avidin.

Expression of TmeA-APEX successfully restored infectivity of the  $\Delta tmeA-lx$  parent strain and showed no significant difference in invasion compared to WT, thus indicating TmeA was functional in the TmeA-APEX chimera. During initial experiments, I was unable to generate a sufficient biotinylation signal at time points corresponding to invasion and entry (30 min pi or 1 hpi) (data not shown); therefore, I examined the profile of biotinylated proteins at 24 hpi. HeLa cells were infected with mock, WT, or TmeA/TmeB-APEX strains, then 24 hpi, biotin-phenol was supplemented to the medium for 30 min before catalyzation with hydrogen peroxide. Whole-culture material was collected, biotinylated proteins were affinity precipitated with avidin resin, and recovered proteins were analyzed via immunoblot or LC-MS/MS. Common contaminants such as keratin, heat shock proteins, and endogenously biotinylated proteins were excluded from the LC-MS/MS results. Proteins with a confidence score below 30 were also excluded, thereby setting an established threshold of a 0.001 probability of peptide identification being random. Consistent with functional TmeA-APEX activity, several uniquely biotinylated proteins were detected in the presence of TmeA-APEX (Figure 19B&C). Immunoblots with protein-specific antibodies revealed the unique presence of N-WASP, EGFR, and CD44, but not SNX9, in TmeA-APEX material. This was an important cross-validation step in identifying biotinylated proteins, especially since N-WASP had a low confidence score in mass spectrometry results.

I also noticed a very prominent and reproducible band at ca. 250 kDa, representing a uniquely biotinylated protein in the TmeA-APEX sample. To identify this protein, I cut the associated region out of a Sypro stained gel, using WT as a control, and submitted it for LC-MS/MS analysis. Negating contaminating proteins and confirming the protein by

immunoblot with specific antibodies, I also identified IQGAP1 as a proximal protein to TmeA (Figure 19C). IQGAP1 binds both Rac1 and Cdc42 and inhibits their intrinsic GTPase activity, thereby stabilizing them in their GTP-bound form (213).

**N-WASP interacts with TmeA and localizes with invading EBs.** Both BirA and APEX2 proximity labeling approaches reproducibly identified N-WASP as proximal to TmeA. I wanted to determine whether TmeA interacts with N-WASP. FLAG-tagged (FT) TmeA was ectopically expressed in HeLa cells, and anti-FLAG coimmunoprecipitation experiments were done. SNX9 was used as a positive control with *C. pneumoniae* Cpn0678 for precipitation (209). 24 hrs post-nucleofection, whole-cell material was collected, and FT proteins were precipitated. Immunoblots were used to detect host proteins precipitated with TmeA-FT or TmeB-FT (Figure 20A). N-WASP coprecipitated with TmeA-FT, while SNX9 did not, suggesting a direct TmeA-N-WASP interaction.

Next, I wanted to determine if N-WASP was recruited to the site of invading EBs in a TmeA-dependent manner. HeLa cells were nucleofected to ectopically express N-WASP tagged with green fluorescent protein (GFP), then infected 24 hrs post nucleofection with either WT,  $\Delta tmeA-lx$ , or *cis-tmeA*. EBs were allowed to invade for 20 min, then cultures were paraformaldehyde-fixed, and EBs were stained for detection by fluorescence microscopy (Figure 20B). Colocalization was also apparent using N-WASP-specific antibodies, and indirect immunofluorescence indicated a peak colocalization of TmeA and N-WASP at 20 to 30 min post-infection (data not shown). The dependence of N-WASP recruitment on TmeA was determined by enumerating the number of invading EBs associated with N-WASP and comparing WT,  $\Delta tmeA-lx$ , and *cis*-TmeA. *Cis*-complemented TmeA expresses WT levels of TmeA and rescued the invasion defect

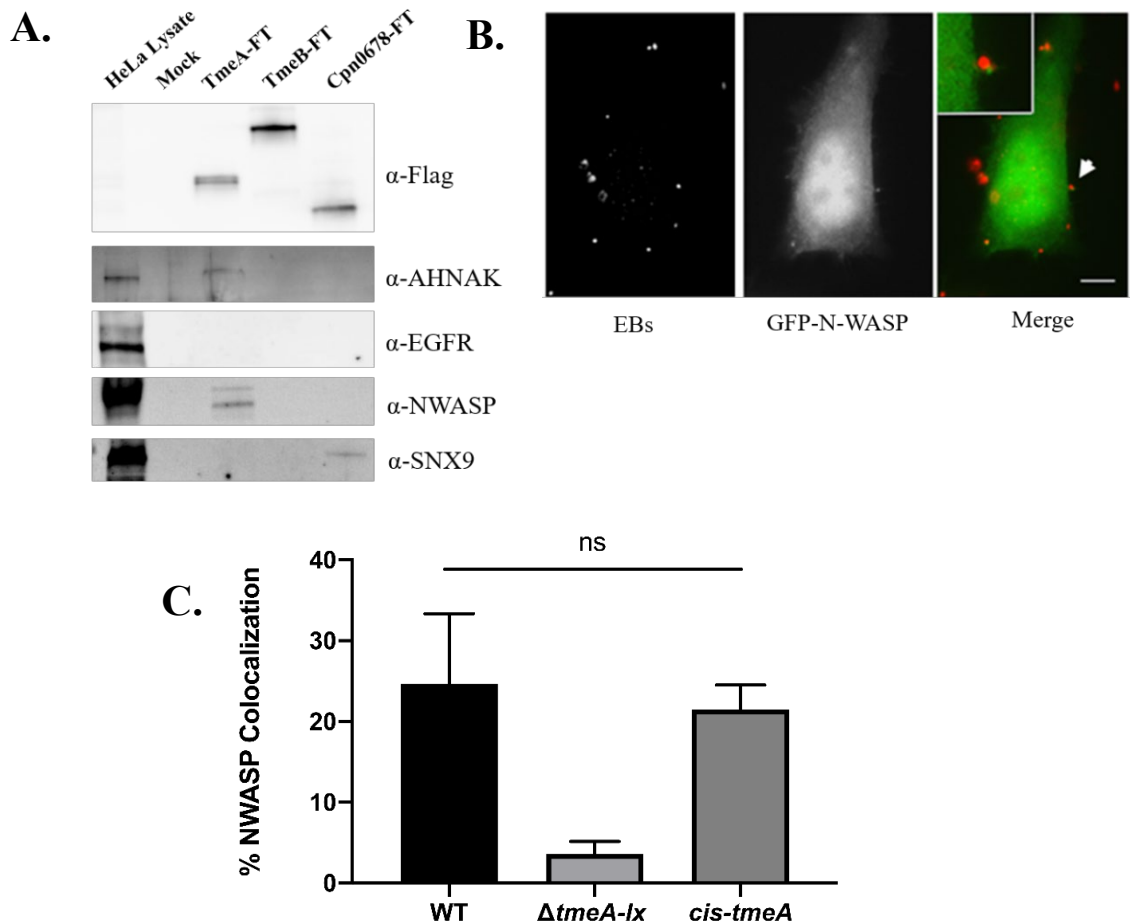


**Figure 20. TmeA interacts with N-WASP, and TmeA is required for N-WASP recruitment to sites of invading EBs.**

(A) FLAG-tagged proteins were immunoprecipitated from whole-cell lysates of HeLa cells ectopically expressing TmeA-FT, TmeB-FT, or Cpn0678-FT for 30 hrs. Immunoprecipitation from mock-treated lysates served as a negative control. The eluted material was probed in immunoblots for tagged chlamydial proteins using anti-FLAG antibodies. Host proteins were detected using antigen-specific antibodies, and HeLa whole-cell lysates were included as a positive control for these antibodies. (B) GFP-N-WASP (green)-expressing HeLa cells were infected for 10 min with WT *C. trachomatis* (red) and visualized by epifluorescence microscopy. The arrow indicates the field of view shown as an inset in the merged image. Bar = 5  $\mu$ m. (C). HeLa cells were cultivated for 20 min after synchronous infection (in triplicate) with WT,  $\Delta tmeA-lx$ , or *cis-tmeA* strains. Monolayers were stained for N-WASP and *Chlamydia* using specific antibodies, and the percentage of colocalization was enumerated for ca. 100 randomly selected EBs. Data are represented as the mean percentage of EBs exhibiting adjacent N-WASP localization. Error bars represent one standard deviation. Statistical significance was computed using Student's t-test with Welch's correction (\*,  $P < 0.04$ ; \*\*,  $P < 0.002$ ).

observed in  $\Delta tmeA-lx$  strains (Appendix 5). When HeLa cells were infected for 20 min, N-WASP colocalized with ca. 20% of WT and *cis-tmeA* EBs, whereas colocalization was < 4% for  $\Delta tmeA-lx$  (Figure 20C). These data indicate that TmeA interacts with and recruits N-WASP during invasion.

**Inhibitor assays reveal Cdc42 and Rac1 signal transduction pathways are differentially related to TmeA and TarP.** The exacerbated invasion defect manifested by  $\Delta tmeA-lx/tarp$  is consistent with a synergistic model for TmeA and TarP during chlamydial entry. The potential pathways regarding actin polymerization were next investigated using pharmacologic inhibitors (Figure 21A). Host cells were treated for 15 min prior to infection by rocking on ice for 1 hr, then shifted to 37 °C for 45 min before fixation with paraformaldehyde. The percentage invasion was determined by differential inside-out staining for both treated and untreated monolayers comparing WT and mutant strains. EIPA (5-[N-ethyl-N-isopropyl] amiloride), a Na<sup>+</sup>/H<sup>+</sup> exchange inhibitor, was used to block macropinocytosis but does not disrupt receptor-mediated endocytosis (214). All strains were susceptible to EIPA treatment and had significantly decreased invasion efficiency. Cdc42 and Rac1 were inhibited with casin and EHop-016, respectively.

Interestingly,  $\Delta tmeA-lx$  invasion was not significantly affected in response to Cdc42 inhibition, nor was it susceptible to N-WASP inhibition (Figure 21B). In contrast,  $\Delta tarp$  invasion was not impacted by Rac1 inhibition. All strains were susceptible to Arp2/3 inhibition by CK666. Where appropriate, *cis*-complemented strains were used to infect drug-treated or untreated monolayers to confirm that the lack of inhibitor susceptibility was due to a loss of TmeA or TarP (Appendix 6). In all cases, *cis*-complementation restored susceptibility to the respective drugs. These data suggest that TmeA and TarP are uniquely

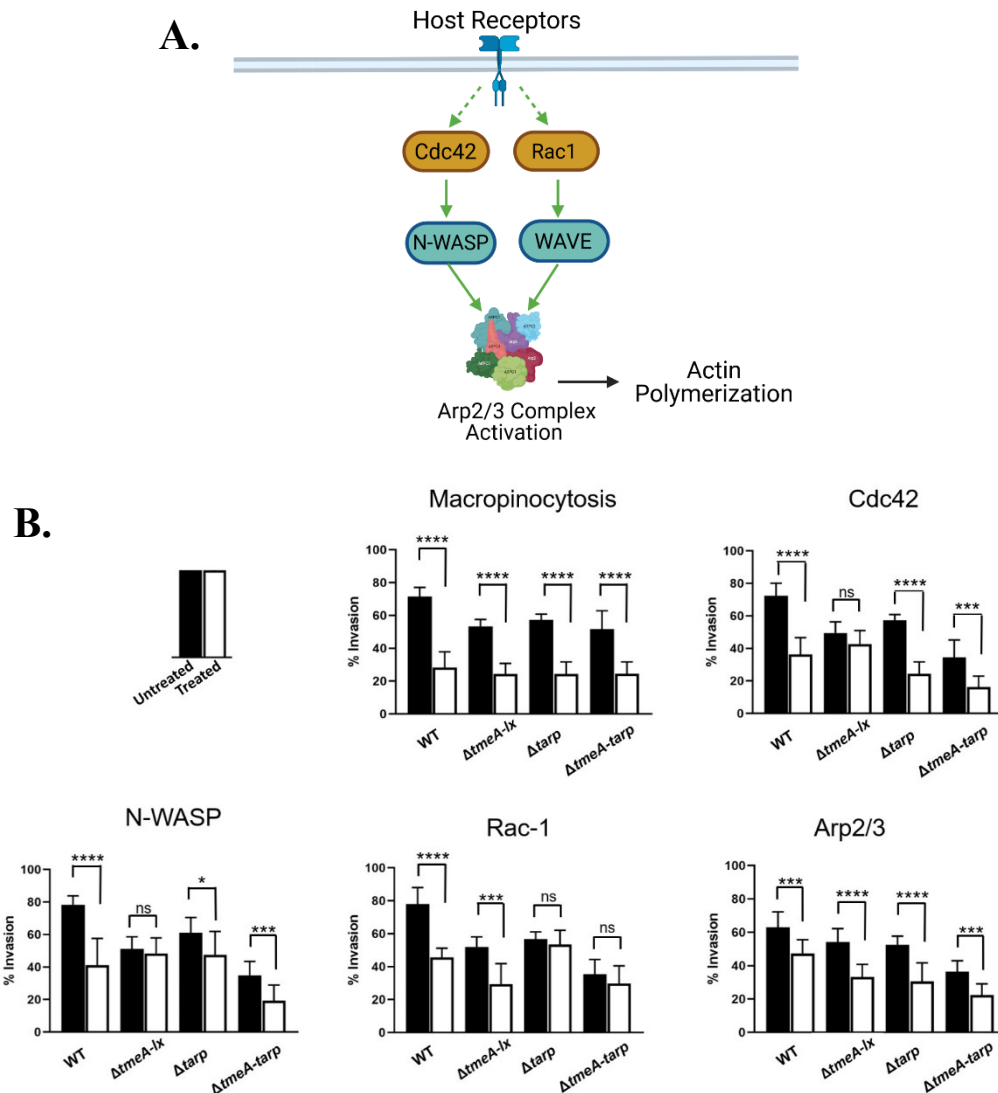


**Figure 21. *C. trachomatis*  $\Delta tmeA-1x$  is less susceptible to Cdc42 and N-WASP inhibition, whereas  $\Delta tarp$  is less susceptible to Rac1 inhibition compared to WT.**

(A) Schematic representation of Arp2/3 complex activation by Cdc42 or Rac1 pathways. (B) HeLa monolayers were infected for 1 hr at 4 °C with WT or mutant strains at an MOI of 10. Infections were carried out in the absence (black bars) or presence (white bars) of specific inhibitors. Pharmacologic disruption of macropinocytosis, Cdc42, N-WASP, Rac1, or Arp2/3 was achieved using 100  $\mu$ M EIPA, 20  $\mu$ M casin, 25  $\mu$ M wiskostatin, 25  $\mu$ M Ehop-016, or 200  $\mu$ M CK666, respectively. Cultures were shifted to 37 °C and maintained for 45 min, with or without drug, then paraformaldehyde-fixed and processed for inside-out staining to assess invasion efficiency. Data are represented as mean values for the percentage of internalized chlamydiae and are shown with error bars at one standard deviation. Statistical significance was computed using Student's t-test with Welch's correction (\*,  $P < 0.002$ ; \*\*\*,  $P < 0.0004$ ; \*\*\*\*,  $P < 0.0001$ ).

involved in Cdc42/N-WASP and Rac1 pathways, respectively, but their functions likely converge with downstream activation of Arp2/3. Interestingly, susceptibility of the  $\Delta tmeA-lx/tarp$  mutant strain to Rac1, Cdc42, and N-WASP inhibition all mirrored the phenotype of the  $\Delta tarp$  strain. These results are consistent with TarP exerting a dominant, upstream function during invasion.

**TmeA promotes Arp2/3-mediated actin polymerization.** Our collaborators investigated whether the interaction with TmeA manifests as activation of N-WASP to promote actin polymerization through N-WASP-mediated activation of Arp2/3. An established *in vitro* assay leveraging pyrene-conjugated actin was employed to examine the kinetics of actin polymerization (215) in the presence of selected proteins. G actin spontaneously assembles into filaments in physiological buffers but is limited by the instability of actin dimers and trimers, thus preventing rapid elongation (216, 217). Known actin nucleators, such as TarP, display a shortened or nonexistent lag phase. GST-tagged proteins were purified, and the tag was subsequently cleaved from TmeA to prevent the possibility of GST dimerization. N-WASP<sup>151-501</sup> lacks the N-terminal EVH1 domain, which facilitates expression in *E. coli*, but does not prevent auto-inhibition (218).

Analysis of proteins in Coomassie-stained material indicates a homogeneous content for the respective proteins (Figure 22A). In Pyrenes assays, neither TmeA alone or in combination with N-WASP<sup>151-501</sup> nor N-WASP<sup>151-501</sup> and Arp2/3 complex without TmeA resulted in polymerization kinetics differing from the actin-only control. The rate of actin polymerization was enhanced when TmeA, N-WASP, and Arp2/3 complex were combined with actin, indicating that TmeA stimulated N-WASP activity and thus led to

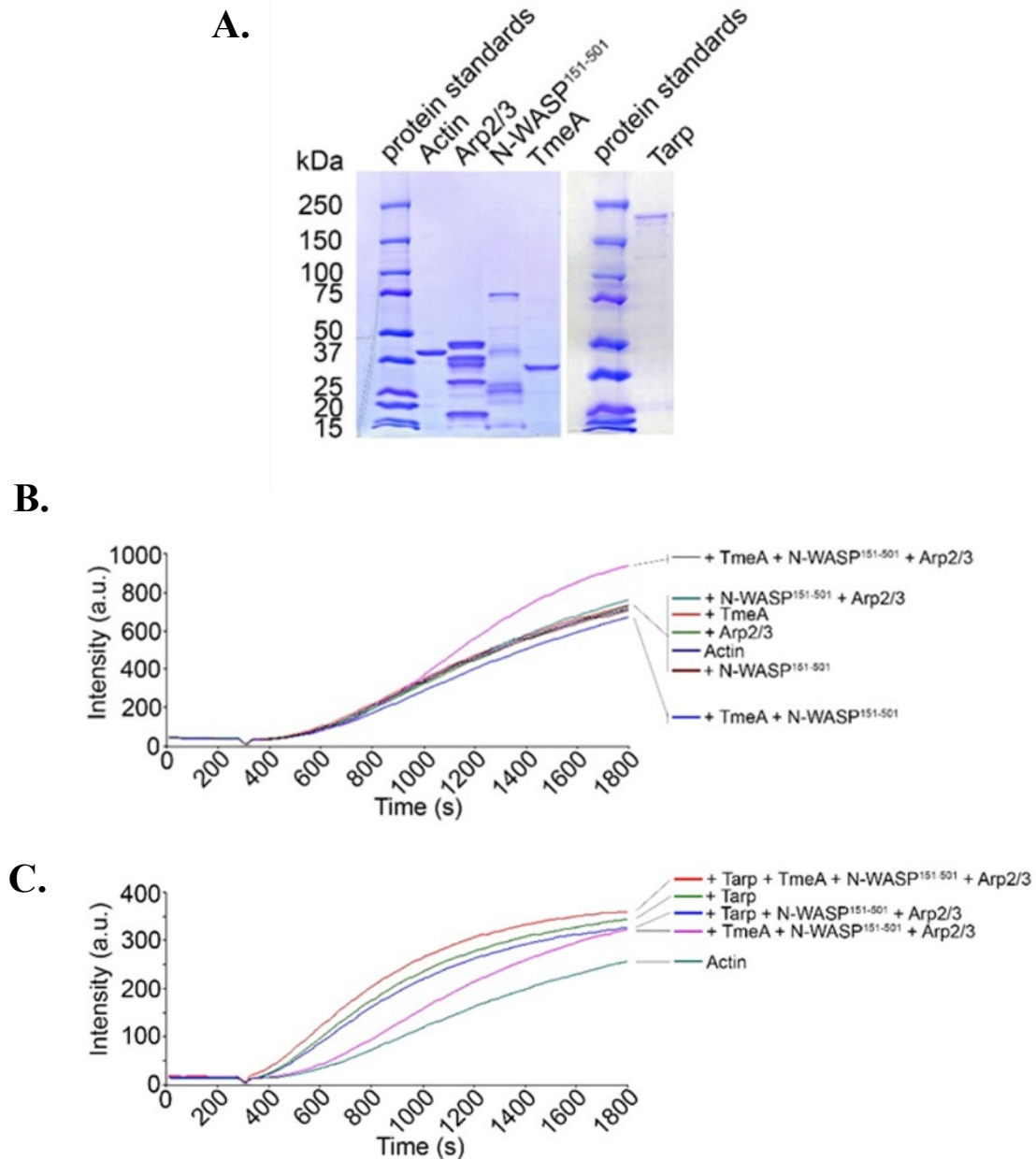


**Figure 22. TmeA activates N-WASP-Arp2/3-dependent actin polymerization, and rates are further enhanced in the presence of TarP.**

(A) Actin, TmeA, TarP, Arp2/3, and N-WASP<sup>151-501</sup> proteins employed in the pyrene actin polymerization assay were resolved by SDS-PAGE and visualized by Coomassie blue staining. (B) TmeA, Arp2/3, and N-WASP were added individually or in combination to monomeric pyrene-labeled actin. A TmeA-mediated increase in actin polymerization after the addition of polymerization buffer at 300 s was measured as the arbitrary fluorescence intensity (arbitrary units [a.u.] over time [s]) with excitation and emission wavelengths of 365 and 407 nm, respectively. (C) Like the assay shown in panel B, with the addition of the actin nucleating effector TarP. Enhanced pyrene actin polymerization was measured in the presence of TarP and TmeA.

Arp2/3 complex activation and increased actin polymerization kinetics (Figure 22B). Our collaborators next tested whether the addition of TarP could further enhance actin polymerization kinetics. Indeed, the combination of TarP, TmeA, N-WASP, and Arp2/3 complex resulted in more rapid actin polymerization kinetics (Figure 22C); therefore, TarP and TmeA can act synergistically to polymerize actin.

#### 5.4. Discussion

The T3S chaperone Slc1 directs the secretion of at least four effectors during chlamydial entry into epithelial cells, including TarP, TepP, TmeA, and TmeB (111). It is well established that *C. trachomatis* TarP influences actin polymerization directly via actin nucleation/polymerization/bundling and in concert with host factors Rac1 and Arp2/3 (reviewed in (120)). Although TmeA is also required for chlamydial entry and impacts actin dynamics, the molecular mechanisms manifesting the invasion function are less clear. TmeA associates with the host plasma membrane via the membrane localization domain (MLD; residues 40 to 80), which is functionally interchangeable with the MLD domains of *Yersinia* and *Pseudomonas* effectors YopE and ExoS, respectively (137). The C terminus of TmeA interacts with host AHNAK, and both TmeA and AHNAK localize adjacent to invading EBs (137, 143). Although TmeA interferes with the F-actin bundling activity of AHNAK, this activity is not responsible for the observed invasion defect manifested by the  $\Delta tmeA$  strain (143). A TargeTron gene disruption of *tepp* reportedly did not impact invasion, yet data were not shown (136). I present evidence that supports a working model whereby TmeA associates with the infection synapse formed between the host cell and an invading EB and initiates Arp2/3-mediated actin polymerization

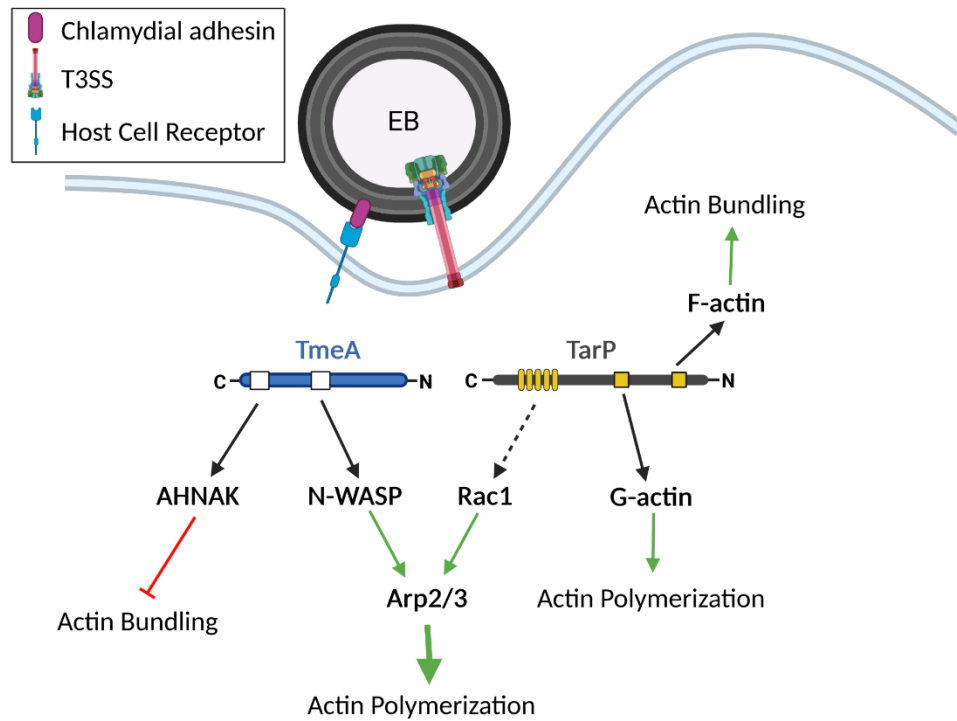


**Figure 23. Proposed model of *C. trachomatis* TmeA and TarP of Arp2/3-mediated actin polymerization.**

TmeA interacts with AHNAK and N-WASP. TarP interacts with Rac1, G-actin, and F-actin. Black arrows represent direct (solid) or indirect (dashed) interactions. Green arrows represent activation, and red lines represent inhibition.

independently of TarP (Figure 23). This model places TmeA downstream of chlamydial attachment and indicates that TmeA is responsible for the direct activation of N-WASP to promote entry. These data also formally exclude the possibility that TepP and TmeB are essential for the invasion process (Appendix 4). Simultaneous to preparing this work, Faris et al. (219) reported an N-WASP binding domain within TmeA and implicated TmeA-dependent N-WASP activation of Arp2/3 during invasion of host cells by *C. trachomatis*. The data presented here are in general agreement with but significantly extend those observations.

Chlamydial invasion requires irreversible attachment of EBs followed by cytoskeletal rearrangements to trigger entry. Cumulative evidence indicates that manipulation of actin can be orchestrated both by activation of cell surface receptors and directly via the action of secreted effector proteins (120). Interestingly, ectopically expressed TmeA-BirA reproducibly resulted in biotinylation of CD44, EGFR, and EphA2 cell surface receptors. While the hyaluronic acid receptor CD44 has not been associated with chlamydial infectivity, host cell RTKs EGFR (151, 220) and EphA2 (86) have been implicated for *C. trachomatis*. EGFR and CD44 were also repeatedly biotinylated via TmeA-APEX chimeric proteins; however, EphA2 was not. This may be indicative of a temporal EphA2 interaction with TmeA. These receptors are activated in response to *C. trachomatis* infection via tyrosine phosphorylation and are separately necessary for chlamydial attachment and invasion. EphA2 (86) becomes activated within minutes of infection, whereas EGFR(151) activation is not apparent until after ca. 2 hrs. Both receptors later associate with the chlamydial inclusion, are essential for development, and inclusion-localized EGFR also colocalizes with F-actin assembly (151). Disruption of RTK

activation is not expected since the loss of TmeA did not alter tyrosine phosphorylation or abundance of these receptors during entry or at later time points (data not shown). This would agree with observations that EphA2 is upregulated during infection by the ERK pathway (86).

PDGFR $\beta$  and ITG $\beta$ 1 were not reproducibly detected by proximity labeling, both of which have been shown to promote *C. trachomatis* attachment and entry (84, 124), yet detection of amino acid transport proteins that are relevant to chlamydial infection was apparent by BioID. SLC3A2 (CD98hc) and SLC7A5 (LAT1) form the heterodimeric glycoprotein CD98, which is capable of regulating ITG $\beta$ 1 in epithelial cells (221). The *C. trachomatis* adhesion Ctad1 engages ITG $\beta$ 1 to promote attachment and entry (84), raising the possibility that CD98 is relevant to *Chlamydia* infection. The glutamine transporter SLC1A5 (ASCT2) has not been implicated during entry but is essential for glutamine-dependent survival of intracellular chlamydiae (222). One consideration to note is that TmeA proximity to receptor and SLC proteins occurred in the absence of *C. trachomatis* infection; yet, host protein labeling required localization to the plasma membrane since they were not biotinylated in the presence of MLD-deficient TmeA-BirA. These data are in contrast to labeling of AHNAK, which did not require the MLD, and raise the possibility that these TmeA associations have spatial requirements. The potential relevance and role of TmeA localizing near these proteins clearly requires further study.

The labeling of N-WASP also required the TmeA MLD in BirA proximity labeling studies. I investigated a physical interaction of TmeA with N-WASP using coimmunoprecipitation. Indeed, N-WASP coprecipitated specifically with FLAG-tagged TmeA expressed in HeLa cells. I also investigated the relevance of this interaction during

infection. In agreement with Faris et al. (219), I observed that N-WASP recruitment to EBs (88) required TmeA and is transient during the entry process. I could not detect colocalization of N-WASP with WT EBs 30 min post-infection (data not shown). The EB-adjacent foci of N-WASP were most evident when bacteria associated with cell edges and surface projections would be consistent with the proposed filopodial capture of *Chlamydia* (88).

Proximity labeling using a TmeA-APEX fusion expressed in *Chlamydia* was also used to confirm the association of TmeA and N-WASP in the context of infection. Although the fusion protein complemented the  $\Delta tmeA-lx$  invasion defect, abundance and sensitivity issues confounded our efforts to capture potential TmeA-N-WASP proximity during the 15- to 20-min window of the invasion process. Experiments were therefore performed at 24 hpi when TmeA-APEX would be present in abundance. Under these conditions, N-WASP was detected in biotin-labeled fractions. Interestingly, these APEX data suggest that TmeA can maintain or reestablish an interaction with N-WASP during later stages of infection. Developing inclusions are enveloped in dynamic actin cages that act as scaffolds and confer stability (152, 223). Neither the N-WASP nor downstream actin branching protein complex Arp2/3 are required for this actin coat assembly (223), yet N-WASP and actin polymerization are later needed for subsequent host cell exit via the extrusion mechanism (99). Extrusion is a complex process involving both host factors and chlamydial T3S effectors (reviewed in (120)). TmeA is also secreted during late-cycle development (139), where the MLD would target this pool of TmeA to the plasma membrane. Indeed, a split GFP technique revealed accumulation of TmeA at the plasma

membrane of infected cells harboring mature inclusions (224). Therefore, this pool of TmeA may contribute to extrusion via activation of N-WASP.

Macropinocytosis is a newly appreciated mechanism for internalization of chlamydiae that requires N-WASP activity (88). We chose to examine pharmacologic inhibitors previously implicated in macropinocytotic internalization of *C. trachomatis* (88), and our comparative sensitivity data reinforced working models and provided interesting new insights. Invasion of single and double *tmeA* and *tarp* mutants were susceptible to EIPA comparable to the WT. This observation is consistent with our model since EIPA inhibits macropinocytosis by lowering submembranous pH, preventing signal transduction through both Cdc42 and Rac1 (225). Mutant strain invasion efficiency was also similarly reduced compared to that of the WT in the presence of CK666 and supports the proposed model (219) of converging TarP and TmeA functions at Arp2/3. Strains lacking *tarp* or *tmeA* lost sensitivity to inhibition with Ehop-016 and wiskostatin, respectively. Hence, Rac1 function is important for TarP-mediated invasion, whereas TmeA-mediated invasion functions through N-WASP.

All strains, except those which lacked only *tmeA*, were susceptible to the Cdc42 inhibitor casin. A role for Cdc42 in *C. trachomatis* entry was initially ruled out based on a lack of robust colocalization of Cdc42 with invading EBs, the absence of Cdc42 detection using coprecipitation with the CRIB domain of PAK1, and insensitivity of chlamydial entry to overexpression of dominant-negative Cdc42 (226). However, Ford et al. (88) noted early colocalization of GFP-Cdc42 with invading EBs and a modest sensitivity of invasion to casin, raising the possibility that Cdc42 has a transient role. The data presented here are consistent with the latter case. The robust level and extended duration of Rac1 activation

(226) could indicate a comparatively more extensive role of Rac1 in chlamydial infection. Cdc42 localization or activity was not examined because the pyrene assay data indicate TmeA bypasses the need for Cdc42 in N-WASP activation. The observation that drug sensitivity of the double mutant always mirrored that of the  $\Delta tarp$  mutant strain may indicate a dominant role for TarP during entry. However,  $\Delta tmeA-lx$  and  $\Delta tarp$  mutant strains are equally deficient for entry in the absence of inhibitor; thus, additional work is required to delineate the comparative roles of these effectors.

Faris et al. (219) identified a specific domain of TmeA (residues 118 to 126), resembling the GBD ligand motif found in the enterohemorrhagic *Escherichia coli* effector EspFu, responsible for interacting with the GBD domain of N-WASP. They surmised that this interaction leads to activation of N-WASP and subsequent Arp2/3-dependent actin polymerization. The EspFu GBD ligand motif associates with the N-WASP GBD domain similarly to Cdc42 (227). EspFu has therefore been proposed to mimic the N-WASP-activating activity of Cdc42 by inducing conformational changes necessary for N-WASP activation of Arp2/3-dependent actin polymerization (227). I present direct evidence that TmeA is sufficient to activate N-WASP, raising the possibility that TmeA also acts as a Cdc42 mimic. *In vitro* reaction mixtures containing TmeA combined with N-WASP and Arp2/3 resulted in elevated rates of pyrene fluorescence indicative of actin polymerization. This polymerization was synergistic with TarP's endogenous actin polymerization activity. Therefore, TmeA's interaction with N-WASP is sufficient to activate association with Arp2/3 and contributes in an additive fashion with TarP to the actin polymerization necessary to promote *C. trachomatis* invasion.

Finally, SNX9 is another essential component of macropinocytosis-mediated entry and has been implicated in the invasion of both *C. trachomatis* (88) and *C. pneumoniae* (209). Although SNX9 was detected in BirA proximity labeling experiments via Western blotting, I did not see evidence of an interaction of TmeA with SNX9. *C. pneumoniae* Cpn0678 and *C. trachomatis tmeA* lack homology but are encoded in the same genomic locus positioned immediately upstream of *tmeB* (138). Cpn0678 binds directly to SNX9 (209). In my hands, FLAG-tagged Cpn0678, but not TmeA, coprecipitated with SNX9. This is consistent with primary sequence analysis indicating that TmeA lacks the apparent proline-rich motifs found in Cpn0678 that mediate the interaction with SNX9. The proline content of TmeA is 4.3% with residues spaced throughout the protein, whereas Cpn0678 contains 12.2% proline with 3 proline-rich repeats spanning residues 137 to 213. Cpn0678 did not appear to interact with N-WASP or AHNAK, and these data emphasize an instance where chlamydial species are functionally divergent. SNX9 was associated with host membrane curvature during *C. pneumoniae* invasion (209) and filopodial capture during *C. trachomatis* infection (88). Based on electron microscopy data, Faris et al. (219) indicated a requirement of TmeA in filopodia formation. This observation would be consistent with robust induction of surface structures induced by chlamydial infection at a high multiplicity of infection (MOI) (129). Still, it is unclear how this fits with data indicating that *Chlamydia* hijacks existing macropinocytosis filopodia instead of inducing the *de novo* assembly of the structures (228). Perhaps functionally distinct protrusions are being manifested when *Chlamydia* associates with host cells.

TmeA and TarP represent two chlamydial effectors that have an intimate and complex relationship. Efficient TarP-mediated entry requires the C-terminal filamentous-

actin binding domain most prominently and the tyrosine-containing repeat domain to a lesser extent (132). The overt role of TmeA during invasion involves activation of N-WASP to promote Arp2/3-dependent actin polymerization. Overall, these data support the notion that TmeA and TarP have distinct functions yet synergistically promote chlamydial invasion by facilitating actin polymerization associated with the macropinocytosis pathway. Moreover, this study demonstrates how markerless gene deletion via FLAEM can be leveraged to generate multi-mutant strains. Previous work has revealed situations where non-physiological levels of expression via trans-complementation schemes can complicate data (143). Cis-complementation overcomes this confounding challenge, and I further demonstrate the efficacy of cis-complementation using allelic replacement in this study. Therefore, this work establishes how evolving and improving genetic approaches now facilitate detailed molecular dissection of effector function in *Chlamydia*.

## **CHAPTER 6: *Chlamydia trachomatis* TmeB Functions Antagonistically to TmeA and Inhibits Arp2/3-Mediated Actin Polymerization**

Contributions: R. Hayman performed experiments with pharmaceutical inhibitors testing percent IFU recovery. K. Fields conducted invasion assays. K.R. Scanlon and K.R. Jewett did pyrene actin polymerization assays. All other experiments were done by myself.

### **6.1. Summary**

This chapter aims to investigate the function of TmeB and identify host targets and potential interacting partners. I have previously found that increased TmeB levels has a

negative effect on *C. trachomatis* invasion and development (Chapter 4). In this chapter, I present evidence that the Arp2/3 complex may be a target for TmeB and that TmeB decreases the rate of Arp2/3-mediated actin polymerization.

## 6.2. Introduction

*Chlamydia trachomatis* TarP, TepP, TmeA, and TmeB all share a common chaperone and are secreted by the T3SS during invasion. TmeA and TarP are directly involved in manipulating the actin cytoskeleton, and TepP has been associated with regulating early immune responses. TmeB is the least characterized of the known Slc1-chaperoned effectors. I have previously shown that TmeB negatively impacts chlamydial development (Chapter 4); however, the function of TmeB is still unknown. The goal of work in this chapter was to determine the host pathways and proteins being targeted by TmeB and determine the role of TmeB.

*C. trachomatis* strains over-expressing *tmeB* have a similar invasion, and progeny phenotypes to *C. trachomatis* lacking *tmeA* (Chapter 4). One function of TmeA is to promote Arp2/3-dependent actin polymerization through interaction with N-WASP (Chapter 5). The Arp2/3 complex is comprised of 7 different subunits. ARP2 and ARP3 resemble actin monomers and give the complex its name (229). The remaining 5 subunits are ARPC1-ARPC5. The complex has little activity on its own, but when engaged by nucleation promoting factors (NPFs), like N-WASP, WAVE, and cortactin, the complex is activated and can form a new “daughter” filament at a 70° branch angle from the “mother” filament.

Actin polymerization can be regulated at many stages along signal transduction pathways involving Rho-family GTPases. For example, N-WASP activation is regulated upstream by the GTPase Cdc42, whereas several NPFs regulate Arp2/3 activation. The Arp2/3 complex can also be negatively regulated by proteins such as glia maturation factor (GMF), Coronin, and Arpin. These inhibitors promote an “open” conformation of Arp2 and Arp3 preventing the formation of an actin nucleation site (230). I hypothesize that TmeB functions along an actin-related pathway, similar to TmeA, and negatively regulates actin reorganization.

I utilized a general approach to investigate signaling pathways that commonly exploit phosphorylated tyrosine residues for regulation to narrow down potential TmeB targets. Biochemical techniques, such as pyrene actin polymerization assays were employed to more precisely investigate the function of TmeB. I found evidence that supports a role for TmeB in negatively targeting actin polymerization and that TmeB interacts with the Arp2/3 complex to inhibit Arp2/3-mediated actin polymerization.

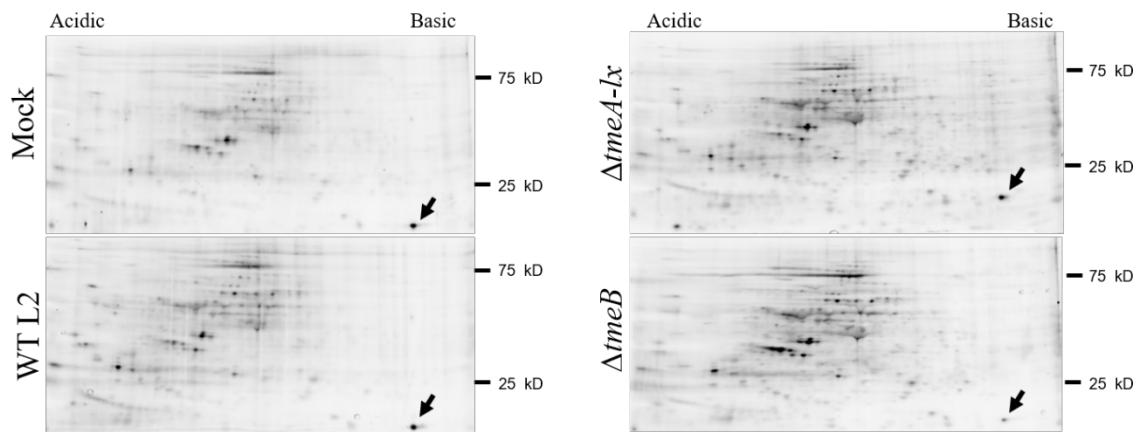
### **6.3. Results**

**Host proteins are differentially phosphorylated in the absence of *C. trachomatis* TmeB.** During *C. trachomatis* L2 infection, global changes occur in the profile of phosphorylated host proteins (231). Because differential tyrosine phosphorylation is a common mechanism for regulating signal transduction pathways through receptor tyrosine kinases like EGFR and EphA2, I reasoned to use this profile to indicate relevant TmeB targets. I infected HeLa cell cultures with mock, WT,  $\Delta tmeA-lx$ , or

*ΔtmeB* for 20 min by rocking. Cultures were then harvested for protein and separated by two-dimensional (2-D) gel electrophoresis. Tyrosine phosphorylated proteins were probed by immunoblot with phospho-tyrosine specific antibodies, and proteins were detected by chemiluminescence (Figure 24A). Images of the blots were analyzed for intensity and uniqueness using PDQuest 2-D analysis software (BioRad). Multiple spots were identified as unique between the *ΔtmeB* and control samples. I cut out spots of interest from 2-D protein gels stained with the phosphoprotein gel stain ProQ Diamond in parallel experiments. LC-MS/MS was used to identify proteins within each of the spots. Cofilin was the only protein identified with sufficient confidence from the areas sampled.

Cofilin is an actin severing protein. In its phosphorylated state, cofilin is inactive, and when dephosphorylated, cofilin is active. Next, I directly looked at the phosphorylation state of cofilin in response to infection with mock, *C. trachomatis* WT, *ΔtmeA-lx*, or *ΔtmeB*

**A.**



**B.**

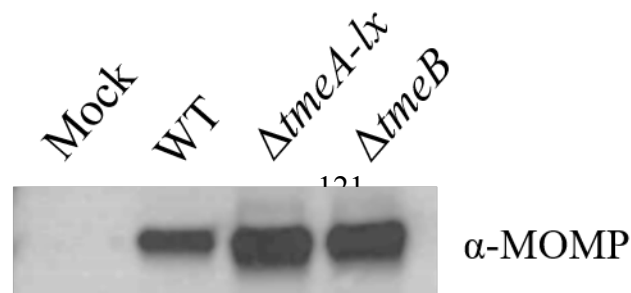


**Figure 24. Levels of phosphorylated cofilin are decreased in the absence of TmeB.**

Whole culture material from HeLa cells infected with mock, WT,  $\Delta tmeA-lx$ , or  $\Delta tmeB$  at an MOI of 1000 for 20 min at 37 °C was harvested and used for (A) two-dimensional analysis or (B) immunoblot. (A) Phosphorylated proteins were detected in two-dimensional blots using phosphotyrosine-specific antibodies. (B) The presence or absence of phosphorylated cofilin was detected using cofilin and phosphorylated-cofilin (cofilin-P) specific antibodies. MOMP was used as a loading control for infection.

(Figure 24B). HeLa cultures were infected at 37 °C for 20 min. Harvested proteins were probed in immunoblots with cofilin or phospho-cofilin specific antibodies and detected by chemiluminescence. In  $\Delta tmeB$  infected cultures, there were decreased levels of phosphorylated cofilin compared to the other strains; however, these data were difficult to repeat consistently. The low reproducibility of these data may suggest a dynamic balance between active and inactive cofilin.

**Susceptibility of *C. trachomatis* TmeB mutant strains to pharmacologic inhibitors.** Cofilin is downstream of the Rac1 pathway. Rac1 activation stimulates PAK and LIMK phosphorylation which ultimately results in cofilin phosphorylation and the inactive state. Pharmacological inhibitors were employed to investigate Rac1 signaling and TmeA related pathways. HeLa cells were pretreated with the inhibitors for 15 min prior to

infection. The monolayers were then infected with *C. trachomatis* WT,  $\Delta tmeA-lx$ ,  $\Delta tmeB$ , WT+pTmeB, or  $\Delta tmeA/B$  by rocking for 1 hr at 37 °C. The  $\Delta tmeA-lx$  and WT+pTmeB strains have increased levels of TmeB (Chapter 4), while  $\Delta tmeA/B$  lack both TmeA and TmeB. Inhibitors were left on cultures for 2 hrs, then washed off and replaced with standard media. 24 hpi, primary inclusions were enumerated by fluorescent staining of fixed cultures. Percent recovery was calculated by comparing treated cultures with untreated cultures (Figure 25). In 1  $\mu$ g/mL cytochalasin D (actin), 50  $\mu$ M NSC (Rac1), and 7.5  $\mu$ M Wiskostatin (N-WASP) treated cultures,  $\Delta tmeA-lx$  and WT+pTmeB (both expressing overabundant TmeB), were more susceptible to treatment relative to WT based on decreased recovery.  $\Delta tmeB$  and  $\Delta tmeA/B$  were equally as susceptible or less susceptible compared to WT for all inhibitors. After treatment with 40  $\mu$ M CK-636 (Arp2/3), the WT+pTmeB strain no longer exhibited increased susceptibility compared to WT.

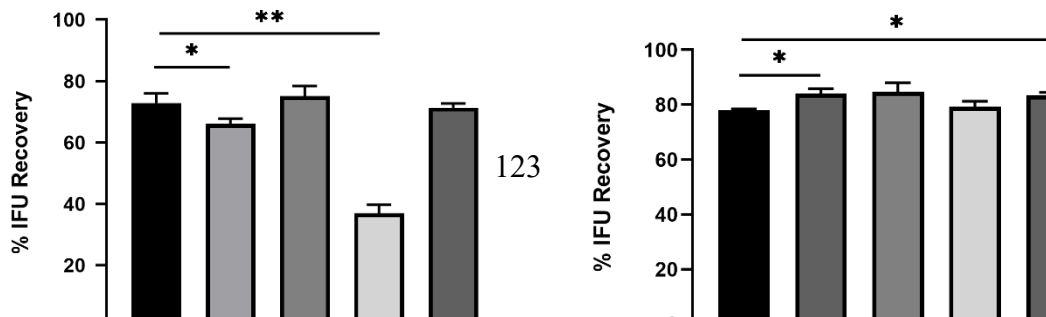
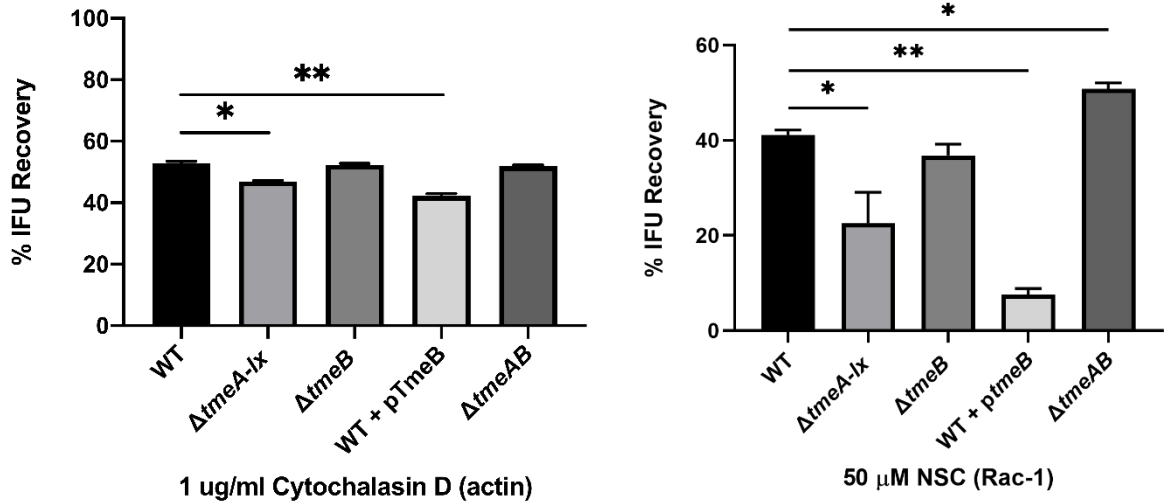


**Figure 25. *C. trachomatis* WT+pTmeB is more susceptible than WT to actin, Rac1, and N-WASP inhibition, but not Arp2/3 inhibition.**

HeLa monolayers were pretreated or not with drug inhibitors for 15 min, then infected for 1 hr at 37 °C with WT or mutant strains at an MOI of 0.5. Inhibitors remained on the cultures for 2 hpi and then were washed off. Pharmacologic disruption of actin polymerization, Rac1, N-WASP, or Arp2/3 was achieved using 1 µg/mL Cytochalasin D, 50 µM NSC, 7.5 µM wiskostatin, or 40 µM CK-636, respectively. Cultures were fixed 24 hpi, and inclusions were fluorescently labeled. Data are represented as mean values for the percentage of inclusions in treated cultures compared to untreated cultures shown with error bars at one standard deviation. Statistical significance was computed using a Student's t-test with Welch's correction (\*, P<0.05; \*\*\*, P<0.001).

These data agree with the notion that TmeB may function along Rac1 or N-WASP related actin polymerization pathways and the loss of susceptibility to inhibitor at Arp2/3 suggests Arp2/3 as a potential target for TmeB.

***C. trachomatis* TmeB may interact with the Arp2/3 complex.** To investigate a potential interaction between TmeB and Arp2/3, I utilized FLAG-tagged (FT) TmeB secreted from *C. trachomatis* (TmeB-FLAG; Figure 26A) or ectopically expressed in HeLa cells (pTmeB-FLAG; Figure 26B&C) and tested whether Arp2/3 could be pulled down concomitantly. First, I transformed  $\Delta tmeB$  with pBOMB TmeB-FLAG, where TmeB was inducible by a *tet* promoter. After transformants were clonally isolated, I maintained chlamydiae in the presence of aTc for two passages to induce expression of TmeB-FLAG. Then HeLa cultures were infected at an MOI of 2 and harvested for protein 24 hpi. FT

proteins were precipitated using anti-FLAG resin and probed in immunoblots with FLAG - or protein-specific antibodies. I detected an Arp2/3 cross-reactive band with WT samples; however, I noticed a higher MW band in the TmeB-FLAG samples with greater intensity than WT. I was unable to determine which band corresponded to Arp2/3 due to inadequate protein abundance.

To overcome this obstacle, I ectopically expressed TmeB-FLAG in HeLa cells. Whole -culture protein was harvested 30 hrs post nucleofection. TmeA-FLAG was used as a positive control for NWASP pull down. *C. pneumoniae* (Cpn) 0677-FLAG and 0678-FLAG were used as additional non-specific controls. I detected a very faint Arp2/3 band for TmeA-FLAG, TmeB-FLAG, and Cpn0677-FLAG samples. This interaction is likely through N-WASP for TmeA-FLAG and Cpn677-FLAG. TmeB-FLAG did not precipitate

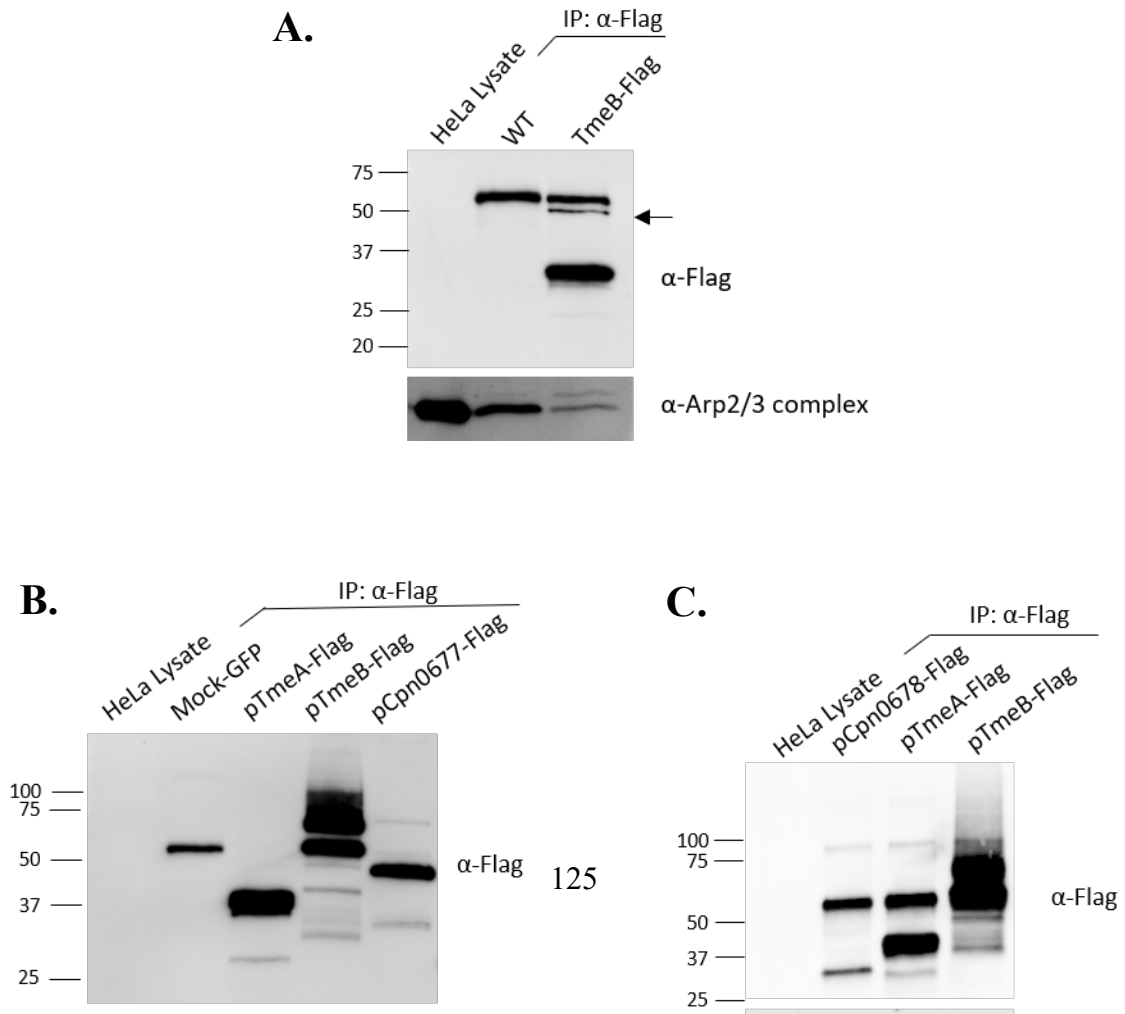


**Figure 26. FLAG-tagged TmeB precipitates with the Arp2/3 complex.**

(A) FLAG-tagged proteins were immunoprecipitated with anti-FLAG resin from whole-culture lysates of HeLa cells infected with *C. trachomatis* WT or TmeB-FLAG 24 hpi. Uninfected HeLa lysate was used as an antibody control. Proteins were probed in immunoblots with antibodies specific for FLAG-tag or the Arp2/3 complex. (B & C) HeLa cells were transfected to ectopically express TmeA-FLAG, TmeB-FLAG, Cpn0677-FLAG, or Cpn0678-FLAG for 30 hrs. Whole-cell material was harvested, and FT-proteins were precipitated with anti-FLAG resin. HeLa lysate was probed as a positive antibody control for host proteins, and Mock samples were used as a negative control.

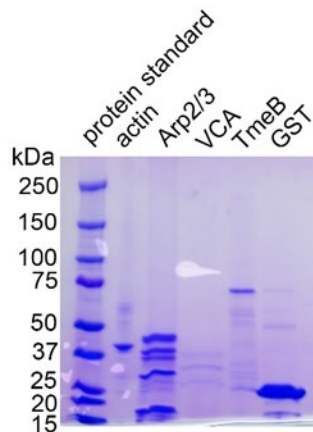
with N-WASP, which suggests an interaction with Arp2/3 may be independent of N-WASP.

***C. trachomatis* TmeB decreases the rate of actin polymerization.** I hypothesized that TmeB functions antagonistically from TmeA; therefore, a possible role for a TmeB interaction with the Arp2/3 complex is to prevent Arp2/3-mediated actin polymerization. Collaborators T. Jewett and K. Scanlon utilized an established *in vitro* assay leveraging pyrene-conjugated actin to examine the kinetics of actin polymerization (215) in the presence of selected purified proteins. G actin spontaneously assembles into filaments in physiological buffers but is limited by the instability of actin dimers and trimers, thus preventing rapid elongation (216, 217). Known actin nucleators, like TarP, increase elongation rate, resulting in increased fluorescence intensity (232). GST-tagged proteins were purified, and the tag was subsequently cleaved to prevent the possibility of GST

dimerization. Analysis of proteins in Coomassie-stained material indicates a homogeneous content for the respective proteins (Figure 27A). In Pyrenes assays, the combination of the Arp2/3 complex proteins and the VCA domain of N-WASP resulted in polymerization kinetics greater than the actin-only control. Notably, the addition of TmeB decreased the rate of polymerization to more closely resemble actin-only (Figure 27B). These data suggest that TmeB can function to inhibit actin polymerization mediated by activated N-WASP and the Arp2/3 complex.

***C. trachomatis* WT+pTmeB form smaller inclusions than WT.** One potential implication for Arp2/3 during *C. trachomatis* development beyond invasion is vesicle fusion. Vesicle fusion is primarily regulated by Rab GTPases and SNAREs, but actin patches have been demonstrated as preferred docking sites for vesicles trafficking to other

**A.**



**B.**

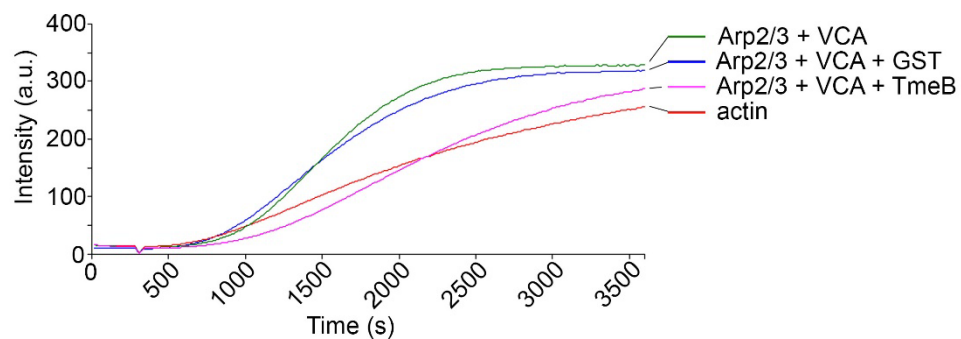


**Figure 27. TmeB decreases the rate of N-WASP-Arp2/3-dependent actin polymerization.**

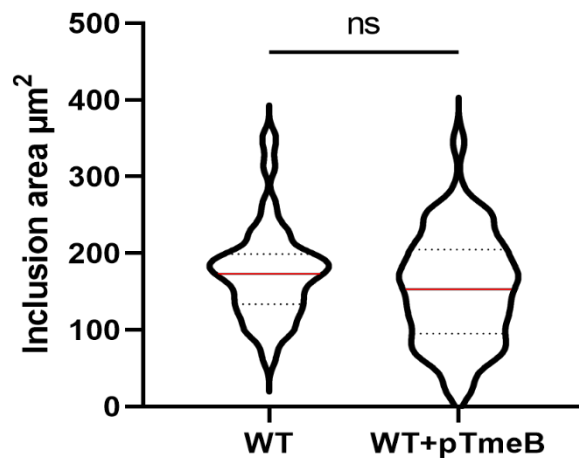
(A) Actin, the Arp2/3 complex, the VCA domain of N-WASP, and TmeB proteins employed in the pyrene actin polymerization assay were resolved by SDS-PAGE and visualized by Coomassie blue staining. (B) TmeB, Arp2/3 complex proteins, and VCA were added individually or in combination to monomeric pyrene-labeled actin. A TmeB-mediated decrease in actin polymerization compared to Arp2/3 + VCA + actin after the addition of polymerization buffer at 300 s was measured as the arbitrary fluorescence intensity (arbitrary units [a.u.] over time [s]) with excitation and emission wavelengths of 365 and 407 nm, respectively.

intracellular pathogen containing vacuoles like *Coxiella burnetii* (233). Therefore, I wanted to investigate whether excess TmeB disrupted inclusion area, which may suggest decreased lipid acquisition. HeLa cells were infected with *C. trachomatis* WT or WT+pTmeB and maintained in either RPMI (Figure 28A) or DMEM media (Figure 28B). DMEM is a more minimal media, so the effects of nutrient deprivation were predicted to be more robust. Cultures were fixed and fluorescently stained for inclusions 24 hpi. Areas were quantified for 100 chlamydial inclusions. There was no significant difference between *C. trachomatis* WT and WT+pTmeB inclusions areas in RPMI media (173  $\mu\text{m}^2$  and 153  $\mu\text{m}^2$ , respectively); however, there was a significant difference when grown in DMEM media (118  $\mu\text{m}^2$  and 84  $\mu\text{m}^2$ , respectively).

**The effect of TmeB during infection of a mammalian host *in vivo*.** Previous studies have shown that the *C. trachomatis* effector TmeA is important for infection in a murine model. During *in vitro* studies, the deletion of TmeB has provided a fitness

advantage to *C. trachomatis* in some instances (Figure 12B and 14C); thus, I wanted to determine if TmeB was also important during infection of a mammalian host. Groups of 5-week-old estrus synchronized mice were infected with  $5 \times 10^5$  IFUs of either *C. trachomatis* L2 WT,  $\Delta tmeB$ ,  $\Delta tmeB + pTmeB$ , or *Cis-tmeB* (Figure 29). Mice were intravaginally swabbed beginning at day 3 post-infection and every 4 days after. Shed IFUs were applied to a fresh monolayer of McCoy cells and infected by centrifugation. Infected monolayers were fixed and stained for IFUs 24 hpi. The overexpression of TmeB has been demonstrated to negatively affect *C. trachomatis* development *in vitro* (Chapter 4); therefore, trans-complemented TmeB *Chlamydia* was not an appropriate control for murine studies. I generated a cis-complemented *tmeB* strain to overcome this obstacle, where the

**A.**



**B.**

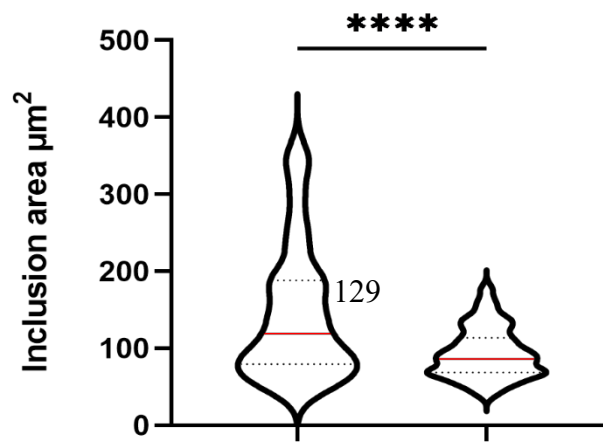
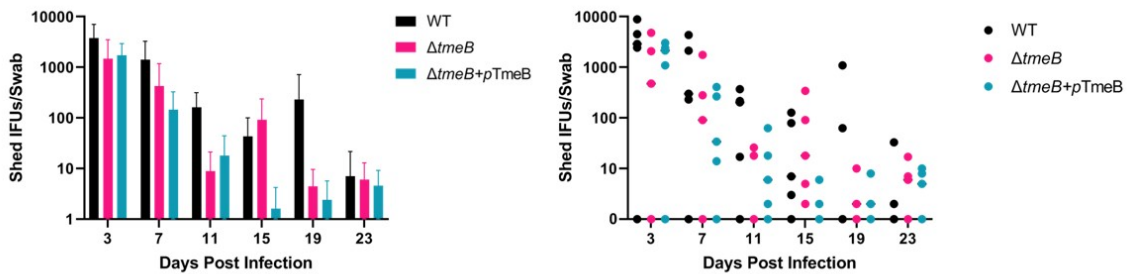


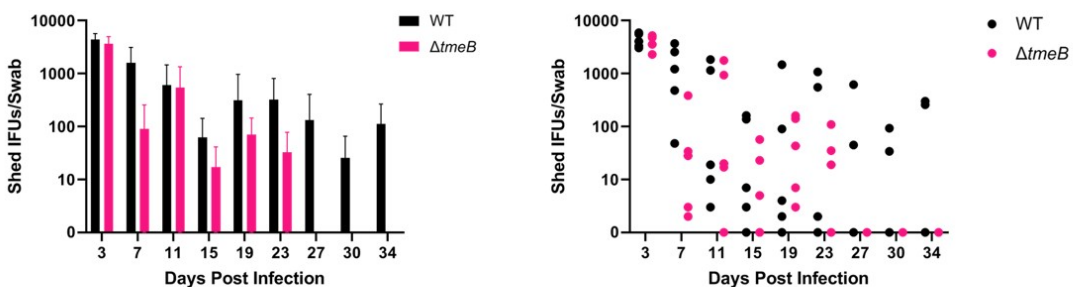
**Figure 28. *C. trachomatis* WT+pTmeB form smaller inclusions than WT.**

HeLa cells were infected using equivalent numbers of WT, or WT+pTmeB at an approximate MOI of 0.1. Cultures were maintained in (A) RPMI or (B) DMEM. At 24 hpi, cultures were methanol fixed and stained to enumerate areas from 100 chlamydial inclusions. Medians are represented by a red line and one standard deviation by dashed lines. Statistical significance was assessed using a Mann-Whitney U test (\*\*,  $P < 0.005$ ; \*\*\*\*,  $P < 0.0001$ ). Outliers were removed according to ROUT analysis with  $Q = 1\%$ .

**A.**



**B.**



**C.**

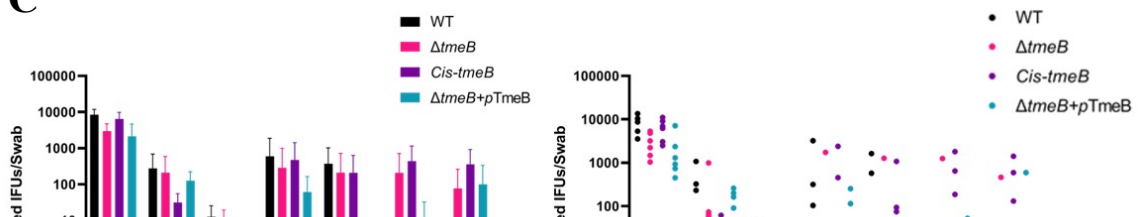


**Figure 29. *C. trachomatis* L2 *tmeB* mutant strains in a murine model.**

Groups of 5 (A&B) or 6 (C) female C3H/HeJ mice were infected intravaginally with  $5 \times 10^5$  IFUs and shed IFUs were enumerated beginning at day 3 and every 4 days following. (Left) Data are represented in bar graphs as means  $\pm$  standard deviation. (Right) Dot plots represent shed IFUs for each animal in the corresponding experiment. Overlapping dots may represent multiple animals at point zero (C; WT D23 & D27, n=5).

entire *tmeA/tmeB* locus was restored by allelic exchange in the  $\Delta tmeB$  mutant strain. Due to the variability of WT L2 infection in mice, I was unable to draw any clear conclusions about the impact of TmeB from these data. One general trend that I noticed was that both WT and TmeB mutant strains had decreased shedding between day 11 and day 15.

#### **6.4. Discussion**

*C. trachomatis* secrete the membrane-associated effectors A and B early during invasion, and they remain localized at the plasma and inclusion membranes, respectively, during later development (138, 139). TmeA and TmeB are encoded by a bicistronic operon and share the common chaperone Slc1. TmeA is directly involved in chlamydial invasion by promoting N-WASP/Arp2/3-mediated actin polymerization and functions synergistically with TarP. I found that TmeB overexpression negatively impacts chlamydial development (Chapter 4); however, the role of TmeB has remained an open

question. I present data that supports TmeB's interaction with the Arp2/3 complex and functions to inhibit Arp2/3-dependent actin polymerization.

Chlamydial invasion has been shown to promote the phosphorylation of many host targets (231). For example, *C. trachomatis* induces phosphorylation of EGFR and EphA2, which are required for chlamydial invasion and development (86, 151). I examined the global tyrosine phosphorylation profile of infected cells to see if any targets were differentially tyrosine-phosphorylated in the absence of TmeB. I identified cofilin as a host target that has decreased phosphorylation in the absence of TmeB. Phosphorylated cofilin is inactive, but when dephosphorylated, it functions to sever filamentous actin. These data suggest at native TmeB levels, cofilin favors the phosphorylated or inactive state. Data from these experiments were not robust in reproducibility, and the change in cofilin status was not observed at 24 hpi (data not shown); however, if cofilin activity is related to the function of TmeB, I speculate that it may be a result of the available pools of G-actin. Inhibition of actin polymerization by TmeB may cause an increase in the available G-actin and simulate negative feedback to promote the inactive form of cofilin. Cells contain multiple proteins to regulate the size and pool of actin monomers (234), so this is one of many explanations for the observed effect.

Many microbial species require cofilin activation and subsequent inactivation to remove the physical barrier of the actin network to complete invasion. Several parasites, such as *Plasmodium*, *Acanthamoeba*, *Trypanosoma*, and *Leishmania*, encode their own cofilin isoforms to regulate the actin cytoskeleton during invasion. Furthermore, HIV-1 induces rapid cofilin inactivation and actin polymerization for stability during attachment, followed by cofilin dephosphorylation during entry (reviewed in (216)). Upon *Legionella*

infection in WT macrophages, cofilin loses its basal phosphorylation status and is accompanied by an increase in the F-actin to G-actin ratio, which promotes fusion of the *Legionella*-containing vacuole with the lysosome (244).

Rac1 is a GTPase upstream of cofilin; therefore, we investigated the susceptibility of TmeB mutant strains to pharmacologic inhibitors of Rac1, actin, Arp2/3, and N-WASP. TmeB is not required for *C. trachomatis* invasion (Figure 11A), so drug inhibitors were left on cells for 2 hpi, and inclusions were examined at 24 hpi. *C. trachomatis*  $\Delta tmeA-lx$  and WT+pTmeB were more susceptible than WT to every inhibitor except Arp2/3, and this trend correlates with increased levels of TmeB. These data raise the possibility that Arp2/3 is a target for TmeB.

I directly investigated an interaction between FLAG-tagged TmeB and Arp2/3 by immunoprecipitation. I was unable to capture robust levels of TmeB-FLAG from infected cultures, which limited protein abundance. I detected a single band in WT infected cultures and a doublet in TmeB-FLAG infected cultures. These data may indicate an interaction but were overall unconvincing. I utilized a second approach with ectopically expressed pTmeB-FLAG to increase protein abundance and include more controls.

I detected N-WASP in pTmeA-FLAG and pCpn0677-FLAG precipitated protein samples. An interaction of Cpn0667 with N-WASP has not been described, so these data are novel. I also noticed weak bands for the Arp2/3 complex and IQGAP1. I did not detect an interaction with cofilin for any of the proteins. Because protein abundance was low, I cannot confidently rule out the possibility that these bands represent background and are not specific.

IQGAP1 can form a complex with Cdc42 and Rac through a domain similar to the catalytic domain of GTPase-activating proteins (GAPs); however, it does not contain GTPase activity (235, 236), and therefore stabilizes activated Rac1 and Cdc42. IQGAP1 seems to function at the interface of many cellular processes and includes binding sites for factors such as actin (237), extracellular signal-regulates kinase-2 (ERK2)(238), calmodulin (213), myosin essential light chain (239),  $\beta$ -catenin (240), and E-cadherin (241); therefore, IQGAP1 may be an intermediate factor in a broad range of TmeA and TmeB mediated effects.

Actin pyrene assays more directly support an interaction between TmeB and the Arp2/3 complex. These experiments utilized the VCA domain of N-WASP (also found in WAVE). The VCA domain consists of a verprolin-homology region that binds G-actin, a central cofilin-homology region, and an acidic region that mediate binding to the Arp2/3 complex. The VCA domain is sufficient to polymerize branched actin filaments and functions to bring an actin monomer to the trimer formed between Arp2/3 and actin, creating a nucleus for new filament formation. TmeB decreased the rate of VCA/Arp2/3-mediated actin polymerization. Because TmeB did not precipitate with N-WASP and does not contain a known actin-binding domain, TmeB is likely directly targeting the Arp2/3 complex or a specific subunit of the complex. Inclusion area data agree with the notion that inhibition of actin polymerization by TmeB negatively effects *C. trachomatis* development. I predict this effect is a result of nutrient acquisition that requires dynamic actin interactions at the inclusion membrane.

*Salmonella* Type III secreted effectors SopB, SopE2, and SptP are important for bacterial invasion and have also been associated with immune responses during

mammalian infection (204, 206); therefore, I wanted to determine if TmeB was important during murine infection. Across 3 replicate experiments,  $\Delta tmeB$  did not display any consistent trends in shed IFUs at later timepoints. One consistent pattern was the decrease in shed IFUs for all strains between day 11 and day 15 and likely correlates with activation of the adaptive immune response in mice (242).

## **CHAPTER 7: Summary and Future Directions**

Over 100 million people are infected each year with sexually transmitted *Chlamydia trachomatis*, an obligate intracellular bacterium (243). In the United States, *C. trachomatis* infection continues to be the number one reported bacterial sexually transmitted infection (8). More than 70% of infections are asymptomatic and asymptomatic infections are still associated with detrimental effects to female reproduction, such as infertility (13). Reproductive pathology is initiated and sustained by infected epithelial cells (19). In the absence of an efficacious vaccine, a basic understanding of how the bacteria invade host cells and maintain infection is an increasingly important area of research.

The type III secretion system (T3SS) is a vital virulence factor for *C. trachomatis* (244). Anti-host proteins are secreted through the apparatus into the host cytoplasm. The translocated membrane-associated effectors A and B (TmeA and TmeB) are secreted within 1 hr of invasion and are encoded by a bicistronic operon (139). TmeA and TmeB share a common bacterial chaperone, Slc1, with the effectors TarP and TepP. TarP is a well-characterized effector and modulates the actin cytoskeleton (131). TepP has been associated with host immune responses (111). The goal of the work presented here was to further characterize the contributions of TmeA and TmeB during host cell invasion and chlamydial development and determine if they were functionally related.

As an obligate intracellular pathogen, *C. trachomatis* has evolved redundant pathways to invade host cells (245). *Chlamydia* bear some inherent infectious properties since EB envelopes alone can enter into non-phagocytic cells and avoid lysosomal fusion (246). Although this pathway occurs with low efficiency, chlamydial surface proteins can mediate invasion independent of type III secretion and represent one mode of entry (91, 200, 247).

Although they are not absolutely essential for invasion, type III secreted effectors (T3SE) contribute to entry efficiency, chlamydial fitness, and have essential contributions during development. *C. trachomatis* strains that lack the effectors TmeA or TarP are attenuated during invasion compared to WT (132, 143). Furthermore, in the absence of chlamydial transcription and translation, inclusions (the chlamydial intracellular niche) are not able to fuse with trafficking vesicles to acquire nutrients, and are eventually targeted by lysosomes (103). The requirement of chlamydial protein synthesis for development suggests *Chlamydia* actively manipulate the host cell through the secretion of effectors.

Whether initiated by chlamydial ligands binding to host receptors or active stimulation by secreted effectors, chlamydial entry depends on signal transduction cascades following Rho family GTPase activity and culminate in the activation of the Arp2/3 complex (226, 248). The Rac1/WAVE2/Abi1/Arp2/3 pathway is required for *C. trachomatis* invasion, but not Cdc42 or RhoA (226). The Rac1 GTPase protein acts on Abi1 and WAVE2 to activate Arp2/3. The precise mechanism of Rac1 activation is not entirely understood; however, it is likely a result of TarP interactions with GEFs. Rac1 activation may also result from *Chlamydia* interactions with host surface proteins similar to *Listeria monocytogenes* InlB signaling. *L. monocytogenes* InlB plays a key role in modulating actin reorganization during invasion into various cell types. InlB interacts with its receptor, Met, and stimulates Rac signal transduction (249). InlB also binds gC1qR, which stimulates the tyrosine phosphorylation of signaling proteins, the activation of phosphatidylinositol 3-kinase (PI3K), and ultimately activation of the Arp2/3 complex (250, 251).

Multiple studies have highlighted additional host factors as being necessary for *C. trachomatis* invasion and actin reorganization. For example, Ephrin A2 (EphA2) is a host surface receptor that facilitates *C. trachomatis* adherence and entry (86). During invasion, EphA2 is strongly upregulated, yet it is depleted from the surface membrane and accumulates around the inclusion. EphA2 and its ligand Ephrin-A1 act at the cross-talk between PI3K, MAPK, Src family kinases, RhoA, and Rac1 (252). EphA2 activation and recruitment of PI3K are also required for chlamydial replication. The epidermal growth factor receptor (EGFR) is also important for *C. trachomatis* attachment and development (151). *C. trachomatis* increases the phosphorylation of EGFR, and the inhibition of EGFR

results in smaller inclusions, decreased intracellular calcium mobilization, and prevents the accumulation of F-actin around the inclusion (151). Healthy inclusions are encased in a network of F-actin and intermediate filaments that confer stability and prevent leakage of inclusion contents into the host cytoplasm (152).

The *C. trachomatis* effector TmeA was previously associated with actin remodeling by inhibiting the actin-bundling activities of host AHNAK (143). TmeA may interact with AHNAK to allow transient actin reorganization events; however, domain analysis studies also indicated that TmeA has additional functions affecting the cytoskeleton independent of AHNAK (137). I hypothesized that TmeA had additional functions that were important for *C. trachomatis* invasion and that TmeA was functionally related to TmeB based on their shared operon and timing of secretion.

Previous attempts to delete *C. trachomatis tmeA* utilized fluorescence-reported allelic exchange mutagenesis (FRAEM), which replaces targeted genes with a selection cassette encoding antibiotic resistance and green fluorescent protein (GFP) (143, 163). This method resulted in the deletion of *tmeA* but also decreased expression of downstream *tmeB* (143). The Fields Lab and I predicted that the FRAEM-selection cassette was exhibiting a polar effect and accounted for the lack of *tmeB* expression. To overcome this obstacle, we utilized Cre-*loxP* genome editing to remove the selection cassette, flanked by *loxP* sites, while transiently expressing Cre recombinase in *C. trachomatis*. We named this method floxed-cassette allelic exchange mutagenesis (FLAEM). The resulting strain contained a markerless *tmeA* deletion with a single *loxP* scar sequence and is referred to as,  $\Delta tmeA-lx$ . This strain restored expression of *tmeB*; however, we noticed that TmeB levels were increased compared to WT strains (Figure 6B).

In the  $\Delta tmeA-lx$  strain, the TmeA start and stop codons remain intact with a 33 bp scar sequence intervening. The TmeB start codon is a noncanonical GUG, which also remains unchanged (Figure 5C). The mechanism resulting in increased TmeB is unknown. One possibility may be that the deletion of the *tmeA* sequence (969 bp) increases the affinity of ribosomes to the ribosomal binding site (RBS) of TmeB. Because TmeA and TmeB share the same promoter region, the TmeA RBS remains on the transcript. One future approach could be to investigate the effect of deleting the DNA sequence associated with the TmeA RBS; however, because the TmeA stop codon remains intact, I do not anticipate that ribosomes are simply not releasing the transcript and continuing to translate TmeB.

Furthermore, if ribosomes did not recognize the stop codon of TmeA and continued to translate the intervening transcript region before the TmeB start codon, the TmeB start codon would be out of frame. Another approach would be to replace *tmeA* with a sequence encoding antibiotic resistance of ca. 900 bp since the increased size of the FRAEM selection cassette may be responsible if TmeB expression was decreased due to lesser affinity of ribosomes. For example, *tmeA* could be replaced with *bla* only (ca. 850 bp) instead of *gfp-bla*. This approach would be laborious without the aid of fluorescent reporting and would only rule out one possibility to explain variability in *tmeB* expression; therefore, I did not pursue these approaches.

I noticed that the *tmeA* deletion strain overexpressing TmeB,  $\Delta tmeA-lx$ , was developmentally attenuated compared to the  $\Delta tmeA$  strain, which lacked TmeA and TmeB. This observation led me to investigate whether TmeB abundance negatively affected *C. trachomatis* development and invasion. By utilizing *C. trachomatis* L2 WT and  $\Delta tmeB$

strains over-expressing TmeB, I concluded that indeed, increased TmeB abundance decreased invasion efficiency (Figure 11B). I also found that the  $\Delta tmeB$  mutant strain had increased developmental fitness compared to WT, indicated by increased ability to produce infectious progeny (Figure 14C) and increased ability to spread in plaquing assays (Figure 12B). Together, these data indicate that the presence of non-physiologic levels of TmeB has a dominant-negative effect on *C. trachomatis* development. Although increased plaque size associated with the  $\Delta tmeB$  strain could indicate a preference to exit host cells by lysis compared to extrusion, I suspect that larger plaques are associated with a developmental advantage based on the observation that  $\Delta tmeB$  chlamydiae produce more infectious progeny.

I was surprised that the  $\Delta tmeB$ +pTmeB strain did not have a greater defect in plaque area since  $\Delta tmeB$ +pTmeB produced fewer infectious progeny (Figure 10B) and genomes (Figure 10C) compared to WT, and the WT+pTmeB strain had decreased invasion efficiency (Figure 11B). One limitation of this study is the lack of antibiotic use. I did not include antibiotics in the agarose media because they would have degraded during the 7-day incubation at 37 °C. Therefore, it is possible that the pCompTmeB plasmid was lost during the course of the experiment. This event is unlikely because the native L2 plasmid is typically lost during FRAEM (163), and maintenance of the pCompAII plasmid becomes essential for virulence, yet this is still an important consideration. Another explanation of these data is that TmeB increases the propensity of chlamydiae to exit by lysis. This effect may compensate for decreased invasion efficiency and support that  $\Delta tmeB$  forms larger plaques due to an increase in progeny. Collectively, these data may indicate a role for TmeB after invasion and during a later stage of development, such as exit.

Experiments investigating the rate of extrusion with fluorescent chlamydiae would provide a greater understanding of a potential TmeB-related exit phenotype.

Progeny experiments enumerating IFUs also highlighted the difficulty in detecting subtle fitness differences between *C. trachomatis* strains. It was beneficial to quantify genomes after multiple passages to amplify the differences between bacterial strains. For example, the  $\Delta tmeAB$  deletion mutant appeared to generate relatively equal infectious progeny compared to WT (Figure 14C). Interestingly, the  $\Delta tmeAB$  double deletion mutant did have significantly fewer progeny genomes after 4 passages than WT (Figure 15A), which may result from a subtle invasion defect that is not easily detected after a single developmental cycle.

The observation that *C. trachomatis* strains lacking TmeA and overexpressing TmeB invade less efficiently and produce fewer progeny supports my hypothesis that these effectors function antagonistically. The levels of these effectors are likely closely balanced by *C. trachomatis*. Although  $\Delta tmeB$  appears to have a developmental advantage *in vitro*, TmeB may play a role *in vivo* or more complex environments.

Because the function of TmeB was utterly unknown, I reasoned that if TmeB works antagonistically to TmeA, identifying additional TmeA targets would narrow the scope of potential targets for TmeB. TarP is a well-characterized effector protein, so I wanted to determine the relationship of TmeA to TarP and utilize established invasion pathways, such as Rac1 signaling, to investigate additional host targets of TmeA. I assumed that three potential outcomes were possible to describe the relationship between TarP and TmeA during invasion. (i) TmeA and TarP function on two independent pathways; (ii) TmeA and

TarP function at different steps along the same pathway; (iii) or TmeA and TarP function on different branches of the same pathway (Figure 30).

Using percent invasion assays, we found that the  $\Delta tmeA-lx$  and  $\Delta tarp$  strains were similarly deficient, yet the double mutant manifested a compounded defect and significantly fewer invading IFUs at 30 min post-infection (Figure 17D). This suggested that TmeA and TarP may function independently or on different branches of the same path. Because signal transduction pathways involving Rac1 and Cdc42 converge at Arp2/3 activation, I predicted that TmeA and TarP likely functioned on individual branches of the same pathways and ultimately resulted in actin polymerization to facilitate invasion; however, the question remained of where TmeA was interacting.

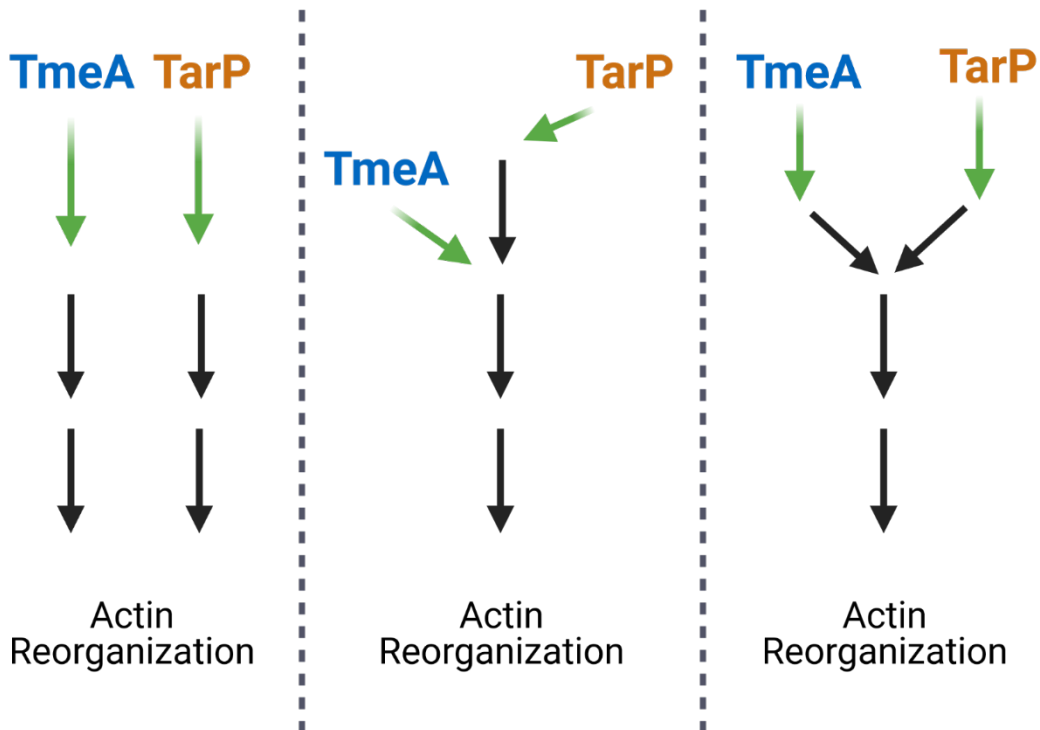


**Figure 30. A schematic representation of the possible relationships between TmeA and TarP.**

TmeA and TarP may function on separate (left), the same (middle), or different branches of the same pathway to promote actin polymerization (right).

Through BirA (J. Ferrel) and APEX proximity biotinylation assays, I identified CD44, EGFR, IQGAP1, and N-WASP as proximal proteins to TmeA (Figure 19). I confirmed an interaction between N-WASP and TmeA through immunoprecipitation assays. I also found that N-WASP transiently localizes at the site of EB entry during invasion in a TmeA-dependent manner. N-WASP is a nucleation promoting factor (NPF) and mediates Arp2/3 complex activation. Under resting conditions, N-WASP exists in an autoinhibited conformation. Interactions between the GTPase-binding domain (GBD) and the C region of the VCA domain obscure the regions that are required for Arp2/3 activation. Regulatory proteins bind the WASP-homology-1 (WH1) domain and modulate activation. Autoinhibition is also regulated by the binding of lipid second messenger molecules, Cdc42 to the GBD, and SH3 proteins to the proline-rich region. These factors can function individually or collaboratively to stimulate N-WASP activation (253). Simultaneous to the preparation of this work, Faris et al. found that TmeA may bind N-WASP at the GBD to

prevent the autoinhibited conformation and promote activity(219); therefore, TmeA may act as a Cdc42 mimic.

During actin polymerization, or actin nucleation, G-actin binds to the fast-growing barbed end of an actin filament or the slow-growing pointed end. Spontaneous actin polymerization must overcome a significant kinetic hurdle; therefore, actin regulators like formins, for linear actin filaments, and the Arp2/3 complex, for branched actin networks, facilitate this process (reviewed in (254)). Signal transduction pathways regulate NPFs. The best-studied pathways involve Class I NPFs, N-WASP and WAVE activation by Rho-family GTPases Cdc42 and Rac1, respectively.

We utilized pharmacological inhibitors to investigate the relationship of TmeA and TarP to Cdc42 and Rac1 signal transduction pathways for Arp2/3 activation (Figure 21). *C. trachomatis*  $\Delta tmeA-lx$  were less susceptible to inhibition of Cdc42 and N-WASP compared to WT. I expected that  $\Delta tmeA-lx$  would be more resistant to N-WASP inhibition due to the predicted interaction of TmeA with N-WASP. Cells infected with *C. trachomatis* lacking TmeA would likely have less N-WASP activation, so treatment with the N-WASP inhibitor is not expected to affect invasion significantly. However, it was interesting that  $\Delta tmeA-lx$  chlamydiae were also less susceptible to Cdc42 inhibition compared to WT. First, Cdc42 was not considered a significant factor in *C. trachomatis* invasion (226), yet these data suggest otherwise. Also, N-WASP is downstream of Cdc42, so I would expect that if Cdc42 activity were important for WT invasion, it would also be important upstream of N-WASP in the absence of TmeA.

I found that *C. trachomatis* TmeA was in proximity to IQGAP and may interact directly or indirectly. Therefore, the  $\Delta tmeA-lx$  chlamydiae may be more resistant to Cdc42

inhibitor treatment because TmeA may be involved in IQGAP1-Cdc42 signaling. This is a complex and exciting area of research since little is known about the molecular mechanisms *Chlamydia* uses to orchestrate cytoskeletal remodeling.

An important consideration for our inhibitor assays is that the  $\Delta tmeA-lx$  strain contains increased levels of TmeB compared to WT. This makes it difficult to draw conclusions about the role of TmeA alone. These studies would be improved with the addition of *C. trachomatis* WT overexpressing TmeB. In Figure 25, I present data from an experiment looking at percent IFU recovery instead of percent invasion. These data show similar susceptibility to N-WASP inhibitors for the  $\Delta tmeA-lx$  strain compared to WT, which are incongruent with what was found during percent invasion assays. Although these experiments are similar, they investigate two different time windows making direct comparisons between the two difficult. Instead, these data should be used as indicators of significant pathways during *C. trachomatis* invasion that require additional investigation.

Pyrene actin polymerization assays were useful to investigate the functions of TmeA and TmeB on actin polymerization more directly. I present evidence that TmeA increases the rate of N-WASP/Arp2/3-mediated actin polymerization and that TmeB decreases the rate of N-WASP/Arp2/3-mediated actin polymerization (Figures 22 and 27). These data fit a model where TmeA and TmeB function to regulate actin polymerization positively and negatively, respectively. Negative control of actin polymerization is an important aspect of bacterial pathogenesis. Many organisms have mechanisms for inhibiting actin or breaking down actin-dense regions. A central host protein involved in these processes is cofilin. When activated, cofilin severs filamentous actin, controls filament turnover, and regulates the pool of G-actin within the cell (255). When

phosphorylated, cofilin is inactivated. In yeast, cofilin is distributed throughout the cell but is specifically enriched at the cortical layers underneath the plasma membrane (256, 257). A variety of signaling molecules regulate cofilin. Activated RhoA can stimulate cofilin phosphorylation through ROCK and LIMK, while Cdc42 and Rac1 promote cofilin phosphorylation through PAK and LIMK (reviewed in (258)).

*Salmonella typhimurium* intricately regulates actin dynamics through employment T3SEs. In one proposed model (reviewed in (259)), SopE, SopE2, and SopB inactivate cofilin through Cdc42/Rac1-LIMK signals leading to F-actin stabilization and polymerization (202, 260-262). Meanwhile, SipA and SipC, actin-binding proteins, promote localized F-actin assembly (263, 264). Subsequently, Slingshot proteins, a family of phosphatases that also bind actin, mediate cofilin activation and increase treadmilling actin filaments at the site of entry to promote membrane protrusions and ruffling (265). Then, cofilin is downregulated by LIMK activation to facilitate final engulfment of the bacteria (251). Finally, a cofilin-independent mechanism is used to disassemble actin which involves other unidentified proteins (reviewed in (259)).

For *C. trachomatis* serovar D, CT166 is implicated in preventing Rho family protein activation by catalyzing their glucosylation (266) and ultimately promote the active state of cofilin. These data indicate that *Chlamydia* also have mechanisms for negative regulation of actin. I found evidence to suggest that *C. trachomatis* L2 TmeB is involved in the phosphorylation state of cofilin (Figure 24). This function is likely the result of indirect cofilin stimulation since cofilin and TmeB do not appear to interact in immunoprecipitation assays (Figure 26). *C. trachomatis* may stimulate cofilin activity during invasion to breakdown actin barriers, and subsequently stimulate cofilin

inactivation via phosphorylation to restore the stability of actin structures at the plasma membrane. The function of Rho-family GTPases and cofilin during *C. trachomatis* invasion are not well understood; thus, these data begin to reveal important factors during this process and shed light on an area requiring future study.

Beyond bacterial invasion, Rho-family GTPases are implicated in immune signaling. For example, during *Staphylococcus aureus* infection, Rac1 signaling was needed for TLR2-mediated activation of nuclear factor- $\kappa$ B (NF- $\kappa$ B) (267). Therefore, the overall effect of TmeA and TmeB activity could influence multiple cell signaling pathways and these effectors may have roles in addition to promoting entry. In APEX proximity labeling experiments, I found that TmeA is proximal to N-WASP at 24 hpi, well after invasion; therefore, this interaction may be important for later developmental events. Additionally, the  $\Delta tmeB$  strain did not invade host cells differently compared to WT in percent invasion assays (Figure 11A); however, this strain did create larger plaques and produced more infectious progeny. Two important developmental events that may be affected by the functions of TmeA and TmeB after invasion are vesicle fusion and extrusion.

Actin structures surround the chlamydial inclusion; however, it must be temporally accessible to intercept and fuse with trafficking vesicles from the Golgi to acquire nutrients (92, 268). *Chlamydia* scavenge lipids such as cholesterol, sphingomyelin, phosphatidylcholine, phosphatidylinositol, and cardiolipin which are incorporated into the outer membrane of both EBs and RBs (269, 270). *Chlamydia* trafficking to the peri-Golgi region and interception of host cell lipids requires chlamydial protein synthesis (103). Vesicle fusion is regulated in part by Rab GTPases and SNARE proteins and multiple

studies have described chlamydial interactions with Rab proteins. WASH has surfaced in recent years as another interesting host factor involved in the pinching off of vesicles and formation of actin patches for vesicle fusion (233). WASH is an Arp2/3 NPF and coats specific vesicles with F-actin (reviewed in (271)). WASH was not detected in my FT precipitation assays (data not shown). In my proposed model, TmeB functions to inhibit Arp2/3-mediated actin polymerization, so it may be that a minimum level of actin polymerization is required for efficient vesicle fusion, and  $\Delta tmeB$  strains are more efficient during these processes and result in greater numbers of progeny. Furthermore, WT+pTmeB bacteria formed smaller inclusions as compared to WT bacteria (Figure 28). These data are consistent with Arp2/3-mediated actin polymerization being required for vesicle fusion. One study I think would be beneficial to this area of research is determining if lipids, iron, and other nutrients differentially accumulate at inclusions of *C. trachomatis*  $\Delta tmeB$ , and WT+pTmeB mutant strains. Microscopy localization assays with nutrient-specific antibodies could be used to determine this effect.

Extrusion is another developmental step that may have implications for effectors involved in Rho-family signal transduction pathways. Rho GTPases, N-WASP, actin, and myosin regulatory light chain (MLC2) are important for pinching and releasing extruded inclusions (99, 272). *In vitro*, extrusion and host cell lysis occur at an equal ratio (99); however, extrusion has not been observed *in vivo*. Extrusion events may happen at different stages of infection and in response to diverse host environments. This may allow the regulation of excessive local inflammatory events in response to host lysis (273). For *C. trachomatis* L2, extruded inclusions also provide a protection strategy for surviving uptake by phagocytic cells and may sustain the chlamydiae until dissemination to new mucosal

tissues (274, 275). Quantifying release by extrusion for TmeA and TmeB strains with fluorescent bacteria would greatly contribute to this area of research.

To corroborate our *in vitro* data, I investigated the relevance of TmeB during *in vivo* infection. Multiple models have been used for chlamydial infection including mouse, guinea pig, and nonhuman primate. I used a mouse model for genital tract infection. *C. trachomatis* infection in mice is used to study the ability of the strain to cause infection; however, this model is not established to study pathogenesis. *C. trachomatis* infection in mice does not ascend to the upper genital tract and thus does not elicit severe pathology, such as hydrosalpinx, fluid-filled regions of the uterine horns (276, 277). Innate immunity is sufficient to clear *C. trachomatis* infection in mice (278).

I chose this model to determine the ability of *C. trachomatis* to invade, establish infection, and maintain infection. Due to the high variability of *C. trachomatis* L2 infection in mice, I was unable to draw any conclusions about the contributions of TmeB in establishing and maintaining infection. This study would be greatly improved by utilizing a mouse genital infection model with *C. muridarum*.

*C. muridarum* naturally infects mice in the wild and is a causative bacterium for mouse pneumonitis (279). The *C. muridarum* genital tract model is the most commonly used animal model for chlamydial infection to study immune responses and disease (280). Mice typically resolve *C. muridarum* infection within 3-4 weeks. *C. muridarum* differs from *C. trachomatis* in multiple ways regarding pathogenesis. *C. muridarum* encode three genes with similarities to large clostridial toxins, while *C. trachomatis* only encodes a partial copy of the cytotoxin (105). Unlike the urogenital *Chlamydia*, the LGV serovars are deficient in both active sites of the toxin and thus are the only serovars that can be infected

at high multiplicity of infection without toxicity to the host cells (281, 282). A high inoculum of *C. trachomatis* IFUs are required for murine infection, and yet is it common that not all animals will become infected. In murine models, this is an important distinction because the toxin is associated with *C. muridarum* resistance to  $\gamma$ -interferon-induced GTPases in murine cells.

FRAEM mutagenesis has not been established for *C. muridarum* and is complicated by plasmid tropism. *C. muridarum* cannot be transformed by the *C. trachomatis* plasmid and vice versa (283). Fortunately, the Fields Lab is developing a method for generating homologous *tmeA* and *tmeB* deletions in *C. muridarum*. These strains will be utilized in future studies to better understand the impact of TmeA and TmeB on chlamydial infectivity in a mammalian host and pathogenesis.

In conclusion, the data presented here support my hypothesis that TmeA and TmeB are functionally linked and have important roles during invasion and development. I utilized novel genetic approaches in *C. trachomatis* and ultimately found an additional function of TmeA in promoting Arp2/3-mediated actin polymerization through N-WASP and that TmeB may counteract this effect by inhibiting Arp2/3-mediated actin polymerization. Because TmeB was not found to interact with N-WASP, I predict actin inhibition is accomplished through an interaction with the Arp2/3 complex. Additional studies will reveal what subunits are involved in this interaction and further elucidate the temporal and spatial role of Arp2/3 during *C. trachomatis* development.

I present a model incorporating the previously discussed cell signaling pathways with the *C. trachomatis* Slc1 chaperoned effectors (Figure 31). This model highlights the redundant pathways stimulated by *Chlamydia* that cooperatively culminate in actin

remodeling. First, *Chlamydia* stimulates receptor-mediated signaling, such as PI3K and Src kinase activation. These factors, along with TarP and TepP, result in the activation of Rho Family GTPases. TarP and TmeA function downstream of these signals more directly to facilitate actin polymerization. TmeB negatively regulates actin polymerization, likely in a manner that has spatial requirements to inhibit actin polymerization. I also propose a model of TmeA and TmeB functions after invasion and later during development where TmeA may contribute to the stability of the host cell and inclusion, and TmeB may be involved in nutrient acquisition, exit, and regulation of host immune responses (Figure 32).

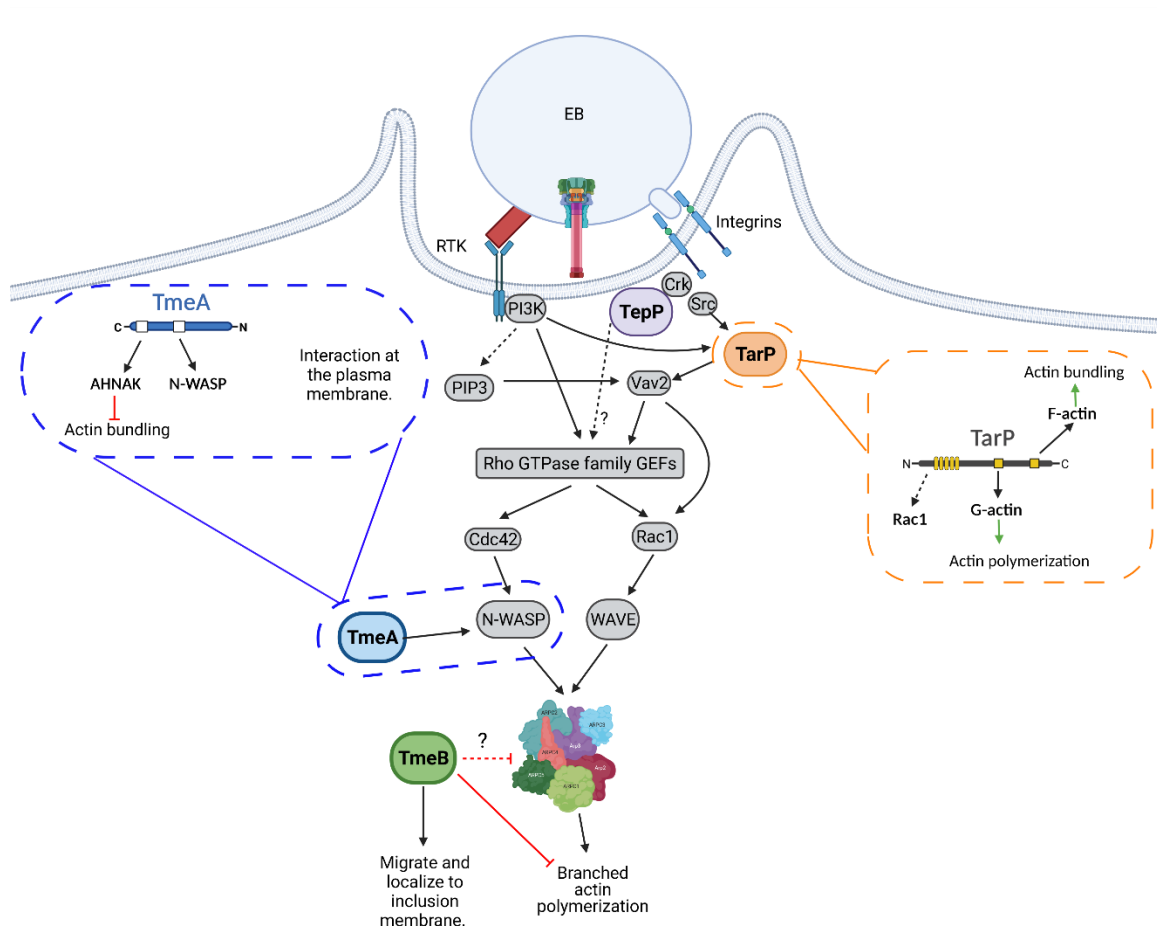


**Figure 31. Proposed model of *C. trachomatis* effectors TmeA, TmeB, TarP, and TepP interacting with host actin signaling pathways.**

*Chlamydia* induce actin polymerization through stimulation of host cell receptors, such as receptor tyrosine kinases (RTKs) and integrins, and by secreting effector proteins through the type III secretion system. The secreted effector TepP (purple) interacts with Crk I/II and may promote Rac1 activation through Rho GTPase guanine exchange factors (GEFs). TarP (orange) promotes Rac1 activation by interacting with Vav2 and other Rho GTPase GEFs. TarP also directly binds G-actin and nucleates actin to promote polymerization and binds F-actin to promote actin bundling. TmeA (blue) localizes to the plasma membrane and stimulates N-WASP activation, likely through a direct interaction, to promote actin polymerization. TmeA also interacts with AHNAK and inhibits actin bundling. TmeB (green) decreases actin polymerization which may be through an interaction with the Arp2/3 complex whereby TmeB prevents activation of the complex. TmeB also localizes to the inclusion membrane after invasion and may have additional function. Solid lines represent direct interactions, dashed lines represent indirect interactions. Question marks represent uncharacterized mechanisms.



## APPENDICES

### APPENDIX 1. List of Abbreviations

DG: Density gradient

EB: Elementary body

EGFR: Epidermal growth factor receptor

EphA2: Ephrin type-A receptor 2

Hpi: Hours post-infection

Hr: Hour

IFU: Inclusion forming unit

IL: Interleukin

ITG $\beta$ 1: Integrin beta-1

LGV: Lymphogranuloma venereum

Min: Minute

MLD: Membrane localization domain

MOI: Multiplicity of infection

N-WASP: Neural Wiskott-Aldrich Syndrome protein

PID: Pelvic inflammatory disease

PNM: Polymorphonuclear monocyte

Rac: Ras-related C3 botulinum toxin substrate 1

RB: Reticulate body

RT: Room temperature

Sec: Second

SNX9: Sorting nexin 9

STD: Sexually transmitted disease

STI: Sexually transmitted infection

TarP: Translocated actin recruiting phosphoprotein

TepP: Translocated early phosphoprotein

TmeA: Translocated membrane-associated effector A

TmeB: Translocated membrane-associated effector B

UGT: Upper genital tract

## APPENDIX 2. Complete List of Materials

Reagent	Company	Catalog Number	Details
Anhydrotetracycline hydrochloride (aTc)	ACROS Organics	233131000	50 ng/mL final concentration. Dissolved in DMSO.
Anti-FLAG M2 Affinity Gel	Sigma-Aldrich	A2220-1ML	
Aurum Total RNA Mini Kit	BioRad	732-6820	
Biotinyl-triamide	Chemodex	B0270	For APEX assays. Dissolved in anhydrous DMSO
Bovine Serum Albumin		12659	Fraction V, low heavy metals
Bromophenol Blue	EMD	Bx1410-7	
CaCl <sub>2</sub> Buffer	EMD Millipore		10 mM Tris pH 7.4, 50 mM Calcium Chloride Dihydrate
Calcium Chloride Dihydrate	Sigma	C7902-500G	Suitable for cell culture
Carbenicillin	Teknova	C2110	50 µg/mL final concentration
Complete Solubilization Solution (CSS; 3x)			For 20 mL: 6 mL SDS (20% w/v), 2.4 mL 2-mercaptoethanol, 6 mL glycerol (100%), 3.75 mL Tris pH 6.8 (1 M), 1.85 mL ddH <sub>2</sub> O, bromophenol blue
Cycloheximide	Sigma	7698-1G	1 µg/mL final concentration
Deoxynucleotide Solution Mix (dNTP)	New England BioLabs	N0447S	
DMEM	Gibco	11995-065	
DMSO	ATCC	4-X	Sterile filtered cell culture tested
DMSO anhydrous	Invitrogen	D12345	For Biotinyl-triamide reconstitution
DTT (DL-Dithiothreitol)	VWR Life Science	M109	

## Materials Continued

Reagent	Company	Catalog Number	Details
EDTA (Ethylenediamine Tetraacetic Acid)	MP	152521	
FLAG Peptide (3x)	Sigma-Aldrich	F4799	
Gentamicin Reagent Solution	Gibco	15750-060	
Gibson Assembly Master Mix	New England BioLabs	E2611L	
Glutamic acid	Sigma	G8415-100G	L-Glutamic acid
Glycerol	VWR Life sciences	0854-1L	
Halt Protease Inhibitor Single Use Cocktail	ThermoScientific	78425	
Hanks' Balanced Salt Solution (HBSS) (1x)	Gibco	24020-117	
HI (Heat Inactivated) FBS (Fetal Bovine Serum)	Gibco	10438-026	
High Capacity Neutravidin Agarose Resin	ThermoScientific	29202	
Hydrogen peroxide solution	Sigma	H1009	
iTaq Universal SYBR Green Supermix	BioRad	1725121	
Laemmli Buffer (6x)			For 10 mLs: 1.2g SDS, 4.7 mL glycerol, 1.2 mL 0.5 M Tris pH:6.8, 2.1 mL water, 0.93 g DTT, bromophenol blue
LE Quick Dissolve Agarose	GeneMate	E-3110-125	
McCoy Cells	ATCC	CRL-1696	
Monarch Plasmid Miniprep Kit	New England BioLabs	T1010L	
MOWIOL 4-88 Reagent	Calbiochem	475904	

## Materials Continued

Reagent	Company	Catalog Number	Details
NaCl (Sodium Chloride)	Fisher Scientific	BP358-10	
NaH <sub>2</sub> PO <sub>4</sub>	Sigma	S3139-250G	Sodium phosphate monobasic
Na <sub>2</sub> HPO <sub>4</sub>	Sigma	S5136-500G	Sodium phosphate dibasic
Neutral Red	VWR Life Science	E470-5G	>90%
Nonidet P 40 (NP40) Substitute	Sigma Life Science	74385-1L	
NP40 Buffer (Nonidet P 40 Substitute)	Sigma	74385	50 mM tris pH 7.5, 150 mM NaCl, 1 mM EDTA, 0.5% or 0.05% NP40
4D-Nucleofector	Lonza		
Penicillin G sodium salt	Sigma	P3032	
Pro-Q Diamond phosphoprotein gel stain	Invitrogen	P33301	
Q5 High-Fidelity DNA Polymerase	New England BioLabs	M0491S	
QIAfilter Plasmid Maxi Kit	Qiagen	12262	
Quenching Solution			10 mM sodium ascorbate, 10 mM sodium azide, 5 mM Trolox in PBS
ReadyPrep 2-D Starter Kit	BioRad	1632105	
ReadyStrip IPG Strips (7 cm)	BioRad	163-2001	pH 4-7
ReadyStrip IPG Strips (11 cm)	BioRad	1632015	pH 4-7
Rifampicin	Alfa Aesar	J60836	5 ng/mL final concentration
RIPA Buffer			50mM Tris HCl, pH7.4; 150mM NaCl, 0.1% SDS, 0.5% sodium deoxycholate

## Materials Continued

Reagent	Company	Catalog Number	Details
RIPA Buffer (Modified)			50mM Tris HCl, pH7.4; 150mM NaCl, 0.1% SDS, 0.5% sodium deoxycholate, 10 mM sodium azide, 10mM sodium ascorbate, 5mM Trolox, 5% Triton X-100, 1% SDS
RPMI 1640 Medium (1x)	Gibco	11875-093	Containing 2mM L- glutamine
SE Cell Line Solution Selection Media	Lonza	PBC1-02250	RMPI 10% FBS, 1 µg/mL cycloheximide, 500 µg/mL spectinomycin, and 50 ng/mL aTc
Sepharose 4B	Sigma	4B200-100 mL	
Sodium L-ascorbate	Sigma Life Science	11140-50G	
Sodium deoxycholic acid	Sigma	D-6750	
SDS (Sodium dodecyl sulfate)	Sigma-Aldrich	L4509	
Sodium orthovanadate (Vanadate)	Sigma	S6508-10G	200 mM stock solution in ddH <sub>2</sub> O
Spectinomycin dihydrochloridepentahydrate,	Alfa Aesar	J61820	100 µg / mL Final concentration. Cell culture grade.
Sucrose	Sigma	S1888-1KG	Bioreagent suitable for cell culture
Sucrose-Phosphate- Glutamate Buffer (SPG)			37.5g sucrose, 1.25 g Na <sub>2</sub> HPO <sub>4</sub> , 0.18 g NaH <sub>2</sub> PO <sub>4</sub> , 0.36 glutamic acid for 500 ml tissue culture grade ddH <sub>2</sub> O
SYPRO Ruby Protein Blot Stain	Lonza	50565	
T4 Polynucleotide Kinase	New England Biolabs	M0201S	
T4 DNA Ligase	New England Biolabs	M0202S	

## Materials Continued

<b>Reagent</b>	<b>Company</b>	<b>Catalog Number</b>	<b>Details</b>
TCA (Trichloroacetic acid)	Sigma	T6399-500G	
Tris	Amresco	0497-5KG	Ultrapure grade
Trolox	Millipore	648471	Solubility steps are described in (180) Note 4.
Trypsin-EDTA (1x)	Gibco	25200-056	0.25%
Tween 20	Amresco	M147-1L	
Water (Cell Culture)	Sigma	W3500-500ML	Sterile-filtered,
Zwittergent 3-14 Detergent	Milipore	693017-5GM	

## APPENDIX 3. Detailed Protocols

### 3.1. Direct IFU Counts

1. Seed  $2 \times 10^5$  HeLa cells in 24-well plates in triplicate for each strain with RPMI +10% RPMI. Incubate at 37 °C + 5% CO<sub>2</sub> for 24 hrs or until confluent.
2. Quantify EB concentration within laboratory stock using acridine orange stain.
  - a. Spike in acridine orange at 1:1000 to EB stock. Incubate at room temperature for 2 min.
  - b. Add the stained solution to 1 well of a 24-well plate containing a 12 mm coverslip.
  - c. Spin the plate at 900 xg for 15 min to adhere EBs to the coverslip.
  - d. Remove the inoculum and mount the coverslip on a slide.
  - e. Count the EBs in 10 fields of view using an epifluorescence microscope with a 100x oil immersion objective.
3. Prepare an equal number of EBs per strain in 15 mL conical tubes with HBSS to achieve an MOI of 0.5 per well.
4. Aspirate growth media from each well and apply 1 mL of HBSS inoculum per well.
5. Centrifuge the plate at 900 xg for 60 min at 20 °C using a swinging bucket rotor.
6. Aspirate the inoculum and add 1 mL RPMI + 10% FBS per well. Incubate the plate at 37 °C for 24 hrs.

7. Aspirate the media from each well and add 300  $\mu$ L MeOH. Incubate at room temperature for 8-10 min.
8. Aspirate the MeOH and wash each well 3 times with 1 mL PBS
9. Block each well with 1 mL TBST + 5% BSA for 1 hr at room temperature with gently rocking.
10. Aspirate the blocking solution and add 1 mL per well TBST + 5% BSA containing anti-HSP60 (mouse) primary antibody diluted at 1:500. Incubate the plate at room temperature for 1 hr with gentle rocking.
11. Aspirate the solution and wash each well 3 times with 1 mL of PBS.
12. Add 1 mL per well TBST + 5% BSA containing anti-mouse AlexaFluor-594 secondary antibody diluted at 1:250. Protect the plate from light and incubate at room temperature for 1 hr with gentle rocking.
13. Aspirate the solution and wash each well 3 times with 1 mL per well PBS.
14. Store the plate (protected from light) at 4 °C until ready to image.
15. Quantify the inclusions using the CellInsight CX5 High-Content Screening platform (ThermoFisher Scientific).

### 3.2. Progeny IFU Enumeration

1. Seed HeLa cells in two 24-well plates at  $2 \times 10^5$  cells per well in RPMI + 10% FBS. Incubate at 37 °C for 24 hrs or until confluent. One plate will be used for a titer plate and one plate will be passaged.
2. Make inoculum solutions by adding approximately equal IFUs to HBSS in a 15 mL conical tube to infect duplicate confluent HeLa monolayers at an MOI of 0.1-0.5.
3. Aspirate RPMI growth media from each well and add 1 mL of inoculum. Centrifuge the plates at 900 xg for 1 hr at 20 °C.
4. Aspirate the inoculum and add 1 mL per well RPMI + 10% FBS.
5. Incubate the plates at 37 °C + 5% CO<sub>2</sub> for 24 hrs.
6. Fix and stain the titer plate according to Appendix 3.1. Steps 7-15.
7. Harvest the remaining plate by mechanically scraping the well and transferring the contents into a 2 mL epitube. Spin the tube at  $>21,000$  xg in a 4 °C microcentrifuge for 30 min to pellet the harvested material.
8. Aspirate the supernatant and resuspend the pellet in 1 mL HBSS. Spin the material at 200 xg in a 4 °C microcentrifuge for 5 min to pellet HeLa cell debris.
9. Pull the supernatant into a fresh 1.5 mL epitube. Serially dilute the material in HBSS ( $10^{-2}$  -  $10^{-5}$ ). Apply 1 mL per well of serially diluted inoculum to fresh HeLa cell monolayers in a 24-well plate.
10. Centrifuge the plate at 900 xg for 60 min at 20 °C. Incubate the plates at 37 °C for 24 hrs.
11. Fix and stain the plate according to *Appendix 3.1. Steps 7-15.*

### 3.3. Quantifying Genomes over Multiple Passages and Penicillin Sensitivity Assay

1. Seed HeLa cells in 6-well plates at  $1 \times 10^6$  cells per well. Incubate the cells at  $37\text{ }^\circ\text{C}$  +  $5\%$   $\text{CO}_2$  for 24 hrs or until confluent.
2. Make up inoculum with approximately equal IFUs in a 15 mL conical tube in HBSS for an MOI of 0.5.
3. Aspirate RPMI growth media from each well and add 1 mL of inoculum to each well. Centrifuge the plates at  $900\text{ }xg$  for 1 hr at  $20\text{ }^\circ\text{C}$ .
4. Aspirate the inoculum and add 1 mL per well RPMI +  $10\%$  FBS containing appropriate antibiotics but not cycloheximide.
5. Incubate the plates at  $37\text{ }^\circ\text{C}$  +  $5\%$   $\text{CO}_2$  for 24 hrs.
6. Harvest the remaining plate by mechanically scraping and transfer the contents into a 2 mL epitube. Spin the tube at  $>21,000\text{ }xg$  in a  $4\text{ }^\circ\text{C}$  microcentrifuge for 30 min to pellet the harvested material.
7. Aspirate the supernatant and resuspend the pellet in 1 mL HBSS. Spin the material at  $200\text{ }xg$  in a  $4\text{ }^\circ\text{C}$  microcentrifuge for 5 min to pellet the HeLa cell debris.
8. Pull the supernatant into a fresh 1.5 mL epitube. Mix by flicking.
9. Transfer  $800\text{ }\mu\text{L}$  into a new tube for NaOH DNA extraction

*Note: If the DNA is not extracted from EBs on the same day it is harvested, the EBs may be pelleted at  $>21,000\text{ }xg$ , resuspended in SPG and frozen at  $-80\text{ }^\circ\text{C}$ .*

- a. Pellet the EBs at  $>21,000\text{ }xg$  in a  $4\text{ }^\circ\text{C}$  microcentrifuge. Aspirate the supernatant.

- b. Resuspended the pellet in 200  $\mu$ L of 0.5 M NaOH. Incubate at room temperature for 2 mins.
  - c. Add 200  $\mu$ L of Tris-Cl pH 8.0 and mix by gently pipetting.
  - d. Add 400  $\mu$ L of phenol-chloroform to the tube and vortex for 1 min.
  - e. Spin the tube in a room temperature microcentrifuge at  $>21,000$  xg for 20 min.
  - f. Pull 200  $\mu$ L of the aqueous phase (Top) into a fresh epitube.
  - g. Use 2  $\mu$ L of the aqueous phase in a qPCR reaction with iTaq Universal SYBR green supermix (Bio-Rad) and 16S specific primers (Table 2).
10. Dilute the remaining 200  $\mu$ L of supernatant in HBSS to infect fresh HeLa monolayers at an MOI of 0.5.

*Note: Typically a dilution of 1:500 or 1:200 is sufficient; however, the key is to dilute the supernatant so that inclusions remain detectable in subsequent infections with an MOI of ~0.5 for WT strains. An MOI of less than 0.3 will not provide enough material for reliable detection by qPCR after DNA extraction.*

11. Infect the plates by centrifuging at 900 xg for 1 hr at 20  $^{\circ}$ C.
12. Aspirate the inoculum and add 1 mL per well RPMI + 10% FBS. Incubate the plates at 37  $^{\circ}$ C + 5% CO<sub>2</sub> for 24 hours.
13. Repeat Steps 6-12 for 4-6 more passages.

### 3.4. 2D Gels

1. Seed HeLa cells at  $2 \times 10^5$  per well of a 24-well plate in RPMI + 10% FBS. Incubate at 37 °C with 5% CO<sub>2</sub> for 24 hrs or until confluent (2 wells per strain per 11 cm strip).
2. For experiments investigating invasion, serum starve the cell layers for 4 hours before infection.
  - a. Remove the media from the confluent monolayer.
  - b. Wash the monolayer once with serum free RPMI.
  - c. Add 1 mL per well of serum free RPMI and incubate for 4 hours at 37 °C with 5% CO<sub>2</sub>.
3. Prior to infection, make up enough lysis solution for 150 µl per well. Add Halt Protease Inhibitor (ThermoFisher Scientific) containing EDTA and freshly thawed vanadate (200 mM) at 1/100 in ice-cold water. Keep on ice until ready to use.
4. To infect, use enough EBs to achieve an MOI of 1000 and dilute with SPG for a final inoculum volume of 200 µl/well. Remove media from the cell monolayers and add 175 µl of inoculum to each well. Incubate the plate at 37 °C for 30 min with gentle rocking.
5. Aspirate the inoculum from the monolayers and wash twice with ice-cold PBS.
6. Set the plates on ice in the hood and add 150 µl lysis solution to each well. Using a p-1000, scrape the cell layers to detach. Transfer the lysate to 2 mL epitube and keep on ice.
7. Clean the samples by chloroform- methanol extraction.

- a. Pre-chill a microcentrifuge to 4 °C.
  - b. Add 600 µl of MeOH to each sample and vortex well
  - c. Add 150 µl of Chloroform to each sample and vortex well
  - d. Add 450 µl ddH<sub>2</sub>O to each sample and vortex well
  - e. Centrifuge at 12,000 RPM for 5 min at 4 °C.
  - f. Discard the top phase and keep the bottom phase including the white disk that sits at the interface of the two layers.
  - g. Add 450µl MeOH and vortex well
  - h. Centrifuge at 12,000 RPM for 5 min at 4 °C.
  - i. Discard the supernatant. Dry the pellet for 10 min.
  - j. Gently resuspend the two pellets in in 93 µl ready prep resuspension buffer (BioRad), then pool together for a total of 186 µl per sample.
8. The remaining steps were done according to the ReadyPrep 2-D Starter Kit Instruction Manual (BioRad, Cat # 163-2105).
9. Rehydrating the IPG Strips and Isoelectric focusing.
- a. Near the end of the day, remove IPG strips from the -20 °C freezer and allow to thaw on bench (20 min). Label the plastic part at the end of the strip with a sample ID.
  - b. Get a clean IEF focusing tray (do not clean the tray with EtOH) and dispense the protein sample evenly along one lane the length of the strip (left to right).
- Note: It helps to prop the long edge of the tray onto something so that the lane is slightly tilted, and the protein sample pools nicely along the edge of the lane.*

- c. Gently peel the plastic backing off the IPG strip using forceps. Lay the strip gel side down onto the protein sample avoiding any air bubbles. Ensure that the positive and negative ends of the strips correspond to the positive and negative electrodes of the tray. Allow to rehydrate for 30-45 min, then overlay each strip completely with mineral oil to prevent drying.
- d. Place the focusing tray into the Protean IEF cell aligning the positive and negative electrodes again and close the cover.
- e. Program the cell for passive rehydration (approx. 12 hrs) and select the appropriate focusing program according to the length of the strip. (For 7cm strip: step 1; 250 V for 20 min with linear ramp. Step 2; 4000 V for 2 hr with linear ramp. Step 3; 4,000 V for 10,000 V-hr with rapid ramp. For 11 cm strip: Step 1; 250 V for 20 min with linear ramp; Step 2; 8000 V for 2.5 hr with linear ramp; Step 3; 8000 V for 20000V-hr with rapid ramp.) The cell temperature should be 20 °C, with the maximum current of 50  $\mu$ A/ strip.
- f. After focusing, strips can be used immediately for separation in the second dimension or the excess mineral oil can be blotted off and the strips can be stored at -80 °C until ready to use.

#### 10. Equilibrate the strips

- a. Remove the strips from the rehydration tray and place on a dry piece of filter paper gel side up. Using a wet piece of filter paper, gently blot off any excess oil. If using strips from the freezer, allow to thaw for 10 min.
- b. Prepare equilibration buffers as described (ReadyPrep 2-D Starter Kit Instruction Manual).

- c. Place the strip, gel side up, into a clean well of the rehydration tray. Add 2 mLs of equilibration buffer I and gently rock for 15 min.
  - d. Empty off the equilibration buffer by tipping the tray over the blunt edge and flicking the tray. Note: if you tip over the curved edge the strips will slip out of the tray.
  - e. Add 2 mLs of Equilibration buffer II to each strip and incubate for 15 min with gentle rocking, then decant the equilibration buffer.
11. Run the strips in the second dimension. Precast gels or hand poured gels can be used for this step so long as the gel comb is long enough to fit the strip and that the gel is poured without the stacking phase.
- a. Remove the comb and the plastic strip along the bottom of the gel cassette. Use a piece of filter paper to blot out the excess water from the comb.
  - b. Remove the IPG strip from the rehydration tray. Wash the strip by dipping it into a cylinder of running buffer to remove excess equilibration buffer.
  - c. Place IPG strip on the gel cassette gel side up. Gently move the strip into the center of well until it is touching the gel.
  - d. Cut a piece of filter paper small enough to fit in the ladder position. Drop 5  $\mu$ l of protein ladder onto the filter paper and load the paper into the gel.
  - e. Microwave the overlay agarose until boiling in the microwave.
  - f. Using a pipette, quickly overlay the hot agarose over the IPG strip. Be careful not to trap any air bubbles. If air bubbles do occur, use forceps to gently push them out.
  - g. Let the agarose solidify 5-10 min, then proceed to run the gel as normal.

### 3.5. Percent Invasion Assay

1. Seed HeLa cells in a 24-well plate with 12 mm coverslips at  $2 \times 10^5$  cells per well.
2. Prepare inoculum by adding approximately equal density gradient purified EBs for an MOI of 20 to a 15 mL conical with HBSS.
3. Aspirate the growth media from each well and add 1 mL per well of inoculum. Infect the plate by rocking on ice for 1 hr, then incubate the plate at 37 °C for 30 min.
4. Fix the cultures with 4% paraformaldehyde for 20 min. Aspirate the paraformaldehyde and wash each well 3 times with PBS.
5. Block the monolayers by adding 1 mL per well PBST + 5% BSA to each well and incubate at room temperature for 1 hr with gentle rocking.
6. Aspirate blocking solution and label extracellular EBs by adding 1 mL per well PBST + 5% BSA containing mouse anti-LPS (Chlamydial) at a dilution of 1:1600. Incubate at room temperature for 1 hr with gentle rocking.
7. Aspirate the solution from each well and wash 3 times with 1 ml PBS.
8. Add 1 ml per well of PBST + 5% BSA containing anti-mouse AlexaFluor-594 diluted at 1:500. Incubate at room temperature for 30 min with gentle rocking. Protect the plate from light for the remaining steps.
9. Aspirate the solution from each well. Permeabilize the cells by adding 300  $\mu$ L of 0.1% Triton X-100 (Sigma) and incubate for 20 min at room temperature.
10. Aspirate the solution from each well and wash 3 times with 1 mL PBS.

11. Add 1 mL PBST + 5% BSA to each well and incubate for 1 hr at room temperature with gentle rocking.
12. Aspirate the blocking solution and add 300  $\mu$ L PBST + 5% BSA containing anti-MOMP (rabbit) 1:5000. Incubate the plate at room temperature for 1 hr with gentle rocking.
13. Add 300  $\mu$ L PBST + 5% BSA containing anti-rabbit AlexaFluor-488 at 1:500 to each well and incubate for 1 hr at room temperature with gentle rocking.
14. Aspirate the solution from each well and wash 3x with 1 mL PBS.
15. Quantify internal (green fluorescent only) and external (red and green fluorescent) EBs using an epifluorescence microscope for 10 fields of view. The percentage EB internalization is calculated using the formula  $([\text{total EBs} - \text{external EBs}] / \text{total red EBs}) \times 100 = \text{percent (\%)} \text{ invasion}$ .

### 3.6. N-WASP Localization

1. Seed HeLa cells in a 24-well plate with 12 mm coverslips at  $2 \times 10^5$  cells per well.
2. Prepare inoculum by adding approximately equal density gradient purified EBs for an MOI of 20 to a 15 mL conical with HBSS.
3. Aspirate the growth media from each well and add 1 mL per well of inoculum. Infect the plate by rocking on ice for 1 hr, then incubate the plate at 37 °C for 20 min.
4. Fix the cultures with 4% paraformaldehyde for 20 min. Aspirate the paraformaldehyde and wash each well 3 times with PBS.
5. Permeabilize the cells by adding 300  $\mu$ L of 0.1% Triton X-100 (Sigma) and incubate for 20 min at room temperature. Wash each well 3 times with PBS.
6. Block the monolayers by adding 1 mL per well PBST + 5% BSA to each well and incubate at room temperature for 1 hr with gentle rocking.
7. Aspirate blocking solution and label EBs by adding 1 mL per well PBST + 5% BSA containing rabbit anti-MOMP at a dilution of 1:5000. Incubate at room temperature for 1 hr with gentle rocking.
8. Aspirate the solution from each well and wash 3 times with 1 ml PBS.
9. Add 300  $\mu$ L per well of PBST + 5% BSA containing anti-rabbit AlexaFluor-594 diluted at 1:500. Incubate at room temperature for 30 min with gentle rocking. Protect the plate from light for the remaining steps.
10. Aspirate the solution from each well and wash 3 times with 1 mL PBS.

11. Add 300  $\mu$ L PBST + 5% BSA containing mouse anti-N-WASP at a dilution of 1:150. Incubate the plate at room temperature for 1 hr with gentle rocking.
12. Aspirate the solution from each well and wash 3 times with 1 mL PBS
13. Add 300  $\mu$ L PBST + 5% BSA containing anti-rabbit AlexaFluor-488 at 1:500 to each well and incubate for 1 hr at room temperature with gentle rocking.
14. Aspirate the solution from each well and wash 3x with 1 mL PBS
15. To mount coverslips onto slides:
  - a. Add 3  $\mu$ L of Mowiol (Calbiochem) onto a glass slide.
  - b. Using forceps, dip the coverslip in ddH<sub>2</sub>O then tap the edge on a kimwipe to remove excess water. Carefully put the edge of the slide in the Mowiol and slowly lower the slide into the oil cell side down.
  - c. Tap the center of the slide gently a few times to encourage air bubbles out.  
Allow the slides to harden on the bench top overnight protected from light.
16. View the slides using an epifluorescence microscope with an oil immersion 100x objective.
17. Localization was blindly scored by viewing labeled EBs (red), then looking for localized green fluorescence that was above background.

### 3.7. Nucleofection

1. Pre-warm the Cell Line Solution to RT and RPMI + 10% FBS to 37 °C.
2. Trypsinize a flask of 70-80% confluent HeLa cells.
3. Resuspend the trypsinized cells in RPMI + 10% FBS for a final volume of 10 mLs. Quantify cell density using a hemocytometer.
4. Transfer  $1 \times 10^6$  to  $5 \times 10^6$  cells into a sterile 15 mL conical tube.
5. Pellet the cells at 90 xg for 10 min at room temperature.
6. During the spin, add 100  $\mu$ l of SE cell line solution and 2 – 5  $\mu$ g DNA to a 1.5 mL epitube. Flick to mix.
7. Turn on the Nucleofector and select the cell line for the experiment program.
8. When the spin is done, quickly aspirate off the media, resuspend the pellet in the DNA solution, and transfer the mixture into a Lonza cuvette.
9. Load the cuvettes into the nucleofector and start the protocol. Once complete, quickly add 1 mL of RPMI + 10% FBS to each cuvette.
10. Remove the contents of each cuvettes with a plastic pasture pipette and dilute in a final volume of 12 mLs RPMI + 10% FBS.
11. Transfer 2 mLs/well in a 6-well plate.
12. Incubate for 24-48 hrs at 37 °C + 5% CO<sub>2</sub>.

### 3.8. Apex Biotinylation

The apex biotinylation procedure is described in detail by Olson et al (180).

1. Seed HeLa cells in a 6 well plate ( $1 \times 10^6$  cells per well) using DMEM supplemented with 10% FBS.
2. Once cells are confluent, remove media and add 2 mLs per well of HBSS inoculum containing enough EBs to achieve an MOI of 2. Infect by spinning the plates at 900 xg for 1 hr at 20 °C.
3. Replace the inoculum with 2 mLs per well DMEM + 10% FBS + 50 ng/mL aTc. Incubate the plates at 37 °C for 24 hrs.
4. Add the biotin-phenol (1.5mM final concentration) to each well 30 minutes before desired reaction time and incubate for 30 min at 37 °C + 5% CO<sub>2</sub>.
5. During the incubation, prechill PBS, lysis buffer, and 1.5 mL epitubes on ice. Prepare H<sub>2</sub>O<sub>2</sub> and quenching solutions and keep at RT.
6. To catalyze the biotin labeling reaction, aspirate the media from each well and add 2 mL per well of 3 mM H<sub>2</sub>O<sub>2</sub> in sterile PBS. Incubate the samples at RT for 1 minute with gentle rocking.

*Note: It is possible to do two plates at a time. If there are more than 2 plates, I find it best to stagger the infection/ biotinylation times by 15 minutes.*

7. After the labeling step, aspirate the H<sub>2</sub>O<sub>2</sub> solution and immediately quench the reaction three times with 1 mL / well washes using the quenching solution

(Appendix 2). During the washes, gently rock the plates for 15-30 seconds and aspirate off the solution between washes.

8. Place the plates on ice and add 166  $\mu$ l of Modified RIPA buffer (Appendix 2) containing protease inhibitors to each well. Scrape the cell layers in 3 different directions to lyse then tilt the plate and scrape the lysates into a pool at the bottom of the well.

*Note: I find it helpful to make a slant in the ice using the bottom of a tip box before setting my plates on ice.*

9. Collect the lysates from each plate into 1.5 mL epi tubes. Incubate the lysates on ice for 1 hr.
10. During the incubation, equilibrate the neutravidin beads and pre-chill a microcentrifuge at 4 °C. Vortex the beads and add 20  $\mu$ l of bead slurry to a 1.5 mL screw cap tube with a rubber gasket for each sample. Wash each tube of beads 3x with 1 mL lysis buffer by adding 1 mL to each tube, rotating on a rotisserie rocker at 4 °C for 5 min, spinning down the beads at max speed for 10 sec, remove the supernatant, and repeat.
11. Remove the insoluble fraction from the cell lysates by spinning them at 17,000  $\times$ g for 3 min. Transfer the supernatant (soluble fraction) onto the equilibrated neutravidin beads. Incubate on a rotisserie rocker at 4 °C overnight.
12. Add 50  $\mu$ l 3xCSS to the insoluble fraction (pellet) and heat at 95 °C for 5 min. Vortex to mix. Store this fraction at -80 °C or use immediately for Western blot analysis.

13. The next day, spin down the neutravidin resin using a pre-chilled microcentrifuge at max speed for 10 sec at 4 °C.
14. Move the supernatant (unbound fraction) into a new tube. This fraction can be saved for TCA or acetone precipitation and be used for western blot analysis.
15. Wash the neutravidin resin 3x 1 mL per sample with RIPA buffer containing protease inhibitors. During each wash, rotate the samples for 5 min at 4 °C on a rotisserie rocker.
16. To elute the proteins, pellet the neutravidin resin by spinning the samples at max speed for 10 sec then remove as much of the supernatant as possible. Add 30 µl of 3x CSS directly to the beads. Heat beads at 95 °C for 5 min.
17. For identification of biotinylated proteins using mass spectrometry, proteins are run into a 12% SDS-PAGE gel for 15 min at 200 V, stained with Sypro Ruby protein blot stain (Lonza), and cut into lanes. The University of Kentucky Proteomics Core performed digestion, preparation, and analysis of samples using Mascot data analysis software. A TSQ Vantage triple quadrupole mass spectrometer was used for liquid chromatography with tandem mass spectrometry (LC-MS/MS) protein identification.

*Note: The Proteomics Core will cut out the specified samples for you; however, I like to cut out my own gel slices. Use tubes that are specified for mass spectrometry such as Eppendorf safe lock tubes. These tubes are also provided by the Proteomics Core. Regular epitubes will not work. Use a fresh surgical blade to cut the desired region from the gel. Cover any area outside of the gel tray with plastic wrap, such as the UV imager, to avoid contamination.*

### 3.9. FLAG-Tag Immunoprecipitations

1. Before starting, pre-chill PBS, lysis buffer, and 1.5 mL epitubes on ice.
2. Remove plates from incubator and set on ice.
3. Aspirate off culture media and wash each well with 2 mLs ice-cold sterile PBS.  
Aspirate to remove.
4. Add 166  $\mu$ l of 0.5% NP40 lysis buffer (Appendix 2) containing Halt Protease Inhibitor Cocktail (ThermoFisher Scientific) and vanadate 1/100 to each well.
5. Scrape cell layer with a cell scraper in three different directions, then gently scrape the lysate down to pool in the bottom of the well.
6. Transfer and combine the lysates from each plate into a 1.5 mL epitubes.
7. Incubate on ice for 1 hr. Pre-chill a refrigerated microcentrifuge to 4 °C.
8. During the incubation, equilibrate Sepharose 4B beads by washing 3 times with lysis buffer.
  - a. Vortex the beads to create a slurry.
  - b. Add 20  $\mu$ l of the bead slurry to a 1.5 mL epitube with a rubber stopper in the cap, to prevent the sample from leaking.
  - c. Add 1 mL of lysis buffer and rotate on a rotisserie rocker for 5 min at 4 °C.
  - d. Pellet the beads by spinning at max speed for 10 sec. Remove lysis buffer without disturbing the beads and repeat two more times.
9. After incubation, centrifuge the cell lysates at 17,000 xg for 3 min at 4 °C to remove the insoluble fraction. Transfer the soluble fraction onto the equilibrated Sepharose 4B beads to preclear the lysates.

10. Incubate the lysates on a rotisserie rocker at 4 °C for 1 hr.
11. Add 50 µl of 3x CSS to the insoluble fractions. Heat at 95 °C for 5 min and vortex to mix. Store the insoluble fractions at -20 °C.
12. While the cell lysates pre-clear. Equilibrate the anti-FLAG M2 resin as described in Step 8.
13. Remove the Sepharose 4B beads from the lysate by centrifuging at max speed for 10 sec. Remove the supernatant without disturbing the bead pellet and transfer onto the equilibrated anti-FLAG M2 affinity resin. Incubate on a rotisserie rocker at 4 °C overnight.
14. The next day, pellet the anti-FLAG M2 affinity resin by centrifuging the samples at max speed for 10 sec at 4 °C in a pre-chilled microcentrifuge.
15. Transfer the unbound fraction into a new tube. This fraction can be saved for TCA or acetone precipitation if desired for analysis by western blot.
16. Wash the anti-FLAG M2 affinity resin 3 times with 1 mL 0.05% NP40 Wash Buffer, containing protease inhibitor and vanadate.  
  
*Note: The Wash buffer has a lesser concentration of detergent and should not be confused with the lysis buffer.*
17. Removes as much wash buffer from the beads as possible, then add 100 µl ice-cold PBS and 4 µl 3x FLAG peptide (Sigma-Aldrich) to the tube. Incubate on a rotisserie rocker for 1 hr.
18. Pellet the beads by spinning the samples at max speed for 10 secs. Transfer the supernatant into a new tube. Add 20 µl of 6x Laemmli buffer. Heat at 95 °C for 5 min.

### 3.9. Plaque Assay

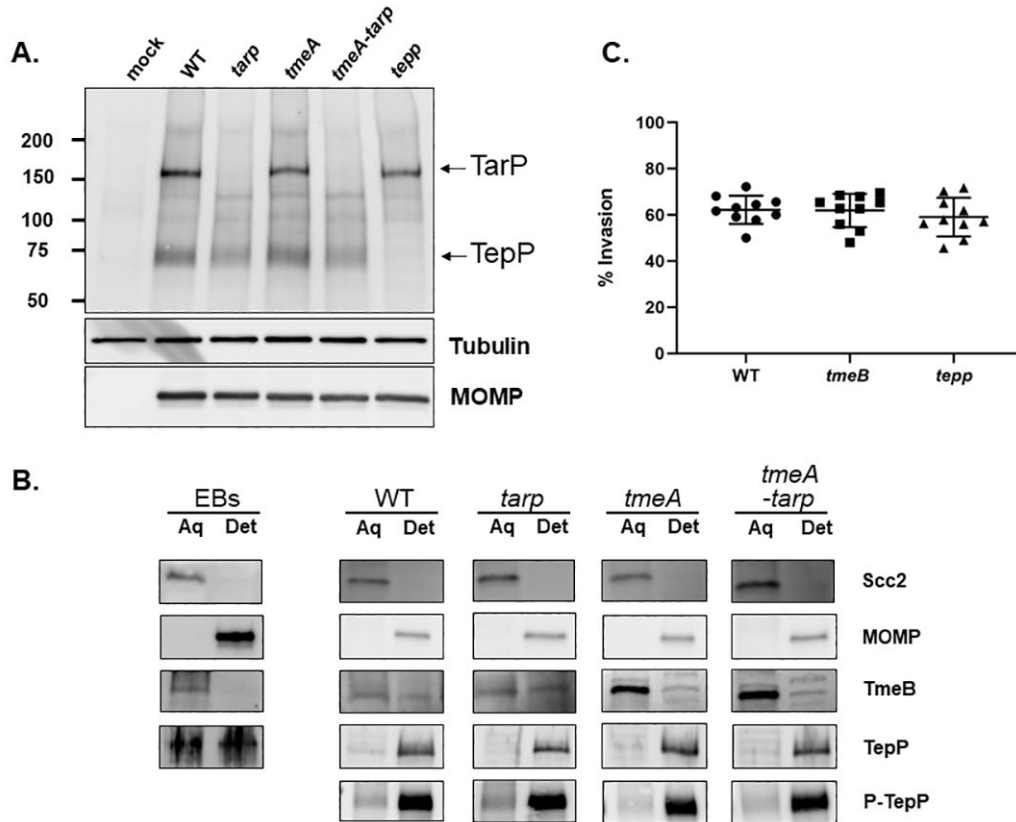
1. Seed  $1 \times 10^6$  Vero cells per well in a 6-well plate using RPMI supplemented with 10% FBS.
2. The next day, autoclave 0.5 g of Quick Dissolve agarose in 10 mL of cell culture grade water using a sterile 20 mL glass vial.

*Note: Fill a beaker with water and autoclave alongside agarose so that when the agarose comes out of the autoclave you have a "water bath" ready to go.*

3. While agarose is in the autoclave, infect Vero cells with approx. 100 EBs per well at 900 xg for 1 hr in HBSS.
4. During infection pre-warm 90 mLs RPMI + 10% FBS in a sterile plastic bottle to 40 °C.
5. Once the agarose comes out of the autoclave, move the vial to the "water bath" and transport to the lab. Place the "water bath" into the hood. The "water bath" will cool quickly. This is okay because you do not want the agarose to be too hot when adding the media, but the warm water will keep it from solidifying while you wait for the infection to complete.
6. After the infection, remove inoculum from each well. Work quickly at this step. Add 90 mLs of prewarmed media to the agarose, mix, and add 4 mLs per well of agarose containing media. Let the agarose solidify for 15 min before moving the plates back into a 37 °C incubator.
7. Plaques will form after 5-7 days.

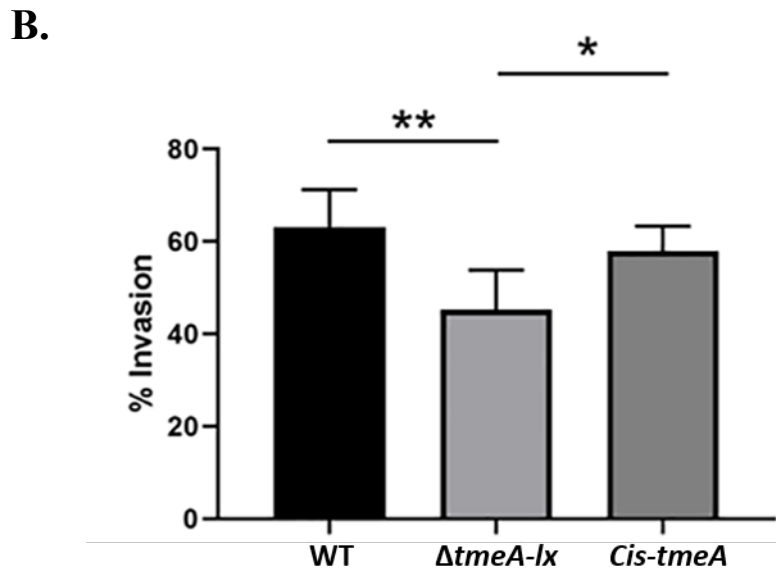
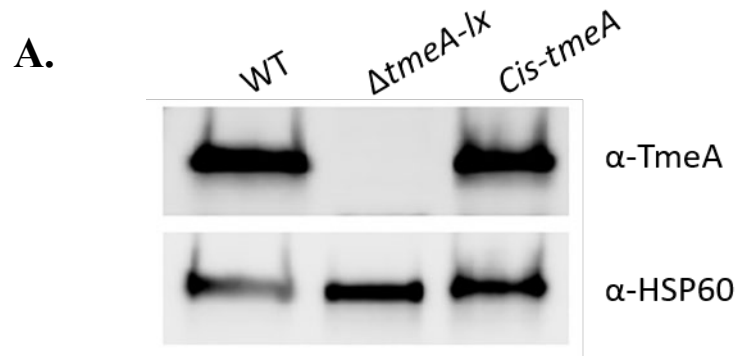
8. To Stain plaques with Neutral red:
  - a. Dissolve 120 mg / 2mL of Neutral red in sterile PBS Warm to 37 °C.
  - b. Autoclave 0.55 g Quick dissolve agarose in 50 mL cell culture water.
  - c. After autoclaving, add the warm neutral red solution to the agarose at a 1/100 dilution (0.06% final concentration).
  - d. Overlay 2 mL per well of neutral red agarose to cell layers.
  - e. Incubate plates at 37 °C for 3 hrs.
  - f. After staining, gently remove the agarose layers with forceps. Loosen the edges, tilt the plate up, and gently peel back the agarose starting from the top.
  - g. Count the plaques by eye or using the CellInsight CX5 High-Content Screening platform (ThermoFisher Scientific).

**APPENDIX 4. Loss of TmeA and Tarp Does Not Indirectly Impact Invasion via Effects on TepP or TmeB**



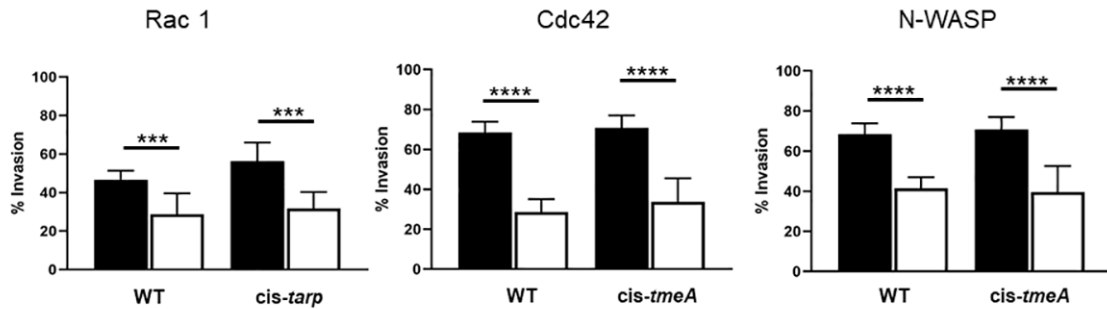
(A). Tyrosine phosphorylation of TarP and TepP was assessed in whole-culture material harvested 45 min after infections with equivalent IFUs of WT or strains lacking, *tarp*, *tmeA*, *tmeA* and *tarp* or *tepp*. SDS-PAGE-resolved material was probed with anti-phosphotyrosine-specific antibodies to visualize phosphor-TarP and TepP, while tubulin and MOMP were detected as loading controls for host and chlamydial material, respectively. (B). Pure WT EBs or HeLa cell monolayers infected with WT and mutant strains at an MOI of 100 for 1 hr were subjected to Triton X-114 detergent extraction. Proteins in detergent (Det) and aqueous (Aq) phases were concentrated, and fractions were probed in immunoblot analysis with TmeB- and TepP-specific antibodies. Material was probed for Scc2 and MOMP as aqueous and detergent controls, respectively. (C). HeLa monolayers were infected for 1 h at 4 °C with WT or strains lacking *tmeB* or *tepp* at an MOI of 10. Cultures were shifted to 37 °C for 30 min and then paraformaldehyde fixed and processed for inside-out staining to assess invasion efficiency. Data are represented as mean values for the percentage of internalized chlamydiae with standard deviations. No statistically significant differences were noted with Student's t-test with Welch's correction.

## APPENDIX 5. Cis Complementation of TmeA



Cis-complementation of  $\Delta tmeA-lx$  restores WT levels of TmeA and invasion efficiency. (A) Protein from equivalent IFU of DG-purified WT,  $\Delta tmeA-lx$ , and *cis-tmeA* EBs was concentrated and resolved for immunoblotting to compare relative levels of TmeA. TmeA was detected via specific antibodies, and detection of *C. trachomatis* Hsp60 was used as a loading control. (B) The ability of *cis-tmeA* to complement the  $\Delta tmeA-lx$  invasion phenotype was tested by infecting HeLa monolayers for 1 h at 4 °C with the WT,  $\Delta tmeA-lx$ , or *cis-tmeA* at an MOI of 10. Cultures were paraformaldehyde fixed and processed for inside-out staining to assess invasion efficiency after 45 min of incubation at 37 °C. Data are represented as the percentage of internalized chlamydiae with standard deviations. Statistical significance was computed using Student's t-test with Welch's correction (\*,  $P < 0.003$ ; \*\*,  $P < 0.0001$ )

## APPENDIX 6. Complementation of Mutants Restores Invasion Efficiency and WT Sensitivity to the Respective Inhibitors



Complementation of mutants restores invasion efficiency and WT sensitivity to the respective inhibitors. Invasion assays were carried out in the absence (black bars) or presence (white bars) of drugs, and levels of invasion for the WT were compared to the respective null mutants cis-complemented with full-length *tarp* or *tmeA*. Assays were carried out with 25  $\mu$ M Ehop-016 (Rac1) for *cis-tarp* and 20  $\mu$ M casin (Cdc42) or 25  $\mu$ M wiskostatin (N-WASP) for *cis-tmeA*. Data are represented as mean values for the percentage of internalized chlamydiae and are shown with standard deviations. Statistical significance was computed using Student's t-test with Welch's correction (\*\*\*,  $P < 0.0004$ ; \*\*\*\*,  $P < 0.0001$ )

## REFERENCES

1. Taylor-Brown A, Vaughan L, Greub G, Timms P, Polkinghorne A. 2015. Twenty Years of Research into *Chlamydia*-like Organisms: a Revolution in our Understanding of the Biology and Pathogenicity of Members of the Phylum Chlamydiae. *Pathogens and Disease* 73:1-15.
2. Dharamshi JE, Tamarit D, Eme L, Stairs CW, Martijn J, Homa F, Jørgensen SL, Spang A, Ettema TJG. 2020. Marine Sediments Illuminate Chlamydiae Diversity and Evolution. *Current Biology* 30:1032-1048.e7.
3. Taylor HRP, Burton MJF, Haddad DMD, West SP, Wright HF. 2014. Trachoma. *The Lancet* 384:2142-2152.
4. Bébéar C, de Barbeyrac B. 2009. Genital *Chlamydia trachomatis* Infections. *Clinical Microbiology and Infection* 15:4-10.
5. Mariotti SP, Pascolini D, Rose-Nussbaumer J. 2009. Trachoma: Global Magnitude of a Preventable Cause of Blindness. *British Journal of Ophthalmology* 93:563-568.
6. Grayston JT, Campbell LA, Kuo CC, Mordhorst CH, Saikku P, Thorn DH, Wang SP. 1990. A New Respiratory Tract Pathogen: *Chlamydia pneumoniae* Strain TWAR. *Journal of Infectious Diseases* 161:618-625.
7. Beeckman DSA, Vanrompay DCG. 2009. Zoonotic *Chlamydophila psittaci* Infections from a Clinical Perspective. *Clinical Microbiology and Infection* 15:11-17.

8. National Center for Hiv/Aids VHSTD, Prevention TBPDOS. 2019. Sexually Transmitted Disease Surveillance 2018. CDC,
9. Owusu-Edusei K, Chesson HW, Gift TL, Tao G, Mahajan R, Ocfemia MCB, Kent CK. 2013. The Estimated Direct Medical Cost of Selected Sexually Transmitted Infections in the United States, 2008. *Sexually Transmitted Diseases* 40:197-201.
10. San-pin W, Cho-chou K, Robert CB, Richard SS, Grayston JT. 1985. Immunotyping of *Chlamydia trachomatis* with Monoclonal Antibodies. *The Journal of Infectious Diseases* 152:791-800.
11. Stephens RS, Sanchez-Pescador R, Wagar EA, Inouye C, Urdea MS. 1987. Diversity of *Chlamydia trachomatis* Major Outer Membrane Protein Genes. *Journal of Bacteriology* 169:3879-3885.
12. Mohammadpour M, Abrishami M, Masoumi A, Hashemi H. 2016. Trachoma: Past, Present and Future. *Journal of Current Ophthalmology* 28:165-169.
13. Farley TA, Cohen DA, Elkins W. 2003. Asymptomatic Sexually Transmitted Diseases: the Case for Screening. *Preventive Medicine* 36:502-509.
14. Paavonen J, Eggert-Kruse W. 1999. *Chlamydia trachomatis*: Impact on human Reproduction. *Human Reproduction Update* 5:433-447.
15. Buckner LR, Amedee AM, Albritton HL, Kozlowski PA, Lacour N, McGowin CL, Schust DJ, Quayle AJ. 2016. *Chlamydia trachomatis* Infection of

Endocervical Epithelial Cells Enhances Early HIV Transmission Events. PloS One 11:e0146663-e0146663.

16. Peterman TA, Newman DR, Maddox L, Schmitt K, Shiver S. 2015. Risk for HIV Following a Diagnosis of Syphilis, Gonorrhoea or Chlamydia: 328,456 women in Florida, 2000-2011. *International Journal of STD and AIDS* 26:113-9.
17. Morré SA, Van den Brule AF, Rozendaal L, Boeke AJP, Voorhorst FJ, De Blok S, Meijer CJ. 2002. The Natural Course of Asymptomatic *Chlamydia trachomatis* Infections: 45% Clearance and no Development of Clinical PID after One-Year Follow-up. *International Journal of STD & AIDS* 13:12-18.
18. Brunham RC, Maclean IW, Binns B, Peeling RW. 1985. *Chlamydia trachomatis*: Its Role in Tubal Infertility. *The Journal of Infectious Diseases* 152:1275-1282.
19. Stephens RS. 2003. The Cellular Paradigm of Chlamydial Pathogenesis. *Trends in Microbiology* 11:44-51.
20. Longbottom D. 2003. Chlamydial Vaccine Development. *Journal of Medical Microbiology* 52:537-540.
21. Poston TB, Gottlieb SL, Darville T. 2017. Status of vaccine research and development of vaccines for *Chlamydia trachomatis* infection. *Vaccine* 37:7289-7294.
22. Abraham S, Juel HB, Bang P, Cheeseman HM, Dohn RB, Cole T, Kristiansen MP, Korsholm KS, Lewis D, Olsen AW, McFarlane LR, Day S, Knudsen S, Moen K, Ruhwald M, Kromann I, Andersen P, Shattock RJ, Follmann F. 2019.

- Safety and immunogenicity of the chlamydia vaccine candidate CTH522 adjuvanted with CAF01 liposomes or aluminium hydroxide: a first-in-human, randomised, double-blind, placebo-controlled, phase 1 trial. *The Lancet infectious diseases* 19:1091-1100.
23. Hafner LM. 2015. Pathogenesis of Fallopian Tube Damage Caused by *Chlamydia trachomatis* Infections. *Contraception* 92:108-115.
  24. Cooper MD, Rapp J Fau - Jeffery-Wiseman C, Jeffery-Wiseman C Fau - Barnes RC, Barnes Rc Fau - Stephens DS, Stephens DS. 1990. *Chlamydia trachomatis* Infection of Human Fallopian Tube Organ Cultures. *Journal of General Microbiology* 136:1109-15.
  25. Rasmussen SJ, Eckmann L, Quayle AJ, Shen L, Zhang Y-X, Anderson DJ, Fierer J, Stephens RS, Kagnoff MF. 1997. Secretion of Proinflammatory Cytokines by Epithelial Cells in Response to *Chlamydia* Infection Suggests a Central Role for Epithelial Cells in Chlamydial Pathogenesis. *The Journal of Clinical Investigation* 99:77-87.
  26. Kiviat NB, Wolner-Hanssen P, Eschenbach DA, Wasserheit JN, Paavonen JA, Bell TA, Critchlow CW, Stamm WE, Moore DE, Holmes KK. 1990. Endometrial Histopathology in Patients with Culture-Proved Upper Genital Tract Infection and Laparoscopically Diagnosed Acute Salpingitis. *The American Journal of Surgical Pathology* 14:167-175.
  27. Van Zandbergen G, Gieffers J, Kothe H, Rupp J, Bollinger A, Aga E, Klinger M, Brade H, Dalhoff K, Maass M, Solbach W, Laskay T. 2004. *Chlamydia*

- pneumoniae* Multiply in Neutrophil Granulocytes and Delay Their Spontaneous Apoptosis. *The Journal of Immunology* 172:1768-1776.
28. Kelly KA, Rank RG. 1997. Identification of Homing Receptors that Mediate the Recruitment of CD4 T Cells to the Genital Tract Following Intravaginal Infection with *Chlamydia trachomatis*. *Infection and Immunity* 65:5198-5208.
  29. Morrison SG, Morrison RP. 2000. *In Situ* Analysis of the Evolution of the Primary Immune Response in Murine *Chlamydia trachomatis* Genital Tract Infection. *Infection and Immunity* 68:2870-2879.
  30. Darville T, C. W. Andrews J, Laffoon KK, Shymasani W, Kishen LR, Rank RG. 1997. Mouse Strain-Dependent Variation in the Course and Outcome of Chlamydial Genital Tract Infection is Associated with Differences in Host Response. *Infection and Immunity* 65:3065-3073.
  31. Taylor MW, Feng G. 1991. Relationship between Interferon- $\gamma$ , Indoleamine 2,3-dioxygenase, and Tryptophan Catabolism. *The FASEB Journal* 5:2516-2522.
  32. Romanik M, Martirosian G, Wojciechowska-Wieja A, Cieřlik K, Kaźmierczak W. 2007. Co-occurrence of Indol-Producing Bacterial Strains in the Vagina of Women Infected with *Chlamydia trachomatis*. *Ginekologia polska* 78:611-615.
  33. Roshick C, Wood H, Caldwell HD, McClarty G. 2006. Comparison of Gamma Interferon-Mediated Antichlamydial Defense Mechanisms in Human and Mouse Cells. *Infection and Immunity* 74:225-238.

34. Kimani J, Maclean IW, Bwayo JJ, MacDonald K, Oyugi J, Maitha GM, Peeling RW, Cheang M, Nagelkerke NJD, Plummer FA, Brunham RC. 1996. Risk Factors for *Chlamydia trachomatis* Pelvic Inflammatory Disease among Sex Workers in Nairobi, Kenya. *The Journal of Infectious Diseases* 173:1437-1444.
35. Shemer-Avni Y, Wallach D, Sarov I. 1988. Inhibition of *Chlamydia trachomatis* Growth by Recombinant Tumor Necrosis Factor. *Infection and Immunity* 56:2503-2506.
36. Shemer-Avni Y, Wallach D, Sarov I. 1989. Reversion of the Antichlamydial Effect of Tumor Necrosis Factor by Tryptophan and Antibodies to Beta Interferon. *Infection and Immunity* 57:3484-3490.
37. Jordan SJ, Gupta K, Ogendi BMO, Bakshi RK, Kapil R, Press CG, Sabbaj S, Lee JY, Geisler WM. 2017. The Predominant CD4+ Th1 Cytokine Elicited to *Chlamydia trachomatis* Infection in Women is Tumor Necrosis Factor Alpha and Not Interferon Gamma. *Clinical and Vaccine Immunology* 24.
38. Darville T, Hiltke TJ. 2010. Pathogenesis of Genital Tract Disease Due to *Chlamydia trachomatis*. *The Journal of Infectious Diseases* 201 Suppl 2:S114-125.
39. Morrison RP, Feilzer K, Tumas DB. 1995. Gene Knockout Mice Establish a Primary Protective Role for Major Histocompatibility Complex Class II-Restricted Responses in *Chlamydia trachomatis* Genital Tract Infection. *Infection and Immunity* 63:4661-4668.

40. Morrison SG, Su H, Caldwell HD, Morrison RP. 2000. Immunity to Murine *Chlamydia trachomatis* Genital Tract Reinfection Involves B Cells and CD4+ T Cells but Not CD8+ T Cells. *Infection and Immunity* 68:6979-6987.
41. Punnonen R Fau - Terho P, Terho P Fau - Nikkanen V, Nikkanen V Fau - Meurman O, Meurman O. 1979. Chlamydial Serology in Infertile Women by Immunofluorescence. *Fertility and Sterility* 31:656-9.
42. Witkin SS, Jeremias J Fau - Neuer A, Neuer A Fau - David S, David S Fau - Kligman I, Kligman I Fau - Toth M, Toth M Fau - Willner E, Willner E Fau - Witkin K, Witkin K. 1996. Immune Recognition of the 60kD Heat Shock Protein: Implications for Subsequent Fertility. *Infectious Diseases in Obstetrics and Gynecology* 4:152-8.
43. Rund S, Lindner B, Brade H, Holst O. 1999. Structural Analysis of the Lipopolysaccharide from *Chlamydia trachomatis* Serotype L2. *The Journal of Biological Chemistry* 274:16819-16824.
44. Heine H, Müller-Loennies S, Brade L, Lindner B, Brade H. 2003. Endotoxic Activity and Chemical Structure of Lipopolysaccharides from *Chlamydia trachomatis* Serotypes E and L2 and *Chlamydophila psittaci* 6BC. *European Journal of Biochemistry* 270:440-450.
45. Ingalls RR, Rice PA, Qureshi N, Takayama K, Lin JS, Golenbock DT. 1995. The Inflammatory Cytokine Response to *Chlamydia trachomatis* Infection is Endotoxin Mediated. *Infection and Immunity* 63:3125-3130.

46. Prebeck S, Brade H, Kirschning CJ, da Costa CP, Dürr S, Wagner H, Miethke T. 2003. The Gram-Negative Bacterium *Chlamydia trachomatis* L2 Stimulates Tumor Necrosis Factor Secretion by Innate Immune Cells Independently of its Endotoxin. *Microbes and Infection* 5:463-470.
47. O'Connell CM, Ionova IA, Quayle AJ, Visintin A, Ingalls RR. 2006. Localization of TLR2 and MyD88 to *Chlamydia trachomatis* Inclusions: Evidence for Signaling by Intracellular TLR2 during Infection with an Obligate Intracellular Pathogen. *The Journal of Biological Chemistry* 281:1652-1659.
48. Darville T, O'Neill JM, Andrews CW, Jr., Nagarajan UM, Stahl L, Ojcius DM. 2003. Toll-Like Receptor-2, but not Toll-Like Receptor-4, Is Essential for Development of Oviduct Pathology in Chlamydial Genital Tract Infection. *The Journal of Immunology* 171:6187-6197.
49. Bas S, Neff L, Vuillet M, Spenato U, Seya T, Matsumoto M, Gabay C. 2008. The Proinflammatory Cytokine Response to *Chlamydia trachomatis* Elementary Bodies in Human Macrophages Is Partly Mediated by a Lipoprotein, the Macrophage Infectivity Potentiator, through TLR2/TLR1/TLR6 and CD14. *The Journal of Immunology* 180:1158-1168.
50. Derbigny WA, Johnson RM, Toomey KS, Ofner S, Jayarapu K. 2010. The *Chlamydia muridarum*-Induced IFN- $\beta$  Response is TLR3-Dependent in Murine Oviduct Epithelial Cells. *The Journal of Immunology* 185:6689-6697.

51. Matsumoto M, Funami K, Tanabe M, Oshiumi H, Shingai M, Seto Y, Yamamoto A, Seya T. 2003. Subcellular Localization of Toll-Like Receptor 3 in Human Dendritic Cells. *The Journal of Immunology* 171:3154-3162.
52. Fox A, Rogers JC, Gilbert J, Morgan S, Davis CH, Knight S, Wyrick PB. 1990. Muramic Acid is not Detectable in *Chlamydia psittaci* or *Chlamydia trachomatis* by Gas Chromatography-Mass Spectrometry. *Infection and Immunity* 58:835-837.
53. Welter-Stahl L, Ojcius DM, Viala J, Girardin S, Liu W, Delarbre C, Philpott D, Kelly KA, Darville T. 2006. Stimulation of the Cytosolic Receptor for Peptidoglycan, Nod1, by Infection with *Chlamydia trachomatis* or *Chlamydia muridarum*. *Cellular Microbiology* 8:1047-1057.
54. Brunham RC, Peeling RW. 1994. Chlamydia trachomatis antigens: role in immunity and pathogenesis. *Infectious Agents and Disease* 3:218-33.
55. Netea MG, Simon A, Veerdonk FLvd, Kullberg BJ, Meer JWMvd, Joosten LAB. 2010. IL-1beta Processing in Host Defense: Beyond the Inflammasomes. *PLoS Pathogens* 6:e1000661-e1000661.
56. Hvid M, Baczynska A, Deleuran B, Fedder J, Knudsen HJ, Christiansen G, Birkelund S. 2007. Interleukin-1 is the Initiator of Fallopian Tube Destruction During *Chlamydia trachomatis* Infection. *Cellular Microbiology* 9:2795-2803.
57. Muhammad TI, Justin HS, Ira MS, John NK, Kyle HR. 2006. Inhibition of Matrix Metalloproteinases Protects Mice from Ascending Infection and Chronic Disease

- Manifestations Resulting from Urogenital *Chlamydia muridarum* Infection. *Infection and Immunity* 74:5513-5521.
58. Sbardella D, Fasciglione GF, Gioia M, Ciaccio C, Tundo GR, Marini S, Coletta M. 2012. Human Matrix Metalloproteinases: An Ubiquitarian Class of Enzymes Involved in Several Pathological Processes. *Molecular Aspects of Medicine* 33:119-208.
59. Ault KA, Kelly KA, Ruther PE, Izzo AA, Izzo LS, Sigar IM, Ramsey KH. 2002. *Chlamydia trachomatis* Enhances the Expression of Matrix Metalloproteinases in an *In Vitro* Model of the Human Fallopian Tube Infection. *American Journal of Obstetrics and Gynecology* 187:1377-1383.
60. Ramsey KH, Sigar IM, Schripsema JH, Shaba N, Cohoon KP. 2005. Expression of Matrix Metalloproteinases Subsequent to Urogenital *Chlamydia muridarum* Infection of Mice. *Infection and Immunity* 73:6962-6973.
61. Barral R, Desai R, Zheng X, Frazer LC, Sucato GS, Haggerty CL, O'Connell CM, Zurenski MA, Darville T. 2014. Frequency of *Chlamydia trachomatis* -Specific T cell Interferon- $\gamma$  and Interleukin-17 Responses in CD4-Enriched Peripheral Blood Mononuclear Cells of Sexually Active Adolescent Females. *Journal of Reproductive Immunology* 103:29-37.
62. Beatty WL, Byrne GI, Morrison RP. 1993. Morphologic and Antigenic Characterization of Interferon  $\gamma$ -Mediated Persistent *Chlamydia trachomatis* Infection *In Vitro*. *Proceedings of the National Academy of Sciences - PNAS* 90:3998-4002.

63. Hogan RJ, Mathews SA, Mukhopadhyay S, Summersgill JT, Timms P. 2004. Chlamydial Persistence: Beyond the Biphasic Paradigm. *Infection and Immunity* 72:1843-1855.
64. Beatty WL, Morrison RP, Byrne GI. 1994. Persistent Chlamydiae: from Cell culture to a Paradigm for Chlamydial Pathogenesis. *Microbiological Reviews* 58:686-699.
65. Keb G, Fields KA. 2020. An Ancient Molecular Arms Race: *Chlamydia* vs. Membrane Attack Complex/Perforin (MACPF) Domain Proteins. *Frontiers in Immunology* 11:1490-1490.
66. McCormack R, de Armas L, Shiratsuchi M, Podack ER. 2013. Killing Machines: Three Pore-Forming Proteins of the Immune System. *Immunologic Research* 57:268-278.
67. Podack ER, Munson GP. 2016. Killing of Microbes and Cancer by the Immune System with Three Mammalian Pore-Forming Killer Proteins. *Frontiers in Immunology* 7:464.
68. Johnson AP, Osborn MF, Rowntree S, Thomas BJ, Taylor-Robinson D. 1983. A Study of Inactivation of *Chlamydia trachomatis* by Normal Human Serum. *The British Journal of Venereal Diseases* 59:369-372.
69. Osborn MF, Johnson AP, Taylor-Robinson D. 1985. Susceptibility of Different Serovars of *Chlamydia trachomatis* to Inactivation by Normal Human Serum. *Genitourinary Medicine* 61:244-246.

70. Lin JS, Yan LL, Ho Y, Rice PA. 1992. Early Complement Components Enhance Neutralization of *Chlamydia trachomatis* Infectivity by Human Sera. *Infection and Immunity* 60:2547-2550.
71. Hall RT, Strugnell T, Wu X, Devine DV, Stiver HG. 1993. Characterization of Kinetics and Target Proteins for Binding of Human Complement Component C3 to the Surface-Exposed Outer Membrane of *Chlamydia trachomatis* Serovar L2. *Infection and Immunity* 61:1829-1834.
72. Yang Z, Tang L, Zhou Z, Zhong G. 2016. Neutralizing Antichlamydial Activity of Complement by *Chlamydia*-Secreted Protease CPAF. *Microbes and Infection* 18:669-674.
73. Tseng C-TK, Rank RG. 1998. Role of NK Cells in Early Host Response to Chlamydial Genital Infection. *Infection and Immunity* 66:5867-5875.
74. Zhao L, Gao X, Peng Y, Joyee AG, Bai H, Wang S, Yang J, Zhao W, Yang X. 2011. Differential Modulating Effect of Natural Killer (NK) T Cells on Interferon- $\gamma$  Production and Cytotoxic Function of NK Cells and its Relationship with NK Subsets in *Chlamydia muridarum* Infection: Differential Modulation of NKT on NK Function. *Immunology* 134:172-184.
75. Perry LL, Feilzer K, Hughes S, Caldwell HD. 1999. Clearance of *Chlamydia trachomatis* from the Murine Genital Mucosa Does Not Require Perforin-Mediated Cytolysis or Fas-Mediated Apoptosis. *Infection and Immunity* 67:1379-1385.

76. Murthy AK, Li W, Chaganty BKR, Kamalakaran S, Guentzel MN, Seshu J, Forsthuber TG, Zhong G, Arulanandam BP. 2011. Tumor Necrosis Factor Alpha Production from CD8+ T Cells Mediates Oviduct Pathological Sequelae following Primary Genital *Chlamydia muridarum* Infection. *Infection and Immunity* 79:2928-2935.
77. Williams DM, Grubbs BG, Schachter J, Magee DM. 1993. Gamma Interferon Levels during *Chlamydia trachomatis* Pneumonia in Mice. *Infection and Immunity* 61:3556-3558.
78. Ni T, Gilbert RJC. 2017. Repurposing a Pore: Highly Conserved Perforin-like Proteins with Alternative Mechanisms. *Philosophical Transactions of the Royal Society of London Series B, Biological Sciences* 372.
79. McCormack RM, de Armas LR, Shiratsuchi M, Fiorentino DG, Olsson ML, Lichtenheld MG, Morales A, Lyapichev K, Gonzalez LE, Strbo N, Sukumar N, Stojadinovic O, Plano GV, Munson GP, Tomic-Canic M, Kirsner RS, Russell DG, Podack ER. 2015. Perforin-2 is Essential for Intracellular Defense of Parenchymal Cells and Phagocytes Against Pathogenic Bacteria. *eLife* 4.
80. Lee JK, Enciso GA, Boassa D, Chander CN, Lou TH, Pairawan SS, Guo MC, Wan FYM, Ellisman MH, Sütterlin C, Tan M. 2018. Replication-Dependent Size Reduction Precedes Differentiation in *Chlamydia trachomatis*. *Nature Communications* 9:45-9.
81. Nelson DE. 2012. Chlamydiales, p 74–96. *In* Tan MB, P. M (ed), *Intracellular Pathogens* vol 1. ASM Press

82. Omsland A, Sixt Bs Fau - Horn M, Horn M Fau - Hackstadt T, Hackstadt T. 2014. Chlamydial Metabolism Revisited: Interspecies Metabolic Variability and Developmental Stage-Specific Physiologic Activities. *FEMS Microbiology Reviews* 38:779-801.
83. Hegemann J, Moelleken K. 2012. Chlamydial Adhesion and Adhesins, p 97-125. *In* Tan M, Bavoil, PM. (ed), *Intracellular Pathogens 1: Chlamydiales*, vol 1. ASM Press, Washington, DC.
84. Stallmann S, Hegemann JH. 2016. The *Chlamydia trachomatis* Ctad1 Invasin Exploits the Human Integrin  $\beta$ 1 Receptor for Host Cell Entry. *Cellular Microbiology* 18:761-775.
85. Mölleken K, Becker E, Hegemann JH. 2013. The *Chlamydia pneumoniae* Invasin Protein Pmp21 Recruits the EGF Receptor for Host Cell Entry. *PLoS Pathogens* 9:e1003325.
86. Subbarayal P, Karunakaran K, Winkler A-C, Rother M, Gonzalez E, Meyer TF, Rudel T. 2015. EphrinA2 Receptor (EphA2) Is an Invasion and Intracellular Signaling Receptor for *Chlamydia trachomatis*. *PLOS Pathogens* 11:e1004846.
87. Conant CG, Stephens RS. 2007. *Chlamydia* Attachment to Mammalian Cells Requires Protein Disulfide Isomerase. *Cellular Microbiology* 9:222-232.
88. Ford C, Nans A, Boucrot E, Hayward RD. 2018. *Chlamydia* Exploits Filopodial Capture and a Macropinocytosis-like Pathway for Host Cell Entry. *PLOS Pathogens* 14:e1007051.

89. Fields KA, Hackstadt T. 2002. The Chlamydial Inclusion: Escape from the Endocytic Pathway. *Annual Review of Cell and Developmental Biology* 18:221-245.
90. Heinzen RA, Hackstadt T. 1997. The *Chlamydia trachomatis* Parasitophorous Vacuolar Membrane is not Passively Permeable to Low-Molecular-Weight Compounds. *Infection and Immunity* 65:1088-1094.
91. Scidmore MA, Rockey DD, Fischer ER, Heinzen RA, Hackstadt T. 1996. Vesicular Interactions of the *Chlamydia trachomatis* Inclusion are Determined by Chlamydial Early Protein Synthesis Rather than Route of Entry. *Infection and Immunity* 64:5366-5372.
92. Hackstadt T, Rockey DD, Heinzen RA, Scidmore MA. 1996. *Chlamydia trachomatis* Interrupts an Exocytic Pathway to Acquire Endogenously Synthesized Sphingomyelin in Transit from the Golgi Apparatus to the Plasma Membrane. *The EMBO Journal* 15:964-977.
93. Clausen JD, Christiansen G, Holst HU, Birkelund S. 1997. *Chlamydia trachomatis* utilizes the host cell microtubule network during early events of infection. *Molecular microbiology* 25:441-449.
94. Grieshaber SS, Grieshaber NA, Hackstadt T. 2003. *Chlamydia trachomatis* uses Host Cell Dynein to Traffic to the Microtubule-Organizing Center in a p50 Dynamitin-Independent Process. *Journal of Cell Science* 116:3793-3802.

95. Hackstadt T, Fischer ER, Scidmore MA, Rockey DD, Heinzen RA. 1997. Origins and Functions of the Chlamydial Inclusion. *Trends in Microbiology* (Regular ed) 5:288-293.
96. KA F. 2012. Chlamydiales, p 192-216. *In* Tan MB, PM (ed), *Intracellular Pathogens* vol 1. ASM Press.
97. Wilson DP, Timms P, McElwain DLS, Bavoil PM. 2006. Type III Secretion, Contact-dependent Model for the Intracellular Development of *Chlamydia*. *Bulletin of Mathematical Biology* 68:161-178.
98. David PW, Judith AW-H, Peter T, Patrik MB. 2009. Kinematics of Intracellular Chlamydiae Provide Evidence for Contact-Dependent Development. *Journal of Bacteriology* 191:5734-5742.
99. Hybiske K, Stephens RS. 2007. Mechanisms of Host Cell Exit by the Intracellular Bacterium *Chlamydia*. *Proceedings of the National Academy of Sciences* 104:11430-11435.
100. Elwell C, Mirrashidi K, Engel J. 2016. *Chlamydia* Cell Biology and Pathogenesis. *Nature Reviews Microbiology* 14:385-400.
101. Galán JE, Lara-Tejero M, Marlovits TC, Wagner S. 2014. Bacterial Type III Secretion Systems: Specialized Nanomachines for Protein Delivery into Target Cells. *Annual Review of Microbiology* 68:415-438.

102. Betts-Hampikian HJ, Fields KA. 2010. The Chlamydial Type III Secretion Mechanism: Revealing Cracks in a Tough Nut. *Frontiers in Microbiology* 1:114-114.
103. Fields KA, Mead DJ, Dooley CA, Hackstadt T. 2003. *Chlamydia trachomatis* Type III Secretion: Evidence for a Functional Apparatus During Early-Cycle Development. *Molecular Microbiology* 48:671-683.
104. Valdivia RH. 2008. Chlamydia Effector Proteins and New Insights into Chlamydial Cellular Microbiology. *Current Opinion in Microbiology* 11:53-59.
105. Read TD, Brunham RC, Shen C, Gill SR, Heidelberg JF, White O, Hickey EK, Peterson J, Utterback T, Berry K, Bass S, Linher K, Weidman J, Khouri H, Craven B, Bowman C, Dodson R, Gwinn M, Nelson W, DeBoy R, Kolonay J, McClarty G, Salzberg SL, Eisen J, Fraser CM. 2000. Genome Sequences of *Chlamydia trachomatis* MoPn and *Chlamydia pneumoniae* AR39. *Nucleic Acids Research* 28:1397-1406.
106. Read TD, Myers GSA, Brunham RC, Nelson WC, Paulsen IT, Heidelberg J, Holtzapple E, Khouri H, Federova NB, Carty HA, Umayam LA, Haft DH, Peterson J, Beanan MJ, White O, Salzberg SL, Hsia RC, McClarty G, Rank RG, Bavoil PM, Fraser CM. 2003. Genome Sequence of *Chlamydophila caviae* (*Chlamydia psittaci* GPIC): Examining the Role of Niche-Specific Genes in the Evolution of the Chlamydiaceae. *Nucleic Acids Research* 31:2134-2147.
107. Thomson NR, Yeats C, Bell K, Holden MTG, Bentley SD, Livingstone M, Cerdeño-Tárraga AM, Harris B, Doggett J, Ormond D, Mungall K, Clarke K,

- Feltwell T, Hance Z, Sanders M, Quail MA, Price C, Barrell BG, Parkhill J, Longbottom D. 2005. The *Chlamydomonas reinhardtii* Genome Sequence Reveals an Array of Variable Proteins that Contribute to Interspecies Variation. *Genome Research* 15:629-640.
108. Azuma Y, Hirakawa H, Yamashita A, Cai Y, Rahman MA, Suzuki H, Mitaku S, Toh H, Goto S, Murakami T, Sugi K, Hayashi H, Fukushi H, Hattori M, Kuhara S, Shirai M. 2006. Genome Sequence of the Cat Pathogen, *Chlamydomonas reinhardtii*. *DNA Research* 13:15-23.
109. Abby SS, Rocha EPC. 2012. The Non-Flagellar Type III Secretion System Evolved from the Bacterial Flagellum and Diversified into Host-Cell Adapted Systems. *PLoS Genetics* 8:e1002983-e1002983.
110. Fattori J, Prando A, Fau - Martins AM, Martins Am Fau - Rodrigues FHdS, Rodrigues Fh Fau - Tasic L, Tasic L. 2011. Bacterial Secretion Chaperones. *Protein and Peptide Letters* 18:158-166.
111. Chen Y-S, Bastidas RJ, Saka HA, Carpenter VK, Richards KL, Plano GV, Valdivia RH. 2014. The *Chlamydia trachomatis* Type III Secretion Chaperone Slc1 Engages Multiple Early Effectors, Including TepP, a Tyrosine-phosphorylated Protein Required for the Recruitment of CrkI-II to Nascent Inclusions and Innate Immune Signaling. *PLoS Pathogens* 10:e1003954.
112. Heinzen RA, Scidmore MA, Rokey DD, Hackstadt T. 1996. Differential Interaction with Endocytic and Exocytic Pathways Distinguish Parasitophorous

- Vacuoles of *Coxiella burnetii* and *Chlamydia trachomatis*. Infection and Immunity 64:796-809.
113. Beatty WL. 2006. Trafficking from CD63-positive Late Endocytic Multivesicular Bodies is Essential for Intracellular Development of *Chlamydia trachomatis*. Journal of Cell Science 119:350-359.
114. Jordan LC, Yadunanda K, Elizabeth RF, Ted H, Raphael HV. 2008. Cytoplasmic Lipid Droplets Are Translocated into the Lumen of the *Chlamydia trachomatis* Parasitophorous Vacuole. Proceedings of the National Academy of Sciences - PNAS 105:9379-9384.
115. Ronzone E, Paumet F. 2013. Two Coiled-Coil Domains of *Chlamydia trachomatis* IncA Affect Membrane Fusion Events during Infection. PloS one 8:e69769-e69769.
116. Henderson IR, Lam AC. 2001. Polymorphic Proteins of *Chlamydia* spp. – Autotransporters Beyond the Proteobacteria. Trends in Microbiology 9:573-578.
117. Brinkworth AJ, Malcolm DS, Pedrosa AT, Roguska K, Shahbazian S, Graham JE, Hayward RD, Carabeo RA. 2011. *Chlamydia trachomatis* Slc1 is a Type III Secretion Chaperone that Enhances the Translocation of its Invasion Effector Substrate TARP. Molecular Microbiology 82:131-144.
118. Saka HA, Thompson JW, Chen YS, Kumar Y, Dubois LG, Moseley MA, Valdivia RH. 2011. Quantitative Proteomics Reveals Metabolic and Pathogenic Properties of *Chlamydia trachomatis* Developmental Forms. Molecular Microbiology 82:1185-1203.

119. Clifton DR, Fields KA, Grieshaber SS, Dooley CA, Fischer ER, Mead DJ, Carabeo RA, Hackstadt T. 2004. A Chlamydial Type III Translocated Protein is Tyrosine-Phosphorylated at the Site of Entry and Associated with Recruitment of Actin. *Proceedings of the National Academy of Sciences of the United States of America* 101:10166-10171.
120. Caven L, Carabeo RA. 2019. Pathogenic Puppetry: Manipulation of the Host Actin Cytoskeleton by *Chlamydia trachomatis*. *International Journal of Molecular Sciences* 21:90.
121. Jiwani S, Alvarado S, Ohr RJ, Romero A, Nguyen B, Jewett TJ. 2013. *Chlamydia trachomatis* Tarp Harbors Distinct G and F Actin Binding Domains That Bundle Actin Filaments. *Journal of Bacteriology* 195:708-716.
122. Pedrosa AT, Murphy KN, Nogueira AT, Brinkworth AJ, Thwaites TR, Aaron J, Chew T-L, Carabeo RA. 2020. A Post-Invasion Role for *Chlamydia* type III Effector TarP in Modulating the Dynamics and Organization of Host Cell Focal Adhesions. *The Journal of Biological Chemistry*  
doi:10.1074/jbc.RA120.015219;jbc.RA120.015219.
123. Jewett TJ, Dooley CA, Mead DJ, Hackstadt T. 2008. *Chlamydia trachomatis* Tarp is Phosphorylated by Src Family Tyrosine Kinases. *Biochemical and Biophysical Research Communications* 371:339-344.
124. Elwell CA, Ceesay A, Kim JH, Kalman D, Engel JN. 2008. RNA Interference Screen Identifies Abl Kinase and PDGFR Signaling in *Chlamydia trachomatis* Entry. *PLoS Pathogens* 4:e1000021.

125. Mehlitz A, Banhart S, Hess S, Selbach M, Meyer TF. 2008. Complex Kinase Requirements for *Chlamydia trachomatis* Tarp Phosphorylation. FEMS Microbiology Letters 289:233-240.
126. Clifton DR, Dooley CA, Grieshaber SS, Carabeo RA, Fields KA, Hackstadt T. 2005. Tyrosine Phosphorylation of the Chlamydial Effector Protein Tarp Is Species Specific and Not Required for Recruitment of Actin. Infection and Immunity 73:3860-3868.
127. Mehlitz A, Sebastian B, André PM, Alexis K, Andrew GG, Julia Z, Gavin M, Thomas FM. 2010. Tarp Regulates Early *Chlamydia*-Induced Host Cell Survival through Interactions with the Human Adaptor Protein SHC1. The Journal of Cell Biology 190:143-157.
128. Lane BJ, Mutchler C, Al Khodor S, Grieshaber SS, Carabeo RA. 2008. Chlamydial Entry Involves TARP Binding of Guanine Nucleotide Exchange Factors. PLoS Pathogens 4:e1000014.
129. Carabeo RA, Grieshaber SS, Fischer E, Hackstadt T. 2002. *Chlamydia trachomatis* Induces Remodeling of the Actin Cytoskeleton During Attachment and Entry into HeLa Cells. Infection and Immunity 70:3793-3803.
130. Carabeo RA, Dooley CA, Grieshaber SS, Hackstadt T. 2007. Rac Interacts with Abi-1 and WAVE2 to Promote an Arp2/3-Dependent Actin Recruitment During Chlamydial Invasion. Cellular Microbiology 9:2278-2288.
131. Ghosh S, Park J, Thomas M, Cruz E, Cardona O, Kang H, Jewett T. 2018. Biophysical Characterization of Actin Bundles Generated by the *Chlamydia*

- trachomatis* Tarp Effector. Biochemical and Biophysical Research Communications 500:423-428.
132. Ghosh S, Ruelke EA, Ferrell JC, Boder MD, Fields KA, Jewett TJ. 2020. Fluorescence-Reported Allelic Exchange Mutagenesis-Mediated Gene Deletion Indicates a Requirement for *Chlamydia trachomatis* Tarp during In Vivo Infectivity and Reveals a Specific Role for the C Terminus during Cellular Invasion. Infection and Immunity 88.
133. He X, Liu J, Qi Y, Brakebusch C, Chrostek-Grashoff A, Edgar D, Yurchenco PD, Corbett SA, Lowry SF, Graham AM, Han Y, Li S. 2010. Rac1 Is Essential for Basement Membrane-Dependent Epiblast Survival. Molecular and Cellular Biology 30:3569-3581.
134. Sun X, Liu S, Wang J, Wei B, Guo C, Chen C, Sun M-Z. 2018. Annexin A5 Regulates Hepatocarcinoma Malignancy via CRKI/II-DOCK180-RAC1 Integrin and MEK-ERK Pathways. Cell Death & Disease 9:637.
135. Keb G, Ferrell J, Scanlon KR, Jewett TJ, Fields KA. 2021. *Chlamydia trachomatis* TmeA Directly Activates N-WASP To Promote Actin Polymerization and Functions Synergistically with TarP during Invasion. mBio 12.
136. Carpenter V, Chen Y-S, Dolat L, Valdivia RH. 2017. The Effector TepP Mediates Recruitment and Activation of Phosphoinositide 3-Kinase on Early *Chlamydia trachomatis* Vacuoles. mSphere 2.

137. Bullock HD, Hower S, Fields KA. 2012. Domain Analyses Reveal That *Chlamydia trachomatis* CT694 Protein Belongs to the Membrane-localized Family of Type III Effector Proteins. *Journal of Biological Chemistry* 287:28078-28086.
138. Hower S, Wolf K, Fields KA. 2009. Evidence that CT694 is a Novel *Chlamydia trachomatis* T3S Substrate Capable of Functioning During Invasion or Early Cycle Development. *Molecular Microbiology* 72:1423-1437.
139. Mueller KE, Fields KA. 2015. Application of  $\beta$ -Lactamase Reporter Fusions as an Indicator of Effector Protein Secretion during Infections with the Obligate Intracellular Pathogen *Chlamydia trachomatis*. *PLOS ONE* 10:e0135295.
140. Keb G, Hayman R, Fields KA. 2018. Floxed-Cassette Allelic Exchange Mutagenesis Enables Markerless Gene Deletion in *Chlamydia trachomatis* and Can Reverse Cassette-Induced Polar Effects. *Journal of Bacteriology* 200:e00479-18, /jb/200/24/e00479-18.atom.
141. Pais SV, Milho C, Almeida F, Mota LJ. 2013. Identification of Novel type III Secretion Chaperone-Substrate Complexes of *Chlamydia trachomatis*. *PloS One* 8:e56292-e56292.
142. Sisko JL, Spaeth K, Kumar Y, Valdivia RH. 2006. Multifunctional Analysis of *Chlamydia*-Specific Genes in a Yeast Expression System. *Molecular Microbiology* 60:51-66.
143. McKuen MJ, Mueller KE, Bae YS, Fields KA. 2017. Fluorescence-Reported Allelic Exchange Mutagenesis Reveals a Role for *Chlamydia trachomatis* TmeA

- in Invasion That Is Independent of Host AHNAK. *Infection and Immunity* 85:e00640-17, /iai/85/12/e00640-17.atom.
144. Lyman MG, Enquist LW. 2009. Herpesvirus Interactions with the Host Cytoskeleton. *Journal of Virology* 83:2058-2066.
  145. Alan H. 1998. Rho GTPases and the Actin Cytoskeleton. *Science (American Association for the Advancement of Science)* 279:509-514.
  146. Cossart P, Sansonetti PJ. 2004. Bacterial Invasion: the Paradigms of Enteroinvasive Pathogens. *Science* 304:242-248.
  147. Gouin E, Welch MD, Cossart P. 2005. Actin-Based Motility of Intracellular Pathogens. *Current Opinion in Microbiology* 8:35-45.
  148. Kate EU, Michael W, Mark M, Laura M, David WH. 2004. Analysis of the Mechanisms of *Salmonella*-Induced Actin Assembly During Invasion of Host Cells and Intracellular Replication. *Cellular Microbiology* 6:1041-1055.
  149. Reynolds DJ, Pearce JH. 1991. Endocytic Mechanisms Utilized by Chlamydiae and their Influence on Induction of Productive Infection. *Infection and Immunity* 59:3033-3039.
  150. Boleti H, Benmerah A, Ojcius DM, Cerf-Bensussan N, Dautry-Varsat A. 1999. *Chlamydia* Infection of Epithelial Cells Expressing Dynamin and Eps15 Mutants: Clathrin-Independent Entry into Cells and Dynamin-Dependent Productive Growth. *Journal of Cell Science* 112:1487-1496.

151. Patel AL, Chen X, Wood ST, Stuart ES, Arcaro KF, Molina DP, Petrovic S, Furdui CM, Tsang AW. 2014. Activation of Epidermal Growth Factor Receptor is Required for *Chlamydia trachomatis* Development. BMC Microbiology 14:277.
152. Kumar Y, Valdivia RH. 2008. Actin and Intermediate Filaments Stabilize the *Chlamydia trachomatis* Vacuole by Forming Dynamic Structural Scaffolds. Cell Host & Microbe 4:159-169.
153. Brothwell JA, Muramatsu MK, Zhong G, Nelson DE. 2018. Advances and Obstacles in the Genetic Dissection of Chlamydial Virulence. Current Topics in Microbiology and Immunology 412:133-158.
154. Rahnama M, Fields KA. 2018. Transformation of *Chlamydia*: Current Approaches and Impact on Our Understanding of Chlamydial Infection Biology. Microbes and Infection 20:445-450.
155. McClure EE, Chávez ASO, Shaw DK, Carlyon JA, Ganta RR, Noh SM, Wood DO, Bavoil PM, Brayton KA, Martinez JJ, McBride JW, Valdivia RH, Munderloh UG, Pedra JHF. 2017. Engineering of Obligate Intracellular Bacteria: Progress, Challenges and Paradigms. Nature Reviews Microbiology 15:544-558.
156. Wang Y, Kahane S, Cutcliffe LT, Skilton RJ, Lambden PR, Clarke IN. 2011. Development of a Transformation System for *Chlamydia trachomatis*: Restoration of Glycogen Biosynthesis by Acquisition of a Plasmid Shuttle Vector. PLoS Pathogens 7:e1002258.
157. Binet R, T. Maurelli A. 2009. Transformation and Isolation of Allelic Exchange Mutants of *Chlamydia psittaci* using Recombinant DNA Introduced by

- Electroporation. Proceedings of the National Academy of Sciences - PNAS 106:292-297.
158. Tam JE, Davis CH, Wyrick PB. 1994. Expression of Recombinant DNA Introduced into *Chlamydia trachomatis* by Electroporation. Canadian Journal of Microbiology 40:583-591.
159. Kokes M, Dunn JD, Granek JA, Nguyen BD, Barker JR, Valdivia RH, Bastidas RJ. 2015. Integrating Chemical Mutagenesis and Whole-Genome Sequencing as a Platform for Forward and Reverse Genetic Analysis of *Chlamydia*. Cell Host & Microbe 17:716-25.
160. Laszlo K, Morgan MG, Linnell BR, Lacey DT, John HC, William MW, Dezso V, Krithika R, Valeria E, Grant M, David EN, Harlan DC, Emil CG. 2011. Generation of Targeted *Chlamydia trachomatis* Null Mutants. Proceedings of the National Academy of Sciences - PNAS 108:7189-7193.
161. LaBrie SD, Dimond ZE, Harrison KS, Baid S, Wickstrum J, Suchland RJ, Hefty PS. 2019. Transposon Mutagenesis in *Chlamydia trachomatis* Identifies CT339 as a ComEC Homolog Important for DNA Uptake and Lateral Gene Transfer. mBio 10.
162. Johnson CM, Fisher DJ. 2013. Site-Specific, Insertional Inactivation of IncA in *Chlamydia trachomatis* using a group II intron. PloS One 8:e83989-e83989.
163. Mueller KE, Wolf K, Fields KA. 2016. Gene Deletion by Fluorescence-Reported Allelic Exchange Mutagenesis in *Chlamydia trachomatis*. mBio 7.

164. Agaisse H, Derré I. 2013. A *C. trachomatis* Cloning Vector and the Generation of *C. trachomatis* Strains Expressing Fluorescent Proteins under the Control of a *C. trachomatis* Promoter. *PloS One* 8:e57090-e57090.
165. Wickstrum J, Sammons LR, Restivo KN, Hefty PS. 2013. Conditional Gene Expression in *Chlamydia trachomatis* Using the Tet System. *PloS One* 8:e76743-e76743.
166. Bauler LD, Hackstadt T. 2014. Expression and Targeting of Secreted Proteins from *Chlamydia trachomatis*. *Journal of Bacteriology* 196:1325-1334.
167. Ouellette SP. 2018. Feasibility of a Conditional Knockout System for *Chlamydia* based on CRISPR Interference. *Frontiers in Cellular and Infection Microbiology* 8:59-59.
168. Song L, John HC, William MW, Laszlo K, Kimmo V, Daniel ES, Heather W, Bing Z, Gail LS, Stephen FP, Grant M, Harlan DC. 2013. *Chlamydia trachomatis* Plasmid-Encoded Pgp4 Is a Transcriptional Regulator of Virulence-Associated Genes. *Infection and Immunity* 81:636-644.
169. Demars R, Weinfurter J Fau - Guex E, Guex E Fau - Lin J, Lin J Fau - Potucek Y, Potucek Y. 2007. Lateral Gene Transfer *In Vitro* in the Intracellular Pathogen *Chlamydia trachomatis*. *Journal of Bacteriology* 189:991-1003.
170. Mueller KE, Wolf K, Fields KA. 2017. *Chlamydia trachomatis* Transformation and Allelic Exchange Mutagenesis. *Current Protocols in Microbiology* 45:11A.3.1-11A.3.15.

171. Olivares-Zavaleta N, Whitmire W, Gardner D, Caldwell HD. 2009. Immunization with the Attenuated Plasmidless *Chlamydia trachomatis* L2(25667R) Strain Provides Partial Protection in a Murine Model of Female Genitourinary Tract Infection. *Vaccine* 28:1454-1462.
172. Wolf K, Rahnama M, Fields KA. 2019. Genetic Manipulation of *Chlamydia trachomatis*: Chromosomal Deletions. *Methods in Molecular Biology*:151-164.
173. Roux KJ, Kim DI, Raida M, Burke B. 2012. A Promiscuous Biotin Ligase Fusion Protein Identifies Proximal and Interacting Proteins in Mammalian Cells. *The Journal of Cell Biology* 196:801-810.
174. Lam SS, Martell JD, Kamer KJ, Deerinck TJ, Ellisman MH, Mootha VK, Ting AY. 2014. Directed Evolution of APEX2 for Electron Microscopy and Proximity Labeling. *Nature Methods* 12:51-54.
175. Keb G, Fields KA. 2020. Markerless Gene Deletion by Floxed Cassette Allelic Exchange Mutagenesis in *Chlamydia trachomatis*. *Journal of Visualized Experiments* doi:10.3791/60848:e60848.
176. Scidmore MA. 2005. Cultivation and Laboratory Maintenance of *Chlamydia trachomatis*. *Current Protocols in Microbiology*.
177. Carpenter V, Chen YS, Dolat L, Valdivia RH. 2017. The Effector TepP Mediates Recruitment and Activation of Phosphoinositide 3-Kinase on Early *Chlamydia trachomatis* Vacuoles. *mSphere* 2:e00207-17.

178. Hussain NK, Jenna S, Glogauer M, Quinn CC, Wasiak S, Guipponi M, Antonarakis SE, Kay BK, Stossel TP, Lamarche-Vane N, McPherson PS. 2001. Endocytic Protein Intersectin-1 Regulates Actin Assembly via Cdc42 and N-WASP. *Nature Cell Biology* 3:927-932.
179. Roux KJ, Kim DI, Burke B. 2018. BioID: A Screen for Protein-Protein Interactions. *Current Protocols in Protein Science* 74:19.23.1-19.23.14.
180. Olson MG, Jorgenson LM, Widner RE, Rucks EA. 2019. Proximity Labeling of the *Chlamydia trachomatis* Inclusion Membrane. *Methods in Molecular Biology* 2042:245-278.
181. Neal MA, Andrew WW, Matthew JR, Defne Y, Cheri SL, Raffi T, Antonius K, Susan ST, Charles B, Sachdev SS, Sandra LS, Gail AH, Jack ED. 2007. The Type III Effector EspF Coordinates Membrane Trafficking by the Spatiotemporal Activation of Two Eukaryotic Signaling Pathways. *The Journal of Cell Biology* 178:1265-1278.
182. Hefty PS, Richard SS. 2007. Chlamydial Type III Secretion System Is Encoded on Ten Operons Preceded by Sigma 70-Like Promoter Elements. *Journal of Bacteriology* 189:198-206.
183. Yarmolinsky M, Hoess R. 2015. The Legacy of Nat Sternberg: The Genesis of Cre-lox Technology. *Annual Review of Virology* 2:25-40.
184. Leibig M, Krismer B, Kolb M, Friede A, Götz F, Bertram R. 2008. Marker Removal in *Staphylococci* via Cre Recombinase and Different lox Sites. *Applied and Environmental Microbiology* 74:1316-1323.

185. Beare PA, Larson CL, Gilk SD, Heinzen RA. 2012. Two Systems for Targeted Gene Deletion in *Coxiella burnetii*. *Applied and Environmental Microbiology* 78:4580-4589.
186. Beare PA, Sandoz KM, Omsland A, Rockey DD, Heinzen RA. 2011. Advances in Genetic Manipulation of Obligate Intracellular Bacterial Pathogens. *Frontiers in Microbiology* 2:97-97.
187. Conway T, Creecy J, Maddox S, Grissom J, Conkle T, Shadid T, Teramoto J, San Miguel P, Shimada T, Ishihama I, Mori H, Wanner B. 2014. Unprecedented High-Resolution View of Bacterial Operon Architecture Revealed by RNA Sequencing. *mBio* doi:10.1128/mBio.01442-14.
188. Tan M. 2012. Temporal Gene Regulation during the Chlamydial Developmental Cycle p149-169. *In* M T, P B (ed), *Intracellular Pathogens I: Chlamydiales* ASM Press, Washington, DC.
189. Albrecht M, Sharma CM, Reinhardt R, Vogel J, Rudel T. 2009. Deep Sequencing-based Discovery of the *Chlamydia trachomatis* Transcriptome. *Nucleic acids research* 38:868-877.
190. Albrecht M, Sharma CM, Dittrich MT, Müller T, Reinhardt R, Vogel J, Rudel T. 2011. The Transcriptional Landscape of *Chlamydia pneumoniae*. *Genome Biology* 12:R98-R98.
191. Van Duyne GD. 2015. Cre Recombinase. *Microbiology Spectrum*

192. Enyeart PJ, Chirieleison SM, Dao MN, Perutka J, Quandt EM, Yao J, Whitt JT, Keatinge-Clay AT, Lambowitz AM, Ellington AD. 2013. Generalized Bacterial Genome Editing Using Mobile Group II Introns and Cre-lox. *Molecular Systems Biology* 9:685-n/a.
193. Mariscal AM, González-González L, Querol E, Piñol J. 2016. All-in-One Construct for Genome Engineering Using Cre-lox Technology. *DNA Res* 23:263-70
194. Pomerantsev AP, Camp A, Leppla SH. 2009. A New Minimal Replicon of *Bacillus anthracis* Plasmid pXO1. *Journal of Bacteriology* 191:6192-6192.
195. Robert D, Jason W. 2008. Interstrain Gene Transfer in *Chlamydia trachomatis* *In Vitro*: Mechanism and Significance. *Journal of Bacteriology* 190:1605-1614.
196. McKimm-Breschkin JL. 2004. A Simplified Plaque Assay for Respiratory Syncytial Virus—Direct Visualization of Plaques without Immunostaining. *Journal of Virological Methods* 120:113-117.
197. Zhong G. 2016. Chlamydial Plasmid-Dependent Pathogenicity. *Trends in Microbiology* 25:141-152.
198. Leigh AK, Aaron B, Caixia M, Imke H-W, Michael H, Bruce AV, Olivia S-M. 2005. Cloning Vectors and Fluorescent Proteins Can Significantly Inhibit *Salmonella enterica* Virulence in Both Epithelial Cells and Macrophages: Implications for Bacterial Pathogenesis Studies. *Infection and Immunity* 73:7027-7031.

199. Ridderhof JC, Barnes RC. 1989. Fusion of Inclusions Following Superinfection of HeLa Cells by Two Serovars of *Chlamydia trachomatis*. *Infection and Immunity* 57:3189-3193.
200. Hackstadt T, Scidmore-Carlson MA, Shaw EI, Fischer ER. 1999. The *Chlamydia trachomatis* IncA Protein is Required for Homotypic Vesicle Fusion. *Cellular Microbiology* 1:119-130.
201. Shmakov SA, Faure G, Makarova KS, Wolf YI, Severinov KV, Koonin EV. 2019. Systematic Prediction of Functionally Linked Genes in Bacterial and Archaeal Genomes. *Nature Protocols* 14:3013-3031.
202. Stender S, Friebel A, Linder S, Rohde M, Mirolid S, Hardt WD. 2000. Identification of SopE2 from *Salmonella typhimurium*, a Conserved Guanine Nucleotide Exchange Factor for Cdc42 of the Host Cell. *Molecular Microbiology* 36:1206-1221.
203. Fu Y, Galán JE. 1998. The *Salmonella typhimurium* Tyrosine Phosphatase SptP is Translocated into Host Cells and Disrupts the Actin Cytoskeleton. *Molecular Microbiology* 27:359-368.
204. Shuping Z, Renato LS, Renee MT, Silke S, Wolf-Dietrich H, Andreas JB, Adams LG. 2002. The *Salmonella enterica* Serotype Typhimurium Effector Proteins SipA, SopA, SopB, SopD, and SopE2 Act in Concert To Induce Diarrhea in Calves. *Infection and Immunity* 70:3843-3855.
205. Renée MT, Adams LG, Michael JH, Christina AS, Tyler K, Robert AK, Thomas AF, Samuel IM, Andreas JB. 2000. SspA Is Required for Lethal *Salmonella*

- enterica* Serovar Typhimurium Infections in Calves but Is Not Essential for Diarrhea. *Infection and Immunity* 68:3158-3163.
206. Shuping Z, Adams LG, Jairo N, Sangeeta K, Renée MT, Andreas JB. 2003. Secreted Effector Proteins of *Salmonella enterica* Serotype Typhimurium Elicit Host-Specific Chemokine Profiles in Animal Models of Typhoid Fever and Enterocolitis. *Infection and Immunity* 71:4795-4803.
207. Wang JTH, Kerr MC, Karunaratne S, Jeanes A, Yap AS, Teasdale RD. 2010. The snx-px-bar Family in Macropinocytosis: The Regulation of Macropinosome Formation by snx-px-bar Proteins. *PloS One* 5:e13763.
208. Carman PJ, Dominguez R. 2018. BAR Domain Proteins—a Linkage Between Cellular Membranes, Signaling Pathways, and the Actin Cytoskeleton. *Biophysical Reviews* 10:1587-1604.
209. Hänsch S, Spona D, Murra G, Köhrer K, Subtil A, Furtado AR, Lichtenthaler SF, Dislich B, Mölleken K, Hegemann JH. 2020. *Chlamydia*-Induced Curvature of the Host-Cell Plasma Membrane is Required for Infection. *Proceedings of the National Academy of Sciences of the United States of America* 117:2634-2644.
210. Rucks EA, Olson MG, Jorgenson LM, Srinivasan RR, Ouellette SP. 2017. Development of a Proximity Labeling System to Map the *Chlamydia trachomatis* Inclusion Membrane. *Frontiers in Cellular and Infection Microbiology* 7:40.
211. Dickinson MS, Anderson LN, Webb-Robertson B-JM, Hansen JR, Smith RD, Wright AT, Hybiske K. 2019. Proximity-Dependent Proteomics of the *Chlamydia*

- trachomatis* Inclusion Membrane Reveals Functional Interactions with Endoplasmic Reticulum Exit Sites. PLoS Pathogens 15:e1007698.
212. Mojica SA, Hovis KM, Frieman MB, Tran B, Hsia R-c, Ravel J, Jenkins-Houk C, Wilson KL, Bavoil PM. 2015. SINC, a Type III Secreted Protein of *Chlamydia psittaci*, Targets the Inner Nuclear Membrane of Infected Cells and Uninfected Neighbors. Molecular Biology of the Cell 26:1918-1934.
213. Hart MJ, Callow MG, Souza B, Polakis P. 1996. IQGAP1, a Calmodulin-Binding Protein with a RasGAP-Related Domain, is a Potential Effector for Cdc42Hs. The EMBO Journal 15:2997-3005.
214. Kim SM, Nguyen TT, Ravi A, Kubiniok P, Finicle BT, Jayashankar V, Malacrida L, Hou J, Robertson J, Gao D, Chernoff J, Digman MA, Potma EO, Tromberg BJ, Thibault P, Edinger AL. 2018. PTEN Deficiency and AMPK Activation Promote Nutrient Scavenging and Anabolism in Prostate Cancer Cells. Cancer discovery 8:866-883.
215. Jewett TJ, Fischer ER, Mead DJ, Hackstadt T. 2006. Chlamydial TARP is a Bacterial Nucleator of Actin. Proceedings of the National Academy of Sciences of the United States of America 103:15599-15604.
216. Cooper JA, Pollard TD. 1982. Methods to Measure Actin Polymerization. Methods in Enzymology 85 182-210.
217. Frieden C, Goddette DW. 1983. Polymerization of Actin and Actin-like Systems: Evaluation of the Time Course of Polymerization in Relation to the Mechanism. Biochemistry 22:5836-5843.

218. Co C, Wong DT, Gierke S, Chang V, Taunton J. 2007. Mechanism of Actin Network Attachment to Moving Membranes: Barbed End Capture by N-WASP WH2 Domains. *Cell* 128:901-913.
219. Faris R, McCullough AA-O, Andersen SA-O, Moninger TO, Weber MA-O. 2020. The *Chlamydia trachomatis* Secreted Effector TmeA Hijacks the N-WASP-ARP2/3 Actin Remodeling Axis to Facilitate Cellular Invasion. *PLOS Pathogens*.
220. Igietseme JU, Partin J, George Z, Omosun Y, Goldstein J, Joseph K, Ellerson D, Eko FO, Pohl J, Bandea C, Black CM. 2020. Epidermal Growth Factor Receptor and Transforming Growth Factor  $\beta$  Signaling Pathways Cooperate To Mediate *Chlamydia* Pathogenesis. . *Infection and Immunity*.
221. Yan Y, Vasudevan S, Nguyen HTT, Merlin D. 2008. Intestinal Epithelial CD98: An Oligomeric and Multifunctional Protein. *Biochimica et biophysica acta General subjects* 1780:1087-1092.
222. Rajeeve KA-O, Vollmuth N, Janaki-Raman S, Wulff TA-O, Baluapuri AA-O, Dejure FR, Huber C, Fink J, Schmalhofer MA-O, Schmitz WA-O, Sivadasan R, Wolf EA-O, Eisenreich W, Schulze A, Seibel JA-O, Rudel TA-O. 2020. Reprogramming of Host Glutamine Metabolism during *Chlamydia trachomatis* Infection and its Key role in Peptidoglycan Synthesis. *Nature Microbiology* 5:1390-1402.
223. Chin E, Kirker K, Zuck M, James G, Hybiske K. 2012. Actin Recruitment to the *Chlamydia* Inclusion Is Spatiotemporally Regulated by a Mechanism That Requires Host and Bacterial Factors. *PLoS ONE* 7:e46949.

224. Wang X, Hybiske K, Stephens RS. 2018. Direct Visualization of the Expression and Localization of Chlamydial Effector Proteins within Infected Host Cells. *Pathogens and Disease* 76:fty001.
225. Koivusalo M, Welch C, Hayashi H, Scott CC, Kim M, Alexander T, Touret N, Hahn KM, Grinstein S. 2010. Amiloride Inhibits Macropinocytosis by Lowering Submembranous pH and Preventing Rac1 and Cdc42 Signaling. *The Journal of Cell Biology* 188:547-563.
226. Carabeo RA, Grieshaber SS, Hasenkrug A, Dooley C, Hackstadt T. 2004. Requirement for the Rac GTPase in *Chlamydia trachomatis* Invasion of Non-Phagocytic Cells. *Traffic* 5:418-425.
227. Garmendia J, Carlier M-F, Egile C, Didry D, Frankel G. 2006. Characterization of TccP-Mediated N-WASP Activation During Enterohaemorrhagic *Escherichia coli* Infection. *Cellular Microbiology* 8:1444-1455.
228. Jarsch IK, Gadsby JR, Nuccitelli A, Mason J, Shimo H, Pilloux L, Marzook B, Mulvey CM, Dobramysl U, Bradshaw CR, Lilley KS, Hayward RD, Vaughan TJ, Dobson CL, Gallop JL. 2020. A Direct Role for SNX9 in the Biogenesis of Filopodia. *Journal of Cell Biology* 219:e201909178.
229. Joseph FK, Simon JA, Thomas DP. 1995. Sequences, Structural Models, and Cellular Localization of the Actin-Related Proteins Arp2 and Arp3 from *Acanthamoeba*. *The Journal of Cell Biology* 131:385-397.
230. Sokolova OS, Chemeris A, Guo S, Alioto SL, Gandhi M, Padrick S, Pechnikova E, David V, Gautreau A, Goode BL. 2017. Structural Basis of Arp2/3 Complex

- Inhibition by GMF, Coronin, and Arpin. *Journal of Molecular Biology* 429:237-248.
231. Birkelund S, Bini L, Pallini V, Sanchez-Campillo M, Liberatori S, Clausen JD, Østergaard S, Holm A, Christiansen G. 1997. Characterization of *Chlamydia trachomatis* L2-Induced Tyrosine-Phosphorylated HeLa Cell Proteins by Two-Dimensional Gel Electrophoresis. *Electrophoresis* 18:563-567.
232. Jiwani S, Ohr RJ, Fischer ER, Hackstadt T, Alvarado S, Romero A, Jewett TJ. 2012. *Chlamydia trachomatis* Tarp Cooperates with the Arp2/3 Complex to Increase the Rate of Actin Polymerization. *Biochemical and Biophysical Research Communications* 420:816-821.
233. Miller HE, Larson CL, Heinzen RA, Heinzen RA. 2018. Actin polymerization in the endosomal pathway, but not on the Coxiella-containing vacuole, is essential for pathogen growth. *PLoS pathogens* 14:e1007005-e1007005.
234. Paavilainen VO, Bertling E, Falck S, Lappalainen P. 2004. Regulation of Cytoskeletal Dynamics by Actin-Monomer-Binding Proteins. *Trends in Cell Biology* 14:386-394.
235. Jon WE, Richard AC, Matthew JH. 1997. Identification of an Actin Cytoskeletal Complex That Includes IQGAP and the Cdc42 GTPase. *The Journal of Biological Chemistry* 272:24443-24447.
236. Owen D, Campbell LJ, Littlefield K, Evetts KA, Li Z, Sacks DB, Lowe PN, Mott HR. 2008. The IQGAP1-Rac1 and IQGAP1-Cdc42 Interactions: Interfaces Differ Between the Complexes. *Journal of Biological Chemistry* 283:1692-1704.

237. Fukata M, Nakagawa M, Kaibuchi K. 2003. Roles of Rho-Family GTPases in Cell Polarisation and Directional Migration. *Current Opinion in Cell Biology* 15:590-597.
238. Roy M, Li Z, Sacks DB. 2004. IQGAP1 Binds ERK2 and Modulates Its Activity. *The Journal of Biological Chemistry* 279:17329-17337.
239. Weissbach L, Bernards A, Herion DW. 1998. Binding of Myosin Essential Light Chain to the Cytoskeleton-Associated Protein IQGAP1. *Biochemical and Biophysical Research Communications* 251:269-276.
240. Fukata M, Kuroda S, Nakagawa M, Kawajiri A, Itoh N, Shoji I, Matsuura Y, Yonehara S, Fujisawa H, Kikuchi A, Kaibuchi K. 1999. Cdc42 and Rac1 Regulate the Interaction of IQGAP1 with  $\beta$ -catenin. *The Journal of Biological Chemistry* 274:26044-26050.
241. Shinya K, Masaki F, Masato N, Katsuhiko F, Tomoko N, Tadashi O, Ichiro I, Takahiro N, Nobuo N, Hideki T, Ikuo S, Yoshiharu M, Shin Y, Kozo K. 1998. Role of IQGAP1, a Target of the Small GTPases Cdc42 and Rac1, in Regulation of E-Cadherin-Mediated Cell-Cell Adhesion. *Science* 281:832-835.
242. Hongyu M, Joseph AH, Martin SZ, Jeanne H-W, Tim RM, Alan SP, Hulin W, David JT. 2010. Quantifying the Early Immune Response and Adaptive Immune Response Kinetics in Mice Infected with Influenza A Virus. *Journal of Virology* 84:6687-6698.
243. 2012. Global Incidence and Prevalence of Selected Curable Sexually Transmitted Infections: 2008: World Health Organization, Department of Reproductive Health

- and Research, 2012 ISBN 978 92 4 150383 9. Reproductive Health Matters 20:207-209.
244. Wolf K, Betts HJ, Chellas-Géry B, Hower S, Linton CN, Fields KA. 2006. Treatment of *Chlamydia trachomatis* with a Small Molecule Inhibitor of the *Yersinia* Type III Secretion System Disrupts Progression of the Chlamydial Developmental Cycle. *Molecular Microbiology* 61:1543-1555.
245. Moulder JW. 1991. Interaction of Chlamydiae and Host Cells *In Vitro*. *Microbiological Reviews* 55:143-190.
246. Eissenberg LG, Wyrick PB, Davis CH, Rumpp JW. 1983. *Chlamydia psittaci* Elementary Body Envelopes: Ingestion and Inhibition of Phagolysosome Fusion. *Infection and Immunity* 40:741-751.
247. Levy NJ, Moulder JW. 1982. Attachment of Cell Walls of *Chlamydia psittaci* to Mouse Fibroblasts (L cells). *Infection and Immunity* 37:1059-1065.
248. Subtil A, Wyploz B, Balañá ME, Dautry-Varsat A. 2004. Analysis of *Chlamydia caviae* Entry Sites and Involvement of Cdc42 and Rac Activity. *Journal of Cell Science* 117:3923-3933.
249. Shen Y, Naujokas M, Park M, Ireton K. 2000. InlB-Dependent Internalization of *Listeria* Is Mediated by the Met Receptor Tyrosine Kinase. *Cell* 103:501-510.
250. Ghebrehiwet B, Cossart P, Braun L. 2000. gC1q-R/p32, a C1q-Binding Protein, is a Receptor for the InlB Invasion Protein of *Listeria monocytogenes*. *The EMBO Journal* 19:1458-1466.

251. Cossart P, Bierne H. 2001. The Use of Host Cell Machinery in the Pathogenesis of *Listeria monocytogenes*. *Current Opinion in Immunology* 13:96-103.
252. Pasquale EB. 2010. Eph Receptors and Ephrins in Cancer: Bidirectional Signalling and Beyond. *Nature Reviews Cancer* 10:165-180.
253. Rajat R, Hsin-yi Henry H, Marc WK. 2000. Mechanism of N-WASP Activation by CDC42 and Phosphatidylinositol 4,5-Bisphosphate. *The Journal of Cell Biology* 150:1299-1309.
254. Welch MD, Goley ED. 2006. The ARP2/3 Complex: an Actin Nucleator Comes of Age. *Nature Reviews Molecular Cell Biology* 7:713-726.
255. Vitriol EA, Wise AL, Berginski ME, Bamburg JR, Zheng JQ. 2013. Instantaneous Inactivation of Cofilin Reveals its Function of F-actin Disassembly in Lamellipodia. *Molecular Biology of the Cell* 24:2238-2247.
256. Moon AL, Janmey PA, Louie AK, Drubin D, G. . 1993. Cofilin Is an Essential Component of the Yeast Cortical Cytoskeleton. *The Journal of cell biology* 120:421-435.
257. Avital AR, Jonathan WT, Pekka L, David GD, David CA. 1999. Aip1p Interacts with Cofilin to Disassemble Actin Filaments. *The Journal of Cell Biology* 145:1251-1264.
258. Sit S-T, Manser E. 2011. Rho GTPases and their Role in Organizing the Actin Cytoskeleton. *Journal of Cell Science* 124:679-683.

259. Zheng K, Kitazato K, Wang Y, He Z. 2016. Pathogenic Microbes Manipulate Cofilin Activity to Subvert Actin Cytoskeleton. *Critical Reviews in Microbiology* 42:677-695.
260. Hardt W-D, Chen L-M, Schuebel KE, Bustelo XR, Galán JE. 1998. *S. typhimurium* Encodes an Activator of Rho GTPases that Induces Membrane Ruffling and Nuclear Responses in Host Cells. *Cell* 93:815-826.
261. Steele-Mortimer O, Knodler LA, Finlay BB. 2000. Poisons, Ruffles and Rockets: Bacterial Pathogens and the Host Cell Cytoskeleton. *Traffic* 1:107-118.
262. Zhou D, Galán J. 2001. Salmonella Entry into Host Cells: the Work in Concert of Type III Secreted Effector Proteins. *Microbes and Infection* 3:1293-1298.
263. Koronakis V, Hayward RD. 1999. Direct Nucleation and Bundling of Actin by the SipC Protein of Invasive *Salmonella*. *The EMBO Journal* 18:4926-4934.
264. Daoguo Z, Mark SM, Jorge EG. 1999. Role of the *S. typhimurium* Actin-Binding Protein SipA in Bacterial Internalization. *Science* 283:2092-2095.
265. Dai S, Sarmiere PD, Wiggan O, Bamberg JR, Zhou D. 2004. Efficient *Salmonella* Entry Requires Activity Cycles of Host ADF and Cofilin. *Cellular Microbiology* 6:459-471.
266. Thalmann J, Janik K, May M, Sommer K, Ebeling J, Hofmann F, Genth H, Klos A. 2010. Actin Re-organization Induced by *Chlamydia trachomatis* serovar D - Evidence for a Critical Role of the Effector Protein CT166 Targeting Rac. *PLoS One* 5:e9887-e9887.

267. Godowski PJ, Kline L, Mira J-P, Guha M, Mackman N, Teusch N, Ulevitch RJ, Knaus UG, Arbibe L. 2000. Toll-like Receptor 2-Mediated NF- $\kappa$ B Activation Requires a Rac1-Dependent Pathway. *Nature Immunology* 1:533-540.
268. Hackstadt T, Scidmore MA, Rockey DD. 1995. Lipid Metabolism in *Chlamydia trachomatis*-Infected Cells: Directed Trafficking of Golgi-Derived Sphingolipids to the Chlamydial Inclusion. *Proceedings of the National Academy of Sciences* 92:4877-4881.
269. Wilbert JNV, Robert BJ. 1983. Disulfide-Linked Oligomers of the Major Outer Membrane Protein of Chlamydiae. *Journal of Bacteriology* 154:998-1001.
270. Wylie JL, Hatch GM, McClarty G. 1997. Host Cell Phospholipids are Trafficked to and then Modified by *Chlamydia trachomatis*. *Journal of Bacteriology* 179:7233-7242.
271. Bear JE. 2009. Sorting Out Endosomes in the WASH. *Developmental Cell* 17:908-908.
272. Nguyen PH, Lutter EI, Hackstadt T. 2018. *Chlamydia trachomatis* Inclusion Membrane Protein MrcA Interacts with the Inositol 1,4,5-trisphosphate Receptor Type 3 (ITPR3) to Regulate Extrusion Formation. *PLOS Pathogens* 14:e1006911.
273. Valdivia MKaRH. 2012. Cell Biology of the Chlamydial Inclusion *In* M. Tan PMB (ed), *Intracellular Pathogens I: Chlamydiales*. ASM Press, Washington, DC.
274. Zuck M, Sherrid A, Suchland R, Ellis T, Hybiske K. 2016. Conservation of Extrusion as an Exit Mechanism for *Chlamydia*. *Pathogens and Disease* 74.

275. Zuck M, Ellis T, Venida A, Hybiske K. 2017. Extrusions are Phagocytosed and Promote *Chlamydia* Survival within Macrophages. *Cellular Microbiology* 19.
276. Huang Y, Sun Y, Qin T, Liu Y. 2019. The Structural Integrity of Plasmid-Encoded Pgp3 Is Essential for Induction of Hydrosalpinx by *Chlamydia muridarum*. *Frontiers in Cellular and Infection Microbiology* 9:13-13.
277. Rank RG. 2007. Chlamydial diseases. *In* Fox J BS, Newcomer C, Smith A, Quimby F & Davisson M (ed), *The Mouse in Biomedical Research*. Academic Press New York, NY.
278. Sturdevant GL, Caldwell HD. 2014. Innate Immunity is Sufficient for the Clearance of *Chlamydia trachomatis* from the Female Mouse Genital Tract. *Pathogens and Disease* 72:70-73.
279. Fox JG, Barthold S, Davisson M, Newcomer CE, Quimby FW, Smith A. 2007. *The Mouse in Biomedical Research: History, Wild Mice, and Genetics*, vol 1. Elsevier Science & Technology, San Diego.
280. Morrison RP, Caldwell HD. 2002. Immunity to Murine Chlamydial Genital Infection. *Infection and Immunity* 70:2741-2751.
281. Robert JB, Marci AS, Deborah DC, Daniel MH, William W, Grant M, Harlan DC. 2001. *Chlamydia trachomatis* Cytotoxicity Associated with Complete and Partial Cytotoxin Genes. *Proceedings of the National Academy of Sciences* 98:13984-13989.

282. John HC, Scott H, Daniel H, Gordon C, Daniel ES, Grant M, Harlan DC, Robert JB. 2004. Polymorphisms in the *Chlamydia trachomatis* Cytotoxin Locus Associated with Ocular and Genital Isolates. *Infection and Immunity* 72:7063-7072.
283. Song L, Carlson JH, Zhou B, Virtaneva K, Whitmire WM, Sturdevant GL, Porcella SF, McClarty G, Caldwell HD. 2014. Plasmid-Mediated Transformation Tropism of Chlamydial Biovars. *Pathogens and Disease* 70:189-193.

## VITA

Gabrielle Keb

### Education

2016 - 2021: University of Kentucky – Lexington, KY

2012 - 2016: Grand Valley State University – Allendale, MI

Bachelor of Science Biomedical Sciences, Chemistry and Biology Minors

### Professional Positions

2016 – 2021: Research Assistant, Fields Lab.

University of Kentucky – Lexington, KY

2019: Fellow, Office of Technology Commercialization,

University of Kentucky – Lexington, KY

2015 – 2016: Research Assistant, Pearl lab

Grand Valley State University – Allendale, MI

2015: Intern, Bacterial Fermentation

Zoetis – Kalamazoo, MI

### Scholastic Awards

2019: NIH F31 Grant

2019: Best Poster, MIMG Department Retreat

2019: Infectious Disease Day 3-Minute Thesis Competition, 2nd Place

2018: Grad Research Live 3-Minute Thesis Competition, Finalist

2018: Infectious Disease Day 3-Minute Thesis Competition, 2nd Place

### Publications

**Keb G**, Ferrell J, Scanlon KR, Jewett TJ, Fields KA. (2020) *C. trachomatis* TmeA directly activates N-WASP to promote actin polymerization and functions synergistically with TarP during invasion. mBio. PMID: 33468693

**Keb G**, Fields KA. (2020) An Ancient Molecular Arms Race: *Chlamydia* vs. Membrane Attack Complex/Perforin (MACPF) Domain Proteins. *Frontiers in Immunology*. PMID: 32760406

**Keb G**, Fields KA. (2020) Markerless Gene Deletion by Floxed Cassette Allelic Exchange Mutagenesis in *Chlamydia trachomatis*. *Journal of Visualized Experiments*. PMID: 32065159

**Keb G**, Hayman R., Fields KA. (2018) Floxed-Cassette Allelic Exchange Mutagenesis Enables Markerless Gene Deletion in *Chlamydia trachomatis* and Can Reverse Cassette-Induced Polar Effects. *Journal of Bacteriology*. PMID: 3022443